

Shaping plastid stromules

DISSERTATION

zur Erlangung des
Doktorgrades der Naturwissenschaften (Dr. rer. nat.)

vorgelegt der

Naturwissenschaftlichen Fakultät I-Biowissenschaften
der Martin-Luther-Universität Halle-Wittenberg,



von Jessica Erickson
geboren am 05.05.1986 in Pincher Creek, AB, Canada

Gutachterinnen bzw. Gutachter:

1. Prof. Dr. Ralf Bernd Klösgen (Martin-Luther-Universität Halle-Wittenberg)
2. Prof. Dr. Bettina Hause (Leibniz-Institut für Pflanzenbiochemie)
3. Prof. Dr. Karin Krupinska (Christian-Albrechts-Universität zu Kiel)

Tag der Verteidigung: 08. April 2019

Martin, I dedicate this thesis to you. You are my mentor, cheerleader
and champion.

Contents

I	General Introduction and Goals	1
1	General Introduction	2
1.1	Plasticity of organelle shape	2
1.2	Stromules	2
1.3	Clarifying the definition of stromule	2
1.4	Stromules are induced under stress	3
1.5	Putative stromule functions	3
1.5.1	Hypothesis 1 - Stromules facilitate exchange between plastids and other organelles	4
1.5.2	Hypothesis 2 - Stromules as a source of plastid-derived vesicles	6
1.5.3	Hypothesis 3 - Stromule as highways for intercellular communication	7
1.6	Requirements for building a stromule	8
1.6.1	Excess membrane	8
1.6.2	Forces	9
2	Goals	12
II	Results	14
3	Plastid-nucleus interactions dictate stromule extension and orientation	15
3.1	Introduction	15
3.2	Publication I	16
3.3	Summary	32
4	A mechanism for myosin dependent stromule formation	33
4.1	Introduction	33
4.2	Results	33
4.2.1	Myosin XI-I is required to maintain basal stromule levels in upper epidermis of <i>A. thaliana</i>	33
4.2.2	Myosin XI-I is important for nucleus movement	34
4.2.3	Mutants with impaired nucleus movement have less stromules	36
4.3	Discussion and outlook	36
4.3.1	Myosin XI-I and nucleus movement is important for basal stromule levels	36
4.3.2	Analysing the stromule-promoting zone in mutants	38
4.3.3	Correlating reduced nucleus movement with reduced stromule initiations	39

4.4	Materials and methods	39
4.4.1	Plant material and growth conditions	39
4.4.2	Bacterial strains and constructs	39
4.4.3	Epifluorescence microscopy	39
4.4.4	Image processing and analysis	40
4.4.5	Data analysis	40
5	Stromule induction during <i>A. tumefaciens</i>-mediated transient assays	41
5.1	Introduction	41
5.2	Publication II	42
5.3	Additional results	62
5.3.1	Expression of the <i>tzs</i> gene influences ACC and OPDA, and ABA levels	62
5.4	Discussion and outlook	63
5.4.1	<i>A. tumefaciens</i> and secreted cytokinins alter endogenous hormones	63
5.4.2	Reliance of stromule induction on ABA	66
5.4.3	RNAseq data to identify stromule-pertinent genes	66
5.4.4	Use of induction via GV3101 as a tool for genetic screens	67
5.5	Additional materials and methods	68
5.5.1	Hormone measurements	68
5.5.2	Plant material for RNA sequencing	68
5.5.3	RNA isolation and sequencing	68
6	Effector screen identifies microtubules as essential to stromule extension	69
6.1	Introduction	69
6.2	Publication III	70
6.3	Additional results	85
6.4	Summary	85
6.5	Additional materials and methods	87
7	VIGS identifies a GRAM protein that regulates stromules	88
7.1	Introduction	88
7.1.1	Methodology of Virus Induced Gene Silencing (VIGS)	88
7.1.2	VIGS screen	89
7.1.3	Identification of SI17E6, a GRAM domain containing protein	91
7.2	Results	92
7.2.1	Confirmation of <i>SI17E6</i> silencing candidate under new conditions	92
7.2.2	Over-expression of <i>SI17E6</i> results in mild stromule induction	96
7.2.3	Identifying silencing targets of <i>SI17E6</i> in <i>N. benthamiana</i>	97
7.2.4	Confirming silencing of <i>Nb17E6-1</i> and <i>Nb17E6-2</i> via real-time PCR	99
7.2.5	Confirming stromule suppressing effect of <i>Nb17E6</i> silencing	100
7.2.6	Over-expression of <i>Nb17E6</i> proteins confirm their relevance to stromule formation	102
7.2.7	Over-expression of GRAM only and no GRAM constructs	103

7.2.8	Identification of <i>N. benthamiana</i> GRAM domain family members	104
7.2.9	Nb17E6 in the context of the GRAM family	107
7.2.10	Nb17E6 homologs required for plant resistance to pathogens	107
7.2.11	<i>Nb17E6</i> silencing inhibits HR in <i>N. benthamiana</i>	108
7.2.12	Nb17E6-1 interacting proteins	109
7.3	Discussion and outlook	125
7.3.1	Nb17E6-1 may have a role in regulating ROS and RNS pools	125
7.3.2	The disturbance of Nb17E6 interactions could influence stromule induction	126
7.3.3	Regulation of Nb17E6-1 via 14-3-3 proteins?	126
7.3.4	Is Nb17E6 important for ETI-induced stromules?	128
7.4	Summary	128
7.5	Materials and methods	128
7.5.1	Plant material and growth conditions	128
7.5.2	Bacterial strains and constructs	128
7.5.3	Virus induced gene silencing	129
7.5.4	Epifluorescence microscopy	129
7.5.5	Image analysis	129
7.5.6	Confocal microscopy	129
7.5.7	Real-time PCR to test VIGS silencing efficiency	130
7.5.8	Generation of the homology tree	130
7.5.9	Ion leakage assay	130
7.5.10	Co-Immunoprecipitation	131
7.5.11	LC-MS/MS	131
7.5.12	Database searching	132
III	General Discussion	133
8	Elucidating cytoskeletal involvement in stromule formation	134
8.1	Actin	134
8.1.1	Actin and myosins influence stromule extension via nucleus movement	134
8.1.2	What anchors stromules to the nucleus?	135
8.1.3	Anchoring of the plastid body	135
8.1.4	Why should the plastid membrane anchor near the nucleus?	136
8.2	Microtubules	137
8.2.1	Microtubule scaffold contributes to stromules formation	137
8.2.2	Microtubules as an interface for interaction	137
8.3	Significance	138
9	Genetic elements contributing to stromule formation	139
9.1	H ₂ O ₂ , a key regulator of stromules?	140
9.2	Significance	141

Contents

10 Conclusion	142
IV Supplemental Data	143
11 Figures	144
12 Tables	153
13 DNA and protein sequences	159
V Appendix	164
14 List of abbreviations	165
15 List of figures	167
16 List of tables	169
17 References	170
18 Publication list	180
19 <i>Curriculum vitae</i> / Lebenslauf	181
20 Declaration / Erklärung	182
21 Acknowledgements	183

Gray boxes

I have chosen to use gray boxes to highlight information that provides context for my work. They are used to remind the reader of important concepts or to draw attention to interesting or controversial ideas from the literature.

Excess membrane generated via *de novo* membrane synthesis? on page 9

A reminder of abbreviations used for the *A. tumefaciens* strains utilized in Erickson et al. (2014). on page 62

A quick reminder about HR. on page 108

Stromules as mediators of H₂O₂ transport? on page 141

Summary

During plant cell evolution the lumen was sequestered into membrane bound compartments, each with a distinct biochemical environment and shape. With the advancement of microscopic techniques it has becoming increasingly clear that organelle shape is not static, and organelles may dramatically change their morphology in times of stress. One striking example of such shape changes can be found in the extension of stromules (dynamic stroma-filled projections) from the surface of plastids. Stromules emanate from all plastid types and have been observed in species scattered throughout the plant kingdom, suggesting that they are important to plant survivability. Stromules are frequently hypothesized to act as a route for retrograde signal transfer between plastids and the nucleus. However, determining the relevance of stromules to cell/plant viability during pathogen attack or under abiotic stress is difficult since there are few known mutations that influence stromule formation. For my thesis I have employed both targeted and untargeted approaches to elucidate the exact mode(s) of stromule formation and regulation in *Nicotiana benthamiana* and *Arabidopsis thaliana*. My goal was to gain insight into function, and/or identify more precise targets for knocking down stromules. Exploring the mechanism of stromule formation led to the discovery that at least two different cytoskeleton-dependent mechanisms contribute to stromule elongation; actin-based nucleus movement and microtubule-dependent extension. This finding suggests that not all stromules are the same, and distinct modes of formation may be important under different circumstances, or produce stromules for a different purpose. Virus Induced Gene Silencing (VIGS) was also used to establish Nb17E6, a GRAM domain containing protein, as an important part of a signaling pathway leading to stromule induction during biotic stress (exposure to *A. tumefaciens*). The identification of Nb17E6 putative interacting proteins points to a role for Nb17E6 in the control of H₂O₂ concentrations, a potent stromule inducer. Now, as opposed to relying only on observational studies for insights into stromule function, as was done in the past, we can use findings presented here to more precisely knockout different stromule types, and manipulate stromule regulatory molecules, to evaluate the relevance of these structures to plant cell survival.

Part I.

General Introduction and Goals

1. General Introduction

1.1. Plasticity of organelle shape

Sequestering of the cellular lumen into membrane-bound compartments is a hallmark of cellular evolution, and resulted in an elaborate and dynamic internal organization (Gabaldón and Pittis, 2015). Creating membrane-bound compartments, hereinafter referred to as organelles, allowed multiple biochemical environments to coexist in a single cell. As a consequence organelles are characterized by typical biochemical properties (Gabaldón and Pittis, 2015). Additionally, organelles exhibit distinct shapes, but may change their morphology drastically in response to external stimuli which cause stress, or during specific developmental programs (Mathur et al., 2012). An emerging concept is that organelle shape contributes to compartment function (Erickson and Schattat, 2018). By exploring the mechanisms governing organelle morphology we come a step closer to understanding the potential adaptive advantage of taking on a certain shape.

1.2. Stromules

This thesis will focus on the plastid, a plant-specific organelle which plays a role in many metabolic processes (Bowsher and Tobin, 2001). One distinctive morphological feature of plastids throughout the green plant lineage is the presence of stromules (Gray et al., 2001), thin stroma-filled tubules formed by the envelope membranes (Köhler et al., 1997). Stromules vary in length, ranging from a few, to more than 65 μm in length, and are approximately 0.4-0.8 μm thick (Gray et al., 2001). The most remarkable characteristic of stromules is their dynamic nature (Gray et al., 2001; Kwok and Hanson, 2004c). Stromules may extend, branch, kink, and retract within minutes (Gunning, 2005; Erickson et al., 2017b,a; Kumar et al., 2018). Although first observed more than 100 years ago (Senn, 1908), stromules went unstudied for years, likely because they are not easily visible with the light microscope. However, with the advent of fluorescence microscopy and the use of stroma-targeted fluorescence proteins, these membrane out-folds became visible (Köhler et al., 1997), and their prevalence in organisms of the plant kingdom indisputable.

1.3. Clarifying the definition of stromule

The initial definition of a stromule was a thin tubule, encompassed by both plastid membranes and filled with stroma (Köhler et al., 1997). In chloroplasts it is easy to distinguish between

the main plastid body and a protruding stromule, since the plastid body is often round and the stromule is visibly thinner and lacks grana stacks (Mathur et al., 2012). However, the definition of 'stromule' becomes confusing when studying other types of plastids, like leucoplasts and etioplasts, which do not possess clearly defined thylakoid stacks and are highly elongated (Schattat et al., 2012). These highly elongated plastids sometimes form thin tubular regions filled with stroma (Figure 1.1 on the following page), which could also be considered stromules under the original definition (Mathur et al., 2012; Schattat et al., 2012). The division of plastids also creates a tubular region between the two new plastid bodies which could also be called a stromule (Schattat et al., 2012). To avoid any confusion, the word 'stromule' will be used to describe organelle extensions that emanate from independent plastids, as described by Mathur et al. (2012) and Schattat et al. (2012). Whereas isthmus will be used to describe stroma-filled connections between dividing plastids (Mathur et al., 2012). The majority of the work in this thesis focuses on epidermal plastids, where the plastid body is easily distinguishable from the stromule, and isthmuses are easily recognized (Figure 1.1 on the next page).

1.4. Stromules are induced under stress

Stromules are a stable characteristic of plant cells under stress, as they are induced under a wide range of biotic and abiotic stress stimuli. Stromules induction has been observed in response to excess salt (Gray et al., 2012), drought (Gray et al., 2012), phosphate deficiency (Vismans et al., 2016), exogenous H_2O_2 (Gray et al., 2012; Caplan et al., 2015), exogenous hormone treatments, including 1 aminocyclopropane-1-carboxylic acid (ACC) (Gray et al., 2012), cytokinins (Erickson et al., 2014), salicylic acid (SA) (Kumar et al., 2018), abscisic acid (ABA) (Gray et al., 2012), methyl jasmonate (MeJa) (Gray et al., 2012), strigolactone (Vismans et al., 2016), as well as exogenous sugar (Schattat and Klösigen, 2011), colonization by mycorrhizae (Fester et al., 2001; Fester and Hause, 2005), or in response to bacteria (Caplan et al., 2015, 2008; Erickson et al., 2014) and viruses (Shalla, 1964; Caplan et al., 2008; Krenz et al., 2010, 2012)¹.

1.5. Putative stromule functions

Based on the wide range of conditions, and the high frequency with which stromules are observed, many different functions have been proposed. Hypotheses about stromule function largely stem from microscopic studies where stromules were observed in association with other organelles, most frequently leading to an inferred role in the exchange of metabolites, proteins and signaling molecules. Although less frequently, stromules have also been implicated in intercellular signaling or autophagy based on similar experimental approaches. Here I will discuss the evidence for the various proposed stromule functions that was available when my PhD began.

¹Some of these stromule inducing conditions were published as part of this thesis, and will be discussed in later chapters.

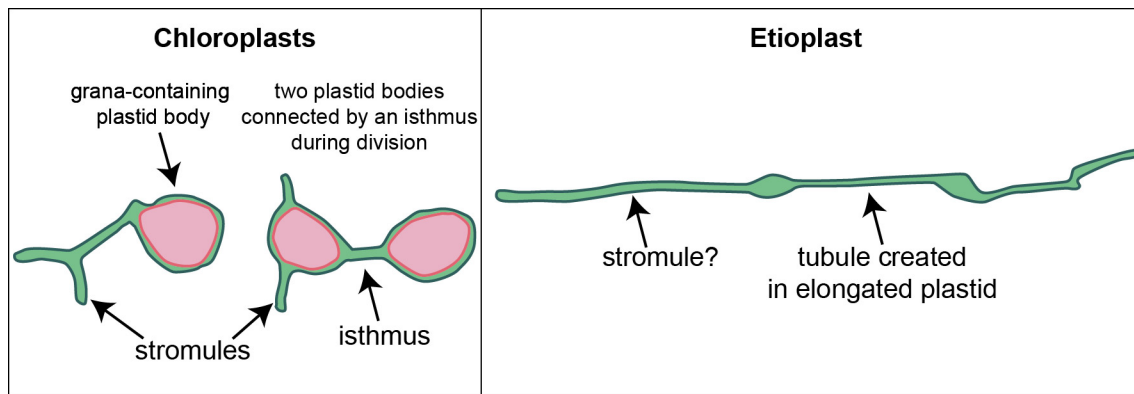


Figure 1.1.: Defining a stromule. Chloroplast stromules are easily distinguished from the main plastid body, which is larger, rounder, and harbours chlorophyll-containing grana stacks (in pink). An isthmus is easily distinguished from a stromule in chloroplasts, since it is typically a short stroma-filled tubule joining two, soon-to-be independent, chlorophyll-containing plastid bodies. Etioplasts are an example of an elongated plastid type which exhibits long-thin 'stromule-like' regions. It is very difficult to distinguish between the plastid body, a stromule and an isthmus. Graphics modeled after plastids depicted in Schattat et al. (2012).

1.5.1. Hypothesis 1 - Stromules facilitate exchange between plastids and other organelles

Mitochondria and peroxisomes

It has been well established that chloroplasts, mitochondria and peroxisomes participate in metabolite exchange, particularly during photorespiration, which requires movement of metabolites through all three compartments (reviewed in Bobik and Burch-Smith, 2015). These three organelles are, indeed, frequently seen in close association (Bobik and Burch-Smith, 2015), perhaps leading to the expectation that stromules increase the surface available for exchange between these organelles (Hanson and Hines, 2018). In some cases, mitochondria and peroxisomes, which are much smaller than the plastid, appear to pile up against extended stromules during cytoplasmic streaming (Gunning, 2005; Kwok and Hanson, 2004a). In many cases mitochondria move along a stromule or associate with an extending stromule tip, perhaps as a result of movement along the same actin scaffold (Gunning, 2005; Kwok and Hanson, 2004a). The associations between stromules and peroxisomes or mitochondria have been described as transient (Barton et al., 2017; Gunning, 2005)² and, in one experiment, an equal number of mitochondria and peroxisomes were shown to associate with the plastid body and the stromule (Barton et al., 2017). This may suggest that stromule extension is not essential for maintaining plastid-mitochondria or plastid-peroxisome interactions (Barton et al., 2017). However, since interactions between stromules and peroxisomes or mitochondria have never been investigated or quantified in detail, few conclusions can be drawn. It is possible that despite the transient nature of such interactions, that stromules act to enhance exchange by catching smaller organelles during cytoplasmic streaming, potentially increasing the duration or number of interactions with the plastid in this way.

²In pavement cell chloroplasts of *A. thaliana*

Endoplasmic Reticulum

The endoplasmic reticulum (ER) is important for the assembly of some types of lipids from chloroplast-derived fatty acids, which are then trafficked back to the plastid where they are incorporated into the thylakoids, contributing to their unique lipid composition (reviewed in Wang and Benning, 2012). Fatty acid and lipid exchange requires a close association between the plastid and ER, and is believed to occur through physical contacts between the membranes of the two organelles (Wang and Benning, 2012). Protein transfer has also been suggested to occur at membrane contact sites (MCSs) (reviewed in Holthuis and Levine, 2005). Stromules have been suggested to increase contact between ER and plastid membrane, perhaps providing more opportunity for exchange (Schattat et al., 2011a). Double labeling of ER and stromules revealed clear alignment of stromules with ER tubules in the cell cortex, with stromules extending into 'ER-lined' channels (Schattat et al., 2011a). Further, extending stromule tips were always associated with ER (Schattat et al., 2011a). Stromules appeared to be tightly associated with ER at defined points, which may represent MCSs. Whether the formation and subsequent movement of ER contact sites are responsible for the highly co-ordinated movement of ER tubules and stromules, or whether these two organelles simply utilize the same cytoskeletal scaffold for extension is unclear so far (Schattat et al., 2011a).

Nucleus

It is widely accepted that chloroplasts evolved from a cyanobacteria engulfed by a mitochondriate eukaryote more than one billion years ago (Dyall et al., 2004). During evolution into the modern-day chloroplast a massive horizontal gene transfer took place, where the majority of essential chloroplast genes were relocated to the nuclear genome (Nott et al., 2006). This arrangement created the need for the plastid to communicate its physiological state to the nucleus to direct the expression of nuclear-encoded chloroplast genes, in a process now known as 'retrograde signaling' (Nott et al., 2006). The exact signals utilized by the plastid for this communication, and the mode with which they are exported from the chloroplast, across the cytoplasm and act in the nucleus remain enigmatic. Stromules have been observed 'reaching' from the plastid surface toward the nucleus during immune reactions (Caplan et al., 2015), in response to *Abutilon* mosaic virus (Krenz et al., 2010, 2012), during high temperature stress (Holzinger et al., 2007a), as well as in unchallenged plants (Holzinger et al., 2007a) (Supplemental Table 1, Erickson et al. 2017b³). Given the abundance of such observations, stromules are often suggested to span the cytoplasm between the plastid and the nucleus for the purpose of directly delivering 'signals' or 'molecules' between these two organelles (Köhler and Hanson, 2000; Kwok and Hanson, 2004b; Natesan et al., 2005; Hanson and Sattarzadeh, 2008; Borucki et al., 2015; Caplan et al., 2008, 2015; Leister, 2012; Bobik and Burch-Smith, 2015). Indeed, striking images of plastid stromules extending into nuclear envelope invaginations (Kwok and Hanson, 2004b), stromules reaching from distant plastids with tips touching the nucleus (Caplan et al., 2015), and stromules completely wrapped around nuclei (Caplan et al., 2015), convince us of the feasibility of this hypothesis (Figure 1.2 on the following page).

³Supplemental data included on SD card

However, one weakness of the current descriptive data on the plastid-nucleus relationship is that stromules and plastids close to the nucleus were the only ones examined, and there is little data describing the appearance of plastids in other parts of the cell. This makes it difficult to assess if stromule-nucleus interactions are truly 'intentional', or if they are simply a coincidence, resulting from overall inflations in stromules frequency.

1.5.2. Hypothesis 2 - Stromules as a source of plastid-derived vesicles

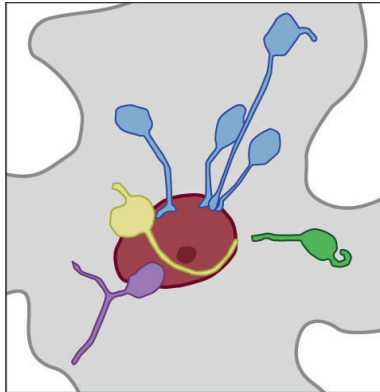


Figure 1.2.: Graphical summary of stromule-nuclear interactions reported in the literature. The cell outline is in gray (cytoplasm in light gray), the nucleus is red (nucleolus in dark red), and plastids are color coded according to the plastid-nucleus interactions they participate in. Blue plastid bodies distant from the nucleus emit stromules that make contact. The green plastid points a stromule in the direction of, but does not contact, the nucleus. The plastid in yellow contacts and wraps a stromule around the nucleus. The purple plastid body is in contact with the nucleus, but projects a stromule towards the cell periphery.

Occasionally, stromules have been observed to undergo 'budding' or 'segmentation', where parts of the stromule are released into the cytosol, to form independent, vesicle-like, organelles (Figure 1.3 on the next page). Gunning (2005) observed that stromules of *Iris unguicularis* sometimes develop a spherical body at the tip and, on one occasion, he captured the release of this vesicle-like body in a movie. Instances of stromule 'segmentation' have also been documented, where stromule pieces released into the cytoplasm take on a mitochondria-like appearance (Wildman et al., 1962). These segments appeared to be able to reintegrate into the plastid body (Wildman et al., 1962), suggesting that stroma could be carried from one plastid to another in this way. As a result of these observations there has been speculation that these 'vesicles' or 'segments' may go on to interact with or fuse with other plastids or organelles (Hanson and Hines, 2018). Indeed, immunoelectron and fluorescence microscopy approaches confirmed the localization of Rubisco and other stromal proteins to small spherical bodies in the cytoplasm (Chiba et al., 2003; Ishida et al., 2008). Release of these bodies from the plastid and their mobilization to the vacuole is

triggered with autophagy, a pathway important for the bulk degradation of proteins during senescence and stress (Ishida et al., 2008). ATG8 (AUTOPHAGY GENE 8), a protein essential for the sequestration of proteins for degradation, sometimes localizes to stromules (Ishida et al., 2008). This suggests that stromules may play a role in the sequestration of stromal proteins to be targeted for degradation in the vacuole (Ishida et al., 2008). Further, when autophagy is induced⁴ in *atg5-1* mutants⁵ spherical bodies do not form and stromule frequency and length increased relative to wild type (Ishida et al., 2008). Ishida et al. (2008) suggest that this increase in stromules may be the result of decreased stromule budding. However, authors also acknowledge that stress induced by impairment of autophagy could also trigger

⁴Excised leaves were incubated in starvation conditions (infiltrated with MES-NaOH) and incubated for 20 h in darkness with the addition of 1 μ m concanamycin A. Concanamycin A suppresses the digestion of stroma containing vesicles in the vacuole by inhibiting H⁺-ATPase activity. This allows for the visualisation of vesicles that would normally be broken down during autophagy.

⁵ATG5 contributes to autophagic vesicle closure and transport to the vacuole (Thompson et al., 2005).

stromules. Although it is clear that these bodies originate from the plastid, it is not clear whether these spherical bodies originate from stromules (Hanson and Hines, 2018).

1.5.3. Hypothesis 3 - Stromule as highways for intercellular communication

Stromules are often hypothesized to function as conduits for the transfer of plastid or nuclear-derived signals to distant regions of the cell, as well as between cells. These ideas come from the frequent observation of stromules which extend toward the cell periphery, sometimes forming close associations with the plasma membrane (Hanson and Sattarzadeh (2008)⁶; Natesan et al. (2005)⁷; Kwok and Hanson (2004b)⁸). Sometimes stromules even appear to intentionally meet on opposite sides

of a shared cell wall, leading to speculation that stromules could facilitate communication through plasmodesmata (Kwok and Hanson, 2004b). Alternatively, stromules in this configuration have also been suggested to act as sensors to detect conditions in other parts of the cell (Tirlapur et al., 1999; Pyke, 2002). So far, however, there has been no stromule-mobilized intercellular signal identified, and no proof that stromules meet in plasmodesmata, making this one of the least cited of the proposed stromule functions.

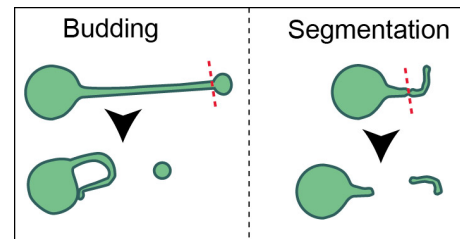


Figure 1.3.: Budding and release of a vesicle-like body from a stromule tip, as reported by Gunning (2005), and segmentation of a stromule as observed by Wildman et al. (1962).

⁶In tobacco callus cell plastids are clustered at the nucleus with stromules extended toward the periphery.

⁷In tobacco seedling hypocotyl epidermis plastids clustered at the nucleus extend stromule toward periphery.

⁸In tobacco hypocotyl epidermis stromules extended from plastids at the nucleus or cell cortex, extended stromules that associated with the plasma membrane.

1.6. Requirements for building a stromule

Despite the frequent observation of stromules there is still relatively little concrete evidence pointing to any specific function, however significantly more work has gone into the investigation of the mechanisms behind stromule formation. Current evidence suggests that there are two basic requirements for a plastid membrane to be quickly re-shaped into a stromule: 1) the plastid must have an excess of envelope membrane and 2) forces must act on the envelope membranes.⁹

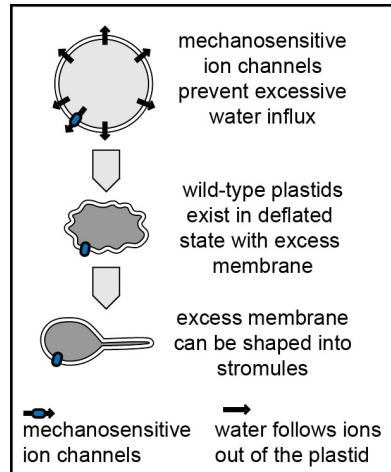


Figure 1.4.: Osmotic status of the plastid dictates the amount membrane available for stromule formation. Ion channels embedded in the plastid membrane control ion flux and therefore, the osmotic potential of the plastid. In a case where the plastid is ‘overinflated’ formation of stromules does not occur (Haswell and Meyerowitz, 2006). When the activity of ion channels maintains the plastid in a ‘deflated’ state there is an excess of membrane. Excess membrane is required for stromule formation to occur (Haswell and Meyerowitz, 2006).

1.6.1. Excess membrane

A perfectly spherical plastid has minimal surface area to volume ratio, and has no membrane available to change shape, conversely an increase in available membrane makes shape change possible (Figure 1.4). This is likely achieved by regulating plastid volume; a principle demonstrated in the examination of two plastid envelope ion channels MSCS-LIKE 2 and MSCS-LIKE 3 (MSL2 and MSL3) from *Arabidopsis thaliana*. Double mutants (*mssl2-1/mssl3-1*) exhibit uncontrolled water influx, resulting in enlarged, spherical plastids, compared to the small, ovoid plastids in wild type (Figure 1.5 on the next page, panels A and B). These ‘over-inflated’ plastids lack stromules and any other surface disturbance (Haswell and Meyerowitz, 2006). In contrast, when water flow into the plastid is tempered (e.g. via supplying double mutants with osmolytes), plastids are normal size and shape, and regain their ability to form stromules (Veley et al., 2012). This clearly indicates that control of plastid osmotic status is required to provide the excess membrane needed for stromule formation.

A second line of evidence showing that membrane availability limits stromule formation comes from in vitro experiments. A tubule reaches its maximum length when excess membrane is

⁹Some of this subsection is published in our review Erickson and Schattat (2018), which is included on the SD card.

used up, and further extension causes tension and ‘stretching’, resulting in a decrease in tubule width (Veley et al., 2012). Assuming the same principle applies to stromule formation in planta, as a stromule reaches its maximum length signs of ‘stretching’ should be observed, i.e. a decrease in stromule width. Indeed, ‘stretching’ events are observed among stromules in planta, and can be quantified to reveal clear decreases in width relative to stromule length (Figure 1.5, panel C).

Excess membrane generated via *de novo* membrane synthesis?

The *de novo* synthesis of membrane could represent an alternative source of excess membrane during stromule extension. However, based on the dynamic and rapid extension of stromules they are more likely to form via stretching of existing membrane. Although plastids appear to be compact, there is evidence to suggest that the plastid envelope is actually ‘wobbly’ or ‘relaxed’ in most circumstances, and deviations from the round plastid shape are often observed in the form of ‘beak-shaped’ protrusions (Schattat et al., 2011a; Gunning, 2005). When ‘wobbly’ membranes are created *in vitro* using sucrose filled liposomes and giant vesicles, osmotic shrinkage can induce similar ‘beak’ shapes (Boroske et al., 1981; Viallat et al., 2004).

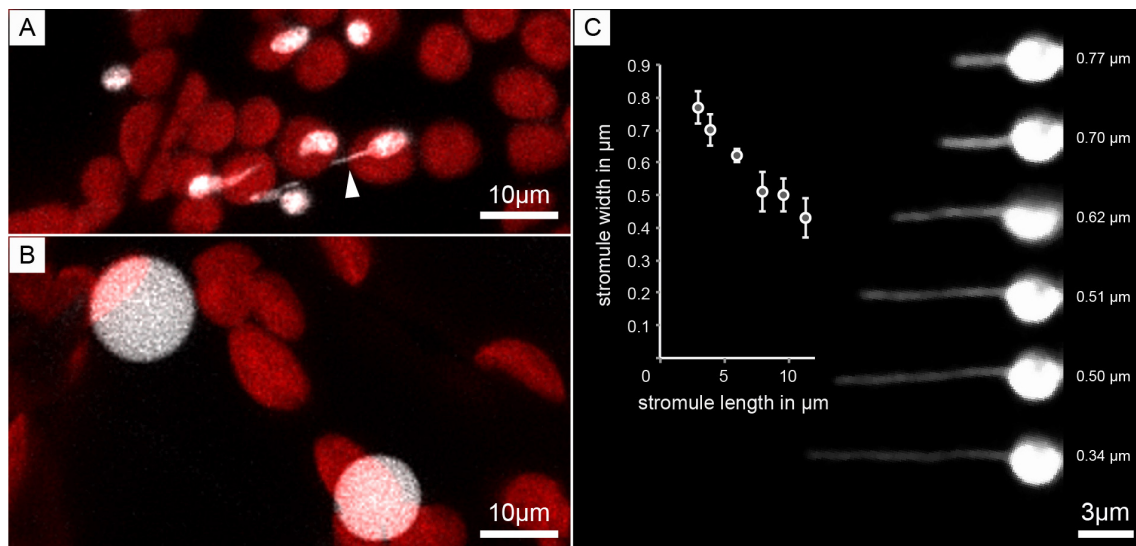


Figure 1.5.: Membrane availability limits stromule formation. (A-B) Upper leaf epidermis of transgenic *A. thaliana* expressing a construct highlighting the plastid stroma (*AtRecA:DsRed*, depicted in white) (refer to Haswell and Meyerowitz (2006) for construct details). Chlorophyll autofluorescence is seen in red. (A) Wild-type plastids are small, with ovoid plastid bodies and occasionally plastid stromules (white arrow). (B) *msl2-1/msl3-1* double mutants have larger, spherical plastids lacking any surface disturbance. (C) A stromule in *N. benthamiana* hypocotyl epidermis (*FNR:eGFP*) is stretched during extension as available membrane declines and tension increases. Stromule width measurements show an obvious decrease as the stromule lengthens (inset scatterplot). Scatter plot values represent the mean stromule width (measurements collected from 5 different positions along the stromule) relative to stromule length (performed with Fiji). Error bars represent standard deviation. Mean stromule width at each time point is also displayed along the right side of the figure.

1.6.2. Forces

If a sufficient amount of membrane is provided, force(s) can act on the membrane and shape it into a tubule. Forces contributing to membrane tubulation discovered during *in vitro* studies on supported lipid bilayers, or liposomes, have been cited when discussing potential modes

of stromule formation (Kwok and Hanson, 2004c; Hanson and Hines, 2018). Indeed, stromules are tubules made of membrane, and as such, comply with the principles of membrane physics discovered *in vitro*. *In vitro* membrane tubulation has identified four basic principles by which a membrane can be shaped into a tubule (Roux, 2013): a) polymerization of internal cytoskeleton, b) induction of spontaneous curvature via protein insertion into the membrane, c) polymerization of membrane-associated proteins and, d) pulling motors. Although principles a), b) and c) are not sufficient to explain the flexibility and dynamic nature of stromules *in planta*. Current data suggests that a mechanism relying on 'pulling-motors', moving along a cytosolic cytoskeleton to generate force, explains much of stromule behavior. I have written a more thorough review of this topic in the form of a review paper (Erickson and Schattat, 2018) included at the end of this thesis.

Actin and microtubules

In 2003 Kwok and Hanson first suggested that actin and microtubules contribute to stromule formation in non-green plastids of tobacco hypocotyl epidermis. Inhibition of actin using cytochalasin D (CD) and latrunculin B (Lat B), or microtubules using oryzalin and aminoprophosmethyl (APM) triggered subtle reductions in both stromule number and length. Interestingly, treatments with actin and microtubule inhibitors caused distinct alterations to plastid morphology (Kwok and Hanson, 2003). Anti-actin drugs caused an increase in stroma-filled loops, which likely represent stromules that have collapsed back onto the plastid body, while anti-microtubule drugs lead to the formation of more short and fat stromules. Simultaneous treatment with both actin and microtubule inhibitors led to an obvious decrease in stromule frequency and had additive effects on stromule length reduction, and plastid morphology (Kwok and Hanson, 2003). This early work suggested that cytosolic cytoskeleton is essential for stromules formation, and that actin and microtubules make distinct contributions to maintenance of stromule morphology and number. Later work in *Nicotiana tabacum* leaf epidermis (Natesan et al., 2009) and in *Oxyria digyna* mesophyll (Holzinger et al., 2007b), suggested that the role of microtubules was minimal, as only actin inhibitors were found to have any impact of stromule frequency. These publications, steered the conversation away from microtubules and towards actin and the identification of potential actin-associated motor proteins responsible for the elongation of stromules.

Role of type XI myosin motors in stromule formation

Myosins are motor proteins that utilize ATP in order to move processively along actin filaments, carrying cargoes throughout eukaryotic cells (Sellers, 2000). Myosins consist of multiple conserved protein domains: the motor domain, which binds ATP and associates with actin, a calmodulin binding IQ motif, a coiled-coil domain that mediates myosin dimerization, and a globular tail domain which binds cargoes (Madison and Nebenführ, 2013). 17 myosins have been characterized in *A. thaliana* and these are divided into two classes VIII, and XI (Reisen and Hanson, 2007). VIII class myosins in Arabidopsis localize to the cell periphery, at the plasma membrane (Avisar et al., 2009), plasmodesmata (Reichelt et al., 1999; Golomb

et al., 2008), and endosomes (Golomb et al., 2008), while myosins of the XI class have been implicated in organelle movement, including the movement of the Golgi, plastids, peroxisomes, mitochondria, and ER (reviewed in Sparkes, 2011).

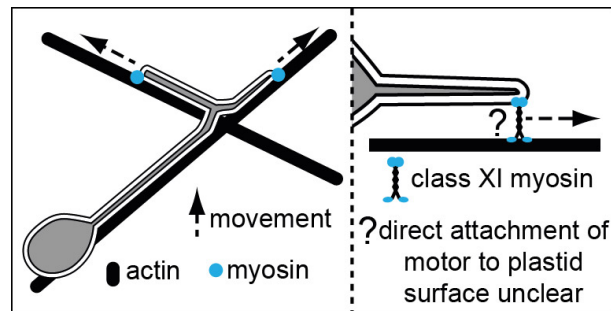


Figure 1.6.: A model for direct pulling of class XI myosins on the plastid membrane during stromule elongation. In this model myosins of the type XI class interact with the plastid membrane, either directly or through adaptor proteins, and pull out stromules as they move along actin filaments.

On several occasions it has been suggested that myosins of the type XI class may pull directly on the plastid membrane during stromules formation (as shown in Figure 1.6), either by associating with the plastid membrane itself or via an interaction with membrane associated adaptor proteins (Gray et al., 2001; Kwok and Hanson, 2004a; Natesan et al., 2009; Hanson and Sattarzadeh, 2011). This stems from work in the epidermis *Nicotiana* species, where treatment with a myosin ATPase inhibitor, and silencing of class XI myosins, led to reduced stromule frequencies (Natesan et al., 2009; Sattarzadeh et al., 2009). One approach that has been used to identify the specific myosin(s) involved in stromule formation was to overexpress and fluorescently tag various pieces of the globular tail domain, creating non-motile myosins that should still specifically bind to cargo. The idea was that tail-domain constructs of myosins important to stromule formation should localized to the plastid or stromules. Using this strategy, myosin XI-2 (cargo-binding tail) (Natesan et al., 2009) and a very small portion of the XI-F tail including only the vacuole-binding domain (41 amino acids) (Sattarzadeh et al., 2009) were shown to labeled chloroplasts when transiently expressed in *Nicotiana* species, with the latter also demonstrating stromule localization. However, the significance of this localization remains uncertain, since the expression of such non-functional myosin truncations is known to interfere with cytoplasmic streaming and general organelle movement (Sparkes et al., 2008; Avisar et al., 2009). In addition, the transient localization of truncated myosins is not readily reproducible, with a single myosin sometimes demonstrating multiple, distinct, sub-cellular distribution patterns within a single experiment, or variable localization depending on protein domains chosen for over-expression (Peremyslov et al., 2012). So, despite there being some evidence in support of a role for myosins in stromule formation, the approaches used thus far have failed to identify the mechanism of myosin involvement or convincingly identify a specific myosin(s) essential for the stromules.

2. Goals

The conservation of dynamic plastid stromules among plants suggests that they make contributions to plant and/or cell viability. Their remarkable flexibility also makes them an ideal model system to determine the mechanisms and molecular machinery required for quick remodeling of membranes. Despite the plethora of stromule observations which followed the visualization of the first stromal-targeted fluorescence proteins there is little data to support any of the proposed functions. So far evidence presented in regard to putative functions has been mostly observational, relying on the descriptions of organelle interactions rather than quantitative data, making it impossible to determine the prevalence of various stromule behaviors or to compare between tissues or treatments. Further, few mutants have been identified that manipulate stromule formation (Mathur et al., 2012), making it difficult to determine what pathways stromules are involved in, and what specific cascades cause their induction.

The central goal of this thesis is to use *Nicotiana benthamiana* and *Arabidopsis thaliana* epidermis as model systems to identify factors involved in regulating and forming stromules. Increased understanding of the cellular components necessary for stromules may provide direct insight into function, or provide us with more precise targets for knocking down stromules to evaluate their significance.

To meet this goal I chose to apply knowledge gained from previous stromule research to devise multiple targeted approaches:

- 1) Stromules are most often implicated in plastid-to-nucleus signaling despite the fact that the relationship between these organelles has never been quantified. I chose a quantitative cell biology approach to evaluate stromule-nucleus relationships and the role of stromules in retrograde signaling.**
- 2) Actin and myosins have been heavily implicated in stromule formation, so I chose to screen myosin mutants with the purpose of identifying the key myosin(s) required to make stromules.**
- 3) *Agrobacterium tumefaciens* strain GV3101 is a known inducer of stromules (Schattat et al., 2012). I chose to identify the 'stromule-inducing' stimuli produced by the bacteria to determine how stromules are being regulated in the presence of this particular bacterial strain.**

I also employed several untargeted approaches to identify novel stromule regulators:

- 4) I employed a unique screen for stromule pertinent cellular processes which utilized the transient expression of effector proteins from pathogenic bacteria.
- 5) Virus induced gene silencing (VIGS) was also used to screen for novel genetic components contributing to stromule formation.

Part II.

Results

3. Plastid-nucleus interactions dictate stromule extension and orientation

3.1. Introduction

As previously mentioned, frequent observations of stromule-nucleus interactions have led many to speculate that stromules are involved in retrograde signaling between plastids and nuclei. This is the most prevalent hypothesis for stromule function in the literature (Summarized in Supplemental Table 1, Erickson et al. 2017b¹). Despite this, at the time when my PhD began the relationship between plastids and the nucleus had never been quantified, and it was still unclear whether this relationship was a coincidence, resulting from overall increases in stromule frequencies throughout the cell, or whether these contacts were truly intentional. If stromules intentionally contact the nucleus, the next question is whether stromules grow in the direction of the nucleus and, if so, how this is achieved. To address these questions, in the following publication we used quantitative cell biology techniques to analyse plastid-nucleus distances, stromules numbers, and directions in *A. thaliana* upper rosette leaf epidermis. We also used live-cell imaging to examine relative movements of plastids and nuclei and suggest a possible mechanism for stromule extension.

¹Supplemental data included on SD card

3.2. Publication I



Plastid-Nucleus Distance Alters the Behavior of Stromules

Jessica L. Erickson, Matthias Kantek and Martin H. Schattat*

Plant Organelle Shape and Dynamics Lab, Plant Physiology, Martin Luther University Halle-Wittenberg, Halle, Germany

Plastids send “retrograde” signals to the nucleus to deliver information regarding their physiological status. One open question concerning this signal transfer is how the signal bridges the cytoplasm. Based on individual reports of plastid derived tubular membrane extensions connecting to nuclei, these so-called stromules have been suggested to function as communication routes between plastids and nuclei in response to biotic stress. However, based on the data currently available it is unclear whether interactions between stromules and nuclei are truly intentional or observed as a result of an inflated stromule frequency throughout the cell, and are thus a random event. The source of this uncertainty stems from missing information regarding the relative distribution of all plastids and stromules within a given cell. A comprehensive analysis of the upper epidermis of *Arabidopsis thaliana* rosette leaves was performed via a combination of still images and time-lapse movies of stromule formation in the context of the whole cell. This analysis could definitively confirm that stromule formation is not evenly distributed. Stromules are significantly more frequent within 8 μm of the nucleus, and approximately 90% of said stromules formed facing the nucleus. Time-lapse movies revealed that this enrichment of stromules is achieved via a 10-fold higher frequency of stromule initiation events within this 8 μm zone compared to the cell periphery. Following the movement of plastids and nuclei it became evident that movement and formation of stromules is correlated to nucleus movement. Observations suggest that stromules “connecting” to the nucleus are not necessarily the result of plastids sensing the nucleus and reaching out toward it, but are rather pulled out of the surface of nucleus associated plastids during opposing movement of these two organelles. This finding does not exclude the possibility that stromules could be transferring signals to the nucleus. However, this work provides support for an alternative hypothesis to explain stromule-nuclear interactions, suggesting that the main purpose of nucleus associated stromules may be to ensure a certain number of plastids maintain contact with the constantly moving nucleus.

Keywords: stromule, retrograde signaling, nucleus movement, plastid positioning, organelle interactions, live-cell imaging, *Arabidopsis thaliana*

INTRODUCTION

It is widely accepted that plastids are descended from a free-living ancestral cyanobacteria that was enveloped by a mitochondriate eukaryote more than one billion years ago (Dyall et al., 2004). Prior to its incorporation it can be assumed that this cyanobacteria contained all coding information necessary to function autonomously as a photoautotroph (Nott et al., 2006). However, during

OPEN ACCESS

Edited by:

Julian Eaton-Prye,
University of Otago, New Zealand

Reviewed by:

Karin Krupinska,
University of Kiel, Germany
Kentaro Tamura,
Kyoto University, Japan

***Correspondence:**

Martin H. Schattat
martin.schattat@
pflanzenphys.uni-halle.de

Specialty section:

This article was submitted to
Plant Cell Biology,
a section of the journal
Frontiers in Plant Science

Received: 20 March 2017

Accepted: 13 June 2017

Published: 06 July 2017

Citation:

Erickson JL, Kantek M and
Schattat MH (2017) Plastid-Nucleus
Distance Alters the Behavior of
Stromules. *Front. Plant Sci.* 8:1135.
doi: 10.3389/fpls.2017.01135

evolution of this symbiont into the present-day chloroplast, there was a massive reduction in the size of the plastid genome, some genes being lost completely, while others were transferred to the nucleus (Dyall et al., 2004). With the reduction of the genome (contemporary plastids are known to have between 60 and 200 ORFs remaining) the chloroplast was no longer autonomous. The majority of protein coding genes necessary for chloroplast development and function in higher plants (>3,000) are now under the control of the nucleus (Nott et al., 2006). With the development of this anterograde control over the plastid it became necessary for the plastid to, in turn, communicate its physiological and developmental state to the nucleus (Nott et al., 2006). Thus, modes of so-called “retrograde signaling” between the plastid and nucleus were developed to regulate the production of nuclear encoded proteins necessary for chloroplast function and maintenance of cell homeostasis (Nott et al., 2006).

Many candidate retrograde signals have been suggested during recent years (recently summarized in Chan et al., 2016). These include carotenoid derivatives (Ramel et al., 2012; Avendaño-Vázquez et al., 2014; Van Norman et al., 2014), the isoprenoid precursor MEcPP (Xiao et al., 2012), tetrapyrrole biosynthesis derivatives (Strand et al., 2003; Woodson et al., 2011), plastid generated ROS molecules (Caplan et al., 2015; summarized in Bobik and Burch-Smith, 2015), phytohormones (Bobik and Burch-Smith, 2015), 3'-phosphoadenosine 5'-phosphate (PAP; Estavillo et al., 2011) and dual localized proteins such as PTM (Sun et al., 2011), WHIRLY1 (Isemer et al., 2012) and NRIP1 (Caplan et al., 2015). These signals can be divided into two main categories. First there are those speculated to be slower acting (e.g., plastid metabolites) because they take time to accumulate and are not capable of directly mediating changes to gene expression (Krause et al., 2012). This category of signals is likely involved in the coordination of nuclear and chloroplast gene expression during plastid development (Pogson et al., 2008). Then there is the second category of signals believed to be involved in rapid response to environmental challenges (Krause and Krupinska, 2009). In contrast to plastid metabolites, protein signals can be stored by the plastid and effectively “released” (and directly influence gene expression) when a cell requires a rapid response by the nucleus (e.g., attack by a pathogen) (Krause and Krupinska, 2009).

It is very difficult to verify the movement of signals from the plastid to the nucleus. However, notable progress has been made in the investigation of dually localized proteins (those believed to be “category 2” signals). Protein export from the plastid to the nucleus has been experimentally demonstrated on very few occasions. The first instance of experimentally detected relocation of a protein from the plastid to the nucleus was demonstrated using *Arabidopsis thaliana* WHIRLY 1 (Isemer et al., 2012). This was achieved via the generation of transplastomic tobacco plants expressing HA-tagged AtWHIRLY1. Following the exclusive synthesis of the protein by the plastid it was then identified in the nucleus, thus confirming the ability of the protein to move from plastids to the nucleus. In addition these transplastomic lines also exhibited an up-regulation of pathogen response related nuclear genes *PR1* and *PR2* (Isemer et al., 2012). A second

example was the confirmed retrograde movement of the protein NRIP1 (N receptor-interacting protein 1), which was provided by Caplan et al. (2008). NRIP1 is localized to the chloroplast in unchallenged *Nicotiana benthamiana* (N-containing, NRIP1-Cerulean expressing plants), but is observed in the plastid, cytoplasm and nucleus when in complex with the Tobacco Mosaic Virus effector p50. This re-localization is further enhanced when the complex is recognized by N, the p50 immune receptor.

Retrograde protein signals, such as WHIRLY1 and NRIP1, face multiple obstacles along the road to altered nuclear gene expression. To enter the nucleus they must cross multiple lipid bilayers, the plastid outer-membrane and the nuclear membrane. In the case of NRIP1 it seems that this is unlikely to occur via simple diffusion across membranes, although the exact mechanism of nuclear entry remains unsolved (Caplan et al., 2008). A second obstacle to re-localization of a protein from the plastid to the nucleus is its movement across the cytoplasm. Several potential modes of transport have been discussed, including passive diffusion as well as active transport across the cytoplasm via as yet unidentified “transporter proteins” (Leister, 2012). In contrast, one theory gaining momentum suggests that proteins (and perhaps other putative signaling molecules) are transferred via direct contact between the plastid and the nucleus, largely suggested to occur via stromules (Caplan et al., 2008, 2015; Leister, 2012; Bobik and Burch-Smith, 2015). Stromules (stroma-filled tubules), as the name suggests, are stroma-filled protrusions of both inner and outer plastid envelopes, which emanate from a plastid body (Köhler et al., 1997; Köhler and Hanson, 2000). Shortly after the plastid stroma was first highlighted via fluorescence proteins (Köhler et al., 1997) the formation of stromules was observed under a wide variety of abiotic and biotic stress conditions (summarized in Mathur et al., 2012). Perhaps coincidentally, these are conditions in which communication between the plastid and the nucleus would be essential for maintaining homeostasis.

The most recent and perhaps the most direct evidence for the hypothesized role of stromules in retrograde signaling comes from Caplan et al. (2008, 2015). Not only were stromules induced following expression of the p50 effector (in N-containing *N. benthamiana*), but NRIP1-Cerulean was localized to plastid stroma and observed in stromules which appeared to contact the nucleus. Additionally Caplan et al. (2015) claim that NRIP1 re-targeting from the plastid to the nucleus during HR-PCD (hypersensitive response-programmed cell death) is enhanced in cells when stromules formed connections with the nucleus. This observation has inspired the model that stromules are formed purposefully to amplify/guide retrograde pro-defense signals to the nucleus (Caplan et al., 2015). Assuming that stromules are established to facilitate communication with the nucleus, this raises the question of how the cell supports the establishment of these plastid-nuclear connections. It could be that under certain conditions select plastids sense the nucleus position and intentionally extend a stromule in the direction of the nucleus. A second possibility is that the stromule-nuclear interactions are the result of excessive stromule induction throughout the cell, thus increasing the probability that a subset of stromules would

contact the nucleus. If the latter were true, then the functional relevance of these structures in the context of plastid-nucleus interactions would likely be called into question.

In order to understand whether the formation of stromule-nuclear interactions is due to the directional formation of stromules toward the nucleus, or a series of random interactions resulting from very high stromule frequencies, it is essential to analyse the position of all plastids of a given cell, both with and without stromules, relative to the nucleus. A literature survey screening for publications that look into stromule-nucleus relations, revealed that plastids with stromules or stromules themselves have frequently been reported to interact with nuclei (Supplementary Table 1). However despite the many reports of stromule-nucleus interactions, this literature survey revealed that most of these observations were not quantified, and additionally none were considered within the context of the entire cell. This means that although there have been thorough descriptions of plastids and stromules in close proximity to the nucleus the remainder of the cell's plastids/stromules were not considered. The behavior of all plastids and stromules within a cell and their relationship to the nucleus is not well understood, and the question of how such interactions are established by the cell is still open. Evaluating stromule behavior in the whole cell situation is essential for directing speculations about stromule function in the context of nuclear-plastid-stromule communication.

In order to test whether stromules intentionally interact with nuclei or whether those interactions are more likely to be coincidental, whole cell stromule levels, directions and behavior in relation to nuclei were quantitatively evaluated in the upper epidermis of *A. thaliana* rosette leaves. Based on the hypotheses present in the literature that stromules are important to nuclear-plastid communication, the first step was to determine if plastids close to the nucleus are more likely to form stromules than those in more distant regions of the cell, and whether these stromules were facing toward or away from the nucleus. Evidence presented here suggests that there is a 'stromule-promoting zone' surrounding the nucleus, and within this zone it was observed that stromules are largely facing toward the nucleus. Surprisingly, results showed that higher stromule frequencies within this zone are the result of an increase in stromule initiation events, rather than increased stromule stability.

MATERIALS AND METHODS

Plant Growth Conditions

For still images transgenic *Arabidopsis thaliana* stably expressing the transit peptide of ferredoxin-NADPH-oxidoreductase fused to eGFP (*FNRtp:eGFP*) was used. Soil grown plants were exposed to 120 $\mu\text{E m}^{-2}\text{s}^{-1}$ under short day conditions (8 h light/16 h dark) at 60% relative humidity and 21°C. Leaf discs were collected from the youngest fully expanded rosette leaves of 10–12 week-old plants and placed in a 1.5 mL tube containing water. A vacuum was applied to this tube using a 10 mL syringe placed on top. When the plunger of the tube is pulled water is forced into the intracellular space making microscopy pictures much clearer. This method is also described in Schattat and Klösgen (2011).

For recording time-lapse z-stacks of plastids and nuclei, fully expanded leaves of primary selected 4 week-old *pLSU4::P_{35S}::FNRtp:eGFP::T_{35S}::P_{UBQ10}::H2B::mCherry::T_{nos}* (hereafter called *pLSU4:pn*) transgenic plants were utilized. The T₀ seeds were germinated and incubated for 4 days on AT media (Ruegger et al., 1997) plates containing 40 $\mu\text{g mL}^{-1}$ hygromycin and 250 $\mu\text{g mL}^{-1}$ cefotaxime. Resistant plants were screened for fluorescence and transferred to soil. After 4 weeks of cultivation on soil at 21°C under short day conditions (8 h light/16 h dark) with a light intensity of 120 $\mu\text{E m}^{-2}\text{s}^{-1}$, mature rosette leaves were harvested and prepared for imaging.

Acquisition of Individual Z-Stacks for Still Images

Data presented in Figures 1–6 originates from a re-analysis of a subset of images acquired as part of the work included in Schattat and Klösgen (2011), but the data set presented here is completely original. Images with labeled nuclei, although originally taken along with the images analyzed in Schattat and Klösgen (2011), were not analyzed in that publication. These images document the 4',6-diamidino-2-phenylindole (DAPI) stained DNA, and effectively label nuclei. These DAPI images were combined with eGFP fluorescence images from Schattat and Klösgen (2011) to analyse stromules/plastid-nucleus relationships.

Details DAPI Staining and Imaging

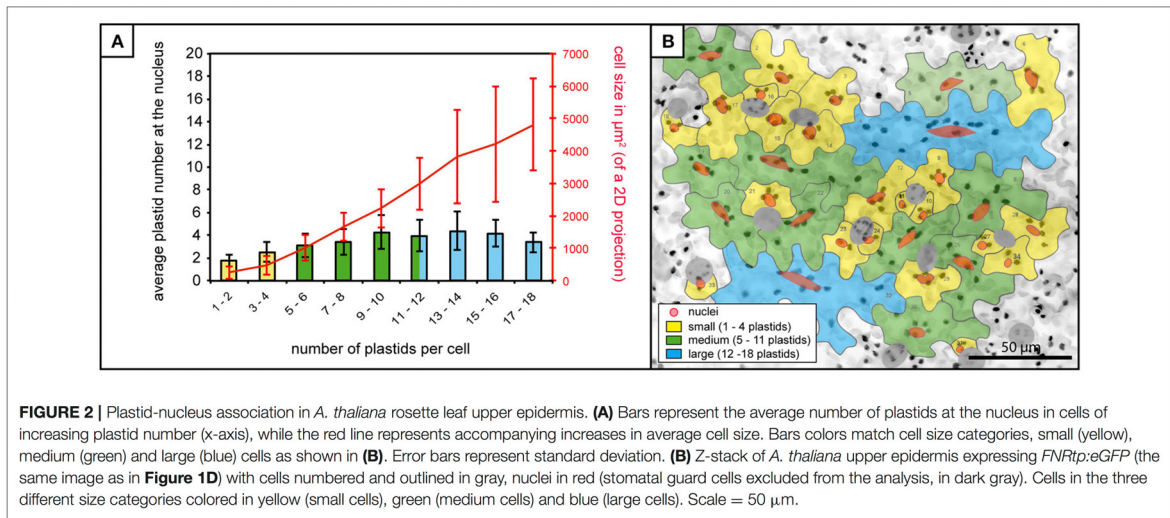
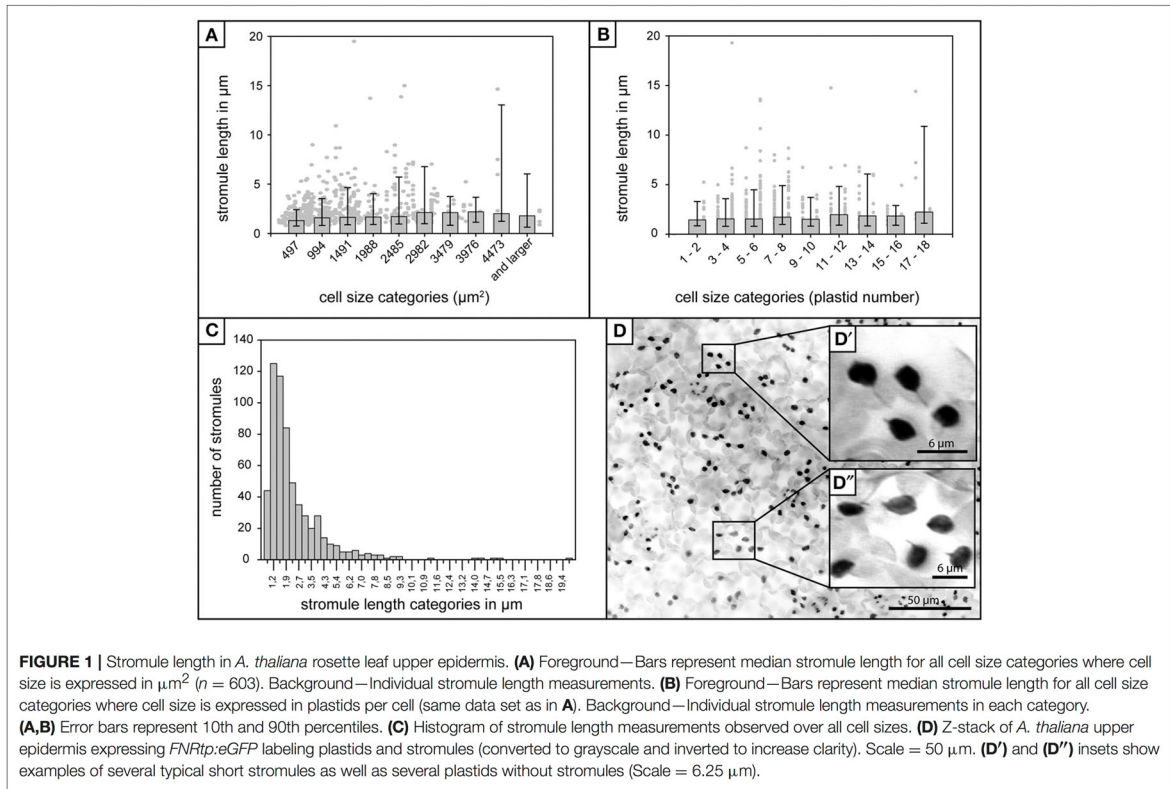
For staining the nuclei in upper epidermis cells, tissue samples were vacuum infiltrated with tap water containing 6 μM (DAPI) and incubated for 10 min at room temperature. A DAPI stock solution was prepared from powder (obtained from Molecular Probes, ThermoFischer Scientific) in double distilled water. Comparison with unstained samples showed that the staining procedure did not change stromule frequency and behavior during these short-term experiments (data not shown). DAPI fluorescence was excited with a HBO100 high-pressure mercury plasma arc-discharge lamp (Carl Zeiss GmbH, Jena, Germany) and imaged using the fluorescence filter set F49 (excitation = G 365; beam splitter = FT 395; emission = BP 445/50) (Carl Zeiss GmbH, Jena, Germany).

Image Processing

Still image stacks were converted into single image projections using CombineZP (Hadley, 2006) and imported into Fiji v.2.0.0-rc-31 (Schindelin et al., 2012). Due to the flat shape of epidermis cells and the location of plastids as well as nuclei on the lower side of cells (facing the mesophyll), 2D projections provide a good representation of the relative position of these organelles in the 3D situation. Measurements of still images were performed via standard analysis tools of Fiji v.2.0.0-rc-31.

Data Analysis

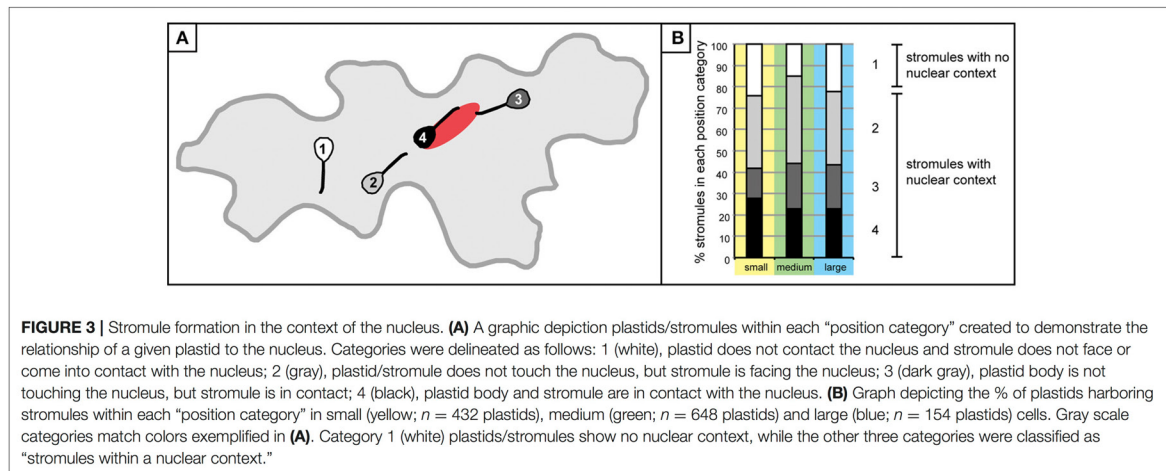
For data handling and analysis Microsoft Excel (version 14.4.4), R (version 3.2.2) and RStudio (version 0.99.484) was used. Statistical tests were performed with SigmaPlot12. Graphs were plotted using Excel or SigmaPlot 12.



Generation of Plastid-Nucleus Double Marker Lines

Since the staining of nuclei with DAPI could damage cells during longer experiments and could potentially alter cell

behavior, an alternative fluorescence based strategy was used to label nuclei during long-term movies. To label nuclei Histone-2B (Wozny et al., 2012) was fused to mCherry (Nelson et al., 2007). Expression was driven by the *AtUBQ10*



promotor fragment described by Grefen et al. (2010) and terminated by the *NOS* terminator (Nelson et al., 2007). For labeling of the plastid stroma the expression cassette *P_{35S}:omegaleader:FNRtp:eGFP:T_{35S}* (described by Marques et al., 2004) was used.

To facilitate efficient cloning of the double protein marker vector Golden Gate cloning was utilized. In order to use this cloning method the *pLSU4* plasmid described by Lee et al. (2012) was turned into a *BsaI* based, Golden Gate compatible vector. To achieve this the *BsaI* site existing in the vector backbone was removed by site-directed mutagenesis and the MCS was replaced by two *BsaI* sites. For cloning the *P_{35S}:omegaleader:FNRtp:eGFP:T_{35S}* as well the second expression cassette, *P_{AtUBQ10}:H2B:mCherry:T_{NOS}*, individual components (e.g., promoters, proteins, tags, and terminators) were amplified via PCR introducing *BsaI* sites. Following a standard Golden Gate protocol the resultant vector *pLSU4:pn* was produced.

For establishing stable transgenic plants *pLSU4:pn* was transferred into *Agrobacterium tumefaciens* strain GV3101 (pMP90) (Koncz and Schell, 1986) by electroporation. These bacteria were used to transform wild-type *A. thaliana* plants by standard floral dipping (Davis et al., 2009).

Time-Lapse Movie Acquisition

To prevent leaves from drying out during movies a chamber was created by applying a c-shaped string of silicon grease to a glass slide. The leaf section was placed with a drop of tap water in the middle of the silicon “c” and covered with a glass coverslip (High Precision No. 1.5H 170 ± 5 μm). Excess water was removed from under the coverslip using a paper towel, thus allowing for gas exchange.

Imaging was done using a Zeiss LSM 780 microscope (Carl Zeiss GmbH, Jena, Germany) based on an inverted AxioObserver and equipped with a 63× lens (C-Apochromat 63×/1.20 W Korr M27, Carl Zeiss GmbH, Jena, Germany). Fluorescence was induced via a 488 nm laser line of a multiline argon laser (25 mW) and a 561 nm laser. Fluorescence was recorded in single-track mode. Individual channels for eGFP (493–556 nm), for mCherry

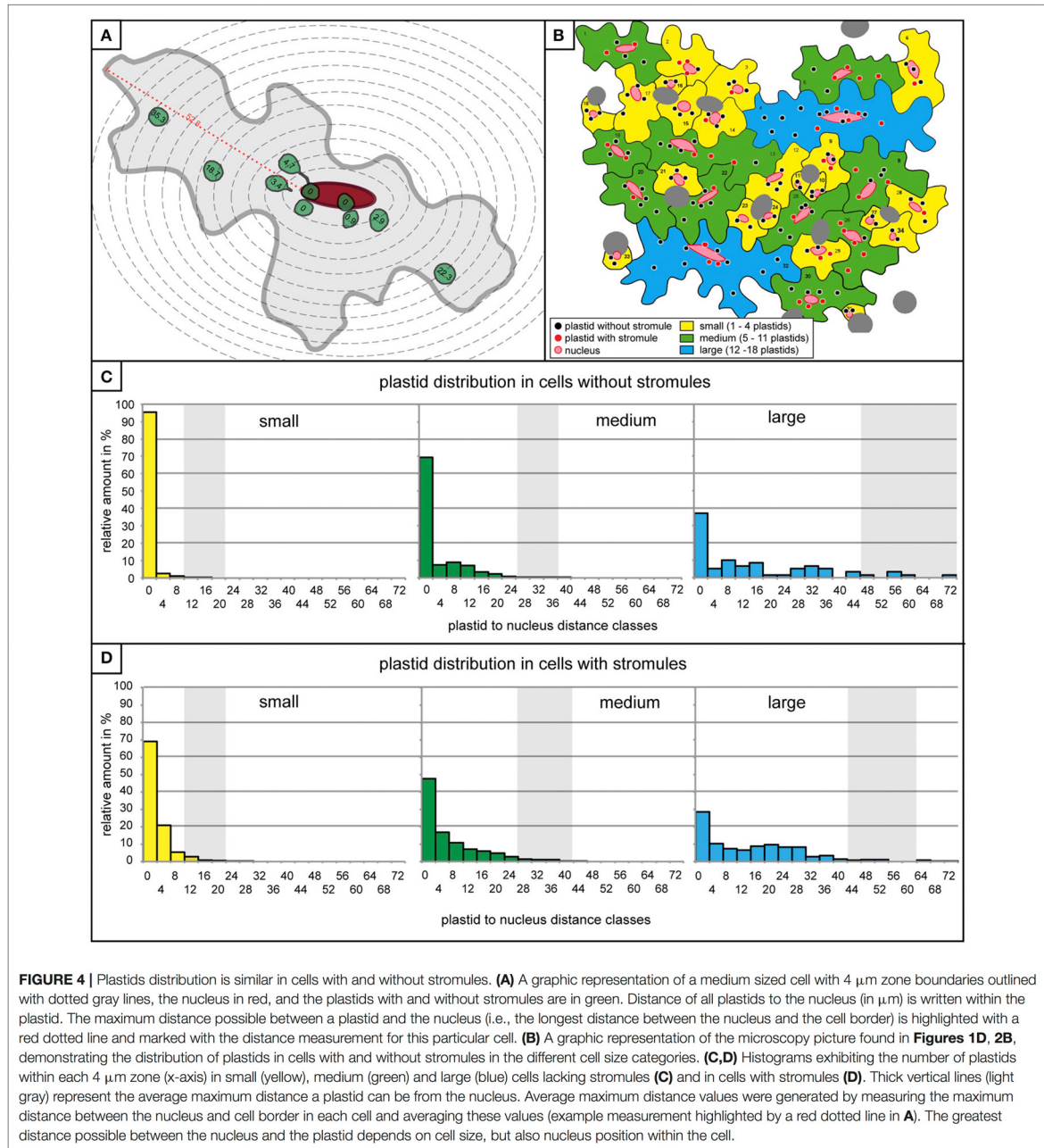
(596–623 nm) and for chlorophyll (653–758 nm) were defined. The transmitted light image was recorded in a separate channel. In preparatory work laser intensity (488 nm 1.8%; 561 nm 2%), pixel dwell time (0.79 μs), line averaging (2 times), pixel number (1,024 × 1,024) as well as the frame rate (3 min) was optimized to minimize the impact of laser light on the cells. Based on its sensitivity to bleaching, the stability of the chlorophyll fluorescence was used to estimate the impact of the laser light on the plant tissue. The microscope setup was controlled with the microscope manufacturer’s software Zen (Carl Zeiss GmbH, Jena, Germany).

Time-Lapse Movie Processing

A total of 7 movies were acquired. Data clearly showed that cell size does not have an impact on the stromule-promoting zone, so it was decided that the analysis would be focused only on medium and large cells. Movies recorded the behavior of 252 plastids in 22 cells. The average plastid number per cell was 11.45 (standard deviation = 5.79; maximum = 30 plastids; minimum = 5 plastids). For analysis, 4D imaging data ($x/y/z/t$) was projected in 3D ($x/y/t$) by creating a maximum intensity projection along the z -axis for each time point using Fiji v.2.0.0-rc-31 (Schindelin et al., 2012).

Time-Lapse Movie Data Analysis

Movie analysis began by outlining all whole cells of interest and labeling them with an ID number. Subsequently the position of each plastid was tracked in relation to the nucleus across 30 frames. For plastids the coordinates of the point closest to the nucleus was tracked, and for nuclei the point closest to the respective plastid was tracked. When plastid and nucleus fluorescence overlapped it was assumed that both organelles “touch” and only one set of coordinates was recorded. The “ManualTrack” PlugIn of Fiji v.2.0.0-rc-31 (Schindelin et al., 2012) was utilized for point tracking. The x - y coordinates provided by the “ManualTrack” PlugIn were used to calculate the Euclidean distance between both points in pixels and subsequently converted to μm.

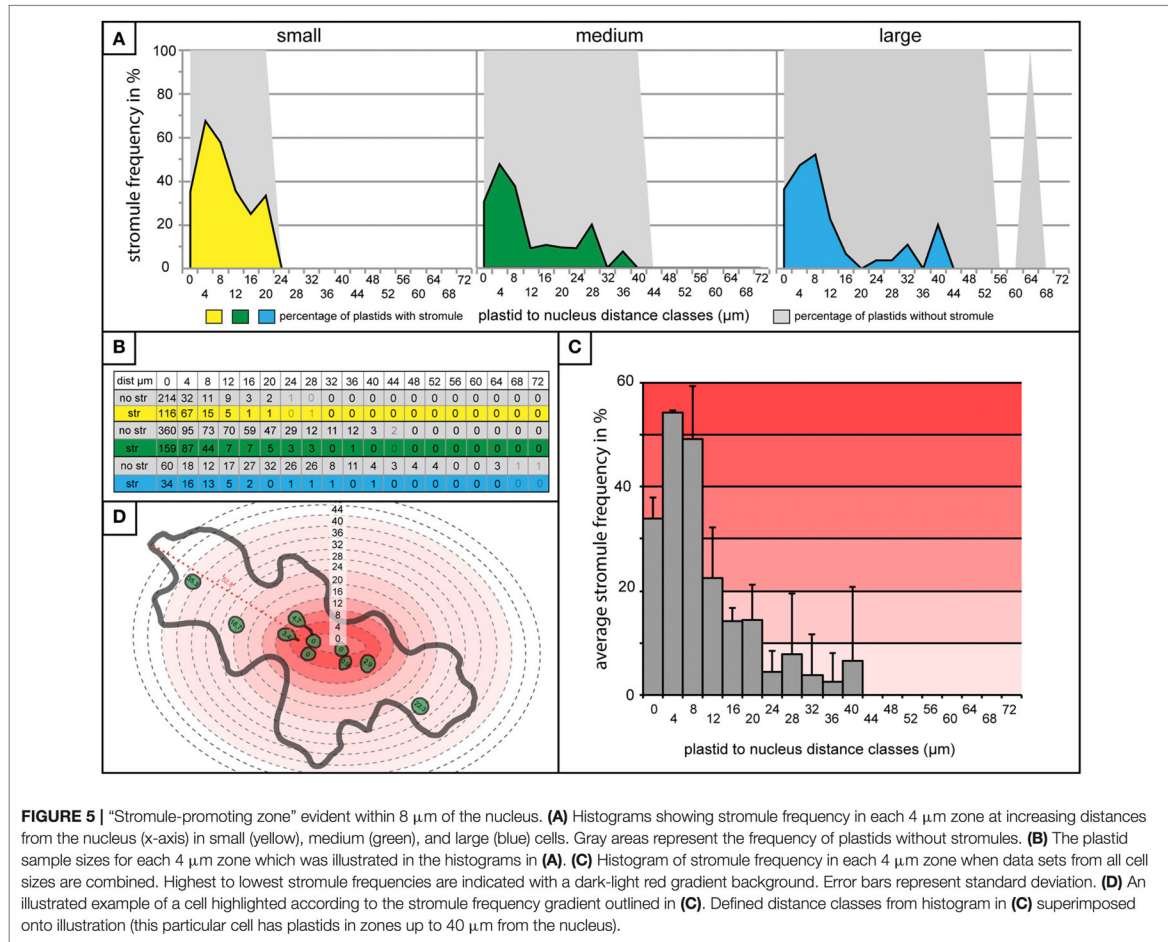


RESULTS

A. *thaliana* Upper Epidermis as a Model System

Before beginning the analysis of stromule-nuclear interactions in the whole cell context an appropriate model tissue had to

be chosen, taking into account any tissue specific influences on stromule frequency. Hypocotyl epidermal cells are very frequently used in the study of stromules. However, Waters et al. (2004) observed that in dark grown tobacco hypocotyl tissue increases in cell size are correlated with a decrease in plastid density, and that this decrease in plastid density is correlated



with increases in stromule abundance. Taking this finding into account, it had to be ensured that the parameters relating to plastid and stromule position would not be heavily influenced by cell size in the model tissue. *A. thaliana* rosette leaf upper epidermis does not exhibit such a correlation, and so was chosen as the model tissue for the following experiments. Schattat and Klösigen (2011) demonstrated that although upper epidermis cells are hugely variable in size, it is clear that the plastid density is constant and that stromule frequency is unlikely to be correlated with cell size. Regardless of cell size, stromule frequency (number of plastids with stromules \div total plastids) of the upper epidermis largely ranges between 0.13 and 0.23 (Schattat and Klösigen, 2011). Plastids are not saturated with stromules, providing the chance to examine the behavior and position of plastids both with and without stromules. Both the independent nature of stromule frequency and cell size, as well as moderate stromule numbers make *A. thaliana* upper epidermis ideal for this study. It should be noted that microscopy images collected by Schattat and Klösigen (2011) were well

suit for this analysis, and were re-evaluated for the purposes of this publication. These experiments utilized 10–12 week-old transgenic *A. thaliana* (Columbia ecotype) rosette leaves stably expressing an *FNRTp:eGFP* plastid label (*FNRTp:eGFP* 7–4; Marques et al., 2003, 2004) and nuclei were labeled with DAPI.

Most Stromules in the Upper Epidermis Are Short

In addition to the influence of cell size and plastid density on stromule number, Waters et al. (2004) also found that stromule length was influenced by these factors, with larger cells/lower plastid density resulting in longer stromule lengths in tobacco hypocotyl. Although the upper rosette leaf epidermis has a constant plastid density the relationship between stromule length and cell size also needed to be assessed to ensure the independence of these two variables. The length of all stromules present in all the images collected ($n = 603$) were measured and it

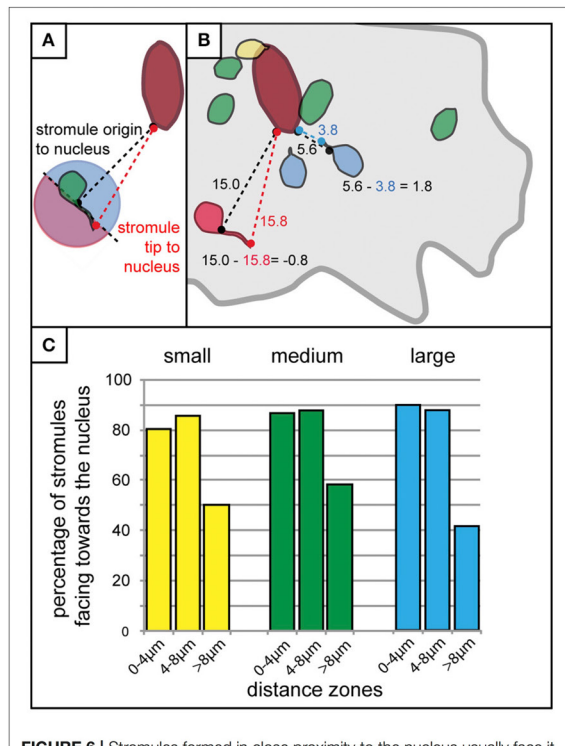


FIGURE 6 | Stromules formed in close proximity to the nucleus usually face it. **(A)** Schematic outline of the method used for the rough determination of whether a stromule faces toward or away from the nucleus. The distance of the base of the stromule as well as the tip of the stromule to the nucleus were measured and compared. If the stromule tip is closer to the nucleus than the base of the stromule (any stromule tip falling within the pink part of the circle for the plastid illustrated here) the stromule would be considered facing away from the nucleus, while any tip that is closer to the nucleus than the base (all those falling within the blue part of the circle) would be considered as facing toward the nucleus. **(B)** Illustration of example measurements taken from a real cell showing four plastids without stromules (green), one with a stromule and plastid body touching the nucleus (yellow), two that were considered to be facing the nucleus (blue), and one that was considered to be facing away from the nucleus (red). Example calculations for a stromule facing the nucleus (i.e., stromule decreasing the distance between the nucleus and plastid body), and a stromule facing away from the nucleus (i.e., stromule increasing the distance between the nucleus and the plastid body), are outlined in blue and red, respectively. Cell border outlined in gray, nucleus outlined in dark red. **(C)** Bar chart illustrating the percentage of stromules facing the nucleus (as determined by the criteria outline in **A,B**) with increasing distance from the nucleus in small (yellow), medium (green), and large (blue) cells.

was found that, in contrast to tobacco hypocotyl, *A. thaliana* leaf upper epidermal tissue showed no obvious correlation between median stromule length and the cell size or number of plastids per cell (**Figures 1A,B**). In fact, median stromule lengths indicate an abundance of very short stromules (between 1 and 2 µm) in all cells (**Figure 1C**). Interestingly, the longest stromule observed (close to 20 µm) was not in the largest cell size class, but was in a cell with only 4 plastids (**Figure 1B**). A histogram of stromule length measurements encompassing all cell sizes shows a drastic

right skew, a median value of 1.9 and an arithmetic mean of 2.7 (**Figure 1C**), thus confirming that in *A. thaliana* upper epidermis, stromules are most often short. It should be noted that stromule measurements in this tissue were simplified by the fact that stromules showed no branching (**Figure 1D**), a phenomenon that is described in other tissues, such as *A. thaliana* cortical root tip and *N. benthamiana* hypocotyl epidermis and leaf epidermis (Schattat et al., 2011).

The Relationship between Plastids and Nuclei in the Upper Epidermis

In order to assess the potential for a relationship between the plastids/stromules and the nucleus of cells the first step was to quantify where the plastids are normally positioned in the cell. In this way it could be determined whether plastids (with or without stromules) preferentially congregate around the nucleus, or whether they are equally distributed throughout the cell. The total number of plastids per cell was counted as well as the number of plastids that appeared to be “in contact” with the nucleus. Based on the analysis of 1,213 cells in 80 images from 8 plants it was found that 99% of cells have at least one plastid in contact with the nucleus. Although plastids at the nucleus increased slightly as plastid number/cell size increased (**Figure 2A**) the mean number of plastids at the nucleus remained below 5 in all cases, despite the fact that larger cells could harbor up to 18 plastids (**Figures 2A,B**). This shows that there is consistently a subpopulation of plastids at the nucleus, which increases little with increases in cell size/plastid number.

Stromule Orientation Gives the Impression That Stromules “Reach” for the Nucleus

Initial efforts were made to establish a clearer picture of how plastids are distributed, and revealed that although there are usually a few plastids at the nucleus, there are also plastids scattered throughout the cell. To evaluate the feasibility of the hypothesis that stromules are formed for the purpose of contacting the nucleus or the cell periphery the next step was to examine how stromules emanating from these plastids were positioned relative to the nucleus. For this analysis only cells with stromules could be assessed, resulting in a decrease in the size of the data set. Of the 1,213 cells that were analyzed for the first experiments 567 cells had one or more plastids with stromules. These cells were divided into three size categories so as not to exclude the possibility that stromule orientation could be influenced by the size of the cell. Small cells were defined as those that had a maximum of 4 plastids, medium cells harbored 5–11 plastids, and large cells harbored 12–18 plastids. Size categories were chosen in a way so as to ensure an adequate number of cells were in each category (small cells, $n = 700$; medium cells, $n = 469$; large cells, $n = 44$). In order to evaluate the relative position and orientation of stromules in regard to the nucleus each plastid with a stromule was visually examined and sorted into one of four categories: (1) plastids and stromules which show no nuclear context, where the plastid body is not in contact with the nucleus and the stromule does not face the nucleus, (2) the plastids and stromules are not in contact with the nucleus, but

the stromule is facing toward the nucleus, (3) the plastid is not in contact with the nucleus, but the stromule is “connecting” the plastid to the nucleus, and 4) the plastid and the whole stromule are in contact with the nucleus (**Figure 3A**). Analysis of stromule position relative to the nucleus showed a similar trend in all cell size classes. Most stromules (75–85%) can be found in a nuclear context, meaning that in most instances stromules are either “reaching toward,” or touching the nucleus, while the remaining stromules show no affinity for the nucleus (**Figure 3B**).

Identification of a “Stromule-Promoting Zone”

The observation that stromules often form within the context of the nucleus, either touching it or “reaching” toward it, provides support for the idea that stromules act to minimize the distance between these two organelles. Given that in this model tissue most stromules are short, it was hypothesized that there is a relatively small distance within which a stromule would be useful for the purpose of communicating with the nucleus. If this were the case, then it would be expected that plastids closer to the nucleus are more likely to form a stromule than those in more distant regions of the cell, given that for these distant plastids the nucleus is effectively “out of reach.” To assess whether this is the case, the entire data set was re-examined and the distance between all plastids and the nucleus was measured in cells both with and without stromules. Due to variations in image quality not all cells could be included in this very detailed analysis reducing the number of cells considered to $n = 527$ cells with no stromules ($n = 2,132$ plastids) and $n = 325$ cells harboring stromules ($n = 1,898$ plastids). Since stromule frequency can only be calculated for a population of plastids and not for an individual plastid they had to be grouped into populations based on their distance from the nucleus. For this purpose zones of increasing distance around the nucleus were defined, each zone being $4 \mu\text{m}$ (example cell shown in **Figure 4A**), which corresponds to the average size of a pavement cell plastid (average plastid size = $3.8 \mu\text{m}$, $n = 4,834$, standard deviation = 0.8). Plastids touching the nucleus were placed into their own distance class. **Figure 4B** shows an animated example of the distribution of plastids with and without stromules in an average microscopy image.

Although it had already been determined that most cells are likely to have at least one plastid near the nucleus independent of whether they had stromules or not (**Figure 2A**), quantification of plastid position using the abovementioned zones provided more precise idea of what these two cell types looked like. Prior to evaluating whether plastids near the nucleus were more likely to show higher stromule frequency, cells with and without stromules were evaluated to determine whether they exhibit comparable plastid distributions. Again, data was divided according to the three cell size categories, small, medium and large (a graphic representation of a microscopy picture outlining the three types of cells can be seen in **Figure 4B**). The result was that cells both with and without stromules showed a similar plastid distribution (**Figures 4C,D**). Based on distance measurements, plastids can be found at almost every possible distance to the nucleus in cells with and without

stromules. However, the large majority of plastids are categorized as touching the nucleus (cells with no stromules: small cells = 95.5%, medium cells = 69.4%, large cells = 37.3% and in cells with stromules: small cells = 69%, medium cells = 47.7%, large cells = 28.4%), or can be found within $8 \mu\text{m}$ of the nucleus (no stromules: small = 99.4%, medium = 85.5%, large = 52.5%, with stromules: small = 95.2%, medium = 75.1%, and large = 46.2%). In both cell types and in all cell sizes there was a sharp decline in the number of plastids in zones at greater distances from the nucleus. One difference between these two cell populations is that there is a noticeably higher frequency of plastids touching the nucleus in cells without stromules (compare **Figures 4C,D**). Overall, the quantification of plastid position in cells with and without stromules revealed that zones further from the nucleus harbor fewer plastids in both cell types. These results suggest that plastid position does not have to change drastically to facilitate stromule induction.

Finding very little difference in plastid distribution between cells with and without stromules, it was then possible to use data from cells with stromules to evaluate whether stromule frequency is higher in zones closer to the nucleus. To do this, stromule frequency was calculated for each zone of $4 \mu\text{m}$ for small, medium and large cells (**Figure 5A**). Zones with less than three plastids present were eliminated based on an insufficient sample size (number of plastids with an without stromules in each zone outlined in **Figure 5B**). The result of this analysis, in the case of all three cell size categories, was that plastids close to the nucleus were up to 10 times more likely to form stromules than those in more distant zones (**Figure 5A**). Peak stromule frequencies of 68, 48, and 52% (for small, medium and large cells, respectively) were observed to fall within $8 \mu\text{m}$ of the nucleus and dropped drastically thereafter (**Figure 5A**). When data from all three cell sizes are combined the same trend is seen (**Figure 5C**). These results demonstrate that stromule frequencies clearly differ between zones, with most stromules specifically occurring in zones close to the nucleus. Independent of cell size, stromule formation is favored within $\sim 8 \mu\text{m}$ of the nucleus and as a result this region was appropriately deemed the “stromule-promoting zone.”

Plastid Position Relative to the Nucleus Influences Stromule Orientation

It was clear that the majority of stromules were found in the context of some kind of nuclear interaction, and that stromules were more likely to form within $8 \mu\text{m}$ of the nucleus. What was not clear was whether the distance of a plastid/stromule from the nucleus influences the direction the stromule is facing. The next step was to roughly determine whether stromules formed in close proximity to the nucleus were more likely to face it. To achieve this each plastid with a stromule was evaluated via measuring the distance between the nucleus and the stromule origin, as well as the distance between the nucleus and the stromule tip (**Figure 6A**). If the difference between these two values (nucleus to stromule origin—nucleus to stromule tip) was greater than 0 the stromule was said to point toward the nucleus (decreasing the distance between the plastid and the nucleus),

while values less than 0 led to the conclusion that the stromule pointed away from the nucleus (**Figure 6B**). Results for all cell sizes showed that within the stromule promoting zone 80–90% of all stromules decrease the distance between the plastid and the nucleus (**Figure 6C**). In zones at greater distances from the nucleus stromule direction appeared to become random (50% of stromules faced the nucleus), or they became more likely to face away from the nucleus (<50% of stromules faced the nucleus). It can be concluded that the frequency of stromules, and the orientation of stromules are influenced by the position of the plastid relative to the nucleus.

Increased Stromule Frequencies Near the Nucleus Are the Result of Increased Stromule Initiation Events, Not an Increase in Stromule Stability

Through the detailed characterization of stromule formation within the whole cell context via still images it has been established that stromules preferentially form around the nucleus. This provides the first quantitative support for the hypothesis that interactions between stromules and nuclei are not solely coincidental but could be functionally relevant, thus confirming the suspicions of many scientists (refer to Supplementary Table 1). Assessment of still images clearly suggested that stromules “reach” for the nucleus, with the potential for retrograde signal transfer. However, this raised a host of mechanistic questions regarding how stromule enrichment is achieved within this 8 μm zone and how stromules are so efficiently directed as they extend toward the nucleus.

The analysis of over 80 individual z-stacks has provided us with snapshots of stromule behavior in time. Snapshots, although very useful for evaluating stromule frequency, do not give us any information about the mode with which this enrichment is occurring. It was therefore postulated that enrichment of stromules in the stromule-promoting zone could be the result of two different scenarios; an increase in stromule stability or more frequent stromule initiation events. To assess the feasibility of these hypotheses required the collection of long-term movies via a confocal microscope, using a new *A. thaliana* transgenic line highlighting both plastids (*FNRtp:eGFP*) and nuclei (*H2B:mCherry*). To determine whether stromules are more stable near the nucleus the persistence of stromules at different distances from the nucleus was measured over 90 min (plastids $n = 252$, cells $n = 22$, videos $n = 7$). Surprisingly, movies revealed that stromules were most often present for between 1 and 4 frames (30 frames, 3 min between frames) independent of how far they were from the nucleus (**Figure 7A**). This analysis suggests that higher stromule frequencies near the nucleus are not the result of increased stromule stability. The same videos were re-evaluated to determine whether there was a difference in the number of stromules initiated in the different zones. The average number of stromules formed per chloroplast was measured over 90 min. It was revealed that plastids closest to the nucleus showed the highest number of stromule initiation events, with a steady decrease in initiations with increasing distance from the nucleus (**Figure 7B**). At the same time the direction of

newly initiated stromules was recorded, revealing that within the stromule-promoting zone over 90% of newly formed stromules face toward the nucleus (**Figure 7C**). These results suggest that the reason more stromules are observed close to the nucleus in snapshots is the direct result of an increase in stromule initiation events, and not due to increased stromule persistence.

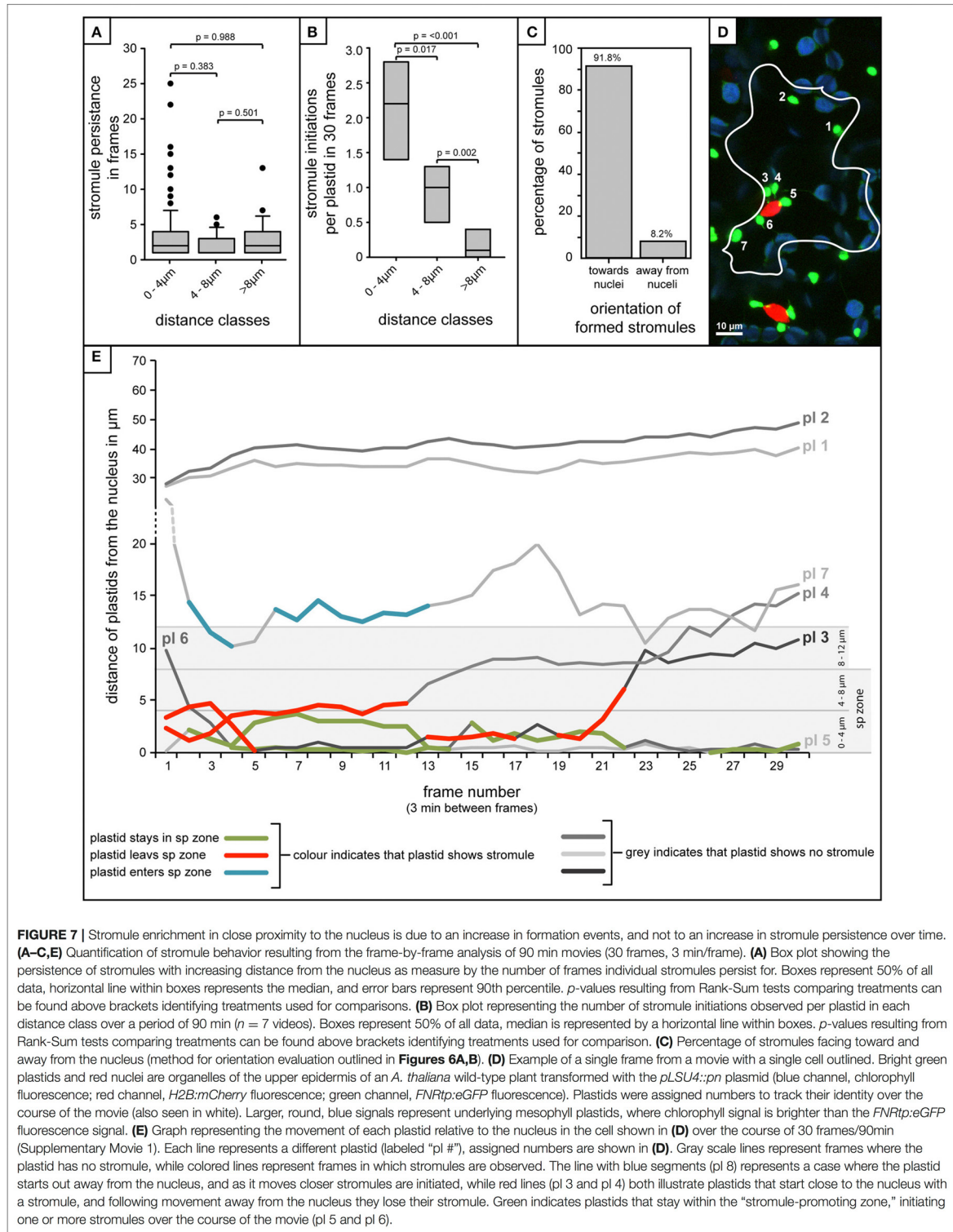
Movement in and Out of the Zone Is Correlated with the Ability of Plastids to Form Stromules

A few plastids observed were capable of moving in and out of the stromule-promoting zone and lost or gained a stromule accordingly. For example, occasionally plastids started out in the stromule-promoting zone with a stromule, sometimes exhibiting several stromule initiations and retractions, and then moved away from the nucleus, immediately losing their stromule, and failing to form another (**Figures 7D,E** pl3 and pl4; in **Figure 7E** the red marked lines). Additionally there were cases where more distant plastids started with no stromule, but gained a stromule when they entered the zone (example in **Figure 7E**, pl7 highlighted in blue). Movement into and out of the stromule-promoting zone was not always a result of the plastid changing its position, but also occurred when the nucleus changed position, moving either closer or further from plastids.

DISCUSSION

It has been suggested that so-called “retrograde” signals are sent from the plastid to the nucleus to deliver important information regarding the physiological status of these endosymbiotic organelles. In recent years a number of potential retrograde signals have been identified, several of which have been suggested to travel to the nucleus via stromules (Caplan et al., 2015), thus implying the intentional extension of stromules for the purpose of communicating with the nucleus. However, based on current data available in the literature it is unclear whether interactions between stromules and nuclei are intentional or observed as a result of an overall increase in stromules throughout the cell, thus increasing the probability that stromules contact the nucleus.

To evaluate whether nucleus-stromule contacts were coincidental, rosette leaves of *A. thaliana* upper epidermis were chosen as a model. Thorough characterization of this tissue has led us to conclude that observed interactions between stromules and nuclei are not coincidental. In fact, a definitive “stromule-promoting zone” was discovered within 8 μm of the nucleus. Within this zone almost all stromules are either facing and/or touching the nucleus (80–90%), while plastids outside this zone are both less likely to form stromules, and stromules that do form appear to lack directionality. Increased stromule frequency in the stromule-promoting zone was further determined to be the result of an increase in stromule initiation events as opposed to increased stromule stability in close proximity to the nucleus. These observations raise two questions, the first being how the stromule-promoting zone and stromule directionality is established and maintained, and the second being whether



these interactions are truly relevant in the context of retrograde signaling.

The Mechanism behind the Stromule Orientation within the Stromule Promoting Zone

Evidence presented here suggests that stromule behavior/formation is heavily influenced by the proximity of plastids to the nucleus. Within the stromule-promoting zone the majority of stromules observed were found to face in the direction of, or directly contact the nucleus. The directionality of stromules toward the nucleus that was observed in still images could be intuitively interpreted as an attempt by plastids that do not contact the nucleus, to “reach out” for the nucleus in order to establish direct contacts. This would imply that plastids “sense” or “know” where to find the nucleus. However, none of the stromules observed in movies demonstrated such clear directional growth toward the nucleus. Instead stromule formation seemed to be correlated with plastid and nucleus movement. Frequently plastids appeared to be anchored with their membrane near or at the nucleus, with the extension of a stromule occurring when there was an increase in distance between the organelles. Movement of the nucleus away from the plastid body often resulted in the formation of stromules that appeared to be “reaching” for the nucleus (Figure 8A, Supplementary Movies 2, 3). In movies it is clear that stromule tips are anchored at a point near or at the nucleus, so that wherever the nucleus moves the directionality of stromules (toward the nucleus) is maintained. Given that 90% of stromules within the stromule-promoting zone are formed facing the nucleus, this provides a convincing mechanistic explanation for most of the stromule formation observed. Although preliminary, this data implies that non-perinuclear plastids within the stromule-promoting zone are not likely forming stromules toward the nucleus to transmit a signal, but rather as a result of the independent movement of both organelles.

Actin Distribution and Rearrangement as an Explanation for the Stromule-Promoting Zone

Currently there is a consensus in the literature that cytoplasmic cytoskeletal elements are essential for maintaining wild-type stromule levels and morphologies. Although the involvement of microtubules in stromule formation appears to differ among tissues/plastid types (Kwok and Hanson, 2003 vs. Holzinger et al., 2007; Natesan et al., 2009), it seems that the involvement of actin is more universally accepted. Actin filaments have been shown to be essential for stromule maintenance in multiple tissues, such as etiolated *Nicotiana tabacum* hypocotyl epidermis (Kwok and Hanson, 2003), *Oxyria digyna* mesophyll (Holzinger et al., 2007), peels of tobacco leaf lower epidermis and onion bulb epidermal cells (Natesan et al., 2009). Kwok and Hanson (2003) found that following treatment with Cytochalasin D (microfilament inhibitor) and Latrunculin B (actin polymerization inhibitor) stromule frequency was reduced, and those that did remain were shorter and thicker than in untreated tissue. Some of the

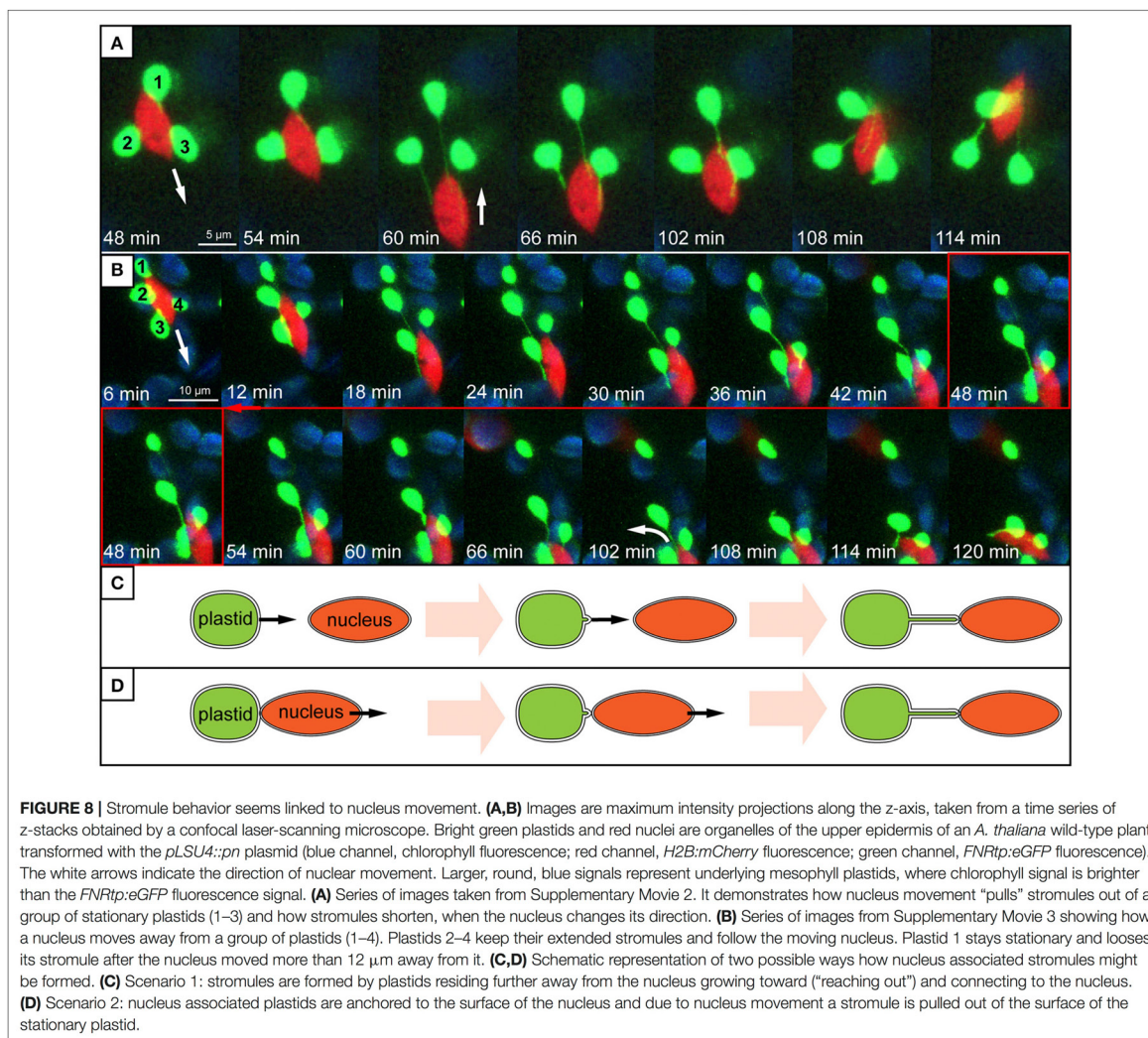
stromules remaining following CD and LatB treatment formed loops (Kwok and Hanson, 2003), as if they had been anchored, extended/stretched and then released from actin to form a loop of slack membrane at the plastid surface, a formation also described in *Iris unguicularis* petals as a “remnant loop” by Gunning (2005). Observations made following actin inhibitor treatments cumulatively suggest that stromules are anchored to actin, and this acts to maintain stromule length, width, number and movement.

Unequal distribution of actin throughout the cell could offer one explanation for why stromules are preferentially enriched when plastids are close to the nucleus. If actin is key to the elongation of stromules, then this could mean that more actin around the nucleus leads to a higher abundance of potential stromule anchor or initiation sites, and so increases the probability that the plastid would initiate a stromule. In support of this hypothesis *A. thaliana* mesophyll cells show high actin densities in close proximity to the nucleus (Kandasamy and Meagher, 1999). Cryofixation of leaves followed by immunofluorescence localization of actin reveals that a high-density basket of thin actin filaments exists around the nucleus (Kandasamy and Meagher, 1999). In pavement cells as well as mesophyll cells the nucleus is also associated with thicker actin bundles that run along the length of the cell (Kandasamy and Meagher, 1999; Higa et al., 2014). From these bundles a series of thin actin filaments extend in random directions into the cell cortex (Kandasamy and Meagher, 1999). Assuming that the likelihood of forming a stromule is positively correlated with the number of actin contact sites, the decreased actin density in this region could, at least in part, cause a decrease in stromule appearance in the cell cortex.

Based on time-lapse movie data, the abundance of stromules near the nucleus appears to be promoted by both a highly mobile nucleus and, perhaps, high actin density in this region. In other words there are many potential actin-anchoring sites available for plastids within the stromule-promoting zone, and the movement of both the nucleus and the surrounding actin is generating the “force” necessary to form stromules. Live-cell imaging of pavement cells has shown that the actin basket surrounding the nucleus is constantly moving together with the encaged nucleus and closely associated plastids (Higa et al., 2014). Movies confirm this rigorous nucleus movement. Based on movie data it could be hypothesized that in cases where plastids do not immediately follow the moving nuclei, plastid-actin contact sites are moved away from the plastid body and thereby “pull” out stromules. Future work will need to utilize actin labeled stable transgenic plants to confirm that the behavior observed is truly correlated with actin distribution and dynamics.

Functional Relevance of Stromules in the Context of Retrograde Signaling

At the beginning of this study it was not clear whether stromule-nucleus associations are occurring by chance. This work has clearly established that in *A. thaliana* leaf model tissue a “stromule-promoting zone” exists. This could be seen as support for the hypothesis that stromules are intentionally



formed as pathways for retrograde signals. However beside its clear existence, the functionality of this zone in the context of plastid-nucleus communication remains open. Through the characterization of unchallenged *A. thaliana* plastid position it was observed that there are typically two or more plastids with or without a stromule in direct “contact” (fluorescence signals overlap) with the nucleus of most cells (**Figures 2B,C**). If direct contact between the nucleus and plastid is a requirement for communication then it could be argued that plastids positioned at the nucleus should not need to form stromules, and yet this frequently occurs. Further, it was observed that approximately half of the epidermis cells (567 out of 1,213) studied in still images lacked stromules completely. Assuming stromules are truly important for communicating plastid “status” to the nucleus, the lack of stromules in unchallenged tissue may indicate that these cells do not require as much plastid-nucleus communication,

but that this process is required for fast response in times of high stress. An alternative explanation is that stromules are not required for retrograde communication at all. The reliable association of plastids with the nucleus in every cell may be enough to ensure that plastid derived signals reach their destination. Interestingly, the number of plastids associated with the nucleus was only partially correlated with the cell size, meaning that although in larger cells the total number of plastids increased, the average number of nucleus associated plastids remained constant (**Figure 2A**). Given these results, one could speculate that only a few nuclear-associated plastids are sufficient to inform the nucleus about the condition of plastids throughout the cell.

As outlined earlier, time-lapse movies suggest that stromule formation within the “stromule promoting zone” appears to be the result of opposing movement of plastids and nuclei.

Interestingly, as illustrated by Supplementary Movie 3 and **Figure 8B**, in the large majority of cases plastids will follow the nucleus when it moves over a significant distance. This gives the impression that the plastid bodies are “dragged” behind the nucleus by stromules. When the nucleus changes its direction, “returning” to the plastids, stromules shrink as the nucleus comes closer to the plastid bodies (**Figures 8A,B**). This type of coupling between plastid body movement, nucleus movement and stromule extension was also observed by Caplan et al. (2015) during hypersensitive response in *N. benthamiana*. The frequent observation of this behavior gives the impression that stromules may simply help keep plastids in contact with the nucleus, analogous to a retractable leash. Considering that in over 99% of all cells plastids are in direct contact with the nucleus, it seems that plastid body-nucleus associations are fundamental in the epidermis. Further the phenomenon of plastids clustering around the nucleus is frequently observed in plants under a wide variety of biotic challenges (Supplementary Table 1), emphasizing the importance of plastid body-nucleus position to stress response. These observations lead to the hypothesis that instead of/in addition to relaying signals to the nucleus, stromules act as anchors to maintain a certain plastid body-to-nucleus proximity. It has been suggested before that stromules could have a role maintaining plastid position within the cell (Hanson and Sattarzadeh, 2008), however this data provides the first support for a role in the context of coupling plastid and nuclear movement in unchallenged plant tissue.

This work does not exclude the possibility that signals, such as H₂O₂, travel through stromules toward the nucleus, as was demonstrated by Caplan et al. (2015). Fundamentally, stromules consist of stroma in which molecules (potentially including retrograde signals) can diffuse. However, as already mentioned, observations presented here suggest that in the upper epidermis of *A. thaliana* leaves stromules are not specifically extended from plastids residing further away from the nucleus to “reach out” for, and connect to it (see **Figure 8C**). Instead, the vast majority of stromule initiations within the stromule-promoting zone seem to be dependent on the relative position of the nucleus and the plastid, potentially to maintain plastid-nucleus contacts despite constant nuclear movement (see **Figure 8D**). Regardless of whether stromules have a significant role in retrograde signaling and/or plastid positioning the result is the same, plastids within 8 μm of the nucleus have stromules facing toward the nucleus. The key difference is that a role for stromules in retrograde signaling implies stromule growth would have to be guided toward the nucleus by an unknown mechanism. In contrast, a theory including a role for stromules acting as plastid anchors is already sufficient to explain stromule directionality and behavior.

CONCLUSION

In recent years there has been a wealth of observations of stromules/plastid bodies associating with nuclei and much

speculation as to the significance of such interactions. Most recently stromules have been implicated in retrograde signaling. However, very few stromule-nucleus observations have been quantified in any way, and none have characterized the position of stromule forming plastids within the context of the whole cell. Originally it was suspected that the result of quantifying the plastid/stromule-nucleus relationship would lead to support for one of two hypotheses, the first being that the stromule is indeed important for nuclear contact and directionally extends toward it, and the second being that stromule contacts are simply formed as a result of an overall inflation of stromule frequency, and are thus coincidental. Still images provided strong support for the former when they revealed that stromules are clearly forming near the nucleus and often appear to be “reaching” toward it, perhaps facilitating retrograde signal transfer. However time-lapse movies renewed doubt regarding a role for these structures in plastid-nuclear communication when they revealed that stromules observed were never seen growing in the direction of the nucleus. Surprisingly, the vast majority of stromules observed were extended as a result of the nucleus and plastid moving in opposing directions. This new evidence suggests that stromules may have a more indirect role in organelle communication, perhaps acting to maintain a certain number of plastid bodies at the nucleus to facilitate signal transfer between these two organelles.

AUTHOR CONTRIBUTIONS

JE collected measurements and wrote the article. MK collected and analyzed data. MS collected data, analyzed data and supervised the writing of the manuscript.

FUNDING

Funding for this project was provided by grants from the state Sachsen-Anhalt (Exzellenznetzwerk Biowissenschaften) and the European Funds for Regional Development (EFRE) provided by the state Sachsen-Anhalt as well as by Martin-Luther University.

ACKNOWLEDGMENTS

We would like to acknowledge Ralf B. Klösigen for providing resources and valuable advice during initial experiments; Nigel Griffiths, Tobias Schröder as well as Nele Stroscher for help with cloning the *pLSU4::pn* T-DNA vector used for live cell imaging; Christina Lampe for help with proofreading of the manuscript. In memory of João Marques.

SUPPLEMENTARY MATERIAL

The Supplementary Material for this article can be found online at: <http://journal.frontiersin.org/article/10.3389/fpls.2017.01135/full#supplementary-material>

REFERENCES

- Avendaño-Vázquez, A.-O., Cordoba, E., Llamas, E., San Román, C., Nisar, N., De la Torre, S., et al. (2014). An uncharacterized apocarotenoid-derived signal generated in ζ -carotene desaturase mutants regulates leaf development and the expression of chloroplast and nuclear genes in *Arabidopsis*. *Plant Cell* 26, 2524–2537. doi: 10.1105/tpc.114.123349
- Bobik, K., and Burch-Smith, T. M. (2015). Chloroplast signaling within, between and beyond cells. *Front. Plant Sci.* 6:781. doi: 10.3389/fpls.2015.00781
- Caplan, J. L., Kumar, A. S., Park, E., Padmanabhan, M. S., Hoban, K., Modla, S., et al. (2015). Chloroplast stromules function during innate immunity. *Dev. Cell* 34, 45–57. doi: 10.1016/j.devcel.2015.05.011
- Caplan, J. L., Mamillapalli, P., Burch-Smith, T. M., Czymmek, K., and Dinesh-Kumar, S. P. (2008). Chloroplastic protein NR1P1 mediates innate immune receptor recognition of a viral effector. *Cell* 132, 449–462. doi: 10.1016/j.cell.2007.12.031
- Chan, K. X., Phua, S. Y., Crisp, P., McQuinn, R., and Pogson, B. J. (2016). Learning the languages of the chloroplast: retrograde signaling and beyond. *Annu. Rev. Plant Biol.* 67, 25–53. doi: 10.1146/annurev-arplant-043015-111854
- Davis, A. M., Hall, A., Millar, A. J., Darrah, C., and Davis, S. J. (2009). Protocol: streamlined sub-protocols for floral-dip transformation and selection of transformants in *Arabidopsis thaliana*. *Plant Methods* 5:3. doi: 10.1186/1746-4811-5-3
- Dyall, S. D., Brown, M. T., and Johnson, P. J. (2004). Ancient invasions: from endosymbionts to organelles. *Science* 304, 253–257. doi: 10.1126/science.1094884
- Estavillo, G. M., Crisp, P. A., Pornsiriwong, W., Wirtz, M., Collinge, D., Carrie, C., et al. (2011). Evidence for a SAL1-PAP chloroplast retrograde pathway that functions in drought and high light signaling in *Arabidopsis*. *Plant Cell* 23, 3992–4012. doi: 10.1105/tpc.111.091033
- Grefen, C., Donald, N., Hashimoto, K., Kudla, J., Schumacher, K., and Blatt, M. R. (2010). A ubiquitin-10 promoter-based vector set for fluorescent protein tagging facilitates temporal stability and native protein distribution in transient and stable expression studies. *Plant J.* 64, 355–365. doi: 10.1111/j.1365-313X.2010.04322.x
- Gunning, B. E. S. (2005). Plastid stromules: video microscopy of their outgrowth, retraction, tensioning, anchoring, branching, bridging, and tip-shedding. *Protoplasma* 225, 33–42. doi: 10.1007/s00709-004-0073-3
- Hadley, A. (2006). *My Software to Combine Pictures to Increase Depth of Field*. Available online at: <http://www.hadleyweb.pwp.blueyonder.co.uk/>
- Hanson, M. R., and Sattarzadeh, A. (2008). Dynamic morphology of plastids and stromules in angiosperm plants. *Plant Cell Environ.* 31, 646–657. doi: 10.1111/j.1365-3040.2007.01768.x
- Higa, T., Suetsugu, N., Kong, S.-G., and Wada, M. (2014). Actin-dependent plastid movement is required for motive force generation in directional nuclear movement in plants. *Proc. Natl. Acad. Sci. U.S.A.* 111, 4327–4331. doi: 10.1073/pnas.1317902111
- Holzinger, A., Wasteneys, G. O., and Lütz, C. (2007). Investigating cytoskeletal function in chloroplast protrusion formation in the arctic-alpine plant *Oxyria digyna*. *Plant Biol.* 9, 400–410. doi: 10.1055/s-2006-92472
- Isemer, R., Mulisch, M., Schäfer, A., Kirchner, S., Koop, H.-U., and Krupinska, K. (2012). Recombinant whirly1 translocates from transplastomic chloroplasts to the nucleus. *FEBS Lett.* 586, 85–88. doi: 10.1016/j.febslet.2011.11.029
- Kandasamy, M. K., and Meagher, R. B. (1999). Actin-organelle interaction: association with chloroplast in *Arabidopsis* leaf mesophyll cells. *Cell Motil. Cytoskeleton* 44, 110–118. doi: 10.1002/(SICI)1097-0169(199910)44:2<110::AID-CM3>3.0.CO;2-O
- Köhler, R. H., Cao, J., Zipfel, W. R., Webb, W. W., and Hanson, M. R. (1997). Exchange of protein molecules through connections between higher plant plastids. *Science* 276, 2039–2042. doi: 10.1126/science.276.5321.2039
- Köhler, R. H., and Hanson, M. R. (2000). Plastid tubules of higher plants are tissue-specific and developmentally regulated. *J. Cell Sci.* 113, 81–89.
- Koncz, C., and Schell, J. (1986). The promoter of TL-DNA gene 5 controls the tissue-specific expression of chimeric genes carried by a novel type of *Agrobacterium* binary vector. *Mol. Gen. Genet.* 204, 383–396. doi: 10.1007/BF00331014
- Krause, K., and Krupinska, K. (2009). Nuclear regulators with a second home in organelles. *Trends Plant Sci.* 14, 194–199. doi: 10.1016/j.tplants.2009.01.005
- Krause, K., Oetke, S., and Krupinska, K. (2012). Dual targeting and retrograde translocation: regulators of plant nuclear gene expression can be sequestered by plastids. *Int. J. Mol. Sci.* 13, 11085–11101. doi: 10.3390/ijms130911085
- Kwok, E. Y., and Hanson, M. R. (2003). Microfilaments and microtubules control the morphology and movement of non-green plastids and stromules in *Nicotiana glauca*. *Plant J.* 35, 16–26. doi: 10.1046/j.1365-313X.2003.01777.x
- Lee, S., Su, G., Lasserre, E., Aghazadeh, M. A., and Murai, N. (2012). Small high-yielding binary Ti vectors pLSU with co-directional replicons for *Agrobacterium tumefaciens*-mediated transformation of higher plants. *Plant Sci.* 187, 49–58. doi: 10.1016/j.plantsci.2012.01.012
- Leister, D. (2012). Retrograde signaling in plants: from simple to complex scenarios. *Front. Plant Sci.* 3:135. doi: 10.3389/fpls.2012.00135
- Marques, J. P., Dudeck, I., and Klösgen, R. B. (2003). Targeting of EGFP chimeras within chloroplasts. *Mol. Genet. Genomics* 269, 381–387. doi: 10.1007/s00438-003-0846-y
- Marques, J. P., Schattat, M. H., Hause, G., Dudeck, I., and Klösgen, R. B. (2004). *In vivo* transport of folded EGFP by the pH/TAT-dependent pathway in chloroplasts of *Arabidopsis thaliana*. *J. Exp. Bot.* 55, 1697–1706. doi: 10.1093/jxb/erh191
- Mathur, J., Mammone, A., and Barton, K. A. (2012). Organelle extensions in plant cells. *J. Integr. Plant Biol.* 54, 851–867. doi: 10.1111/j.1744-7909.2012.01175.x
- Natesan, S. K. A., Sullivan, J. A., and Gray, J. C. (2009). Myosin XI is required for actin-associated movement of plastid stromules. *Mol. Plant* 2, 1262–1272. doi: 10.1093/mp/ssp078
- Nelson, B. K., Cai, X., and Nebenführ, A. (2007). A multicolored set of *in vivo* organelle markers for co-localization studies in *Arabidopsis* and other plants. *Plant J.* 51, 1126–1136. doi: 10.1111/j.1365-313X.2007.03212.x
- Nott, A., Jung, H.-S., Koussevitzky, S., and Chory, J. (2006). Plastid-to-nucleus retrograde signaling. *Annu. Rev. Plant Biol.* 57, 739–759. doi: 10.1146/annurev-arplant.57.032905.105310
- Pogson, B. J., Woo, N. S., Förster, B., and Small, I. D. (2008). Plastid signaling to the nucleus and beyond. *Trends Plant Sci.* 13, 602–609. doi: 10.1016/j.tplants.2008.08.008
- Ramel, F., Birtic, S., Ginies, C., Soubigou-Taconnat, L., Triantaphylidès, C., and Havaux, M. (2012). Carotenoid oxidation products are stress signals that mediate gene responses to singlet oxygen in plants. *Proc. Natl. Acad. Sci. U.S.A.* 109, 5535–5540. doi: 10.1073/pnas.1115982109
- Ruegger, M., Dewey, E., Hobbie, L., Brown, D., Bernasconi, P., Turner, J., et al. (1997). Reduced naphthylphthalamic acid binding in the tir3 mutant of *Arabidopsis* is associated with a reduction in polar auxin transport and diverse morphological defects. *Plant Cell* 9, 745–757. doi: 10.1105/tpc.9.5.745
- Schattat, M., Barton, K., Baudisch, B., Klösgen, R. B., and Mathur, J. (2011). Plastid stromule branching coincides with contiguous endoplasmic reticulum dynamics. *Plant Physiol.* 155, 1667–1677. doi: 10.1104/pp.110.170480
- Schattat, M. H., and Klösgen, R. B. (2011). Induction of stromule formation by extracellular sucrose and glucose in epidermal leaf tissue of *Arabidopsis thaliana*. *BMC Plant Biol.* 11:115. doi: 10.1186/1471-2229-11-115
- Schindelin, J., Arganda-Carreras, I., Frise, E., Kaynig, V., Longair, M., Pietzsch, T., et al. (2012). Fiji: an open-source platform for biological-image analysis. *Nat. Methods* 9, 676–682. doi: 10.1038/nmeth.2019
- Strand, A., Asami, T., Alonso, J., Ecker, J. R., and Chory, J. (2003). Chloroplast to nucleus communication triggered by accumulation of Mg-protoporphyrinIX. *Nature* 421, 79–83. doi: 10.1038/nature01204
- Sun, X., Feng, P., Xu, X., Guo, H., Ma, J., Chi, W., et al. (2011). A chloroplast envelope-bound PHD transcription factor mediates chloroplast signals to the nucleus. *Nat. Commun.* 2:477. doi: 10.1038/ncomms1486
- Van Norman, J. M., Zhang, J., Cazzonelli, C. I., Pogson, B. J., Harrison, P. J., Bugg, T. D. H., et al. (2014). Periodic root branching in *Arabidopsis* requires synthesis of an uncharacterized carotenoid derivative. *Proc. Natl. Acad. Sci. U.S.A.* 111, E1300–E1309. doi: 10.1073/pnas.1403016111
- Waters, M. T., Fray, R. G., and Pyke, K. A. (2004). Stromule formation is dependent upon plastid size, plastid differentiation status and the density of plastids within the cell. *Plant J.* 39, 655–667. doi: 10.1111/j.1365-313X.2004.02164.x

- Woodson, J. D., Perez-Ruiz, J. M., and Chory, J. (2011). Heme synthesis by plastid ferrochelatase I regulates nuclear gene expression in plants. *Curr. Biol.* 21, 897–903. doi: 10.1016/j.cub.2011.04.004
- Wozny, M., Schattat, M. H., Mathur, N., Barton, K., and Mathur, J. (2012). Color recovery after photoconversion of H2B::mEosFP allows detection of increased nuclear DNA content in developing plant cells. *Plant Physiol.* 158, 95–106. doi: 10.1104/pp.111.187062
- Xiao, Y., Savchenko, T., Baidoo, E. E. K., Chehab, W. E., Hayden, D. M., Tolstikov, V., et al. (2012). Retrograde signaling by the plastidial metabolite MEcPP regulates expression of nuclear stress-response genes. *Cell* 149, 1525–1535. doi: 10.1016/j.cell.2012.04.038

Conflict of Interest Statement: The authors declare that the research was conducted in the absence of any commercial or financial relationships that could be construed as a potential conflict of interest.

Copyright © 2017 Erickson, Kantek and Schattat. This is an open-access article distributed under the terms of the Creative Commons Attribution License (CC BY). The use, distribution or reproduction in other forums is permitted, provided the original author(s) or licensor are credited and that the original publication in this journal is cited, in accordance with accepted academic practice. No use, distribution or reproduction is permitted which does not comply with these terms.

3.3. Summary

The central question of the above publication was to determine if close relationships between nuclei and stromules observed by us and others were the result of overall increases in stromule abundance throughout the cell, or were the result of intentional interactions. Further, we wanted to evaluate the feasibility of stromules as transporters of retrograde signals, as well as consider possible mechanisms for stromule extension. Using *A. thaliana* as a model system, we clearly demonstrated that stromule-nuclear associations are not a coincidence resulting from inflated stromule frequency, but are likely a functional characteristic of cells in the upper epidermis. Stromules were highly enriched among plastids positioned within 8 μm of the nucleus (the so-called 'stromule promoting zone'), and 80-90% of stromules formed faced toward, or touched the nucleus. Alone, this data creates the impression that stromules 'reach' for the nucleus and lends support for the hypothesis that stromules intentionally grow toward the nucleus to make contact. However, live-cell imaging never revealed a case where a stromule grew in the direction of the nucleus in *A. thaliana* upper epidermis. Instead, we found evidence for an alternative mechanism where stromule extension relies on plastid and/or nucleus movement. Our observations suggest that stromules elongate when the plastid membrane is anchored at, or near the nucleus (possibly to actin), and the distance between the two organelles increases. Particularly, nucleus movement away from closely associated plastid bodies resulted in the extension of stromules; all of which faced the nucleus. Rather than suggesting a direct role for stromules in the transfer of signals, observations of nucleus-stromule relations give the impression that stromules act as anchors between the plastid and nucleus, and thus, act to keep track of the nucleus and maintain plastid-nucleus associations. Whether the maintenance of plastid-nucleus distance is significant in facilitating communication between these organelles remains open for investigation.

4. A mechanism for myosin dependent stromule formation

4.1. Introduction

As previously described, published work by Natesan et al. (2009) and Sattarzadeh et al. (2009) provide the first indications that myosins are important for stromule formation. However, so far the specific myosin, or subset of myosins responsible for stromule elongation has not been identified and the mechanism with which a myosin would act during stromule elongation is unknown. One clear cut approach to assessing the involvement of individual myosins in stromule formation is to evaluate stromule frequencies in mutants of all 13 *A. thaliana* type XI myosins compared to wild type. Surprisingly, no one has adopted this strategy, likely because of the time it takes to generate multiple stable transgenic lines with plastids and stromules labeled.

We chose to take this approach to get a clear answer to the question of whether any single myosins are essential for stromule formation. With the help of Caroline Alfs (Hiwi) and Alexandra Gurowietz (Hiwi) stable transgenics were generated that express *FNRtp:eGFP*, labeling plastids and stromules of wild-type *A. thaliana* (ecotype Columbia) and T-DNA insertion mutants for all XI-type myosins (transgenic lines listed in Table 12.1 on page 154). Stromule frequencies were quantified from upper epidermal tissue of rosette leaves, where plastid position and stromules have been very thoroughly characterized (Schattat and Klösigen, 2011; Erickson et al., 2017b). Expecting that myosins may function redundantly (Prokhnevsky et al., 2008), we also acquired and transformed the previously characterised triple (*xi-k*, *xi-1*, *xi-2*; 3KO) and quadruple (*xi-k*, *xi-1*, *xi-2*, *xi-i*; 4KO) knockout plants that lack the most highly expressed myosins present in vegetative tissues (Peremyslov et al., 2010).

4.2. Results

4.2.1. Myosin XI-I is required to maintain basal stromule levels in upper epidermis of *A. thaliana*

Most myosin mutants showed mean stromule frequencies between 15-24%, within 5% of wild type. Several myosin mutant lines showed a subtle, but significant, difference from wild type (Figure 4.1 on page 35). The exception was *xi-i*, which showed a more substantial drop in stromule frequency (down to only 10% plastids with stromules) (Figure 4.1). This result

was surprising, because although XI myosins have been implicated in stromule formation and morphology in general, and portions of *N. benthamiana* XI-F¹ and XI-2² cargo domains have been localized to plastids³, this is the first evidence to suggest a link between XI-I and stromules. Additionally, it was not expected that any single mutant would create a clear reduction in stromule frequency, but that we would be most likely to see a stromule phenotype when multiple myosins were missing. Contrary to this, wild-type-like stromule frequencies were observed in the triple mutant line. The 3KO is known to suffer severe impairment of organelle movement (Golgi and peroxisomes), and alterations to actin and ER structure (Peremyslov et al., 2010), both of which have been shown to interact with stromules (Kwok and Hanson, 2004a; Schattat et al., 2011a). However, this appeared to have a surprisingly minimal effect on stromule abundance and no obvious effect on morphology relative to wild type (Figure 4.1 on the facing page). It was only when myosin XI-I was knocked out alone, or in the 4KO, that plants showed a drastic reduction in stromule frequency. These results clearly indicate the importance of myosin XI-I to the maintenance of wild-type stromule levels in *A. thaliana* upper leaf epidermis.

4.2.2. Myosin XI-I is important for nucleus movement

Myosin XI-I has a known role in maintaining nucleus shape and movement in the root epidermis, root hair, and is also required for dark-induced movement of nuclei in mesophyll cells (Tamura et al., 2013). Specifically, mutants in XI-I exhibit slow-moving, spherical, nuclei in root epidermis, as opposed to the 'spindle-shaped', faster moving nuclei seen in wild type (Tamura et al., 2013). Myosin XI-I tail domains are known to localize to both motile 'punctate structures' (Avisar et al., 2009) and to the nuclear envelope (Tamura et al., 2013; Avisar et al., 2009). Further, a full-length XI-I-GFP construct also labeled the nuclear membrane of cultured tobacco protoplasts. Taken together, these findings suggest that, at least in the root epidermis and root hair, XI-I localized to the nuclear envelope is responsible for nucleus movement along actin (Tamura et al., 2013). Although initially surprising, the finding that a myosin involved in nucleus movement exhibits a phenotype with a reduced stromule frequency fits well within the context of work presented in Part I of this thesis. In Erickson et al. (2017b) we reported that most stromules in *A. thaliana* upper epidermis form within 8 μm of the nucleus, within the so called 'stromule-promoting zone', and that most of these stromules face the nucleus. Movie data showed instances where the plastid membranes appear to be anchored close to the nucleus and stromules were 'pulled out' when the nucleus moved away from the plastid body (Figure 4.2 on page 36). Based on our observations we suggested that nucleus movement is key to the mechanism of stromule formation and directionality within the stromule-promoting zone. The finding that myosin *xi-i* exhibits clear decreases in stromule frequencies provides clear support for a mechanism of nuclear movement-driven stromule formation and warrants further investigation.

¹The vacuole-binding domain (41 amino acids) (Sattarzadeh et al., 2009).

²A small portion of coiled-coil and dilute domain (505 amino acids) (Natesan et al., 2009).

³Transient assays in *Nicotiana* species (Sattarzadeh et al., 2009; Natesan et al., 2009).

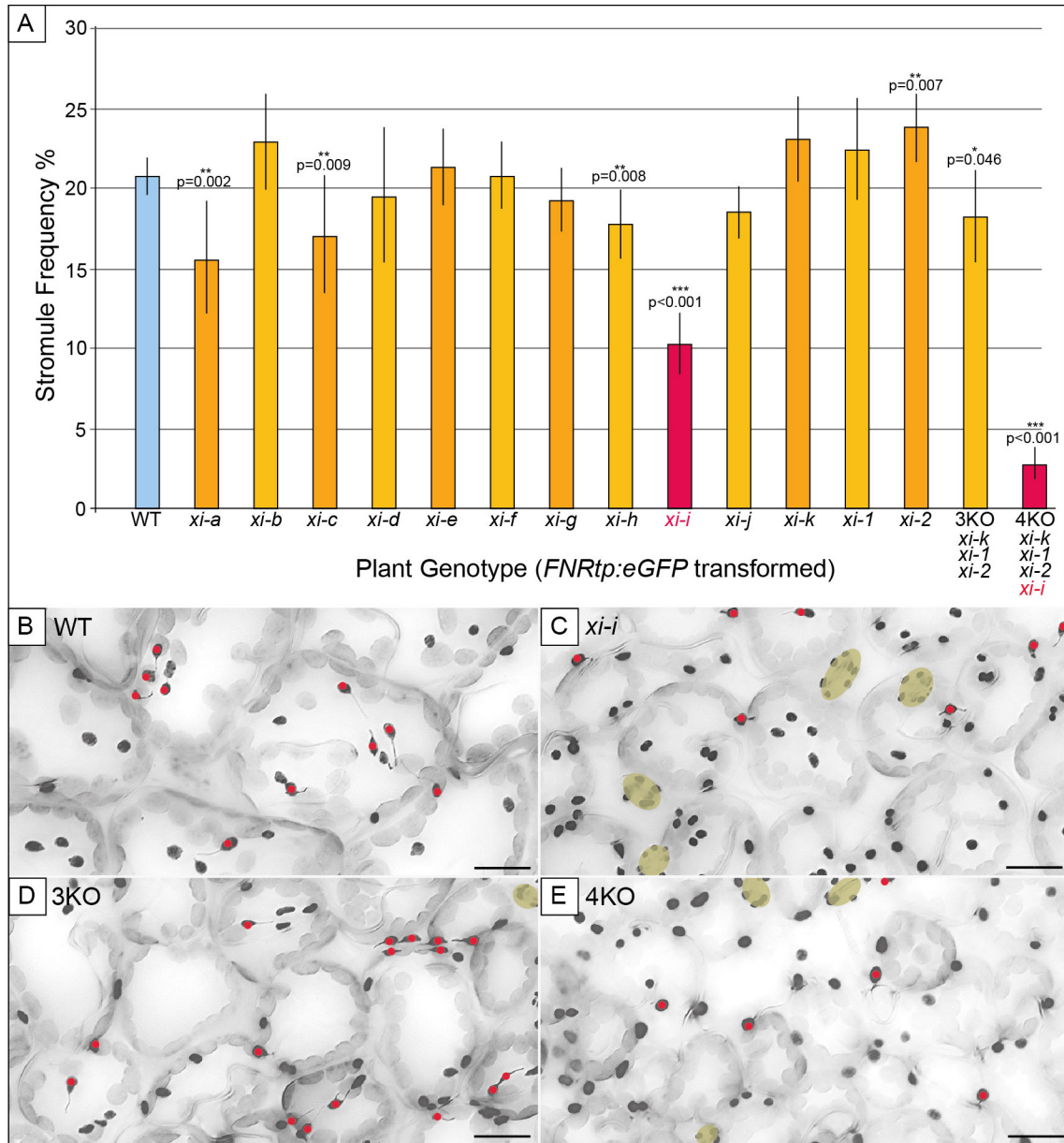


Figure 4.1.: Mutants lacking functional myosin XI-I show the most severe decreases in stromule frequency in *A. thaliana* upper epidermis. (A) Mean stromule frequencies in the upper epidermis of *A. thaliana* (ecotype Columbia-0 expressing *FNRtp:eGFP*) wild type (WT-blue bar), compared to myosin mutants (orange and red bars). Three wild-type plants (independent transformants) were grown alongside every mutant line and placed in the same tray to ensure quantification of stromules under similar conditions. Sample sizes and details of plant lines utilized can be seen in Table 12.1 on page 154. Myosin *xi-i* and the 4KO are highlighted in red, these lines showed the most drastic decreases in stromule frequency relative to the wild type. Raw data was arcsine transformed and bars represent back-transformed means. Error bars represent back-transformed 95% confidence intervals. Rank-Sum test results compared WT and mutants and significant differences ($p < 0.05$) are reported above the mutant bar. (B-E) Examples of epifluorescence images of (B) wild-type plants (WT), (C) myosin *xi-i* mutants, (D) triple (3KO) and (E) quadruple (4KO) myosin knockouts used for the quantification of stromules. For ease of visualization images were converted to gray scale and inverted, so plastids and stromules are visible in dark gray-black. Stomata guard cells are indicated in light green (stromules in guard cell were not part of quantification). Plastids with stromules indicated with red dots. Scale bars = 20 μm .

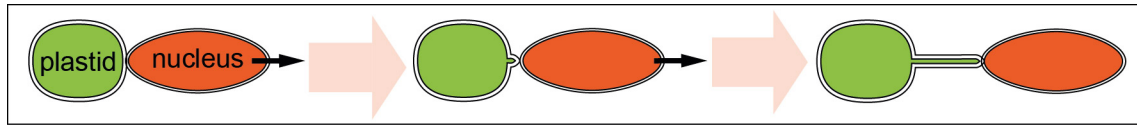


Figure 4.2.: Nucleus movement-driven stromule elongation within the 'stromule-promoting zone'. Plastids in close proximity to the nucleus (within 8 μm ; the so called 'stromule-promoting zone') are anchored at or near the surface of the nucleus. Nucleus movement causes a stromule to be 'pulled out' of the surface of the stationary plastid. Figure modified from Erickson et al. (2017b).

4.2.3. Mutants with impaired nucleus movement have less stromules

The next step was to test whether the reduction in stromule frequency observed in *xi-i* plants can be linked more definitively to impaired nucleus movement, and is not dependent on another, yet unknown function of myosin XI-I. To do this, we chose to analyse mutants in WIT1 and WIT2 (WPP DOMAIN-INTERACTING TAIL-ANCHORED PROTEIN 1 and 2). WIT 1 and 2 integrate into outer nuclear membrane and mediate the interaction between XI-I and the nuclear envelope (Tamura et al., 2013). In root cells of *wit12* double mutants, myosin XI-I is no longer localized to the nuclear membrane (Tamura et al., 2013). Additionally, nuclei exhibit the same round shape and reduced movement rate as that observed in *xi-i* plants (Tamura et al., 2013). We transformed *wit12* with a plastid-nucleus (pn) marker construct containing both *FNR:eGFP* (labels plastid stroma and stromules) as well as *H2B:mCherry* (labels nucleus) to simultaneously label the plastid stroma and nuclei⁴. This allowed us to visualize plastids and stromules as well as the morphology of nuclei. To enable comparison between the previously analysed wild type, *xi-i*, 3KO and 4KO mutants, these lines were also stably transformed with the pn marker. Excitingly, the *wit12* double mutant showed a 43% reduction in stromule frequency compared to wild-type grown in the same tray, a decrease comparable to *xi-i* and 4KO mutants (43% and 53% respectively, Figure 4.3 on the facing page). 3KO mutants showed a less dramatic drop in stromule frequency (approx. 25%) compared to wild type, a similar result to that shown in Figure 4.1 on the previous page. Analysis of the *wit12* double mutant provides encouraging evidence for a nucleus movement-based mechanism of stromule formation.

4.3. Discussion and outlook

4.3.1. Myosin XI-I and nucleus movement is important for basal stromule levels

Almost 10 years ago treatments with myosin ATPase inhibitors and silencing of type XI myosins showed that myosin function is generally important to stromule formation (Natesan et al., 2009; Sattarzadeh et al., 2009). This led to speculation that myosins localise to the plastid membrane, either directly or through adaptor proteins, and act to pull stromules from the plastid surface (Figure 1.6 on page 11). So far evidence for this model is indirect, and mutant plant lines were never analysed to evaluate the importance of individual myosins to

⁴The generation of 'pn' construct is described in Erickson et al. (2017b).

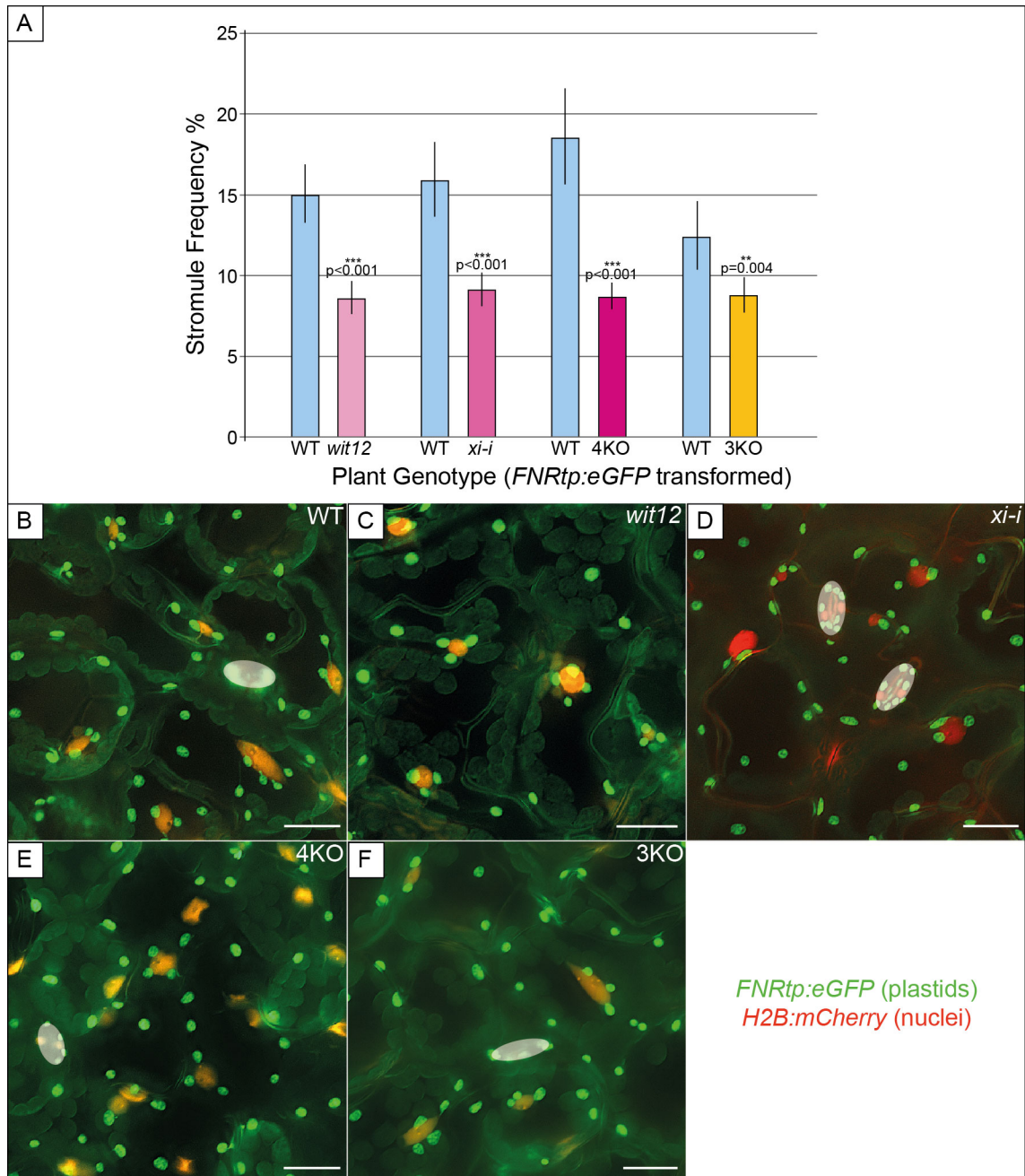


Figure 4.3: Mutants with impaired nucleus movement show the most severe decreases in stromule frequency in *A. thaliana* upper epidermis (stably expressing *pn* marker). (A) Mean stromule frequencies in the upper epidermis of *A. thaliana* (ecotype Columbia-0) wild type (WT, blue bars) compared to *wit1-1/wit2-1* (*wit12*, light pink bars), *xi-i* (medium pink), 4KO (*xi-i, xi-k, xi-2, xi-1*, dark pink bar) and 3KO (*xi-k, xi-1, xi-2*, yellow bar). Pink bars represent mutants with impaired nucleus movement. At least three wild-type *pn* transformed lines and 9 or more plants per line were examined for all mutants (samples sizes and plant lines utilized can be found in Table 12.2 on page 155). Raw data was arcsine transformed and bars represent back-transformed means. Error bars represent back-transformed 95% confidence intervals. Rank-Sum test results comparing WT and mutants are indicated above the corresponding mutant bar. Example epifluorescence images of (B) wild type, (C) *wit12*, (D) *xi-i*, (E) 4KO and (F) 3KO. Plastids are in visible green (*FNR:eGFP*), while nuclei are visible in red (*H2B:mCherry*). Stomata guard cells are indicated in transparent white ovals (stromules in guard cell were not part of quantification). Labeling of nuclei with mCherry reveals elliptical nuclei in wild type and 3KO, while the double mutant *wit12, xi-i* and 4KO (also lacking myosin *xi-i*) show characteristic round nuclei.

stromule formation. Through the analysis of all individual myosin mutants in unstressed *A. thaliana* upper epidermis, we have shown that most individual myosins do not have a drastic impact on stromule frequency. Surprisingly, myosin XI-I was the only myosin that caused an obvious reduction in stromule frequencies when singly knocked out in this tissue. Full length myosin XI-I does not associate with the plastid membrane, but rather to that of nuclei (Tamura et al., 2013), making it highly unlikely that this myosin contributes to stromule frequency based on a 'direct pulling' model (Figure 1.6 on page 11). Rather, it appears that basal stromule levels are maintained by nuclear movement, which is inhibited in the *xi-i* mutant. This hypothesis is supported by the finding that another mutant with impaired nucleus movement (*wit12*) shows the same clear reduction in stromule frequency. These findings support the hypothesis put forward in Erickson et al. (2017b) that the plastid membrane is anchored near or at the nucleus (perhaps to actin), and subsequent movement of the nucleus away from the associated plastids creates the force necessary to generate stromules. This model would explain the enrichment of stromules in close proximity to the nucleus in this tissue.

While our data suggest that myosin XI-I is involved in stromule formation in close proximity to the nucleus, it does not explain stromule formation in more distant regions of the cell, which likely employ other mechanisms. It is possible that stromules formed elsewhere in the cell are dependent on 'direct pulling' on the plastid membrane by redundantly functioning myosins. Although we examined all individual myosin mutants for stromule phenotypes in *A. thaliana*, more multi-gene knockouts would have to be screened to determine if myosins act redundantly to pull on the plastid membrane during stromule extension. What we can decisively conclude from data presented here, is that there is no single myosin responsible for pulling directly on stromules in *A. thaliana* upper epidermis.

4.3.2. Analysing the stromule-promoting zone in mutants

Time-lapse movies suggested movement of the nucleus away from plastids within the stromule-promoting zone appears to provide the force necessary to pull a stromule out of the main plastid body, and provides an explanation for the directionality of stromules toward the nucleus in this part of the cell (Figure 4.2 on page 36). If our hypothesis is correct reductions in stromule frequency resulting from impaired nucleus movement should specifically be occurring within the stromule-promoting zone, where this mechanism is active, and should have little impact on stromules formed outside this zone. Although mutants with impaired nucleus movement showed clear and reproducible decreases in stromule frequency, images will have to be re-analysed to confirm that stromule frequency drops are specific to those plastids close to the nucleus. The distance of each plastid from the nucleus, the presence of a stromule, and the direction of all stromules will have to be evaluated in order to compare the configuration of stromule promoting zones for each mutant line to confirm our model.

4.3.3. Correlating reduced nucleus movement with reduced stromule initiations

Although this preliminary work provides strong indications that nucleus movement influences stromule elongation in the upper epidermis, it should be noted that a reduction in nucleus motility has only been shown in root cells (Tamura et al., 2013) and has not yet been confirmed for *xi-i*, 4KO or *wit12* in rosette leaf upper epidermis. However, the nucleus marker (*H2B:mCherry*) revealed that these mutants exhibited round nuclei (Figure 4.3 on page 37), similar to that seen in root cells. This is in contrast to the elliptical nuclei observed in wild type and the 3KO mutant (Figure 4.3), both of which still have myosin XI-I. This suggests that XI-I, WIT1 and WIT2 likely have comparable functions in the root and rosette. Time-lapse movies are currently being collected in pn marker lines for the analysis of nucleus velocity as well as total nucleus movement. Stromule behavior will be analysed to determine if the decreased nucleus velocity in mutants is truly correlated with the extension of associated stromules. This work is done by Jolina Marx as part of her bachelor's thesis.

4.4. Materials and methods

4.4.1. Plant material and growth conditions

Growth conditions and sample preparation of plant material for microscopy can be found in Erickson et al. (2017b). Information on the plant lines and sample sizes used for the quantification of stromules can be found in Tables 12.1 on page 154 and 12.2 on page 155.

4.4.2. Bacterial strains and constructs

A. tumefaciens strain GV3101 (pMP90) (Koncz and Schell, 1986) was used to mediate stable transformations of plant lines. Bacteria were transformed with plasmids using electroporation with a Bio-Rad, E.coli Pulser (Munich, Germany). *A. thaliana* plants were transformed with marker constructs using the floral dip method (Davis et al., 2009).

Erickson et al. (2017b) contains a description of the plasmids utilized for transformation of plant lines; *FNRtp:eGFP* and the double construct featuring *FNRtp:eGFP* and *H2B:mCherry* (*pLSU::pn* (pn) marker).

4.4.3. Epifluorescence microscopy

Z-stacks for the analysis of stromule frequency were collected with an AxioObserver with an AxioCamMRm-CCD-Camera. Samples were excited with a HXP 120V illuminator with a 120W short arc lamp X-cite 120. eGFP was imaged using a 38HE filter, and mCherry required a 43HE filter. The EC Plan-Neofluar x40/0.75 Ph2 lens was used. ZenBlue software was used to control the microscope and to capture images. All equipment and software was provided by Zeiss GmbH (Jena, Germany).

4.4.4. Image processing and analysis

Single images were prepared from z-stacks collected at the epifluorescence microscope as outlined in Erickson et al. (2017b,a). Quantification of stromules in transgenic plant lines was performed using ImageJ/Fiji as outlined in Erickson et al. (2017a).

4.4.5. Data analysis

Information on stromule frequency data handling can be found in Erickson et al. (2017a).

5. Stromule induction during *A. tumefaciens*-mediated transient assays

5.1. Introduction

A. tumefaciens-based expression assays in *N. benthamiana* and *N. tabacum* are commonly used to transiently express proteins for a wide variety of applications (protein localization studies, protein-protein interaction studies, labeling and observing organelles, etc.) due to their quick and inexpensive nature. During the PhD thesis of Martin Schattat (MLU, Halle), infiltrations utilizing two different bacterial strains were used to facilitate expression of a stroma-localized fluorescence protein (*FNRtp:eGFP*) in order to visualize stromules in *N. benthamiana* lower leaf epidermis. During preliminary experiments it was discovered that stromules were reliably induced and plastids clustered around the nucleus during transient assays utilizing the common lab strain, GV3101. In contrast, plastid phenotypes were much less pronounced following inoculation with a second strain, LBA4404. In the publication that follows we chose to examine the differences between these two bacterial strains in order to determine the 'stromule-inducing stimuli' and changes to the sub-cellular environment, thus identifying conditions conducive to stromule formation. In addition to learning more about stromules, characterisation of cellular conditions in the presence of GV3101 should be of general interest to those using transient assays.

5.2. Publication II

Erickson et al. *BMC Plant Biology* 2014, **14**:127
<http://www.biomedcentral.com/1471-2229/14/127>



RESEARCH ARTICLE

Open Access

Agrobacterium-derived cytokinin influences plastid morphology and starch accumulation in *Nicotiana benthamiana* during transient assays

Jessica L Erickson¹, Jörg Ziegler², David Guevara^{3,4}, Steffen Abel², Ralf B Klösgen¹, Jaideep Mathur⁴, Steven J Rothstein⁴ and Martin H Schattat^{1,4*}

Abstract

Background: *Agrobacterium tumefaciens*-based transient assays have become a common tool for answering questions related to protein localization and gene expression in a cellular context. The use of these assays assumes that the transiently transformed cells are observed under relatively authentic physiological conditions and maintain 'normal' sub-cellular behaviour. Although this premise is widely accepted, the question of whether cellular organization and organelle morphology is altered in *Agrobacterium*-infiltrated cells has not been examined in detail. The first indications of an altered sub-cellular environment came from our observation that a common laboratory strain, GV3101(pMP90), caused a drastic increase in stromule frequency. Stromules, or 'stroma-filled-tubules' emanate from the surface of plastids and are sensitive to a variety of biotic and abiotic stresses. Starting from this observation, the goal of our experiments was to further characterize the changes to the cell resulting from short-term bacterial infestation, and to identify the factor responsible for eliciting these changes.

Results: Using a protocol typical of transient assays we evaluated the impact of GV3101(pMP90) infiltration on chloroplast behaviour and morphology in *Nicotiana benthamiana*. Our experiments confirmed that GV3101(pMP90) consistently induces stromules and alters plastid position relative to the nucleus. These effects were found to be the result of strain-dependant secretion of cytokinin and its accumulation in the plant tissue. Bacterial production of the hormone was found to be dependant on the presence of a *trans*-zeatin synthase gene (*tzs*) located on the Ti plasmid of GV3101(pMP90). Bacteria-derived cytokinins were also correlated with changes to both soluble sugar level and starch accumulation.

Conclusion: Although we have chosen to focus on how transient *Agrobacterium* infestation alters plastid based parameters, these changes to the morphology and position of a single organelle, combined with the measured increases in sugar and starch content, suggest global changes to cell physiology. This indicates that cells visualized during transient assays may not be as 'normal' as was previously assumed. Our results suggest that the impact of the bacteria can be minimized by choosing *Agrobacterium* strains devoid of the *tzs* gene, but that the alterations to sub-cellular organization and cell carbohydrate status cannot be completely avoided using this strategy.

Keywords: *Agrobacterium tumefaciens*, *Nicotiana benthamiana*, Transient assays, GV3101(pMP90), LBA4404, Plastid, Stromules, Bacteria-derived, Cytokinin, *Trans*-zeatin synthase

* Correspondence: martin.schattat@pflanzenphys.uni-halle.de

¹Abteilung Pflanzen Physiologie, Institut für Biologie-Pflanzenphysiologie, Martin-Luther-Universität Halle-Wittenberg, Weinbergweg 10, Halle/Saale 06120, Germany

⁴Department of Molecular and Cellular Biology, University of Guelph, Guelph, ON N1G 2 W1, Canada

Full list of author information is available at the end of the article



© 2014 Erickson et al.; licensee BioMed Central Ltd. This is an Open Access article distributed under the terms of the Creative Commons Attribution License (<http://creativecommons.org/licenses/by/2.0>), which permits unrestricted use, distribution, and reproduction in any medium, provided the original work is properly credited. The Creative Commons Public Domain Dedication waiver (<http://creativecommons.org/publicdomain/zero/1.0/>) applies to the data made available in this article, unless otherwise stated.

Background

The soil-borne bacterium *Agrobacterium tumefaciens* is the cause of crown gall disease in various plant species. The Ti-plasmid of virulent *A. tumefaciens* strains is essential for tumor induction during bacterial infection. A distinct part of this plasmid (the T-DNA) is excised and transferred to the plant cell via a type IV secretion apparatus, then transported to the nucleus where it is finally inserted into the plant genome. The transferred wild type T-DNA encodes genes that force the transformed plant cell to synthesize the plant hormones auxin and cytokinin as well as amino acid–sugar conjugates (opines). The resulting increase in auxin and cytokinin levels in the plant tissue induces cell proliferation resulting in tumor formation. The opines, which are produced only by transformed cells, are utilized by *A. tumefaciens* as a carbon and nitrogen source. The type of opine(s) produced is used to classify the infectious *A. tumefaciens* strains as octopine, nopaline or agropine-type strains (reviewed in [1-4]).

The removal of the T-DNA region of wild type Ti-plasmids yields bacterial strains that are no longer capable of stimulating tumor formation or opine production in plant cells. In place of the wild type, tumor inducing, T-DNA, modified T-DNAs located on binary T-DNA vectors have been designed and utilized to efficiently mediate the transfer of genes to plant cells (reviewed in [1,5]). The ability to transfer genes of interest to plant genomes without inducing tumors made such 'disarmed' *A. tumefaciens* strains invaluable to plant gene technology (reviewed in [2,4,6]).

Today *A. tumefaciens* is routinely used to generate transgenic plant lines for biotechnology or research purposes. However, the process of establishing transgenic lines is time consuming, and for several applications, not mandatory. The use of *A. tumefaciens* in transient assays provides a time saving alternative to the generation of stable transgenic plants. In most of these assays, 'disarmed' *A. tumefaciens* suspensions containing the construct of interest are infiltrated into leaf tissue. Cells exposed to the bacteria are subsequently transformed with the sequence of interest and can be assayed for expression a few days after infiltration. This method of plant cell transformation is often preferable to particle bombardment as it introduces fewer copies of the sequence, with a lower frequency of rearrangement (reviewed in [7]). Based on their high transformation efficiency, leaves of *Nicotiana tabacum* and *Nicotiana benthamiana* are commonly used for *A. tumefaciens* mediated transient expression.

Although infiltration of *N. tabacum* and *N. benthamiana* with 'disarmed' *A. tumefaciens* causes seemingly minor macroscopic effects [8], there is a growing body of evidence suggesting that even 'disarmed' strains are recognized by these *Nicotiana* species as a pathogen, and that pathogen related responses can interfere with transient

gene expression assays [8,9]. Although the mechanism of these interactions is not well understood, it clearly indicates that the use of *A. tumefaciens* in a transient system has limitations. The use of such assays is based on the assumption that plant cells expressing the gene(s) of interest are maintaining authentic sub-cellular behaviour. However, aside from the mentioned effect of *A. tumefaciens* on pathogen related responses, the impact of the bacteria on other aspects of cell biology, such as protein localisation, organelle movement and organelle morphology, has not been studied or reported in detail. During standard transient assays using the 'disarmed' laboratory strain GV3101 (pMP90) it became evident to us that *A. tumefaciens* can indeed have a pronounced effect on organelle morphology in *N. benthamiana*. Specifically, we observed that infiltration with this bacterial strain lead to the increased formation of stroma-filled-tubules (stromules) emanating from the surface of plastids and seemed to alter plastid position relative to the nucleus [10].

Stromules are approximately 0.1 to 0.8 μm in diameter (reviewed in [11]) and can range from only a few μm to 45 μm in length [12]. They are a common morphological feature of all plastid types, and have been observed in both vascular and non-vascular plants (monocotyledons, dicotyledons, moss and green algae) (reviewed in [13]), suggesting that these structures have been conserved during *Viridiplantae* evolution. It is known that stromules form at certain developmental stages, and the frequency of these protrusions is elevated when plants are exposed to a variety of stresses (biotic as well as abiotic) (reviewed in [14]). Although this suggests that stromules support plant cells in coping with unfavorable conditions, the specific subcellular function remains speculative.

Based on the sensitivity of stromule formation to stress, we interpreted our initial observation that GV3101(pMP90) induces stromules as a first indication of potential sub-cellular changes induced by short-term infestation of *A. tumefaciens* during transient assays. Our goal was to identify the specific elicitor responsible for the observed changes, thus better understanding how the 'disarmed' strain alters the sub-cellular environment of *N. benthamiana*, and simultaneously gain insight into the phenomenon of stromule formation.

Our results have confirmed that GV3101(pMP90) reliably induces stromules, and additionally, we have observed changes in plastid positioning relative to the nucleus following bacterial infiltration. These changes induced by GV3101(pMP90) are strain specific, and were found to be dependant on the presence of a Ti-plasmid specific *trans-zeatin synthase* gene (*tzs*). Further, we demonstrate that the production of cytokinins by the bacteria during transient assays is sufficient to alter cell physiological status, increasing both soluble sugar level and starch accumulation and that this can

partially be avoided by utilizing alternative 'disarmed' strains.

Results

To study the effect of *A. tumefaciens* infiltration on plastid behavior and morphology we utilized transgenic *N. benthamiana* lines constitutively expressing the chimeric protein FNR-EGFP, which highlights the plastid stroma and stromules [15,16]. Using these stable transgenic lines the effect of *A. tumefaciens* infiltration can be easily estimated by comparison of infiltrated and non-infiltrated tissue using fluorescence microscopy. To simplify the description of the results we have assigned acronyms to all bacterial strains utilized and listed them in Table 1, along with their antibiotic resistance.

Infiltration with GVR induces stromule formation as well as plastid repositioning

A 'disarmed' *A. tumefaciens* strain, GV3101(pMP90) (abbreviated - GV) [17] was employed in this study due to its wide-spread use for transient gene expression in *N. benthamiana*. In order to monitor transformation activity of *A. tumefaciens*, GV was transformed with the binary vector pCP60-35S-DsRed2 to yield GV3101(pMP90)/pCP60-35S-DsRed2 (abbreviated - GVR). This vector facilitates the expression of untagged DsRed2 [10]. Three days after infiltration, DsRed2 was detectable in infiltrated areas as bright fluorescence signals in the cytoplasm and nucleoplasm, indicating successful transfer and expression of the reporter gene from *A. tumefaciens* to the plant (Additional file 1: Figure S1C). In contrast, cells of non-infiltrated areas did not show any fluorescence signal using the same or even more sensitive microscope settings (Additional file 1: Figure SD and S1F respectively).

In the leaves of FNR-EGFP transgenic plants the plastids are clearly highlighted by the EGFP fluorescence. Following infiltration with GVR there were drastic alterations to plastid morphology and plastid position when compared to untreated tissue. The most obvious difference

following GVR treatment was the large number of stromules compared to the control (Figure 1A and 1B). The average stromule frequency (SF) in GVR-infiltrated leaf areas was approximately 53%, which was significantly higher than the 3% observed in non-infiltrated tissues (Figure 1C).

Stromule morphology also appeared altered in cells infiltrated with GVR. In non-infiltrated tissues there was an abundance of short stromules, mostly in the range from 3 to 5 μm , only in rare cases exceeding 10 μm . In contrast to this, in cells which were exposed to GVR, 50% of stromules demonstrated lengths of 5 μm or higher, with a maximum length of approximately 27 μm (Figure 1D). In addition to exhibiting substantially longer stromules, there was also frequent observation of crooked and branched stromules (Figure 1B). These branches originate from triangular dilations along the 'main stromule tubule' and were described in earlier publications [16,18].

It was also observed that, in many GVR-infiltrated cells, a subpopulation of plastids clustered around the nucleus (Figure 1B) in contrast to the untreated tissue, in which plastids are largely observed as part of evenly distributed pairs (Figure 1A). For quantification of this parameter we counted the number of plastids associated with individual nuclei, which we have named 'Plastid-Nuclear Association Index' (PNAI). Nuclei were labeled via DsRed2 accumulation in the nucleoplasm of GVR-infiltrated tissue, whereas in untreated tissue nuclei were detected after incubating the leaf disks in DAPI for 10 minutes. The box plot in Figure 1E clearly shows that after GVR treatment, the number of plastids in close proximity to the nucleus increases significantly, changing from a PNAI median of 2 (minimum of 1; maximum of 6) in untreated areas, to a PNAI median of 5 in infiltrated tissues (minimum 1; maximum of 18).

Our initial experiments confirmed the previous observation that the chosen strain, GVR, induces drastic changes in stromule frequency. In control experiments performed previously [10], the infiltration itself, and the agrobacterium

Table 1 Antibiotic resistance of *Agrobacterium tumefaciens* strains

<i>A.tumefaciens</i> strain				
Full strain name	Acronym	Genome	Ti Plasmid	T-DNA vector
GV3101(pMP90)	GV	Rif	Gent	-
GV3101(pMP90)/pCP60-35S-DsRed2	GVR	Rif	Gent	Kan
LBA4404	LBA	Rif	Strep	-
LBA4404/pCP60-35S-DsRed2	LBR	Rif	Strep	Kan
GV3101/pCP60-35S-DsRed2 (cured)	GVC	Rif	-	Kan
LBA/pLSU-ptzs-tzs	LtZ	Rif	Strep	Kan

Disarmed *A. tumefaciens* strains (column 1), acronyms used (column 2) and location of the genes conferring resistance to the various antibiotics, this includes the resistance located in the bacterial genome (column 3), the Ti plasmid (column 4) and the T-DNA vector (column 5). Antibiotics are abbreviated as follows: Rif = rifampicin, Gent = gentamicin, Strep = Streptomycin, Kan = kanamycin, and the absence of the T-DNA vector or Ti plasmid is indicated by a dash (-).

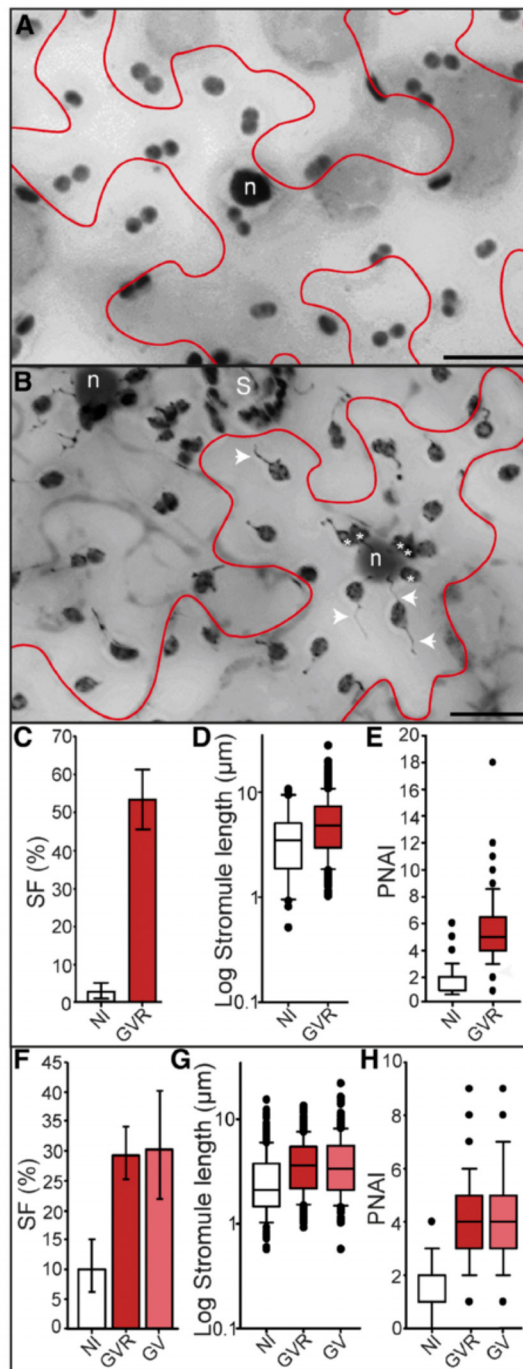


Figure 1 (See legend on next page.)

(See figure on previous page.)

Figure 1 Impact of infiltration with *A. tumefaciens* strains GVR and GV on stromule induction and plastid position. ‘Stacked’ fluorescence images of *N. benthamiana* lower epidermis with FNR-EGFP labeled plastids (single cells outlined in red). Nuclei of non-infiltrated cells were labeled via DAPI staining, while the nuclei of GVR-infiltrated cells were labeled via nucleoplasmic DsRed2. Epidermal plastids are dark grey, nuclei labeled ‘n’, location of stomata labeled ‘S’ (plastids surrounding are within guard cells). Plastids in close proximity to the nucleus are indicated by asterisks ‘*’. Images were converted to gray scale and inverted for easier viewing of stromules. Images were taken 3 days post-infiltration. Scale bars=20 μ m (**A, B**). **A** Non-infiltrated tissue. **B** GVR-infiltrated tissue. Examples of stromules indicated with white arrows. **C** Bar graph illustrating average stromule frequency (SF) in non-infiltrated (NI) and GVR-infiltrated (GVR) tissues. Rank sum (NI-GVR): $U=0$, $p<0.001$. Sample sizes: $n(\text{NI},\text{GVR})=9$. **D** Box plot illustrating the distribution and median stromule lengths in non-infiltrated (NI) and GVR-infiltrated (GVR) tissues. Rank sum (NI-GVR): $U=3002$, $p=0.022$. Sample sizes: $n(\text{NI})=30$, $n(\text{GVR})=269$. **E** Box plot illustrating median plastid nuclear association index (PNAI) in non-infiltrated (NI) and GVR-infiltrated (GVR) tissues. Rank sum (NI-GVR): $U=593$, $p<0.001$. Sample sizes: $n(\text{NI})=100$, $n(\text{GVR})=73$. **F** Bar graph illustrating average stromule frequency (SF) in non-infiltrated (NI), GVR-infiltrated (GVR) and GV-infiltrated (GV) tissues. Rank sum (NI-GVR): $U=1$, $p<0.001$; (NI-GV): $U=4$, $p=0.001$; (GV-GVR): $U=34$, $p=0.596$. Sample sizes: $n(\text{NI},\text{GV},\text{GVR})=9$. **G** Box plot of median stromule lengths in non-infiltrated (NI), GVR-infiltrated (GVR) and GV-infiltrated (GV) tissues. Rank sum (NI-GVR): $U=56132$, $p<0.001$; (NI-GV): $U=28578.5$, $p<0.001$; (GV-GVR): $U=68971.5$, $p=0.652$. Sample sizes: $n(\text{NI})=325$, $n(\text{GVR})=535$, and $n(\text{GV})=263$. **H** Box plot illustrating the median plastid nuclear association index (PNAI) in non-infiltrated (NI), GVR-infiltrated (GVR) and GV-infiltrated (GV) tissues. Rank sum (NI-GVR): $U=7356.5$, $p<0.001$; (NI-GV): $U=6266$, $p<0.001$; (GV-GVR): $U=12097.5$, $p=0.082$. Sample sizes: $n(\text{NI})=259$, $n(\text{GVR})=157$, and $n(\text{GV})=173$. **C, F** Raw data was arcsine transformed and bars represent back-transformed means. Error bars represent back-transformed 95% confidence intervals. **D, E, G, H** Boxes contain 50% of data, the median is represented by black line, and error bars represent 90% confidence intervals.

infiltration medium (AIM) used for solubilizing the bacteria, were ruled out as the stromule inducing stimuli, providing evidence that the inducing factor most likely originates from the bacteria. The goal of the second set of experiments was to identify the bacterial factor responsible for these ‘stromule inducing’ changes to the sub-cellular environment.

The expression of the reporter protein has no influence on the observed changes that follow GVR infiltration

The over-expression of proteins in stable as well as transient systems has the potential to interfere with normal cell metabolism as well as organelle behaviour [19-21]. In order to test if overexpression of the reporter protein was responsible for the observed effects, infiltration experiments were repeated utilizing GV lacking the pCP60-DsRed2 T-DNA vector. As a positive control we also infiltrated with GVR into the same leaves. GV and GVR-infiltrated tissues showed comparable levels of stromule induction, with both treatments yielding significantly higher SF values compared to the non-treated areas (Figure 1F). There was also no significant difference in stromule length (Figure 1G), or PNAI values (Figure 1H). Like GVR-infiltrated tissues, GV infiltration resulted in a higher tendency of plastids to associate with the nucleus (PNAI median of 4, minimum 1; maximum 9) when compared to untreated cells (Figure 1H). These results demonstrate that the transient expression of DsRed2 is not the cause for the GVR induced changes, but confirms that the source of stromule induction is intrinsic to the bacteria itself. GV is a disarmed derivative of the nopaline wild-type strain C58, which is the parental isolate for many disarmed laboratory strains (reviewed in [5]). We repeated the experiments using a different *A. tumefaciens* lab strain, originating from a different wild type isolate.

Infiltration of LBA and LBR does not induce plastid morphology and position changes to the same extent as GV and GVR

In order to evaluate whether the capacity for stromule induction was specific to C58 derived strains, or was more likely to be a general characteristic of *A. tumefaciens*, we transformed LBA4404 with pCP60-35S-DsRed2 (abbreviated - LBR) and repeated the experiments as outlined for GVR. LBA4404 (abbreviated - LBA) is one of the few ‘disarmed’ lab strains derived from the octopine wild type Ach5, a different wild type isolate than C58 (reviewed in [5]). Furthermore, to exclude an influence on the phenotype by over-expression of the reporter protein we also infiltrated with untransformed LBA. Again GVR was infiltrated into the same leaves to act as positive control for stromule induction.

In comparison to GV and GVR, LBA and LBR-infiltrated tissue had significantly fewer stromules, and cells looked much like non-infiltrated cells (Figure 2A, 2B and 2E). However, stromules observed after LBA and LBR treatments were slightly, but significantly longer (medians of 2.11 and 2.58 μ m, respectively) than in non-infiltrated tissues (median of 1.86 μ m), though still shorter than after GVR treatment (median of 3.68 μ m) (Figure 2F). PNAI results were very similar (Figure 2G). Clustering of plastids around the nucleus was observed more frequently in both LBA treatments when compared to untreated tissue (Figure 2C and 2D). Notably the PNAI of LBR-infiltrated tissue was not significantly different from that in the GVR treatment (Figure 2G).

SF measurements clearly show that strong induction of stromules is specifically induced by GV and GVR but not by LBA and LBR strains. However, LBA and LBR infiltrations still have an effect on the respective tissue, which is reflected in stromule length and the PNAI. Based on the

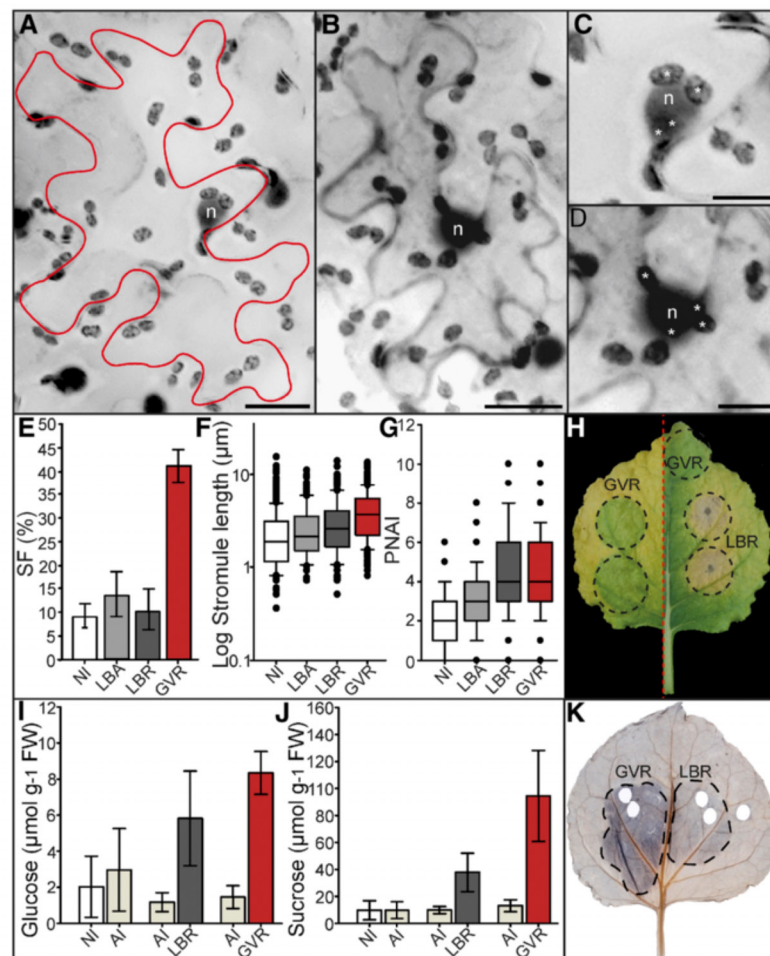


Figure 2 Infiltration with LBA and LBR induces mild alterations to plastid morphology and position relative to GVR infiltrated cells. 'Stacked' fluorescence images of *Nicotiana benthamiana* lower epidermis with FNR-EGFP labeled plastids. In non-infiltrated and LBA-infiltrated treatments nuclei were stained via DAPI, while nuclei of LBR and GVR treatments were labeled via nucleoplasmic DsRed2. Epidermal plastids are dark grey, nuclei labeled 'n'. Images were converted to gray scale and inverted for easier viewing of stromules. Images were taken 3 days post-infiltration. Scale=20 µm (A, B), or 10 µm (C, D). **A** Infiltrated with LBA. Cell boundary marked in red. **B** Infiltrated with LBR. Cell boundary marked by cytosolic DsRed2. **C, D** Enlargements of nuclei in **A** and **B** respectively, showing plastids in close proximity to the nucleus (indicated by asterisks **). **E** Bar graph of mean stromule frequency (SF) in non-infiltrated (NI), LBA-infiltrated (LBA), LBR-infiltrated (LBR), and GVR-infiltrated (GVR) tissues. Rank sum (NI-LBA): U=48, p=0.131; (NI-LBR): U=73, p=0.872; (LBA-LBR): U=28, p=0.289; (GVR-NI, LBA and LBR): U=0, p<0.001. Sample sizes: n(NI)=17, n(LBA)=9, n(LBR)=9, and n(GVR)=18. Raw data were arcsine transformed and bars represent back-transformed means. Error bars represent back-transformed 95% confidence intervals. **F** Box plot illustrating median stromule lengths in non-infiltrated (NI), LBA-infiltrated (LBA), LBR-infiltrated (LBR), and GVR-infiltrated (GVR) tissues. Rank sum (NI-LBA): U=34726, p=0.005; (NI-LBR): U=25226.5, p<0.001; (LBA-LBR): U=11983.5, p=0.053; (NI-GVR): U=95386.5, p<0.001; (LBA-GVR): U=46698, p<0.001; (LBR-GVR): U=45923, p<0.001. Sample sizes: n(NI)=448, n(LBA)=181, n(LBR)=151, and n(GVR)=805. **G** Box plot illustrating median plastid nuclear association index (PNAI) in non-infiltrated (NI), LBA-infiltrated (LBA), LBR-infiltrated (LBR), and GVR-infiltrated (GVR) treatments. Rank sum (NI-LBA): U=8772, p<0.001; (LBA-LBR): U=3380.5, p<0.001; (LBR-NI): U=2384, p<0.001; (GVR-NI): U=7738, p<0.001; (GVR-LBA): U=10906, p<0.001; (LBR-GVR): U=9450.5, p=0.359. Sample sizes: n(NI)=182, n(LBA)=147, n(LBR)=83, and n(GVR)=244. **F, G** Boxes contain 50% of data, the median is represented by black line. Error bars represent 90% confidence intervals. **H** Two senescing leaves (divided by a red dotted line) showing the maintenance of 'green islands' in GVR-infiltrated regions, and premature senescence of LBR-infiltrated regions. Infiltration zones outlined with black dotted lines. **I** Mean absolute glucose content of non-infiltrated (NI), AIM-infiltrated (AI), LBR-infiltrated (LBR) and GVR-infiltrated (GVR) tissues. Rank sum (NI-AI): U=14, p=0.209; (AI-LBR): U=0, p<0.001, t-test (AIM-GVR): t=13.577, p<0.001; (LBR-GVR): t=2.323, p=0.039. Sample sizes: n(NI, AI, LBR, GVR)=7. Error bars represent standard deviations. **J** Mean absolute sucrose content of non-infiltrated (NI), AIM-infiltrated (AI), LBR-infiltrated (LBR) and GVR-infiltrated (GVR) tissues. Rank sum (NI-AI): U=24, p=1, t-test (AIM-LBR): t=5.082, p<0.001, Rank sum (AIM-GVR): U=0, p<0.001, t-test (LBR-GVR): t=4.098, p=0.001. Sample sizes: n(NI, AI, LBR, GVR)=7. Error bars represent standard deviations. **K** Starch staining of a leaf infiltrated with GVR and LBR 3 days post-infiltration. Infiltration zones outlined with black dotted lines.

chosen parameters, this indicated that the presence of LBA and LBR also changes cell physiology, but to a lesser extent than GV and GVR. The stronger effects of GV and GVR infiltration on stromule induction and plastid repositioning compared to those obtained with LBA and LBR infiltration suggest that they are due to differences in either the bacterial chromosome or the disarmed Ti-plasmid present in these strains.

GVR-infiltrated tissues exhibit symptoms indicative of elevated cytokinin

Another phenomenon observed after infiltration concerns the senescence of infiltrated leaf tissue, which is detected as yellowing of leaf tissue approximately 6 weeks post-infiltration. GVR-infiltrated tissues were maintained as green islands (Figure 2H) in a manner reminiscent of cytokinin treatments described in the literature (reviewed in [22]). Infiltration with AIM buffer or LBR did not show the same effect. While GVR treatment delayed tissue senescence, infiltration with LBR actually induced a premature yellowing and, in some cases, even necrosis starting from the point of infiltration (Figure 2H). AIM infiltration caused neither the formation of green islands, nor premature senescence (data not shown). The ability of GVR to induce the formation of green islands suggests the possible accumulation of cytokinins in tissue infiltrated with this particular bacterial strain.

An alternative phenomenon after treatment of tobacco cell cultures with cytokinins is the pronounced and immediate accumulation of starch in plastids, as visualized by iodine staining [23,24]. The accumulation of starch was analyzed in GVR as well as LBR-infiltrated tissue by iodine staining three days post-infiltration. The result was that GVR-infiltrated areas showed a darker staining than the surrounding non-infiltrated tissue, indicating high levels of starch accumulation (Figure 2K). Microscopy of starch stained epidermal cells showed that this accumulation also took place in cells of the lower epidermis and is not restricted to mesophyll tissue (data not shown). Re-evaluation of fluorescence images taken for previous experiments revealed that starch accumulation was visible in GVR as well as in GV treatments as EGFP and chlorophyll fluorescence free areas in the plastid stroma (data not shown). LBA-infiltrated areas were, in most cases, indistinguishable from non-infiltrated leaf tissue. In rare cases infiltration with LBR showed a slightly darker staining than the surrounding tissue (Figure 2K). The pronounced accumulation of starch in GVR and GV compared to the low accumulation in LBA treatments, indicates that cytokinin accumulation is specifically induced following infiltration with GVR and GV, and that this effect is not common to all *A. tumefaciens* strains.

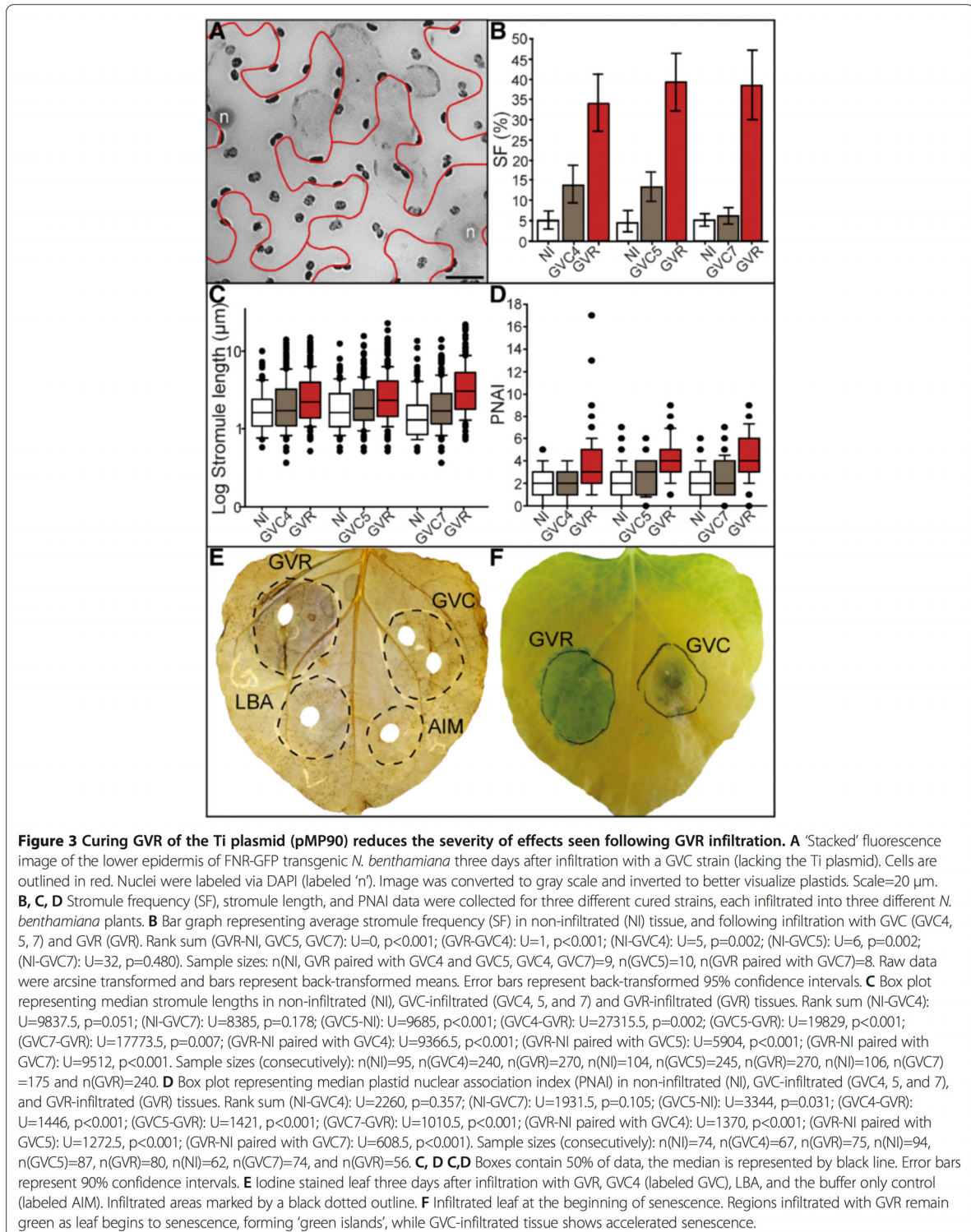
Cytokinins are known to be involved in the regulation of source-sink relationships. In addition to altering starch

accumulation this could also be reflected by a change in soluble sugar levels [25,26]. In order to test if soluble sugar levels are influenced by *A. tumefaciens* treatment, glucose and sucrose concentration of GVR, LBR, AIM and non-infiltrated tissues was measured (Figure 2I and 2J). Infiltration with AIM does not induce any significant changes in the sugar concentrations when compared to non-infiltrated tissues ($\sim 3 \mu\text{mol g}^{-1}$ FW glucose and $\sim 10 \mu\text{mol g}^{-1}$ FW sucrose) after AIM treatment, compared to non-infiltrated tissues which had $\sim 2 \mu\text{mol g}^{-1}$ FW glucose and $\sim 10 \mu\text{mol g}^{-1}$ FW sucrose). In contrast to AIM infiltration, both LBR and GVR induced clear and significant increases in glucose as well as sucrose concentration. LBR infiltration induced a 5-fold increase in glucose concentration ($5.8 \mu\text{mol g}^{-1}$ FW glucose), and a 4-fold increase in sucrose ($37.7 \mu\text{mol g}^{-1}$ FW sucrose). GVR infiltration induced a greater increase in soluble sugars, with a 5.5-fold increase in glucose concentration ($8.3 \mu\text{mol g}^{-1}$ FW glucose) and a 7-fold increase in sucrose concentration ($94.46 \mu\text{mol g}^{-1}$ FW sucrose). As already seen for the other parameters the induced glucose and sucrose accumulation is more severe for GVR than as it is for LBR. Comparing both *A. tumefaciens* strains it becomes increasingly evident that GV and GVR strains induce more severe physiological changes than LBA and LBR.

Cured GVR fails to induce stromule formation, plastid relocation and cytokinin related effects

In order to evaluate the possible differences between the GV and LBA strains that could be responsible for the observed physiological effects we reviewed their parentage. The Ti-plasmid of the GV strain, pMP90, is a derivative of the pTi-C58 of the C58 isolate [5]. This plasmid carries a gene involved in *trans*-zeatin synthesis close to the *vir*-gene region but outside of the deleted T-DNA region, the *tzs* gene [27]. This suggests that it may be the source of *trans*-zeatin accumulating in infiltrated regions. In order to eliminate the source of bacterial derived *trans*-zeatin, we depleted GVR of its Ti-plasmid (pMP90), and infiltrated the resulting GV3101 'cured' strains (abbreviated GVC, and labeled with a colony number) into leaf tissue. We then evaluated the ability of these strains to induce the effects observed in GVR. Indeed, the starch staining as well as the green island tests (Figure 3E and 3F) revealed that GVC strains lost the ability to induce pronounced starch accumulation, and no 'green islands' were observed during senescence. This suggests a decreased capacity to produce and maintain high cytokinin levels in the treated areas as observed with GVR.

Three separately cured GVC lines were analyzed. Microscopic inspection of GVC treated tissue revealed that in all cases stromule frequency was significantly lower than in the positive control infiltrations with GVR (Figure 3A). Infiltrations with the GVR positive control



resulted in a stromule frequency of about 35-40%, which is significantly higher than the 7-14% stromules induction following infiltration with GVC strains and the 5% observed in untreated tissue (Figure 3B). All the cured strains induced less than 15% stromules, i.e. a relatively minor increase in stromule frequency relative to non-treated (Figure 3B), which is in the same range as SF values in LBA and LBR treatments (Figure 2E). Stromule length and PNAI results revealed a similar relationship between treatments, in which GVR showed a clear induction of changes, and the three GVC strains were comparable to the non-infiltrated condition (Figure 3C and 3D).

Using starch accumulation and the presence of 'green islands' as indicators of cytokinin activity it can be concluded that the loss of the pMP90 and the *tzs* gene in GVC strains leads to a drastic reduction in cytokinin levels. This reduction was accompanied by a drastically reduced impact of GVC on the quantified plastid parameters to a level comparable to LBR treatments. This indicated that the GVR induced effects were indeed caused by a gene product encoded on the pMP90 Ti-plasmid. Additionally, it suggests that the contribution of the GVR genome to the observed reactions can be neglected.

Addition of *tzs* to LBA facilitates changes to plastid morphology and increases starch accumulation

To specifically test for the involvement of the *tzs* gene (a gene encoded in the pMP90 plasmid) in upregulating cytokinin indicators and plastid-based parameters, we tested if the addition of this gene into LBA would result in a gain of function, GVR/GV-like, phenotype. The *tzs* gene was cloned (coding region plus approximately 2 kb upstream and downstream) from GV and inserted into the small binary vector pLSU [28], simultaneously removing both T-DNA borders and the sequence between to avoid the transfer of the *tzs* from GV to the plant upon infiltration. The vector was then transformed into LBA and four of the subsequent transformants (abbreviated LtZ1-4) were infiltrated into FNR-GFP plants. All four strains induced a drastic increase in stromule frequency relative to NI and LBR strains, with stromule frequencies between 39% and 51% (Figure 4A). Three out of four strains showed no significant difference in SF when compared to GVR control infiltrations (LtZ1, 2 and 4). Median stromule lengths of tissues infiltrated with LtZ1-4 were significantly higher than NI and LBR controls, but significantly lower than GVR (Figure 4B). Although plastid clustering around the nucleus was apparent, and often extreme (see Figure 4C), we were not able to reliably locate the nucleus using DAPI staining or DIC, and so we could not quantify PNAI. Intensity of starch staining of the LtZ-infiltrated regions was comparable to GVR and remained within the infiltrated area as in GVR treatments (Figure 4D).

Measuring cytokinin accumulation in infiltrated tissues

Up to this point the increase of cytokinin in the plant tissue following infiltration has been indicated by starch staining, and by the maintenance of green islands. To quantify the strain dependant differences in cytokinin production within leaf tissue, liquid chromatography mass spectrometry (LC-MS/MS) was used to directly measure *trans*-zeatin, as well as *trans*-zeatin-9-riboside (Figure 4E and 4F). The same trend was observed for both hormones measured. Cytokinin levels of tissue infiltrated with AIM (infiltration buffer), GVC7, and LBR were below 0.2 ng/g (*trans*-zeatin) and 0.1 ng/g (*trans*-zeatin-9-riboside), while infiltration with both GVR and LtZ showed at least a three-fold increase in cytokinin accumulation (Figure 4E and 4F). Interestingly, LtZ-infiltrated tissues exhibited *trans*-zeatin levels that were about 3 times higher and *trans*-zeatin-9-riboside levels that were about 9 times higher than GVR-infiltrated tissues.

Tissue infiltrated with cytokinins mimic tissue infiltrated by GV, GVR and LtZ

As final proof that cytokinin accumulation and stromule induction are causally linked, even in the absence of all bacterial factors, we infiltrated plants with the hormone to test if we could mimic the effects observed with GVR treatment. For this purpose we infiltrated the tissue with 100 $\mu\text{g ml}^{-1}$ of *trans*-zeatin, administered three times over three consecutive days. 100 $\mu\text{g ml}^{-1}$ kinetin was also tested to determine if stromule induction as well as plastid repositioning is specific to *trans*-zeatin or if this is due to general changes induced by cytokinins. In addition a control solution was also infiltrated to ensure the stress of multiple infiltrations did not induce stromules. After a 3-fold infiltration with each cytokinin and a recovery period of two days we observed, in both instances, an increased stromule frequency (Figure 5A). Average stromule frequency was approximately 23.4% for *trans*-zeatin and 38.6% for kinetin, which were significantly higher than in the NaOH control-infiltrated tissues, but significantly lower than the GVR positive controls, which were found to be close to 60%. Stromule length was also altered by the hormone treatment in a similar way as observed after bacteria treatments, showing a small, but significant increase in stromule length relative to control treatments (Figure 5B). As in tissue infiltrated with GV, GVR and LtZ strains, clustering of plastids around the nucleus was visible in *trans*-zeatin and kinetin treatments (Figure 5E and 5F), but again the efficiency of the DAPI staining was very low so PNAI could not be quantified. Starch also accumulated in a manner reminiscent of GV infiltrations, although staining was not as dark as after the bacterial treatments (Figure 5C and 5D). Although we infiltrated in a restricted region of the leaf (outlined in Figure 5C and 5D with dotted lines) dark starch staining was

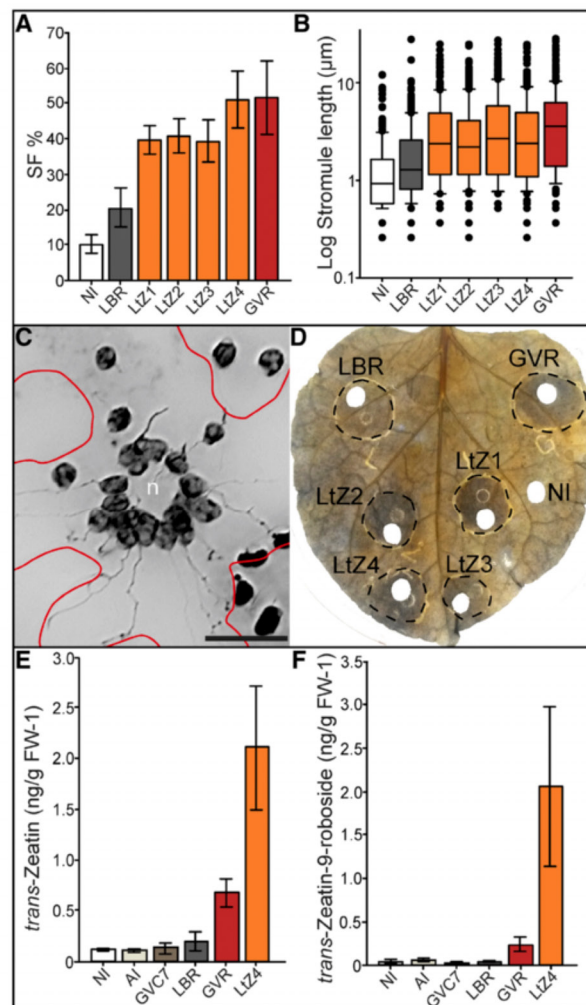


Figure 4 LBA transformed with 4.3 kb *tzs* gene from pMP90 induces a GVR-like phenotype. Four different LBA/pLSU-*ptzs-tzs* transformants (LtZ1-4) were infiltrated into the lower epidermis of three different *N. benthamiana* plants. **A** Bar graph of average stromule frequency (SF) in non-infiltrated (NI) LBR-infiltrated (LBR), LtZ-infiltrated (LtZ1-4) and GVR-infiltrated (GVR) tissue. Rank sum (NI-LtZ1, 2, 3, 4): $U=0$, $p<0.001$; (LtZ1-LBR, LtZ2-LBR): $U=7$, $p<0.001$; (LtZ3-LBR): $U=8$, $p<0.001$; (LtZ4-LBR): $U=4$, $p<0.001$; (LtZ1-GVR): $U=39$, $p=0.061$; (LtZ2-GVR): $U=40$, $p=0.069$; (LtZ4-GVR): $U=62$, $p=0.829$; (LtZ3-GVR): $U=32$, $p=0.039$. Sample sizes: $n(GV, NI, LtZ1, LtZ2)=12$, $n(LtZ3, LtZ4)=11$. Raw data were arcsine transformed and bars represent back-transformed means. Error bars represent back-transformed 95% confidence intervals. **B** Box plot representing median stromule lengths in non-infiltrated (NI) tissue, LBR-infiltrated (LBR), LtZ-infiltrated (LtZ1-4) and GVR-infiltrated (GVR) tissues. Rank sum (LtZ1-GVR): $U=54007$, $p<0.001$; (LtZ2-GVR): $U=51988$, $p<0.001$; (LtZ3-GVR): $U=53068.5$, $p=0.015$; (LtZ4-GVR): $U=50161$, $p<0.001$; (LtZ1-LBR): $U=38767$, $p<0.001$; (LtZ2-LBR): $U=39391.5$, $p<0.001$; (LtZ3-LBR): $U=33777$, $p<0.001$; (LtZ4-LBR): $U=35246.5$, $p<0.001$; (LtZ1-NI): $U=21007$, $p<0.001$; (LtZ2-NI): $U=21005$, $p<0.001$; (LtZ3-NI): $U=18181.5$, $p<0.001$; (LtZ4-NI): $U=19019.5$, $p<0.001$. Sample sizes: $n(NI)=235$, $n(LBR)=308$, $n(LtZ1)=360$, $n(LtZ2)=360$, $n(LtZ3)=330$, $n(LtZ4)=330$, $n(GVR)=360$. Boxes contain 50% of data, the median is represented by black line. Error bars represent 90% confidence intervals. **C** 'Stacked' fluorescence image of extreme clustering of plastids around the nucleus three days post-infiltration with LtZ4. The cell is outlined in red and the nucleus is indicated by 'n'. Image was converted to gray scale and inverted to better visualize plastids. Scale=20µm. **D** Iodine stained leaf three days after infiltration with GVR, LtZ strains 1-4, LBR and non-infiltrated control (NI). Infiltrated areas marked by a black dotted outline. **E** LC/MS/MS measurements of absolute *trans*-zeatin in fresh *N. benthamiana* leaf tissue 3 days post-infiltration with AIM buffer (AI), GVC7 (GVC7), LBR (LBR), GVR (GVR), and LtZ4 (LtZ4). Rank sum (GVR-NI, GVR-AI, GVR-GVC7, GVR-LBR, LtZ4-NI, LtZ4-AI, LtZ4-GVC7): $U=0$, $p=0.029$; (LtZ4-GVR): $U=0$, $p=0.029$. Sample size: $n=4$ for each. **F** LC/MS/MS measurements of absolute *trans*-zeatin-9-ribose in fresh *N. benthamiana* leaf tissue 3 days post-infiltration with AIM buffer (AI), GVC7 (GVC7), LBR (LBR), GVR (GVR), and LtZ4 (LtZ4). Rank sum (for all pair wise comparisons): $U=0$, $p=0.029$. Sample size: $n=4$ for each.

not limited to the infiltrated region, but spread to adjacent tissue, implying the spread of the hormone. In some cases this affected the non-infiltrated control

samples (Figure 5C) providing an explanation for the higher than average values of stromule frequency in the control treatments.

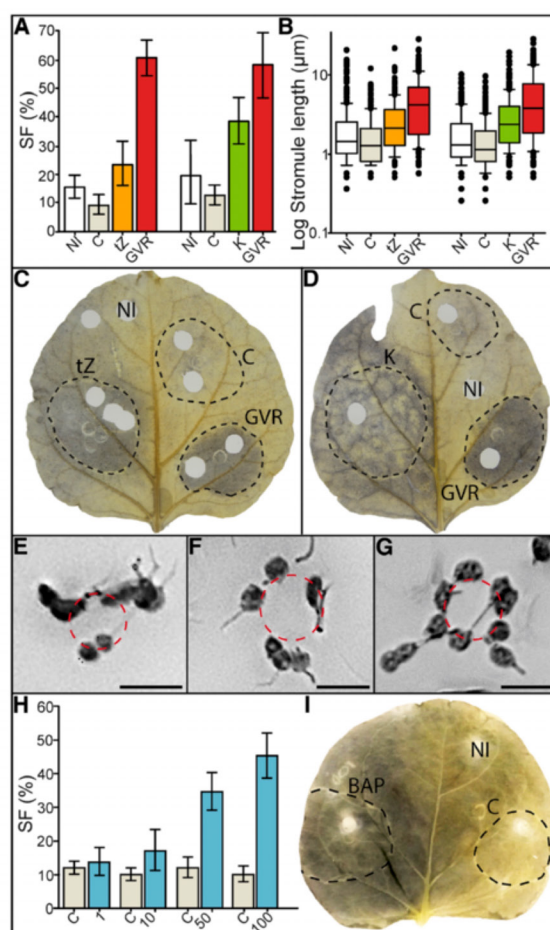


Figure 5 Treatment with *trans*-zeatin, kinetin or BAP mimics the effects of GVR infiltration. **A** Bar graph illustrating stromule frequency (SF) in non-infiltrated (NI), NaOH control-infiltrated (C), *trans*-zeatin-infiltrated (tZ), and kinetin-infiltrated (K) tissues. Rank sum for *trans*-zeatin infiltrated leaf (NI-C): $U=13$, $p=0.017$; (NI-GVR, C-GVR, tZ-GVR): $U=0$, $p<0.001$; (C-tZ): $U=12$, $p=0.013$; (tZ-NI): $U=20$, $p=0.077$. Rank sum for kinetin infiltrated leaf (NI-K): $U=13$, $p=0.017$; (NI-GVR): $U=13$, $p=0.001$; (C-K, C-GVR): $U=0$, $p<0.001$; (K-GVR): $U=11$, $p=0.01$, (NI-C): $U=27$, $p=0.251$. Sample size (consecutively): $n(\text{NI}, \text{C}, \text{tZ}, \text{NI}, \text{C}, \text{K}, \text{GVR})=9$, $n(\text{GVR on } \textit{trans}\text{-zeatin-infiltrated leaf})=8$. **B** Box plot representing median stromule lengths in non-infiltrated (NI), NaOH control-infiltrated (C), *trans*-zeatin-infiltrated (tZ) and kinetin-infiltrated (K) tissues. Rank sum for *trans*-zeatin-infiltrated leaf (NI-tZ): $U=24467$, $p<0.001$; (NI-GVR): $U=15101.5$, $p<0.001$; (C-GVR): $U=9931.5$, $p<0.001$; (C-tZ): $U=17141$, $p<0.001$; (tZ-GVR): $U=19279$, $p<0.001$; (tZ-NI, tZ-C): $U=23933.5$, $p=0.023$. Rank sum for kinetin-infiltrated leaf (NI-K): $U=18243$, $p<0.001$; (NI-C): $U=24938$, $p<0.001$; (NI-GVR): $U=14310.5$, $p<0.001$; (C-GVR): $U=11592.5$, $p<0.001$; (C-K): $U=14851$, $p<0.001$; (K-GVR): $U=23276.5$, $p<0.001$. Sample sizes (consecutively): $n(\text{NI})=256$, $n(\text{C})=213$, $n(\text{tZ})=249$, $n(\text{GVR})=240$ for the *trans*-zeatin-infiltrated leaf, and $n(\text{NI})=239$, $n(\text{C})=253$, $n(\text{K})=270$, $n(\text{GVR})=270$ for the kinetin-infiltrated leaf. Boxes contain 50% of data, the median is represented by black line. Error bars represent 90% confidence intervals. **C** Iodine stained leaf showing non-infiltrated (NI) regions as well as regions infiltrated with *trans*-zeatin (tZ), the NaOH control (C), and GVR (GVR). Infiltrated regions outlined with black dotted line. **D** Iodine stained leaf showing non-infiltrated (NI) regions as well as regions infiltrated with kinetin (K), the NaOH control (C), and GVR (GVR). Infiltrated regions outlined with black dotted line. **E-G** Plastids clustered around the nucleus in cells of the lower leaf epidermis following treatments with *trans*-zeatin (**E**), kinetin (**F**) and BAP (**G**), respectively. Images have been converted to gray scale and inverted for easier viewing of stromules. Bright field microscopy was used to locate nuclei and position was marked with red-dotted circles. Scale=20 μm . **H** Bar graph illustrating stromule frequency (SF) in NaOH control-infiltrated (C) and BAP-infiltrated (1, 10, 50, 100 $\mu\text{g ml}^{-1}$) tissues. Rank sum (C-1): $U=32$, $p=0.48$; (C-10): $U=13$, $p=0.017$; (C-50): $U=0$, $p<0.001$; (C-100): $U=0$, $p<0.001$. n (each treatment)=9. **I** Iodine stained leaf showing non-infiltrated (NI) NaOH control-infiltrated (C), and 100 $\mu\text{g ml}^{-1}$ BAP-infiltrated (BAP) regions. Infiltrated regions outlined with black dotted line. Starch staining spread throughout the leaf, extending beyond the infiltrated area. **A, H** Raw data were arcsine transformed and bars represent back-transformed means, and error bars represent back-transformed 95% confidence intervals.

3-fold infiltrations of kinetin and *trans*-zeatin were performed to counteract potential degradation of the cytokinins by the plant, which was suspected after single

infiltrations of 100 $\mu\text{g ml}^{-1}$ resulted in inconsistent stromule induction and starch accumulation after 2–3 days (data not shown). To minimize the influence of hormone

degradation, single infiltrations were performed using the synthetic cytokinin 6-Benzylaminopurine (BAP). This hormone is broken down much slower than other cytokinins when applied exogenously and can still be detected in plant tissue 6 weeks after infiltration [29]. A gradient of 1 $\mu\text{g ml}^{-1}$, 10 $\mu\text{g ml}^{-1}$, 50 $\mu\text{g ml}^{-1}$ and 100 $\mu\text{g ml}^{-1}$ BAP was infiltrated into tissue and stromule frequency was evaluated. At only 2 days post-infiltration there was a significant induction of stromules at all concentrations except 1 $\mu\text{g ml}^{-1}$, which was comparable to the control infiltration (Figure 5H). 100 $\mu\text{g ml}^{-1}$ BAP-infiltrated tissue had an average SF value of 45%, a SF comparable to that of GV and GVR evaluated at 3 days post-infiltration (compare Figure 5H to Figures 1C, 2E, 3B, 4A). Plastids were also seen to form clusters around nuclei (Figure 5G) and extensive starch staining (Figure 5I), similar to observation made following hormone infiltration and treatment with *tzs* containing bacterial strains. Although the physiological symptoms induced following bacterial infiltrations are not as severe, it appears that direct infiltration with cytokinin is capable of mimicking the effects of *tzs* expression by *A. tumefaciens*.

Discussion

Stromules are induced under a wide range of biotic and abiotic stresses, and based on our previous observation that the number of stromules increases following infiltration of GVR into *N. benthamiana* leaf tissue [10], we suspected this phenotype may be indicative of cellular changes during *Agrobacterium*-mediated transient assays. Under conditions typical of transient assays ($\text{OD}_{600} = 0.8$, microscopy 2–3 days post-infiltration) we confirmed the previously reported stromule induction by GV3101 (pMP90) (GV) and found that GV triggers alterations to plastid position and starch accumulation. The use of transient assays assumes that the cells observed are displaying authentic sub-cellular behaviour, but these significant changes in chloroplast morphology, position and carbohydrate content indicate that cells assumed to be 'normal' might actually be very different from non-infiltrated neighbouring tissue. The determination of the 'inducing agent' responsible for such cellular changes was imperative to understanding the magnitude of GV's impact on plant physiology within transient systems. Based on the observation that infiltrated tissue was displaying symptoms characteristic of increased cytokinins, such as the formation of green islands during senescence and increased starch accumulation, we performed experiments to determine if this was the 'inducing' agent responsible for the plastid related changes observed.

Agrobacterium strain dependant secretion of cytokinins correlates with stromule induction and starch accumulation

Wild type *A. tumefaciens* strains are known to harbour cytokinin synthesis genes, which are transferred with the

T-DNA to the plant cell forcing transformed cells to produce cytokinins. In the course of disarming the wildtype *A. tumefaciens* strains for laboratory use, the tumor inducing T-DNA was removed from the wildtype Ti-plasmid, thus removing the ability of the bacteria to induce cytokinin production by the plant. However, some *A. tumefaciens* strains, such as C58 (the wild type ancestor of GV), are capable of secreting a significant amount of cytokinin, specifically *trans*-zeatin, into the culture medium even in the absence of plant cells (concentrations of up to 35 μM measured by [30]). Cytokinin accumulation in culture was found to be the direct result of the activation of the *tzs* (*trans-zeatin synthase*) gene [30], an isopentenyl transferase (IPT) gene situated outside of the wild type T-DNA boundaries, in very close proximity to the *vir* region of the Ti plasmid [30,31]. The *tzs* gene was not removed during the creation of the disarmed Ti-plasmid pMP90 [17] harbored by GV [32]. The ability of GV cells to stay viable in leaf tissue for more than two weeks after infiltration [9], coupled with our observation that infiltrated tissue developed strong physiological symptoms characteristic of high cytokinin levels (Figure 2H and 2K), suggests that GV is also a constant and significant source of cytokinin in plant tissue in the days following infiltration. In support of this hypothesis LC-MS/MS measurements indicated the accumulation of *trans*-zeatin in GV-infiltrated tissues (Figure 4E).

In contrast to GV, we found that LBA (LBA4404), which is an octopine strain, does not induce the same level of starch accumulation (Figure 2K), the green island phenotype (Figure 2H), or any significant increase in either *trans*-zeatin or its riboside (Figure 4E, 4F). This is in line with previously published data suggesting that octopine strains lack the *tzs* gene on their Ti-plasmids, and are thus incapable of secreting high levels of *trans*-zeatin in culture [30,32].

Evidence supporting the role of the *tzs* gene in the production of the 'inducing agent' responsible for altering plastid-based parameters came from our curing of GV, which resulted in a drastic decrease in cytokinin indicators and stromule induction. More definitive evidence for the causal link between *tzs* derived cytokinin and stromule induction was derived from the cloning of *tzs* into pLSU and transformation into LBA. The resulting strains (LtZ1-4) increased stromule frequency, stromule length and dark starch staining reminiscent of GV and GVR infiltrations. Additionally, all these symptoms were correlated with an increase in both *trans*-zeatin and its riboside within infiltrated tissues, confirming that the cloned *tzs* gene was functional. The 'gain-of-function' phenotype of LBA following addition of a single gene, *tzs*, defines a role for this gene in the production of bacteria-derived cytokinins as well as significant changes to the cell.

After establishing causality between the *tzs* gene and alterations to plastids via the generation of the LtZ strain, causation between cytokinins themselves and the effects observed was established via direct infiltration with three different cytokinins, *trans*-zeatin, kinetin and BAP. Infiltrated cytokinins were found to influence plastid morphology and starch accumulation, but our ability to produce the same magnitude of change as that induced by *tzs* containing *A. tumefaciens* strains was limited. We suggest several possible explanations for this. The first being that it was very difficult to assess what concentration of hormone should be used in our infiltrations, as it was very difficult to determine the amount of cytokinin the bacteria produced to elicit the given response in plant tissue. *A. tumefaciens* anchors to the plant cell wall during infection [33], and secretion of the cytokinin by the immobilized bacteria would likely lead to a highly localized accumulation of cytokinin and a non-homogeneous distribution of hormone within the plant tissue. In addition, free-base cytokinins (like *trans*-zeatin) preferentially accumulate in the chloroplast, leading to the non-uniform distribution of hormone at the cellular level, further hindering the ability to determine their concentration at their point of action [34]. Thus, although our method of measuring whole leaf homogenate provides a good first estimation of the changes in *trans*-zeatin induced by *A. tumefaciens*, it could lead to the underestimation of the absolute amount of cytokinin required to elicit the observed changes to plant physiology. The second problem we faced in attempting to infiltrate hormones directly was that single infiltrations with *trans*-zeatin or kinetin did not consistently induce stromules or starch staining, suggesting their possible inactivation. Cytokinin oxidases, important cytokinin inactivators [35], are actually known to be up-regulated by the presence of the hormone itself [35,36], meaning that upon infiltration with cytokinins we could simultaneously have triggered their increased inactivation. The third issue was the possible diffusion of infiltrated hormones away from the infiltration zone, as indicated by extensive starch staining of infiltrated leaves (Figure 5C, 5D and 5I). This likely resulted in a decrease in the concentration of the hormone in the infiltrated region and additionally prevented us from controlling the amount of hormone in the infiltration zone. Although we could not prevent hormone diffusion, we have used BAP as an alternative to *trans*-zeatin and kinetin in infiltrations, due to an increased resistance to degradation [29]. A gradient of BAP showed that single infiltrations of the hormone with concentrations as low as 10 $\mu\text{g ml}^{-1}$ were capable of significant stromule induction at only two days post-infiltration (Figure 5H). It should be noted that the concentration of *trans*-zeatin measured in the supernatants of C58 cultures by Powell et al. [30] was

comparable to this value (35 $\mu\text{M} = 7.67 \mu\text{g ml}^{-1}$). Increasing concentrations of the hormone (1–100 $\mu\text{g ml}^{-1}$) resulted in a corresponding increase in stromule number, thus causally linking the hormone and the formation of these protrusions from the plastid body.

The expression of the *tzs* gene increases the abundance of multiple cytokinin species

Multiple infiltrations with pure *trans*-zeatin indicated that this hormone is sufficient to mimic the effects of *tzs* expression by the bacteria and induce changes to plastid morphology and position. However, it is important to note that the expression of the *tzs* gene is known to increase the abundance of other cytokinins [37], which could also influence the measured plastid parameters. The *tzs* gene product exhibits catalytic activity specific to both HMBDP (precursor of *trans*-zeatin-type cytokinins) and DMAPP (precursor for iP-type cytokinins) substrates, meaning that this enzyme is capable of acting in multiple cytokinin biosynthesis pathways that produce multiple cytokinin species [37]. The cloning of the C58 *tzs* gene into *E. coli* and subsequent measurements of cytokinins secreted into culture fluids showed that although the increase in *trans*-zeatin was the most obvious (from 11 ngL^{-1} before *tzs* added to 19,900 ngL^{-1} after the addition), there was also a increase in *iso*-pentenyladenine (iP)-type cytokinins (from 120 to 8,700 ngL^{-1}), *trans*-ribosylzeatin (from <1 to 236 ngL^{-1}) and *iso*-pentenyladenosine (iPA)-type (25 to 85 ngL^{-1}) cytokinins [27]. The sensitivity of the cell to the different species seems to depend largely on the ligand preference of the cytokinin receptors present [38,39]. Based on data from *Arabidopsis* and maize it seems that iP and *trans*-zeatin are most often preferred [38,39], but the sensitivity of *N. benthamiana* receptors is unknown. For this reason, although we can say that cytokinins are changing plastid morphology, at this point we cannot speculate further as to which product of the *tzs* gene has the greatest influence on the measured parameters.

Exposure to *tzs*-derived cytokinins alters cell physiology

Our experiments establish that GV and other *tzs* containing strains are a constant source of significant amounts of cytokinin when infiltrated into leaf tissue, and that this is the cause for the observed changes to plastid morphology in the relatively short time-scale of transient assays. Previous studies have also observed changes to chloroplast structure following exposure to elevated cytokinins. For example, the formation of crystalloids or an 'amoeboid-like' morphology is characteristic of plastids in the leaves of stable transgenic tobacco overexpressing cytokinin synthesis genes [34,40]. Although we never observed crystalloids, the description of the 'amoeboid-like' plastid structure is reminiscent of

our observations of multiple stromules emanating from a single plastid body. Thus, it seems that, although the exposure of plants to *tzs*-derived cytokinins is limited to a few days in the transient assay system, the physiological changes triggered by this short exposure are significant enough to favour the alteration of the plastid membrane in a manner similar to long term exposure.

We have shown that the short duration of GV-based transient assays is also sufficient to induce changes in carbohydrate content, as evident by an increase in starch and soluble sugar (sucrose and glucose) content in infiltrated tissue. This finding is concurrent with literature reports that implicate cytokinins in the regulation of tissue carbohydrate status and carbohydrate partitioning, thereby influencing the source/sink status of a tissue (reviewed in [25,26,41]). This suggests that during a typical transient assay the secretion of *tzs*-derived cytokinins may be significant enough to switch the carbohydrate status tissue from a source to a sink.

The formation of stromules has been frequently observed in tissues considered to be sinks for carbohydrates [42]. This idea is supported by the work of Schattat and Klösgen [43], which showed that treatment with exogenous glucose and sucrose induced stromules in *Arabidopsis thaliana* upper leaf epidermis. This could suggest that the observed stromule induction is a consequence of elevated soluble sugar levels induced by *tzs* cytokinins. However, in contrast to *A. thaliana*, the increases in soluble sugars were not as clearly correlated with an increase in stromule frequency. Despite the absence of the *tzs* gene in LBR, there was a significant increase in soluble sugars that was accompanied by only very small changes to stromule frequency relative to non-infiltrated treatments (Figure 2E, 2I and 2J). Although the increase in sugar level was more pronounced in GVR-infiltrated tissues, a direct connection between elevated sugar and altered plastid morphology in *N. benthamiana* remains to be established.

Plastid relocation appears independent of stromule formation

The intermediate phenotype of LBR observed during sugar measurements was also observed when PNAI was measured. In contrast to stromule induction, relocation of plastids to the nucleus was not completely abolished in strains lacking the *tzs* gene (LBR or GVC), which resulted in intermediate or GV-like phenotypes (Fig 2G). Plastid proximity to the nucleus and the incidence of stromules has often been discussed as though these two phenomena are functionally related [44-46]. However, clustering of plastids around the nucleus has been reliably observed preceding cell division, and is suggested to ensure unbiased organelle inheritance [47], and this phenomenon may be unrelated to the formation of stromules. It has

long been known that treatment with a very minimal amount of exogenous cytokinin ($1\mu\text{g L}^{-1}$) is capable of inducing cell division in tobacco tissue culture [48]. We found that single treatments with *trans*-Zeatin (100 mg ml^{-1}) induces plastids to reliably cluster around the nucleus (data not shown), a treatment that did not reliably induce stromules, suggesting that plastid position seems to be independent of stromule formation, and possibly more sensitive to the hormone. A higher sensitivity of PNAI to cytokinins could offer one explanation for the frequent association of plastids with nuclei in some LBA and cured treatments, which occurred in conjunction with low levels of stromule induction.

Are stromule induction, starch accumulation and plastid relocation pathogen related responses?

Our experiments are not the first to elucidate the effect of disarmed *A. tumefaciens* strains on infiltrated leaf tissue. In two other studies, which focused on plant-pathogen interactions, it was found that infiltration of tobacco with standard disarmed laboratory strains (including GV3101 (pMP90)) interferes with subsequent infections with tobacco mosaic virus (TMV) and *Pseudomonas syringae* [8,9]. In addition to reducing infection symptoms, infiltration of 'disarmed' *Agrobacterium* strains altered the expression of pathogen responsive gene PR-1 (pathogen related 1), induced chlorosis, inhibited leaf expansion and reduced ABA levels and SA production induced by *P. syringae* [8,9]. Cells cured of the Ti-plasmid elicited these responses to nearly the same extent as the original strains, leading the authors of both studies to the conclusion that these pathogen related responses occur independent of Ti-plasmid encoded gene products [8,9]. In contrast to these Ti-plasmid independent phenotypes, we found stromule formation, plastid relocation and starch accumulation to be highly dependent on Ti-plasmid derived cytokinins. Although we cannot exclude that *Agrobacterium*-derived factors might modulate the induction of these processes to some extent, the fact that we were able to mimic the infiltration of *tzs* harbouring bacteria with hormone solutions shows that other bacteria-derived factors are not essential to induce the observed reactions. Therefore it seems most likely that stromule formation is not a result of a pathogen specific reaction of the cells.

Evaluating *Agrobacterium*-mediated transient assays

GV is a favoured laboratory strain, likely due to its high transformation efficiency. In most protocols the bacteria is adjusted to an OD of 0.8, as we did in our experiments, however lower densities have been found to yield sufficient expression of transgenes [49]. This leads to the hypothesis that lowering the concentration of bacteria used during GV-based experiments might reduce the adverse effects of this particular strain, while maintaining a

sufficient amount of transient gene expression. Using the induction of stromules as a 'bio-indicator' for cytokinin accumulation, we have briefly tested whether there is a concentration of GVR where we observe the transgene, but do not observe stromules. Preliminary results indicate that even at an OD₆₀₀ of 0.01, when very little DsRed2 was detected, GVR can still induce SF values close to 30% 3 days post-infiltration (data not shown). Suggesting that despite a drastic decrease in the amount of bacteria, cytokinin still accumulates to a level sufficient to induce changes to the plastid. Using stromules as an indicator, the viability of this strategy could be further tested for highly expressed and stable transgene products. This may allow for the reduction of the OD to a level where stromules are no longer induced but the visibility of the proteins is maintained.

An alternative strategy to lower the impact of the bacteria-born cytokinins is to limit exposure time by analysing tissue as soon as expression of the transgene is detectable. However studies in *Arabidopsis* have revealed the impact of cytokinin on gene expression and the proteome is widespread and immediate [50-52]. For example, treatment of seedlings with 5 μ M exogenous cytokinin results in the differential expression of 82 genes [50] and the differential regulation of 96 proteins within the first 15 minutes [52]. Most of the proteins were localized to the chloroplast (52%), but others were predicted to localize to the cell wall, cytoplasm, ER, nucleus, mitochondria, and vacuole [52]. Although such responses must be evaluated for *N. benthamiana* in the context of transient experiments, it appears that even short-term exposure to low levels of hormone have the potential to affect the composition of multiple cellular compartments, and the influence of bacteria-derived cytokinins during transient assays may be much more extensive than originally hypothesized.

In addition to changing parameters of the infiltration and analysis protocol, an obvious solution is to use an *A. tumefaciens* strain that is devoid of the *tzs* gene. Thus the LBA strain, which lacks the *tzs* gene, may be more appropriate for use in a transient system. However, even this strain induces weak changes to chloroplast morphology, position, and soluble sugar levels. This is most likely due to the accumulation of additional cytokinin species. Both nopaline (e.g. GV and GVR) and octopine *A. tumefaciens* strains (e.g. LBA and LBR) secrete iP, and the production of this cytokinin continues in both strains even after the removal of the Ti-plasmid [31]. Although our data suggests that the largest impact of *A. tumefaciens* is the result of strain-dependant secretion of *tzs*-born cytokinin, other bacterial factors should not be discounted when interpreting the results of transient assays. The variable impact of different bacterial strains observed here highlights the need for appropriate

controls that evaluate the impact of each bacterial strain on the process under observation.

Conclusion

There is no denying that *Agrobacterium*-mediated transient assays provide a valuable tool for the investigation of protein localization and gene expression in the context of living cells. However, whether the cells visualized during these assays represent 'normal' cells has been called into question. We have reported that drastic changes to chloroplast shape, position, and carbohydrate status are the result of the strain-dependant secretion of cytokinin into plant tissue by the bacteria. Although we have only examined the effect of transient *A. tumefaciens* infestation on one organelle, altered plastid shape and starch content are indicative of an effect on the physiology of the entire cell. We emphasize the importance of designing appropriate controls to test the influence of the bacteria on the structures under observation, as well as confirming transient assay results via the generation of stable transgenic lines when possible.

Methods

Plant material and growth conditions

Plant material was grown on soil under short day conditions (8 h light/16 h dark) at a temperature of approx. 20°C (day and night) and a light intensity of approx. 120 μ E m⁻². Infiltrations were performed in the third or fourth leaf of four to six week old plants grown on soil. For visualization of plastids and stromule morphology transgenic *N. benthamiana* lines expressing a stroma targeted eGFP were used (generation of plants lines described in [10]); chimeric FNR-EGFP described in [15]. To rule out the possibility that observed effects are caused by T-DNA insertion in a certain region of the genome of transgenic plants all experiments were performed in three independent transgenic lines (FNR-EGFP_7-25; FNR-EGFP_6-24; FNR-EGFP_3-20) originating from independent transformation events.

Bacterial strains and culture

Agrobacterium strains used for experiments are listed in Table 1. Both GV [17] and LBA [53], were transformed by electroporation (Bio-Rad, *E.coli* Pulser) with the T-DNA vector pCP60-35S-DsRed2 source described in [10]. This vector harbours a 35S-promotor driven expression cassette expressing untagged DsRed2, and confers resistance to kanamycin in bacteria. *A. tumefaciens* strains were grown on YEB agar plates or YEB liquid medium according to [54] and were supplied with the respective antibiotics (rifampicin 100 μ g ml⁻¹; gentamycin 20 μ g ml⁻¹; kanamycin 100 μ g ml⁻¹; streptomycin 100 μ g ml⁻¹) (Duchefa Biochemie, Haarlem, Netherlands).

Curing GV3101(pMP90)

In order to cure the *A. tumefaciens* strain GV3101 (pMP90) of its Ti-plasmid (pMP90) a modified protocol based on the method described by Engler et al. [55] was used. To cure GVR we grew streaks of single colonies on YEB plates at 37°C for a period of 5 days. The plates contained kanamycin and rifampicin. Gentamycin resistance is specified by the Ti-plasmid, and so was not included in the media, thus eliminating pressure to retain the plasmid (summary of strain antibiotic resistance in Table 1). For selection of cured GV3101 (absence of pMP90) 30 single colonies were picked and transferred to two plates harbouring different antibiotic combinations, one with kanamycin/rifampicin and one with kanamycin/rifampicin/gentamycin, and allowed to grow at room temperature. 12 out of 30 picked colonies showed no growth on gentamycin containing plates after 7 days, indicating potential curing, 3 of these are shown in supplementary Additional file 1: Figure S1A. 4 out of these 12 strains were tested for the presence of the *tzs* gene via PCR (Additional file 1: Figure S1B) with primers specific to the *tzs* gene (Additional file 2: Table S1). Primers specific to the nptIII gene (Additional file 2: Table S1) of the pCP60-35S-DsRed2 acted as a positive PCR control (Additional file 1: Figure S1B), as this vector should have been retained during the curing process (primers from Eurofins MWG Operon, Ebersberg, Germany). As an additional check three of these were chosen for infiltration into *N. benthamiana* and the lower epidermis of screened for expression of DsRed2 using a confocal microscope. Cured lines, presumably lacking the virulence genes contained on the Ti plasmid, were not capable of facilitating DsRed2 expression in plants (Additional file 1: Figure S1E and S1G).

Cloning *tzs* from GV and transformation into LBA

A 4.3 kb fragment including the *tzs* coding region and approximately 2 kb upstream and 1.7 kb downstream was amplified using primers specifically designed for RF cloning (described by [56]) of the fragment into the pLSU binary vector (*tzs*4kb_pLSU_F:gctagcgcgcggacaagctaggattggctcaggcagcttcgcagcgaac, *tzs*4kb_pLSU_R: ttgagacacaacgtggatctaattgctgatagaggagaccagagtaact). RF cloning was followed by transformation into DH5 α and selection on LB containing kanamycin, DNA from four different colonies was isolated and transformed into LBA. Resistant LBA colonies were tested via PCR for the presence of *tzs* using primers internal to the *tzs* coding region (Refer to Additional file 2: Table S1).

Infiltration of *Agrobacterium* into *N. benthamiana* leaves

Infiltrations were carried out according to standard transient expression protocols. 1 ml of the bacterial 'over night' culture was pelleted, re-suspended and allowed to incubate in the acetosyringone (Sigma-Aldrich, Deisenhofen,

Germany) containing infiltration media (AIM consisting of 10 mM MgCl₂, 5 mM MES pH 5.3 (both from Roth, Karlsruhe, Germany) and 150 μ M acetosyringone) prior to infiltration. Following 2 h incubation the optical density of the suspension was adjusted to OD_{600nm} = 0.8. AIM alone (buffer control) and the *A. tumefaciens* strains were infiltrated into the bottom side of the third or fourth leaf of 6–8 week old *N. benthamiana* plants with a needleless syringe. To allow for better comparison between the results of independent infiltrations in different leaves, we infiltrated one half of the leaf with the control and the other half with the treatment. After 48–72 hrs leaf discs of the infiltrated areas, as well as a non-infiltrated control were harvested and the lower leaf epidermis was observed using an epifluorescence microscope or confocal microscope.

Staining and tissue preparation for microscopy

To stain nuclei of *N. benthamiana*, leaf disks were incubated in 20 μ M DAPI (Roth, Karlsruhe, Germany) for 10 minutes.

For visualising starch, leaves were excised from plants and placed in petri-dishes containing 100% ethanol (Roth, Karlsruhe, Germany) where they were allowed to de-stain overnight at room temperature. Once fully bleached, leaves were rinsed with water, and 6 mL iodine (Roth, Karlsruhe, Germany) was added to stain starch. After 30 min - 1 hr stained leaves were rinsed and excess stains was removed via suspension of leaves in water for 4–5 hrs at room temperature.

Measurement of sucrose and glucose concentration

For glucose and sucrose measurements of non-infiltrated, buffer-infiltrated (AIM), as well as bacteria-infiltrated tissue, treatments were administered as described previously. For biological and experimental replicates 3 leaves (3rd, 4th and 5th) of 7 plants were infiltrated. Each leaf was infiltrated with AIM on one half and the other half went untreated or was infiltrated with one of the bacteria strains. After 48 hours leaf disks were harvested and frozen in liquid nitrogen. Sucrose and glucose quantification was performed as described in [57].

Cytokinin measurements

Frozen plant material was homogenized to a fine powder with a mixer mill MM301 (Retsch, Haan, Germany) at a frequency of 25 s⁻¹ for 50 s with a single 5 mm diameter steel bead in a 2 ml Eppendorf tube. The resulting powder was extracted with 200 μ l methanol containing 5 ng each of [²H₅]trans-zeatin and [²H₅]trans-zeatin 9-riboside (OlChemIm Ltd. Olomouc, Czech Republic) as internal standards. After vigorous shaking for 20 min, the slurry was centrifuged twice at 10,000 g for 5 min. The final supernatant was diluted with 800 μ l aqueous formic acid solution (2% v/v) and subjected to solid phase extraction

(SPE). The SPE 96-well plate was prepared by distributing dry HR-XC-resin (Macherey-Nagel, Düren, Germany) into the wells of a 96-well filtration plate (50 mg per well). The resin was conditioned by 1 ml of methanol followed by 1 ml of water. In this and all subsequent steps, the liquid was passed through the resin by centrifugation at 250xg for 5 min using a JS5.3 swing-out rotor in an Avanti J-26XP centrifuge (Beckman Coulter, Fullerton, CA, USA). After loading the samples, the resin was washed with 1 ml of water, followed by 1 ml of methanol and eluted with 0.35 M NH₄OH in methanol into a 96 deep well plate (Roth, Karlsruhe, Germany). The eluates were transferred to 2 ml Eppendorf tubes and the solvent was evaporated under vacuum in Savant SC210A Speed Vac Concentrator at 45°C (ThermoFisher Scientific, Waltham, MA, USA). The dry residue was dissolved in 40 µl 10% (v/v) methanol. After dilution with 40 µl of water and centrifugation at 10,000 g for 10 min, the samples were transferred to auto-sampler vials for LC-MS/MS analysis.

Separations were performed on a Nucleoshell RP18 column (50 × 3 mm, particle size 2.7 µm; (Macherey-Nagel, Düren, Germany) at 30°C using an Agilent 1290 Infinity HPLC system. Eluents A and B were water and acetonitrile, respectively, each containing 0.2% (v/v) acetic acid. After an initial hold at 2% B for 0.5 min, the percentage of B was increased to 28% over 3 min, further increased to 98% in 0.5 min followed by an isocratic period of 1.5 min at 98% B. The starting conditions were restored within the next 0.5 min, and the column was allowed to re-equilibrate for 1 min at 2% B. The flow rate was set to 0.5 ml/min. The analytes were detected on-line by ESI-MS/MS using an API 3200 triple-quadrupole LC-MS/MS system equipped with an ESI Turbo Ion Spray interface, operated in the positive ion mode (AB Sciex, Darmstadt, Germany). The ion source parameters were set as follows: curtain gas: 50 psi, ion spray voltage: 3500 V, ion source temperature: 650°C, nebulizing and drying gas: 70 psi and 50 psi, respectively. Triple quadrupole scans were acquired in the multiple reaction monitoring mode (MRM) with Q1 and Q3 set at “unit” resolution. Scheduled MRM was performed with a window of 90 s and a target scan time of 0.1 s. Selected MRM transitions and compound specific parameters are given in Supplemental Additional file 3: Table S2.

Peak areas were calculated automatically using the IntelliQuant algorithm of the Analyst 1.6.2 software (AB Sciex, Darmstadt, Germany) and manually adjusted if necessary. All subsequent calculations were performed with Excel (Microsoft Office Professional Plus 2010). Hormones were quantified using the internal standards.

Hormone treatments

Stock solutions of *trans*-zeatin and kinetin (both from Duchefa Biochemie, Haarlem, Niederlande) were made

by first dissolving powdered hormone in 0.5 mL 1 N NaOH (Roth, Karlsruhe, Germany). These stock solutions were then used to prepare the 100 µg ml⁻¹ working solutions that were used for subsequent infiltrations. A control infiltration was performed that contained NaOH solution at the same concentration (2.28 mM NaOH) as in the treatment condition (basic solution used to increase solubility of hormones). *trans*-zeatin and kinetin were administered with a needleless syringe via the same method outlined for *A. tumefaciens* infiltration. Solutions were infiltrated 3 times into the same area of the leaf over the course of 3 consecutive days, and microscopy was performed 2 days after the final infiltration. The procedure was the same for BAP gradient infiltrations (1, 10, 50 and 100 mg L⁻¹), except that infiltrations were performed only once, with microscopy completed 2 days post-infiltration. Infiltrated control solutions contained NaOH in same concentration as in treatment condition.

Microscopy and image processing

Confocal microscopy was performed with an Axiovert mot LSM 510 from Carl Zeiss GmbH, Jena, Germany. DsRed2 and chlorophyll were imaged simultaneously in separate channels. DsRed2 was excited by a 543 nm laser line and the emitted light was filtered by a 560 – 615 nm band pass filter. Chlorophyll fluorescence was excited by a 633 nm laser line and the emitted fluorescence was filtered by a 650 nm long pass filter.

Epifluorescence images were taken with a non-motorised Axioskop2 Zeiss GmbH, Jena, Germany equipped with an Axiocam HRc CCD-Camera (Carl Zeiss, Jena, Germany). Fluorescence illumination was realised with an HBO100 Lamp house equipped with a mercury light bulb (HBO 100 W/2 from Osram, Munich, Germany). EGFP, DsRed2 and DAPI were imaged using the following filter from AHF-Analysetechnik (Tübingen, Germany): DsRed/GFP (F51-019), DsRed (F46-005), endowGFP (F41-017), DAPI/GFP (F51-012).

Image processing and image analysis

Epifluorescence images were taken as z-stacks. The series of images was exported as a set of individual ‘.tif’ files. The exported images were sharpened in Adobe Photoshop CS6 by applying an unsharpen mask to the single images. Images of one z-stack were subsequently flattened to obtain single images with an extended depth of focus. For the stacking process the free software package CombineZPBatch [58] was utilized, as outlined in [59]. For presentation purposes Epifluorescence images were converted to black and white, and inverted, allowing for better viewing of stromules on printed media. Therefore dual-band filter set images lose their colour difference of DAPI stain or DsRed2 to eGFP. However

the nucleus can still easily be identified in the images due to its size and position.

Stromule number, stromule lengths and the association of plastids with the nucleus were counted using the 'cell counter' plugin and the 'measure' feature of Fiji [60]. Counts and length measurements were made per image neglecting plastids in guard cells. For stromule frequency every fully imaged epidermal plastid was counted. The mean stromule frequency for each treatment represents an average of counts from 9 different images ($n = 9$), each containing approximately 250–350 plastids (each treatment is represented by 2000 to 3000 plastids). For stromule length measurements 30 stromules were measured per image. In order to avoid biased measurements, stromules were measured in a rectangle in the upper left corner of the respective images. We considered the formation of short stromule branches as being independent from the elongation of the main stromule body. Based on this assumption stromule measurements were made on the longest stromule branches.

Statistical analysis

For each treatment three different plants from three independent FNR-EGFP lines (3, 6, and 7) were infiltrated, and one disk was punched from the infiltrated region. 3 images were taken per leaf disk, for a total of 9 images. Due to similarity between data sets from the different plant lines the data of the repeats were pooled. Stromule frequency (SF%) represents the proportion of plastids with one or more stromules. For calculation of SF% the number of plastids with stromules was counted and divided by the total number of plastids. The resulting data was arcsin transformed, and statistical analysis was performed on the transformed data. 95% confidence intervals and arithmetic averages were calculated, and back-transformed data was represented in bar graphs (transformations completed using Excel). We introduced PNAI to describe the absolute number of plastids in close association with a given nucleus. Stromule length and PNAI were represented as medians and box plots to better show the distribution of the data.

Glucose and sucrose concentration were obtained from 7 leaves ($n = 7$) per treatment. In each case the AIM control was infiltrated into the same leaf as one of the treatments, AIM and treatment conditions of each of the 7 leaves was pooled and averaged (arithmetic average). To describe variance the standard deviation was calculated and T-tests were performed to compare normally distributed data, while the Mann–Whitney Rank Sum Test was used to compare data that failed a Normality Test, or Equal Variance Test. Comparisons were made between AIM and treatment conditions administered to the same set of leaves. Sigma Plot was used for statistical analysis of all data.

Additional files

Additional file 1: Figure S1. Evidence of successful curing of GVR of (pMP90).

Additional file 2: Table S1. Primers for amplification of *tzs* and *nptII*.

Additional file 3: Table S2. MS parameters for MRM-transitions.

Competing interests

The authors declare that they have no competing interests.

Authors' contributions

JLE and MHS were responsible for experimental design, analysis, and wrote the article; JZ performed hormone measurements under the supervision of SA; DG performed sugar measurements under the supervision of SJR; JM and RBK contributed advice on the manuscript and technical support.

Acknowledgements

We would like to acknowledge Sarah Griffiths, and Sebastian Schornack for reviewing early versions of the manuscript and providing valuable advice.

Financial sources

Research was funded through grants from the Natural Sciences and Research Council of Canada to S.J.R. and J.M. Additional funding was provided to J.M. through the Canada Foundation for Innovation, and the Ministry of Research and Innovation, Ontario. The contributions by J.Z. and S.A. were funded by the Leibniz Association (SAW-PAKT 2011–2015). Funding for M.H.S. is provided by EFRE funds of the EU.

Author details

¹Abteilung Pflanzen Physiologie, Institut für Biologie-Pflanzenphysiologie, Martin-Luther-Universität Halle-Wittenberg, Weinbergweg 10, Halle/Saale 06120, Germany. ²Abteilung Molekulare Signalverarbeitung, Leibniz-Institut für Pflanzenbiochemie, Weinberg 3, Halle/Saale 06120, Germany. ³Present Address: Pioneer Hi-Bred, 12111 Mississauga Rd, Georgetown, ON L7G 4S7, Canada. ⁴Department of Molecular and Cellular Biology, University of Guelph, Guelph, ON N1G 2 W1, Canada.

Received: 26 November 2013 Accepted: 24 April 2014

Published: 9 May 2014

References

- McCullen CA, Binns AN: *Agrobacterium tumefaciens* and plant cell interactions and activities required for interkingdom macromolecular transfer. *Annu Rev Cell Dev Biol* 2006, **22**:101–127.
- Escobar MA, Dandekar AM: *Agrobacterium tumefaciens* as an agent of disease. *Trends Plant Sci* 2003, **8**:380–386.
- Gelvin SB: *Agrobacterium*-mediated plant transformation: the biology behind the "gene-jockeying" tool. *Microbiol Mol Biol Rev* 2003, **67**:16–37.
- Zhu J, Oger PM, Schrammeijer B, Hooykaas PJJ, Farrand SK, Winans SC: The bases of crown gall tumorigenesis. *J Bacteriol* 2000, **182**:3885–3895.
- Hellens RP, Edwards EA, Leyland NR, Bean S, Mullineaux PM: **pGreen: a versatile and flexible binary Ti vector for *Agrobacterium*-mediated plant transformation.** *Plant Mol Biol* 2000, **42**:819–832.
- Lee L-Y, Gelvin SB: T-DNA binary vectors and systems. *Plant Physiol* 2008, **146**:325–332.
- Kuta DD, Tripathi L: *Agrobacterium*-induced hypersensitive necrotic reaction in plant cells: a resistance response against *Agrobacterium*-mediated DNA transfer. *Afr J Biotechnol* 2005, **4**:752–757.
- Rico A, Bennett MH, Forcat S, Huang WE, Preston GM: **Agroinfiltration reduces ABA levels and suppresses *Pseudomonas syringae*-elicited salicylic acid production in *Nicotiana tabacum*.** *PLoS One* 2010, **5**:e8977.
- Pruss GJ, Nester EW, Vance V: **Infiltration with *Agrobacterium tumefaciens* induces host defense and development-dependent responses in the infiltrated zone.** *MPMI* 2008, **21**:1528–1538.
- Schattat MH, Griffiths S, Mathur N, Barton K, Wozny MR, Dunn N, Greenwood JS, Mathur J: **Differential coloring reveals that plastids do not form networks for exchanging macromolecules.** *Plant Cell* 2012, **24**:1465–1477.

11. Hanson MR, Sattarzadeh A: **Dynamic morphology of plastids and stromules in angiosperm plants.** *Plant Cell Environ* 2008, **31**:646–657.
12. Gunning BES: **Plastid stromules: video microscopy of their outgrowth, retraction, tensioning, anchoring, branching, bridging, and tip-shedding.** *Protoplasma* 2005, **225**:33–42.
13. Kwok EY, Hanson MR: **Stromules and the dynamic nature of plastid morphology.** *J Microsc* 2004, **214**:124–137.
14. Mathur J, Mammone A, Barton KA: **Organelle extensions in plant cells.** *J Integr Plant Biol* 2012, **54**:851–867.
15. Marques JP, Schattat MH, Hause G, Dudeck I, Klösgen RB: **In vivo transport of folded EGFP by the DeltapH/TAT-dependent pathway in chloroplasts of *Arabidopsis thaliana*.** *J Exp Bot* 2004, **55**:1697–1706.
16. Schattat M, Barton K, Mathur J: **Correlated behavior implicates stromules in increasing the interactive surface between plastids and ER tubules.** *Plant Signal Behav* 2011, **6**:715–718.
17. Koncz C, Schell J: **The promoter of TL-DNA gene 5 controls the tissue-specific expression of chimaeric genes carried by a novel type of *Agrobacterium* binary vector.** *Mol Gen Genet* 1986, **204**:383–396.
18. Schattat M, Barton K, Baudisch B, Klösgen RB, Mathur J: **Plastid stromule branching coincides with contiguous endoplasmic reticulum dynamics.** *Plant Physiol* 2011, **155**:1667–1677.
19. Sparkes IA, Teanby NA, Hawes C: **Truncated myosin XI tail fusions inhibit peroxisome, Golgi, and mitochondrial movement in tobacco leaf epidermal cells: a genetic tool for the next generation.** *J Exp Bot* 2008, **59**:2499–2512.
20. Ketelaar T, Anthony RG, Hussey PJ: **Green fluorescent protein-mTalin causes defects in actin organization and cell expansion in arabidopsis and inhibits actin depolymerizing factor's actin depolymerizing activity in vitro.** *Plant Physiol* 2004, **136**:3990–3998.
21. Holweg CL: **Living markers for actin block myosin-dependent motility of plant organelles and auxin.** *Cell Motil Cytoskeleton* 2007, **64**:69–81.
22. Winkler A, Roitsch T: **Metabolic regulation of leaf senescence: interactions of sugar signalling with biotic and abiotic stress responses.** *Plant Biol* 2008, **10**:50–62.
23. Miyazawa Y, Sakai A, Miyagishima S, Takano H, Kawano S, Kuroiwa T: **Auxin and cytokinin have opposite effects on amyloplast development and the expression of starch synthesis genes in cultured bright yellow-2 tobacco cells.** *Plant Physiol* 1999, **121**:461–469.
24. Enami K, Ozawa T, Motohashi N, Nakamura M, Tanaka K, Hanaoka M: **Plastid-to-nucleus retrograde signals are essential for the expression of nuclear starch biosynthesis genes during amyloplast differentiation in tobacco BY-2 cultured cells.** *Plant Physiol* 2011, **157**:518–530.
25. Roitsch T, Ehness R: **Regulation of source/sink relations by cytokinins.** *Plant Growth Regul* 2000, **32**:359–367.
26. Werner T, Holst K, Pors Y, Guivarc'h A, Mustroph A, Chriqui D, Grimm B, Schmülling T: **Cytokinin deficiency causes distinct changes of sink and source parameters in tobacco shoots and roots.** *J Exp Bot* 2008, **59**:2659–2672.
27. Beaty JS, Powell GK, Lica L, Regier DA, Macdonald EMS, Hommes NG, Morris RO: **Tzs, a nopaline Ti plasmid gene from *Agrobacterium tumefaciens* associated with trans-zeatin biosynthesis.** *Mol Gen Genet* 1986, **203**:274–280.
28. Lee S, Su G, Lasserre E, Aghazadeh MA, Murai N: **Small high-yielding binary Ti vectors pLSU with co-directional replicons for *Agrobacterium tumefaciens*-mediated transformation of higher plants.** *Plant Sci* 2012, **187**:49–58.
29. Werbrouck S, Strnad M, VanOnckelen HA, Debergh PC: **Meta-topolin, an alternative to benzyladenine in tissue culture?** *Physiol Plant* 1996, **98**:291–297.
30. Powell GK, Hommes NG, Kuo J, Castle LA, Morris RO: **Inducible expression of cytokinin biosynthesis in *Agrobacterium tumefaciens* by plant phenolics.** *MPMI* 1988, **1**:235–242.
31. Regier DA, Morris RO: **Secretion of trans-zeatin by *Agrobacterium tumefaciens*: a function determined by the nopaline Ti plasmid.** *Biochem Biophys Res Commun* 1982, **104**:1560–1566.
32. Han Z-F, Hunter DM, Sibbald S, Zhang J-S, Tian L: **Biological activity of the *tzs* gene of nopaline *Agrobacterium tumefaciens* GV3101 in plant regeneration and genetic transformation.** *MPMI* 2013, **26**:1359–1365.
33. Matthyse AG, Holmes KV, Gurliitz RH: **Elaboration of cellulose fibrils by *Agrobacterium tumefaciens* during attachment to carrot cells.** *J Bacteriol* 1981, **145**:583–595.
34. Polanská L, Vicánková A, Nováková M, Malbeck J, Dobrev PI, Brzobohaty B, Vankova R, Machácková I: **Altered cytokinin metabolism affects cytokinin, auxin, and abscisic acid contents in leaves and chloroplasts, and chloroplast ultrastructure in transgenic tobacco.** *J Exp Bot* 2007, **58**:637–649.
35. Brugière N, Jiao S, Hantke S, Zinselmeier C, Roessler JA, Niu X, Jones RJ, Habben JE: **Cytokinin oxidase gene expression in maize is localized to the vasculature, and is induced by cytokinins, abscisic acid, and abiotic stress.** *Plant Physiol* 2003, **132**:1228–1240.
36. Motyka V, Vankova R, Capkova V, Petrasek J, Kaminek M, Schmülling T: **Cytokinin-induced upregulation of cytokinin oxidase activity in tobacco includes changes in enzyme glycosylation and secretion.** *Physiol Plant* 2003, **117**:11–21.
37. Ueda N, Kojima M, Suzuki K, Sakakibara H: ***Agrobacterium tumefaciens* tumor morphology root plastid localization and preferential usage of hydroxylated prenyl donor is important for efficient gall formation.** *Plant Physiol* 2012, **159**:1064–1072.
38. Yonekura-Sakakibara K, Kojima M, Yamaya T, Sakakibara H: **Molecular characterization of cytokinin-responsive histidine kinases in maize. Differential ligand preferences and response to cis-zeatin.** *Plant Physiol* 2004, **134**:1654–1661.
39. Stolz A, Riefler M, Lomin SN, Achazi K, Romanov GA, Schmülling T: **The specificity of cytokinin signalling in *Arabidopsis thaliana* is mediated by differing ligand affinities and expression profiles of the receptors.** *Plant J* 2011, **67**:157–168.
40. Synková H, Schnablová R, Polanská L, Husák M, Siffel P, Vácha F, Malbeck J, Machácková I, Nebesárová J: **Three-dimensional reconstruction of anomalous chloroplasts in transgenic ipt tobacco.** *Planta* 2006, **223**:659–671.
41. Hwang I, Sheen J, Müller B: **Cytokinin signaling networks.** *Annu Rev Plant Biol* 2012, **63**:353–380.
42. Waters MT, Fray RG, Pyke KA: **Stromule formation is dependent upon plastid size, plastid differentiation status and the density of plastids within the cell.** *Plant J* 2004, **39**:655–667.
43. Schattat MH, Klösgen RB: **Induction of stromule formation by extracellular sucrose and glucose in epidermal leaf tissue of *Arabidopsis thaliana*.** *BMC Plant Biol* 2011, **11**:115.
44. Kwok EY, Hanson MR: **Plastids and stromules interact with the nucleus and cell membrane in vascular plants.** *Plant Cell Rep* 2004, **23**:188–195.
45. Caplan JL, Mamillapalli P, Burch-Smith TM, Czymbek K, Dinesh-Kumar SP: **Chloroplastic protein NRIP1 mediates innate immune receptor recognition of a viral effector.** *Cell* 2008, **132**:449–462.
46. Krenz B, Jeske H, Kleinow T: **The induction of stromule formation by a plant DNA-virus in epidermal leaf tissues suggests a novel intra- and intercellular macromolecular trafficking route.** *Front Plant Sci* 2012, **3**:291.
47. Sheahan MB, Rose RJ, McCurdy DW: **Organelle inheritance in plant cell division: the actin cytoskeleton is required for unbiased inheritance of chloroplasts, mitochondria and endoplasmic reticulum in dividing protoplasts.** *Plant J* 2003, **37**:379–390.
48. Miller CO, Skoog F, Von Saltza MH, Strong FM: **Kinetin, a cell division factor from deoxyribonucleic acid.** *J Am Chem Soc* 1955, **77**:1392–1392.
49. Sparkes IA, Runions J, Kearns A, Hawes C: **Rapid, transient expression of fluorescent fusion proteins in tobacco plants and generation of stably transformed plants.** *Nat Protoc* 2006, **1**:2019–2025.
50. Brenner WG, Romanov GA, Köllmer I, Bürkle L, Schmülling T: **Immediate-early and delayed cytokinin response genes of *Arabidopsis thaliana* identified by genome-wide expression profiling reveal novel cytokinin-sensitive processes and suggest cytokinin action through transcriptional cascades.** *Plant J* 2005, **44**:314–333.
51. Brenner WG, Ramireddy E, Heyl A, Schmuelling T: **Gene regulation by cytokinin in *Arabidopsis*.** *Front Plant Sci* 2012, **3**:8.
52. Cerny M, Dycka F, Bobalova J, Brzobohaty B: **Early cytokinin response proteins and phosphoproteins of *Arabidopsis thaliana* identified by proteome and phosphoproteome profiling.** *J Exp Bot* 2011, **62**:921–937.
53. Hoekema A, Hirsch PR, Hooykaas PJJ, Schilperoort RA: **A binary plant vector strategy based on separation of vir-region and T-region of the *Agrobacterium tumefaciens* Ti-plasmid.** *Nature* 1983, **303**:179–180.
54. Wise AA, Liu Z, Binns AN: **Culture and Maintenance of *Agrobacterium* Strains.** In *Agrobacterium Protocols, Volume 1*. 2nd edition. Edited by Wang K. Totowa: Humana Press; 2006:2–13.

55. Engler G, Holsters M, Van Montagu M, Schell J, Hernalsteens JP, Schilperoort: **Agrocin 84 sensitivity: a plasmid determined property in *Agrobacterium tumefaciens***. *Mol Gen Genomics* 1975, **138**:345–349.
56. van den Ent F, Löwe J: **RF cloning: a restriction-free method for inserting target genes into plasmids**. *J Biochem Biophys Methods* 2006, **67**:67–74.
57. Coneva V, Guevara D, Rothstein SJ, Colasanti J: **Transcript and metabolite signature of maize source leaves suggests a link between transitory starch to sucrose balance and the autonomous floral transition**. *J Exp Bot* 2012, **63**:5079–5092.
58. Hadley A: **My Software to Combine Pictures to Increase Depth of Field**. In; 2006. <http://www.hadleyweb.pwp.blueyonder.co.uk/>.
59. Schattat MH, Klösigen RB: **Improvement of plant cell microscope images by use of "depth of field" - extending software**. *Endocytobiosis Cell Res* 2009, **19**:11–19.
60. Schindelin J, Arganda-Carreras I, Frise E, Kaynig V, Longair M, Pietzsch T, Preibisch S, Rueden C, Saalfeld S, Schmid B, Tinevez J-Y, White DJ, Hartenstein V, Eliceiri K, Tomancak P, Cardona A: **Fiji: an open-source platform for biological-image analysis**. *Nat Methods* 2012, **9**:676–682.

doi:10.1186/1471-2229-14-127

Cite this article as: Erickson et al.: *Agrobacterium*-derived cytokinin influences plastid morphology and starch accumulation in *Nicotiana benthamiana* during transient assays. *BMC Plant Biology* 2014 **14**:127.

Submit your next manuscript to BioMed Central and take full advantage of:

- Convenient online submission
- Thorough peer review
- No space constraints or color figure charges
- Immediate publication on acceptance
- Inclusion in PubMed, CAS, Scopus and Google Scholar
- Research which is freely available for redistribution

Submit your manuscript at
www.biomedcentral.com/submit



5.3. Additional results

As we have summarized in the paper, we found that stromule induction, as well as plastid relocation and the formation of green islands was likely a consequence of the secretion of cytokinins by the bacteria. Accumulation of *trans*-Zeatin and *trans*-Zeatin-9-riboside in plant tissue was correlated with the presence of the *tzs* gene in the *A. tumefaciens*, which is located on the Ti-plasmid of GV3101, but is not found in LBA4404. Prior to this publication the effect of cytokinins on stromules was unknown, and cytokinin levels in plant tissue during GV3101-based transient assays in *N. benthamiana* had not been measured. Accompanying elevated cytokinins, we found an increase in starch accumulation and soluble sugar levels in plant tissue, clearly suggesting that even short-term exposure alters cell physiology and metabolism. Work in *A. thaliana* suggests that cytokinins also influence the abundance of other phytohormones such as ABA (Nishiyama et al., 2011), auxin (Jones and Ljung, 2011) and ethylene (Chae et al., 2003). Further, cytokinin signaling pathways are not isolated and cross-talk between hormone signaling cascades is expected (El-Yazal et al., 2015). Since stromules are observed in response to a wide variety of hormones (Section 1.4), it was suspected that cytokinin may not directly act to induce stromules, but alter the balance of endogenous hormones to influence stromule frequency. To gain insight into global changes to hormones which occur in the presence of *tzs*-derived cytokinin, we chose to compare hormone profiles among strains with and without *tzs* to better understand the hormonal interactions occurring in conjunction with stromule formation.

5.3.1. Expression of the *tzs* gene influences ACC and OPDA, and ABA levels

During a collaboration with Jörg Ziegler, he developed a method by which apolar phytohormones can be quantified via LS-MS/MS alongside 1-aminocyclopropan-1-carboxylic acid (ACC), a polar ethylene precursor (Ziegler et al., 2014)¹. Using this protocol he was able to provide a hormone profile for tissues that were non-infiltrated (NI), or infiltrated with buffer (AIM), strains lacking the *tzs* gene (LBR, GVC7, 4, 5), and strains containing the *tzs* gene (GVR, LtZ4).

A reminder of abbreviations used for the *A. tumefaciens* strains utilized in Erickson et al. (2014):

LBR - LBA4404 harbouring a plasmid facilitating the synthesis of dsRed *in planta*.

GVC - GV3101 strain cured of the Ti-plasmid, pMP90 (strain lacks the *tzs* gene). Numbers represent the three distinct cured strains chosen for analysis. All strains also harbour a second plasmid facilitating the synthesis of dsRed *in planta*.

GVR - GV3101 strain harbouring pMP90, plus a second plasmid facilitating the synthesis of dsRed *in planta*.

LtZ4 - LBA4404 harbouring a plasmid with the *tzs* gene amplified from pMP90 (coding region plus 2kb upstream and downstream). T-DNA border sequences were removed from the plasmid to ensure it was only expressed in *A. tumefaciens*.

¹This publication can be found on the SD card.

In addition to the cytokinin measurements reported in Erickson et al. (2014), Figure 5.1 on the following page displays unpublished measurements of abscisic acid (ABA), indole-3-acetic acid (IAA), salicylic acid (SA), jasmonic acid (JA), jasmonic acid-isoleucine (JA-Ile), and 12-oxo-phytodienoic acid (OPDA) obtained from the same samples analysed in the publication. Hormone measurements revealed subtle and mostly non-significant differences in JA, JA-Ile, and IAA between infiltration medium controls and bacterial infiltrations. In contrast, SA was elevated in the presence of all bacterial strains regardless of whether they harboured the *tzs* gene. ABA showed a general decrease in response to *A. tumefaciens*, but most obviously in the presence of strains harbouring the *tzs* gene. ACC showed a general increase in the presence of *A. tumefaciens*, but the largest increase was in the presence of the Ltz4 strain, which induces the most *trans*-Zeatin and *trans*-Zeatin-9-riboside accumulation (Erickson et al., 2014). OPDA, in contrast, did not react to all *A. tumefaciens* stains, but very specifically increased in response to those harbouring the *tzs* gene. In summary, in treatments where stromules are moderately induced (between 10-20%), i.e. infiltration with LBR and GVC4, 5, 7, there was a decrease in ABA and an increase in ACC. High stromule frequencies (30-50%) induced by GVR and Ltz4 coincided with a more drastic decrease in ABA, a more drastic increase in ACC, and a specific increase in *trans*-Zeatin, *trans*-Zeatin-9-riboside and OPDA.

5.4. Discussion and outlook

Cytokinin affects the abundance of other plant hormones during development (Jones et al., 2010; Jones and Ljung, 2011), during salt and drought stress (Nishiyama et al., 2011) and in response to exogenously applied hormone (Chae et al., 2003). In the context of plant-microbe interactions, cytokinin accumulation is interpreted as a defense signal by the plant (Naseem et al., 2014), priming the plant immune system through its influence on the abundance of other hormones (Großkinsky et al., 2014; Argueso et al., 2012; Swartzberg et al., 2007). As previously mentioned, in addition to cytokinins, stromule abundance is altered by multiple phytohormones, suggesting that stromule frequency is the cumulative product of multiple phytohormone inputs. Therefore, changes to phytohormones induced by *tzs*-containing bacterial strains may reveal more about the hormonal conditions interacting to produced stromule frequency outputs. As expected, *tzs*-derived cytokinins did have an impact on endogenous hormone levels in *N. benthamiana* tissue, including the down-regulation of ABA, and the up-regulation of ACC and OPDA; clearly creating conditions conducive to stromule formation.

5.4.1. *A. tumefaciens* and secreted cytokinins alter endogenous hormones

ABA

ABA was clearly reduced following infiltration with all *A. tumefaciens* strains (Figure 5.1 on the next page, panel A), with the largest decrease seen in strains harbouring the *tzs* gene, which induce the most cytokinin accumulation in plant tissue (Figure 4, on page 51, Erickson et al. 2014). This data clearly fits with the experiments of Rico et al. (2010), which showed

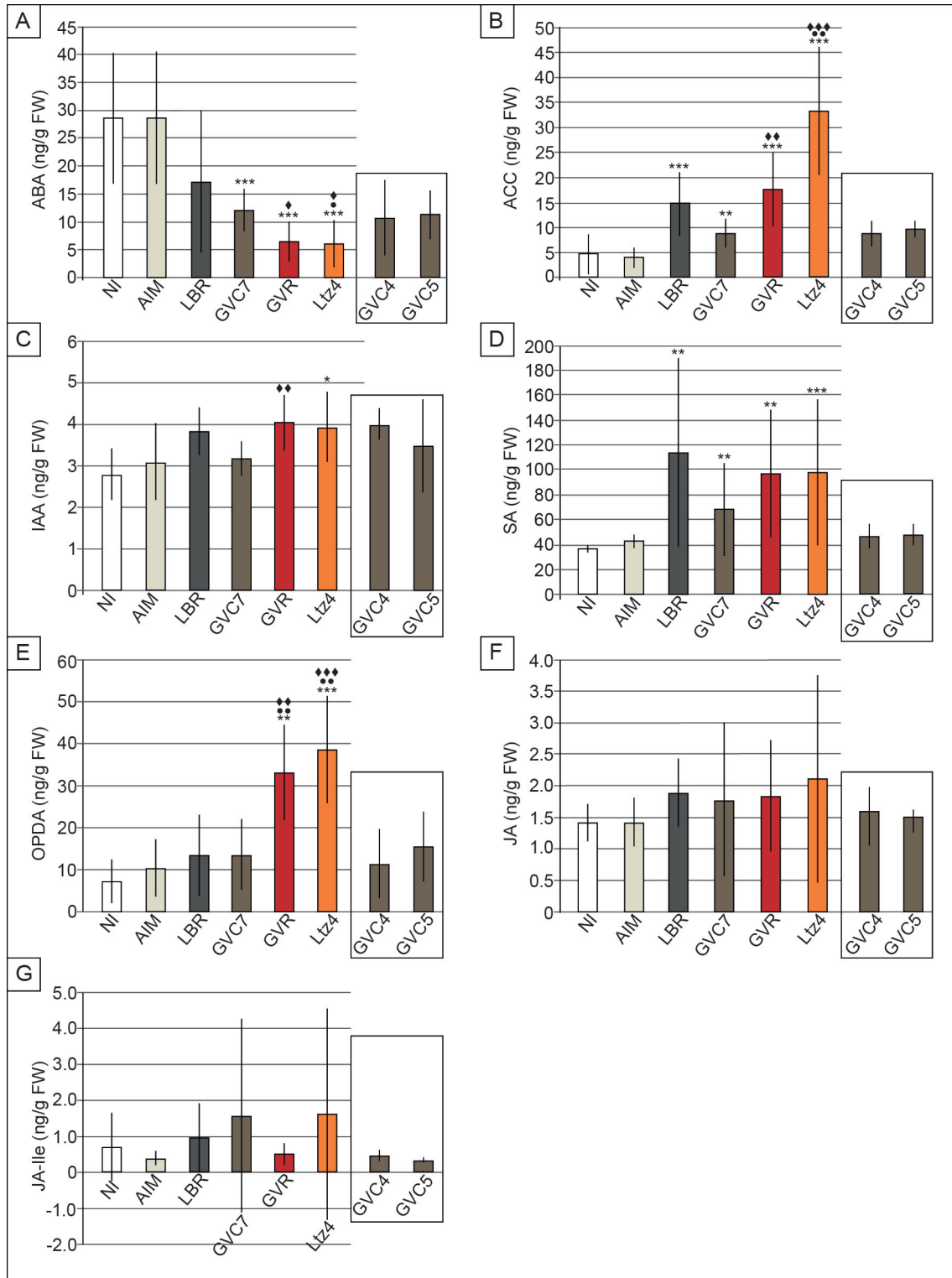


Figure 5.1.: Infiltration with *A. tumefaciens* derivatives expressing the *tzs* gene is correlated with a reduction of ABA and increases in OPDA and ACC. LC/MS/MS measurements of absolute (A) ABA, (B) ACC, (C) IAA, (D) SA, (E) OPDA, (F) JA, and (G) JA-Ile in non-infiltrated (NI) *N. benthamiana* leaves, and leaves infiltrated with AIM buffer (beige bars), LBR (dark grey bars), GVC7, GVC4, GVC5 (brown bars), GVR (red bars), or Lz4 (orange bars) at 3 dpi. Bars represent average hormone levels, error bars are standard deviation, asterisks indicate a significant difference from the AIM treatment, circles indicate a significant difference between the LBR and *tzs* containing strains and diamonds indicate a significant difference between GVC7 treatments and *tzs* containing strains (Rank sum tests summarized in Table 12.3 on page 156). Experiments were performed twice, examining 8 plants total, except in the case of ACC, IAA, SA, OPDA, JA, JA-Ile, where $n = 7$ for GVR and LBR. GVC4 and 5 are included in the figure (surrounded by box) to demonstrate the similarity between tissues infiltrated with different GV3101 cured lines, but since they were only included in one experiment ($n = 4$) these were not included in the statistical analysis.

that infiltration with GV3101 results in decreases in ABA to below that of untreated tissue. A reduction in endogenous ABA in the presence of *A. tumefaciens* is typically beneficial to the plant, since ABA is required for tumor development by wild-type *A. tumefaciens* strains (Lee et al., 2009). Interestingly, the resistance of *N. tabacum* to infection with another pathogenic bacterium, *P. syringe*, was shown to be dependent on the antagonistic relationship between cytokinin and ABA (Großkinsky et al., 2014). The application of cytokinin alone, like GV3101 infiltrations, also suppresses endogenous ABA and increases resistance to subsequent infection with *P. syringe*, while ABA treatments increase proliferation of bacteria (Großkinsky et al., 2014). Together, these results suggest that, even during transient infiltrations with disarmed *A. tumefaciens* strains, bacteria-derived cytokinin, and perhaps other bacterial factors, are priming the plant immune system.

Ethylene

1-Amino cyclopropane-1-carboxylic acid (ACC) is the rate limiting intermediate in the ethylene biosynthesis pathway, and as such, measurements of ACC are considered to reflect ethylene production (Ziegler et al., 2014). General increases in ACC seen during inoculations with *A. tumefaciens* strains are not surprising, given that plant ethylene production is known to increase during the initial stages of *A. tumefaciens* infection (Subramoni et al., 2014), and during plant transformations utilizing disarmed strains (Nonaka et al., 2008). ACC interferes with expression of virulence genes on the Ti-plasmid and thus inhibits *A. tumefaciens*-mediated transformation of plant cells (Nonaka et al., 2008). Interestingly, it has long been known that ethylene production also increases in leaf tissue treated with exogenous cytokinins in multiple monocot and dicot species (Suttle, 1986). In fact, ethylene production and signaling is actually required for some cytokinin-dependent effects on plant development, suggesting that it acts downstream of cytokinin (El-Yazal et al., 2015). Ethylene production during *A. tumefaciens* inoculation could represent a direct response to the amount of cytokinin secreted by the various *A. tumefaciens* strains. Indeed, our data shows that ACC levels are highest in tissue inoculated with Ltz4, the strain which induces the most cytokinin accumulation (Figure 4, on page 51, Erickson et al. 2014).

OPDA

OPDA is a biologically active precursor of jasmonic acid, a molecule with known roles in both biotic and abiotic stress signaling (Robert-Seilaniantz et al., 2011). In our experiments JA levels were very low, exhibiting high standard deviations, however, OPDA showed a clear and specific induction following infiltrations with *tzs*-containing *A. tumefaciens* strains (Figure 5.1 on the facing page, panel E). OPDA was shown to promote defense response in tomato independent of JA (Scalschi et al., 2015). However, overall, little is known about OPDA during plant-pathogen interactions or in response to exogenously applied cytokinins.

5.4.2. Reliance of stromule induction on ABA

In our experiments ABA was lowest in treatments where stromules were highest (GVR and LtZ4 inoculations). This was surprising in the context of work published by Gray et al., (2012), which suggested that ABA plays a key role in stromule induction under a variety of stress conditions (Figure 5.2 on the next page outlines findings by Gray et al., 2012). ABA induces stromules within hours of application in a concentration-dependent manner, and among the many hormones tested, showed the most reliable and dramatic induction of stromules. Stromule induction was also shown to occur via MeJA and ACC (both induced in response to pathogen attack), mannitol (osmotic stress) and H₂O₂ (generally induced under stress conditions). Simultaneous application of these stress/hormone treatments with ABA synthesis inhibitors suppressed stromule induction, leading Gray et al. (2012) to conclude that many stromule-inducing stimuli are dependent on ABA biosynthesis. This work seemed to suggest that the ABA biosynthesis pathway integrates multiple stress signals, ultimately resulting in stromule induction. In contrast to the findings of Gray et al. (2012), we found that in *N. benthamiana* lower epidermis challenged with *tzs* containing *A. tumefaciens* strains ABA does not seem to play such a pivotal role in stromule induction. During transient assays, our work shows that stromules occur in the presence of elevated cytokinins, ACC and OPDA despite a lack of ABA accumulation, indicating that stromule induction is occurring via an ABA-independent pathway (as shown in Figure 5.2 on the facing page). In the future one should confirm this idea via the co-infiltration of tissue with GV3101 and ABA synthesis inhibitor. If stromule induction occurs via an ABA-independent pathway, ABA synthesis inhibitor should have little impact on GV3101-induced increases in stromule frequency. One could also test the reliance of cytokinin-induced stromule induction on OPDA and ACC.

Differences between our findings and those of Gray et al. (2012) may be explained by differences in ABA response and interaction between plant hormone signaling pathways under different environmental stimuli. Cells are re-programmed according to the type of stress they face. For example, when confronted with *A. tumefaciens* it is likely beneficial to have low ABA (Rico et al., 2010), while it is known that ABA biosynthesis is beneficial in response to osmotic stress caused by high salt or drought (Sah et al., 2016). Fundamental differences in the reliance of stromule formation on ABA could also come from the fact that Gray et al. (2012) did not challenge plants with live bacteria, but instead simulated stresses via the application of purified signaling molecules. Additionally, authors examined different tissues (hypocotyl and root hair) and a different developmental stage (seedlings), which could create fundamental differences in hormone biosynthesis, response and subsequent stromule induction.

5.4.3. RNAseq data to identify stromule-pertinent genes

As another approach to get an overview of the sub-cellular conditions that promote stromules we collected RNA samples from three independent plants infiltrated with 100mg/mL

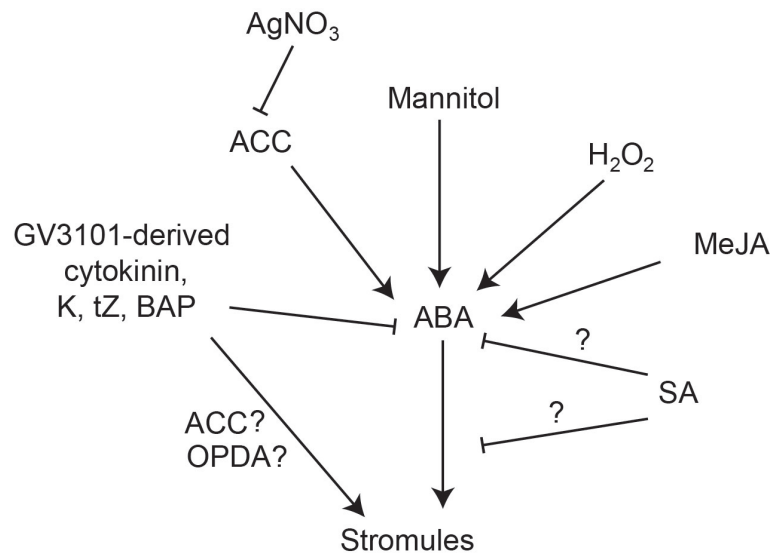


Figure 5.2.: Exogenous application of stress-associated compounds leads to stromule formation. Gray et al. (2012) found that in wheat root hair and tobacco hypocotyl, multiple compounds associated with both biotic and abiotic stress induce stromules. Stromule induction via 1-aminocyclopropanecarboxylic acid (ACC), mannitol, hydrogen peroxide (H_2O_2) and methyl jasmonate (MeJA) depends on abscisic acid (ABA) biosynthesis. Application of silver nitrate ($AgNO_3$), an ethylene inhibitor, and salicylic acid (SA) was found to inhibit stromule formation. Whether the inhibition of stromules by SA occurs via the inhibition of ABA biosynthesis was not tested. Work presented in this thesis suggests that induction of stromules via GV3101-triggered stromule induction occurs via an ABA independent pathway, perhaps one that relies on the accumulation of ACC or 12-oxo-phytodienoic acid (OPDA), which are both induced by secreted-cytokinins. Cytokinins found to induce stromules in Erickson et al. (2014) were 6-benzylaminopurine (BAP), *trans*-Zeatin (*tZ*), and kinetin (K).

6-Benzylaminopurine (BAP)², GV3101³, or non-infiltrated, and sent them to MWG Eurofins⁴ for RNA sequencing⁵. As previously mentioned, we believed that the magnitude of changes to the *N. benthamiana* transcriptome following GV3101 infiltrations would be of general interest to all those performing transient assays. More important for us, however, was that both GV3101 and BAP consistently induce stromules (Erickson et al., 2014), and by identifying transcripts that are co-regulated in both treatments we could identify genes or pathways which are important for stromule formation and function. The RNA sequencing has not yet been analysed, but in the future one could focus on a subset of co-regulated genes, perhaps on those encoding specific classes of proteins, such as transcription factors or kinases. Alternatively, with the knowledge that the abundance of ABA, OPDA and ACC are altered in correlation with stromules, one could also look into genes known to act in biosynthesis and signaling pathways of these hormones.

5.4.4. Use of induction via GV3101 as a tool for genetic screens

Besides induction via GV3101, little to no treatments had been identified that consistently induced stromules in *N. benthamiana* leaf epidermis. The ability to induce stromules in this tissue represents an invaluable tool for the further study of stromule form and function, since *N. benthamiana* is a common platform for the transient over-expression of proteins of interest

²Tissue was harvested at 2dpi.

³Tissue was harvested at 3dpi.

⁴Ebersberg, Germany

⁵Illumina HiSeq 2000, v3.0 chemistry

and common screening approaches, such as Virus Induced Gene Silencing (VIGS). Therefore, in the next two parts of this thesis GV3101 is used extensively to identify cellular components necessary for stromule formation.

5.5. Additional materials and methods

5.5.1. Hormone measurements

Information on the growth of plant material, and the generation, growth and infiltration of bacterial strains utilized for hormone measurements is described in Erickson et al. (2014). The same tissue analyzed for *trans*-Zeatin and *trans*-Zeatin-9-riboside content in Erickson et al. (2014), was used for the measurements of all other hormones displayed in Figure 5.1 on page 64. As part of a collaboration, Jörg Ziegler developed a method of detecting apolar ACC, along with polar hormones, *trans*-Zeatin and *trans*-Zeatin-9-riboside, ABA, IAA, SA, JA, JA-Ile and OPDA. This collaborative work was also published in 2014 and can be found on the SD card provided.

5.5.2. Plant material for RNA sequencing

Plants were grown in soil under short day conditions (8h light and 16h dark), under a light intensity of $120 \mu\text{Em}^{-2}$ at 20°C . RNA was collected from three transgenic *N. benthamiana* plants (*FNR:eGFP*, labeling plastid stroma/stromules; described in Erickson et al., 2014) that were untreated, treated with $100 \text{ mg} \cdot \text{mL}^{-1}$ 6-Benzylaminopurine (BAP) (2 dpi), or with GV3101 (3 dpi). Treatments were administered via infiltration using a needless syringe into fully expanded leaves of 6-week-old plants as described in Erickson et al. (2014). To confirm that tissue was responding to treatments as expected, infiltrations spots were examined for the presence of stromules, which typically occur in BAP and GV3101 treatments.

5.5.3. RNA isolation and sequencing

RNA isolation and sequencing is described in a collaborative publication with the bioinformatics department of Martin Luther University Halle-Wittenberg (Keilwagen et al., 2016), which can also be found on the SD card provided.

6. Effector screen identifies microtubules as essential to stromule extension

6.1. Introduction

Using a targeted approach, Part I and II of this thesis made us aware of several mutants that alter stromule abundance in the upper epidermis of *A. thaliana*, and revealed that in unstressed plants basal stromule levels depend on nucleus movement. However, stromule induction is strongly induced when the plant is confronted with abiotic or biotic stress, and very little is known about the regulation of stromules under these conditions. We believed that a new, untargeted, approach was required in order to gain new insight into the processes stromules are involved in, or the cellular components necessary for their formation.

We chose to utilize type III effector proteins (T3Es) from *Xanthomonas campestris* pv. *vesicatoria* (*Xcv*), a Gram-negative plant-pathogenic bacteria, as tools to screen for stromule-related processes. T3Es are typically translocated directly into the host cytoplasm via the type III secretion system of *Xcv*, where they specifically manipulate host cell processes to benefit the bacteria (Büttner and He, 2009). Effector sequences previously isolated from *Xcv* (refer to Table S1, Erickson et al., 2017a), were transiently expressed in *N. benthamiana* and screened for their ability to suppress or enhance stromule formation. *A. tumefaciens* strain GV3101 was chosen to mediate transient over-expression due to its ability to consistently induce stromules (Part III), and effectors producing increases or decreases in stromule frequency were chosen for further study.

6.2. Publication III

the plant journal

SEB
Society for
Experimental Biology

The Plant Journal (2018) 93, 856–870

doi: 10.1111/tpj.13813

The *Xanthomonas* effector XopL uncovers the role of microtubules in stromule extension and dynamics in *Nicotiana benthamiana*

Jessica L. Erickson^{1,2,†}, Norman Adlung^{1,†}, Christina Lampe^{1,2}, Ulla Bonas^{1,*} and Martin H. Schattat^{2,*}

¹Department of Genetics, Institute for Biology, Martin Luther University Halle-Wittenberg, D-06099 Halle, Germany, and

²Department of Plant Physiology, Institute for Biology, Martin Luther University Halle-Wittenberg, D-06099 Halle, Germany

Received 1 September 2017; revised 4 December 2017; accepted 8 December 2017; published online 29 December 2017.

*For correspondence (e-mails martin.schattat@pflanzenphys.uni-halle.de or ulla.bonas@genetik.uni-halle.de).

[†]These authors contributed equally to this work.

SUMMARY

Xanthomonas campestris pv. *vesicatoria* type III-secreted effectors were screened for candidates influencing plant cell processes relevant to the formation and maintenance of stromules in *Nicotiana benthamiana* lower leaf epidermis. Transient expression of XopL, a unique type of E3 ubiquitin ligase, led to a nearly complete elimination of stromules and the relocation of plastids to the nucleus. Further characterization of XopL revealed that the E3 ligase activity is essential for the two plastid phenotypes. In contrast to the XopL wild type, a mutant XopL lacking E3 ligase activity specifically localized to microtubules. Interestingly, mutant XopL-labeled filaments frequently aligned with stromules, suggesting an important, yet unexplored, microtubule–stromule relationship. High time-resolution movies confirmed that microtubules provide a scaffold for stromule movement and contribute to stromule shape. Taken together, this study has defined two populations of stromules: microtubule-dependent stromules, which were found to move slower and persist longer, and microtubule-independent stromules, which move faster and are transient. Our results provide the basis for a new model of stromule dynamics including interactions with both actin and microtubules.

Keywords: actin, E3 ubiquitin ligase, microtubules, *Nicotiana benthamiana*, stromule dynamics, stromule morphology, stromule velocity, *Xanthomonas campestris* pv. *vesicatoria*, XopL.

6.3. Additional results

In Erickson et al. (2017a) we showed that the transient expression of the *Xcv* effector XopL (an E3 ubiquitin ligase) virtually wiped out GV3101-induced stromules in *N. benthamiana* lower epidermis. In the publication we suggest that one explanation for the stromule phenotype induced by XopL is that it likely targets the microtubule network. This is supported by the observation that an E3 dead variant of XopL (XopLmut), which still contains the substrate binding domain (LRR domain) but is unable to ubiquitinate substrates, localizes to microtubules (Figure 4, Erickson et al., 2017a, on page 77). However, the exact impact of XopL on microtubules was not investigated in the context of the article and remained an open question. In order to answer this question I obtained stable *N. benthamiana* transgenics expressing GFP-labeled α -tubulin (GFP-TUBULIN α -6; Gillespie et al. (2002)), courtesy of Manfred Heinlein¹. GFP-TUBULIN α -6 (GFP-TUA6) is expressed in all cells in untreated plants, labeling microtubules and, to a lesser extent, the cytosol (Figure 6.1 on the next page, panel C). In stark contrast, when XopL-mOrange2 was transiently expressed microtubules were no longer visible in the GFP channel and only the cytosolic signal remained (Figure 6.1, panel A). XopL did not express in all cells (transient expression is generally less uniform), and in those cells lacking XopL, microtubules remained intact (arrows in Figure 6.1, panel A). As a control the XopLmut was expressed, and once again exhibited microtubule localization (Figure 6.1, panel B), as described in Erickson et al. (2017a). Inverted images of the microtubules in non-infiltrated, XopL and XopLmut-infiltrated tissues are shown in Figure 6.1, panels C, D, and E to increase the visibility of filaments for print. The result from this experiment was clear, microtubules are absent in cells expressing XopL. Based on the pivotal role of microtubules in stromule dynamics that was defined in Erickson et al. (2017a), it is not surprising that cells lacking microtubules would have severely reduced stromule frequencies. Once again, this emphasizes the importance of microtubules for maintaining stromules in tissue under stress from GV3101.

6.4. Summary

The original idea behind Erickson et al. (2017a) was to utilize *Xcv* effectors as part of an untargeted approach to gain insight into stromules formation. Quite unexpectedly, we found an effector that disrupts the microtubule network, XopL, induces a dramatic decrease in stromule frequencies. Although it was previously reported that microtubules contribute to stromule length and number in etiolated tobacco hypocotyl (Kwok and Hanson, 2003), the exact role of microtubules in this process was never defined, and the relationship between microtubules and stromules was never examined in detail. Through the use of double labeling of stroma/stromules and microtubules, we clearly showed that microtubules create a scaffold for stromule growth and shape. Growth along microtubules suggests that kinesins are likely involved in the extension of stromules. Indeed, we found that stromule growth along microtubules occurs at velocities that compare with kinesin velocities measured *in vitro*. The role

¹Institut de Biologie Moléculaire des Plantes du CNRS, Strasbourg, France

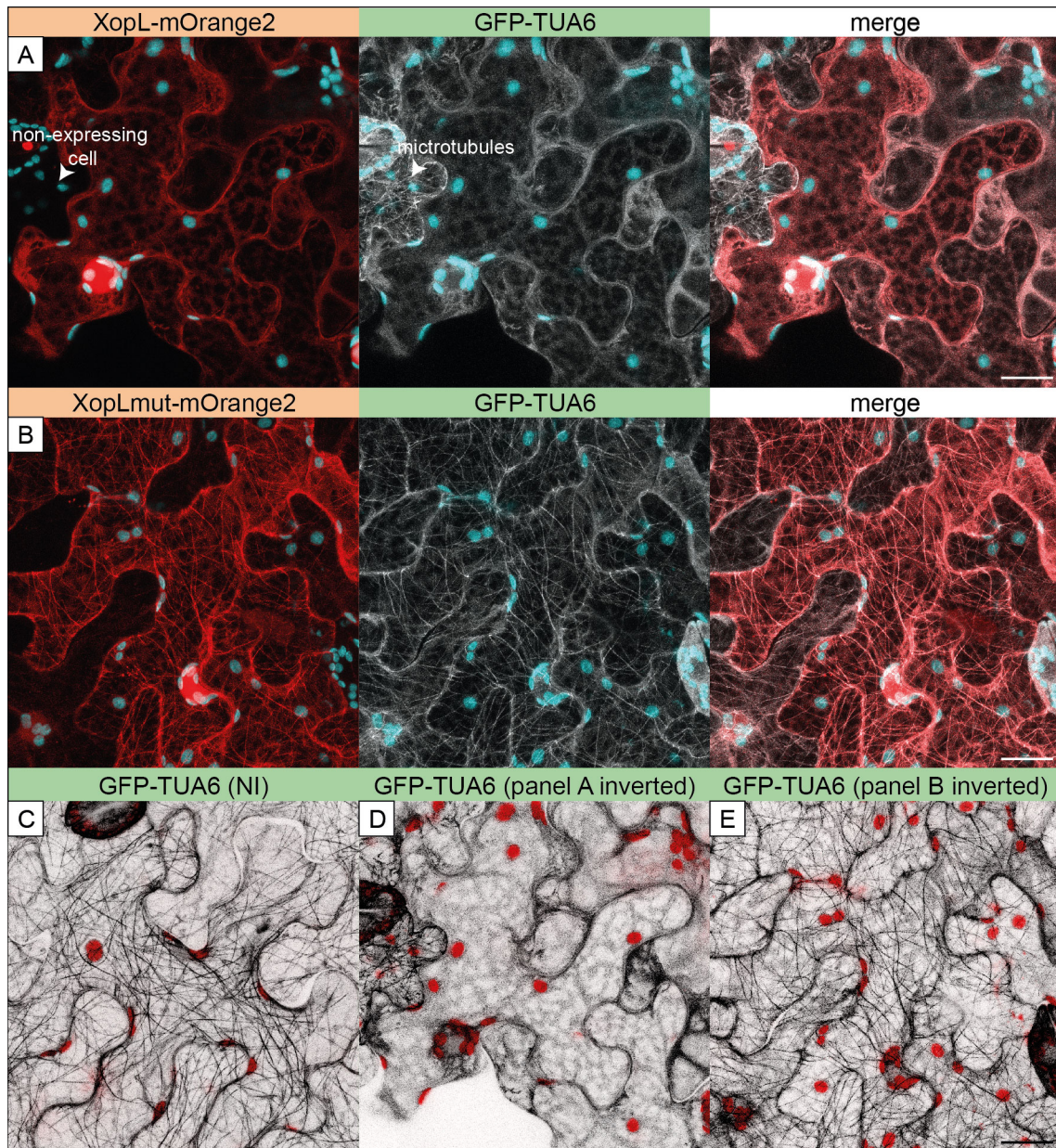


Figure 6.1.: XopL triggers depolymerization of microtubules. CLSM images of GFP-TUA6 (microtubules in white) stable transgenic *N. benthamiana* lower leaf epidermis inoculated with *A. tumefaciens* GV3101-derivatives mediating the expression of (A) XopL-mOrange2 (red) and (B) XopLmut-mOrange2 (red). (A) XopL expression (first panel) results in a loss of microtubules (second panel). White arrows show a cell that is not expressing XopL, which still has microtubules. (B) XopLmut (first panel) co-localizes with GFP-TUA6 at microtubules (second panel). (C-E) Inverted images of GFP-TUA6-labeled microtubules (in black) in (C) non-infiltrated, (D) *xopL* expressing or (E) *xopLmut* expressing plants. Chlorophyll autofluorescence is present in all images and is false-colored blue in (A and B) and is red in (C-E). Scale bars are on the right hand panels and are the same for all panels (20 μm). Images are Z-projections.

of kinesins in stromule formation has not been explored thus far, but represents a promising avenue for stromule research going forward.

6.5. Additional materials and methods

All methods used in experiments with GFP-TUA6 are the same as those described for transient expression experiments in *N. benthamiana* outlined in Erickson et al. (2017a).

7. VIGS identifies a GRAM protein that regulates stromules

7.1. Introduction

During the time it took to complete this thesis significant steps were taken that contributed to elucidation of mechanisms and cellular components necessary for stromules formation. However the function of stromules, and their contributions to plant fitness remain elusive. This is partially due to the fact that very few mutants have been identified that reduce stromule number, and nearly none (with the exception of the ion channel double mutant, *mssl2-1/mssl3-1*) that knock out stromules completely. In addition to the effector screen described in part IV, a second untargeted approach was chosen that aimed to identify novel stromule regulators via the use of a blind **Virus Induced Gene Silencing (VIGS)** screen.

7.1.1. Methodology of Virus Induced Gene Silencing (VIGS)

VIGS is a method utilizing a viral system to facilitate the transient knock-down of specific transcripts in host plants via the induction of **post-transcriptional gene silencing (PTGS)**. PTGS is suggested to have evolved as a anti-viral defense mechanism employed by plants to degrade specific viral RNAs, and can be initiated by the presence of viral **double stranded RNA (dsRNA)**, or in the presence of transgenes which generate dsRNAs (reviewed in Burch-Smith et al., 2004). PTGS specifically involves the cleavage of dsRNA into small interfering RNAs (siRNAs) of approximately 21-25 nucleotides in length (Hamilton and Baulcombe, 1999; reviewed in Velásquez et al., 2009). The anti-sense strand of siRNAs is then used as a guide to direct the degradation of target mRNAs (either viral, or endogenous) by the Dicer ribonuclease (reviewed in Bartel, 2004; Velásquez et al., 2009). VIGS uses viral vectors containing host-derived cDNAs to specifically target homologous plant transcripts for silencing, and so highjacks the plant defense system to degrade its own mRNAs in a sequence specific manner (reviewed in Burch-Smith et al., 2004; Velásquez et al., 2009).

Although there have been multiple VIGS viral vector systems developed over the years the tobacco rattle virus (TRV) is known for high silencing efficiency, its ability to spread efficiently through meristems, and induction of minimal viral side effects which could mask knock-down phenotypes (Burch-Smith et al., 2004). The TRV system is bipartite and requires the combination of both *TRV1* (encodes RNA-dependent RNA polymerase and movement protein) and *TRV2* (encodes viral coat protein and cDNA insert homologous to desired target mRNA) for initiation of PTGS (Liu et al., 2002). Vectors are introduced into plants via *A. tumefaciens*,

whereby bacterial cultures containing *TRV1* and *TRV2* are mixed and infiltrated into young plants (Liu et al., 2002). Silencing with the TRV system is limited to new leaves, and will not affect pre-existing or infiltrated leaves (Liu et al., 2002). Refer to Figure 7.1 on the following page for a graphic depiction of VIGS.

7.1.2. VIGS screen

Since silencing using VIGS is relatively fast, efficient, inexpensive and simple to perform, it is easily adaptable to large scale genetic screens. Through a collaboration with Sebastian Schornack¹ from AG Bonas of the Genetics Department (MLU), Martin Schattat performed a VIGS screen to identify genes relevant to stromule formation. Wild-type *N. benthamiana* plants were silenced blindly with a *TRV2*² cDNA library from *Solanum lycopersicum* (tomato). Silencing was done in *N. benthamiana* due to higher silencing efficiency in this species compared to tomato, and is facilitated by high sequence similarity between these species (Bombarely et al., 2012). Silencing was allowed to occur over 10-15 days, after which the lower epidermis of new, and presumably silenced leaves, were inoculated with *A. tumefaciens* strain GV3101 mediating the expression of stromal-targeted GFP (*FNRtp:eGFP*) to transiently label plastids and stromules in the lower epidermis (Figure 7.2 on page 91). GV3101 is known for its ability to induce stromules (Erickson et al., 2014), so plants were screened for suppression of stromule formation.

¹Currently in The Sainsbury Laboratory, Cambridge, UK.

²Plasmid name = *pYL276a*; *YL276* from Liu et al. (2002) modified by S. Schornack to include an ampicillin resistance cassette.

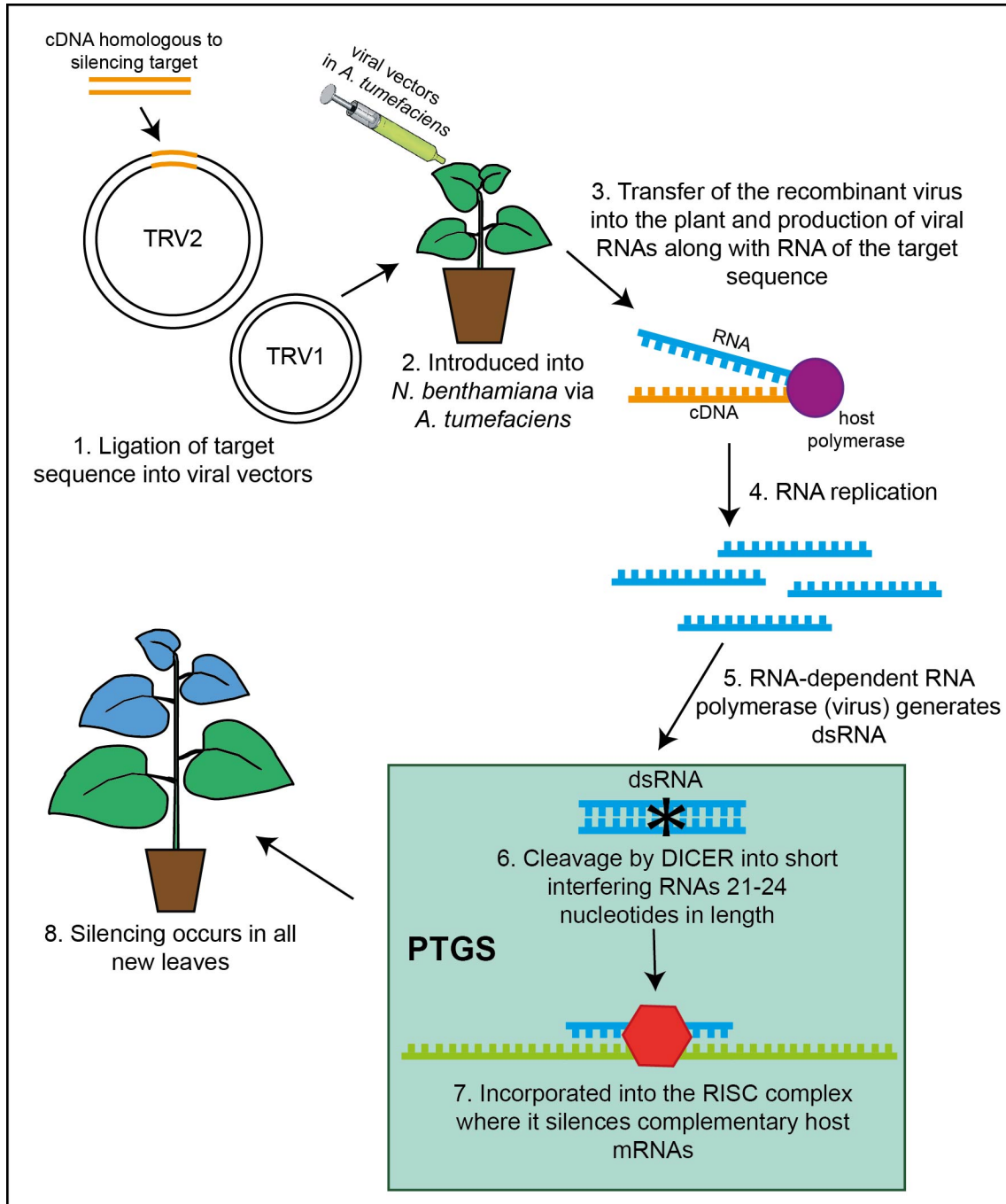


Figure 7.1.: Mechanism of Virus Induced Gene Silencing. Green box indicates post-transcriptional gene silencing (PTGS) initiated by the plant.

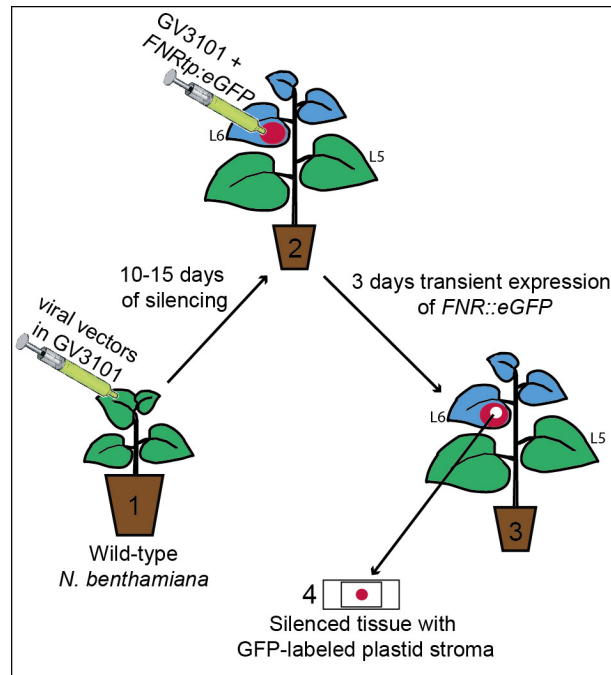


Figure 7.2.: Schematic of blind VIGS screen for stromule-relevant genes. In the VIGS screen performed by M. Schattat and S. Schornack the procedure was as follows: **1)** Young, wild-type *N. benthamiana* plants (four leaf stage) were infiltrated with GV3101-derivates harbouring plasmids containing the recombinant virus, and the tomato full-length cDNA library (one silencing construct per plant). **2)** Silencing occurred in all new leaves after approximately 15 days (silenced leaves marked in blue), and at this point a silenced leaf was infiltrated with a GV3101-derivative harbouring *FNRtp:eGFP* (infiltration spot outlined in red) which simultaneously induces stromules and mediates the expression of a stromal-targeted eGFP. **3)** At 3 dpi leaf punches were collected from the silenced tissue and **4)** were evaluated via epifluorescence microscopy, and stromules were quantified.

7.1.3. Identification of SI17E6, a GRAM domain containing protein

When silencing of any given construct resulted in the suppression of GV3101-induced stromules, this was chosen as a candidate for further analysis. Out of the 425 silencing constructs tested only 2 were identified and confirmed as stromule suppressors in a second test (refer to M. Schattat's thesis). One of these candidates, clone number 17-E-6 (referred to here as *SI17E6*) was sequenced and identified via a BLAST to 'Tomato Genome cDNAs' ³, revealing its identity as Solyc08g078510 (Figure 11.1 on page 144), a GRAM domain containing/ABA responsive protein. It was at this point that I took over the project. A search of the 'Protein families database (Pfam)' (Finn et al., 2013) with the *SI17E6* amino acid sequence using 'MOTIF search' ⁴, identified only the GRAM domain, predicted to span amino acids 160-276 (Table 7.1).

³ITAG release 2.40, <https://solgenomics.net/tools/blast/>

⁴<https://www.genome.jp/tools/motif/>

Pfam motif identified	Amino acid position (Independent E-value)	Pfam annotation, description
GRAM	160-276 (2.6e ⁻²⁵)	PF02893, GRAM domain

Table 7.1.: The GRAM domain is the only conserved protein domain identified in *SI17E6*. 'Motif Search' output following analysis of the translated ORF of the *SI17E6* sequenced clone. Pfam database was used, E-value cut-off = 1.

Conservation of the GRAM (Glucosyltransferases, **R**ab-like GTPase activators and **M**yotubularins) domain, as the name suggests, was first recognised during sequence comparisons between the glucosyltransferases of slime mold and yeast, and subsequently in Rab-like GTPases and myotubularins in yeast, *Caenorhabditis elegans*, and humans (Doerks et al., 2000). The GRAM domain was predicted to form a β sheet consisting of four β strands, each of which harbours one conserved aromatic residue (Doerks et al., 2000). In eukaryotes GRAM domains have been proposed to act in protein-protein interaction and lipid-binding, and are often found in combination with non-catalytic domains typical of membrane-associated proteins (C2 domain in plants) (Doerks et al., 2000). GRAM domain proteins identified in plants often occur in proteins that are ABA responsive, and participate in biotic and abiotic stress response reactions (Doerks et al., 2000; Jiang et al., 2008). As mentioned throughout this thesis, stromules are a common feature of plastids in plants under stress. In particular, ABA biosynthesis has been suggested to be essential for the stromule induction following treatment with a variety of stress inducing stimuli (Gray et al., 2012). Therefore, Sl17E6, an ABA-responsive protein from the GRAM family, was chosen for further characterisation.

7.2. Results

7.2.1. Confirmation of *Sl17E6* silencing candidate under new conditions

Optimizing the VIGS system in AG Schattat

Before delving into the function of Sl17E6 in stromule formation, the stromule suppression phenotype observed by M. Schattat during silencing experiments had to be confirmed. As previously mentioned, the original screen utilized *A. tumefaciens*-mediated transient expression of *FNRtp:eGFP* for the visualization of stromules. Although this was the best option for labeling stromules at the time, expression was patchy. As a result, between the time of the initial screen and the confirmation experiments, stable *FNRtp:eGFP* transgenics were generated. These plants were used to confirm the suppression of GV3101-induced stromules.

In order to confirm the phenotype the VIGS system had to be established in our growth conditions. The efficiency and reproducibility of VIGS silencing using the *TRV1/TRV2* system is largely dependent on plant growth conditions such as light and temperature, which are known to influence the interaction between the host plant and the virus (reviewed in Burch-Smith et al., 2004). The step of optimizing silencing using a positive silencing control is particularly important when evaluating phenotypes at the cellular and organelle level, as small unsilenced patches may easily be chosen for microscopy and skew stromule frequency data. Optimization of VIGS was performed via silencing of *PHYTOENE DESATURASE (PDS)*, a standard positive control for VIGS systems (Liu and Page, 2008). *PDS* encodes an enzyme involved in carotenoid biosynthesis and silencing of this gene is known to reduce the abundance of carotenoids essential for protection against photo-oxidative damage (Kumagai et al., 1995). As a consequence of *PDS* silencing, chlorophyll is destroyed and a white phenotype appears (Kumagai et al., 1995). *PDS* silencing was tested under three different light cycle conditions:

8 h day/16 h night, 16 h day/8 h night, and 24 h light (Figure 7.3 on the following page) and chambers were approximately 22°C. *FNRtp:eGFP* plants at the 4 leaf stage were inoculated with *A. tumefaciens* harbouring *TRV1*⁵ and *TRV2::NbPDS*⁶ and silencing was allowed to occur over 14-17 days. Results showed a clear light-dependent silencing gradient. Plants grown in 8 h day/16 h night exhibited very weak silencing (Figure 7.3, panel A), with most tissues retaining green coloration. Followed by the 16 h day/8 h night conditions which exhibited well bleached and moderately bleached patches (Figure 7.3, panel B). Finally, plants grown in 24 h light showed an abundance of bright white tissue (Figure 7.3, panel C). Closer examination of 16 h and 24 h day conditions showed that effective silencing occurs earlier in 24 h treatments, as is evident by effectively bleached/silenced tissue as early as leaf 5 (leaves numbered according to the order of emergence; Figure 7.3, panel E, L5), while silencing in the 16 h day condition takes effect in later leaves (Figure 7.3, panel D, L6 and L7). It should be noted that most effective silencing occurs near the leaf petiole in both conditions, and so this area was chosen as the site for microscopy in further silencing experiments.

Although I observed that *PDS* showed the most efficient silencing under 24 h day conditions, I questioned whether plastid morphology would be altered under such excessive light. For the silencing setup to be effective it was essential to maximize silencing and minimize plastid shape alterations induced by light stress. To this end, I examined plastid phenotypes in both untreated plants, and plants silenced with a *TRV2* control in both 16 h and 24 h light conditions to look for changes to the plastid shape and general signs of plant stress. Leaf 6 was found to be ideal for microcopy in both light conditions, since leaves were fully expanded and plastids were clearly visible. Leaf 6 also showed reasonable silencing efficiency in both light treatments using the *PDS* control, indicating that VIGS is likely to be active in this leaf (Figure 7.3 on the next page, panels D and E, L6). Despite thorough silencing in leaves 7 and higher, they were not suitable for evaluating plastid morphology due to the high density of small and expanding cells (data not shown). Under 16 h light conditions plastids in untreated (Figure 7.4 on page 95, panel A) and *TRV2* control silencing conditions (Figure 7.4, panel B) demonstrated morphologies and positions reminiscent of untreated control plants described by Erickson et al. (2014) (grown under 8 h day light conditions), where plastids were often found in pairs and were more or less equally distributed throughout the cell. Very few stromules were observed. However, plants under 24 h light showed signs of extreme stress and aberrant plastid phenotypes (Figure 7.4, panels C and D). Plastids frequently showed extreme clustering in untreated tissues (Figure 7.4, panel C), mild clustering in *TRV2*-silenced tissues, and excessive amounts of starch in both cases (Figure 7.4, panel C and D). Few stromules were observed, but this could be the result of a decrease in clarity of the plastid outline, as well as potential obscuring of stromules via clustering. Leaves were brittle and were darker green. Given the obvious stress induced by the 24 h treatment, we chose to use the 16 h light condition for further silencing, despite a slight decrease in silencing efficiency as indicated by the *PDS* control. Importantly, the *TRV2* silencing control did not alter stromule frequencies or plastid morphology relative to the untreated control and so was deemed a suitable VIGS

⁵YL192, purchased from ABRC - www.arabidopsis.org, stock number: CD3-1039

⁶*PDS* isolated from *N. benthamiana*, provided by S. Schornack.

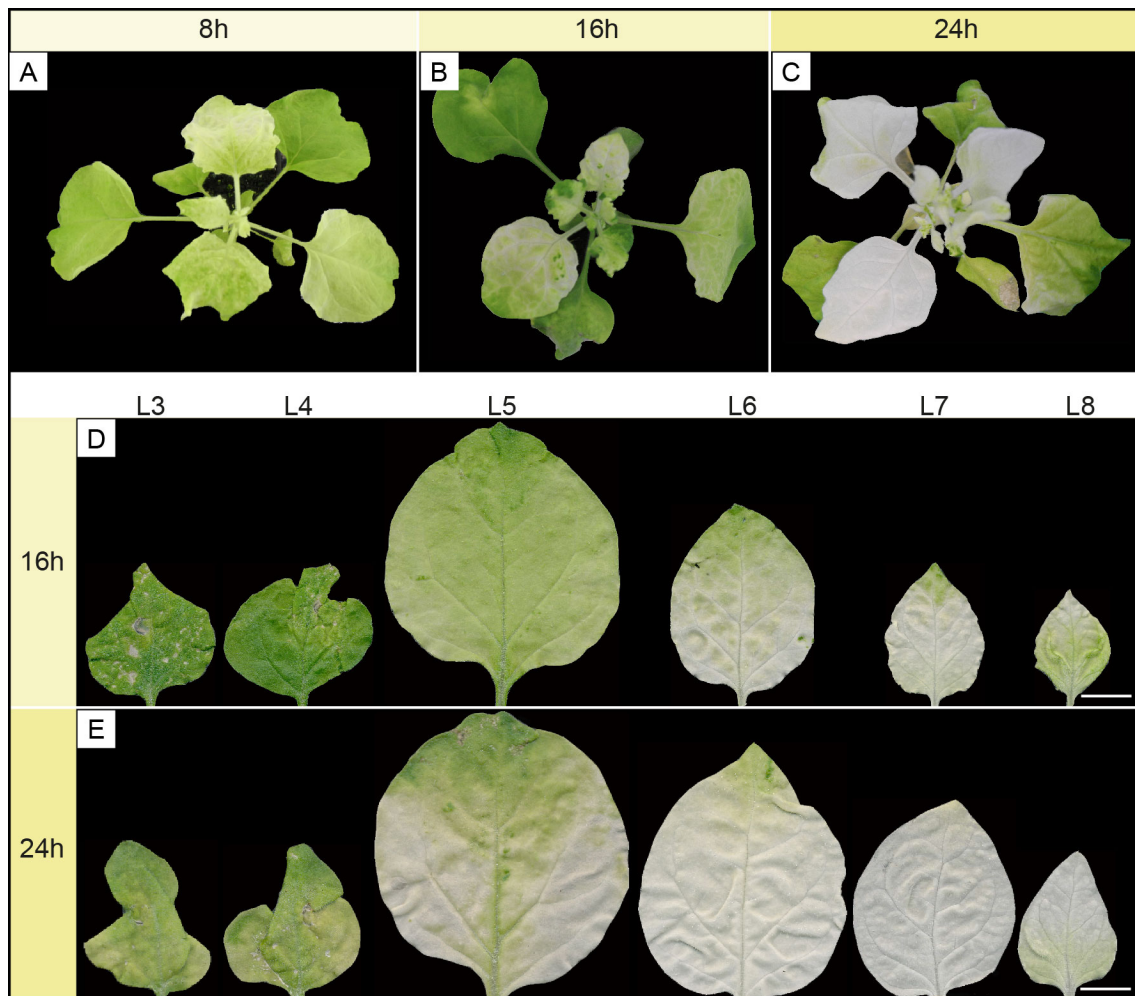


Figure 7.3.: VIGS silencing of *PDS* in *N. benthamiana* is most efficient under 24 h light conditions. *PDS* silencing of *FNRtp:eGFP* transgenics under (A) 8 h day/16 h night, (B) 16 h day/8 h night and (C) 24 h light. White tissue is indicative of effective silencing. (D and E) Leaves from *PDS*-silenced plants under (D) 16 h day/8 h night and (E) 24 h light, after 14 days of silencing. Leaves were numbered as they emerged, with VIGS infiltrations into leaves 3 (L3) and 4 (L4). All subsequent, and newly formed leaves showed varying degrees of silencing in the two treatments (L5-L8). Scale = 1 cm.

negative control for further silencing experiments (Figure 7.4 on the next page, panels B and D).

Replicating stromule suppression phenotype utilizing *Sl17E6*

Following the optimization of the VIGS system, we re-tested the stromule suppression phenotype of *Sl17E6* according to the schematic outlined in Figure 7.5 on page 110, panel A. As described in Erickson et al. (2014), *N. benthamiana* lower epidermis typically exhibits very low basal stromules levels, but following infiltration with GV3101 the stromule frequency jumps up to approximately 30% (Figure 7.5, panel B-No VIGS). This also held true in *TRV2*-silenced plants inoculated with GV3101, with GV3101 inducing significantly higher stromule frequencies than non-infiltrated zones (Rank Sum: $U = 0$, $p < 0.001$) and absolute stromule frequencies comparable to unsilenced plants (Figure 7.5 panel B, and compare images in C and D). This indicates that silencing with the negative control does not alter stromule frequencies. In contrast, silencing using *Sl17E6* severely suppressed GV3101-induced stromules,

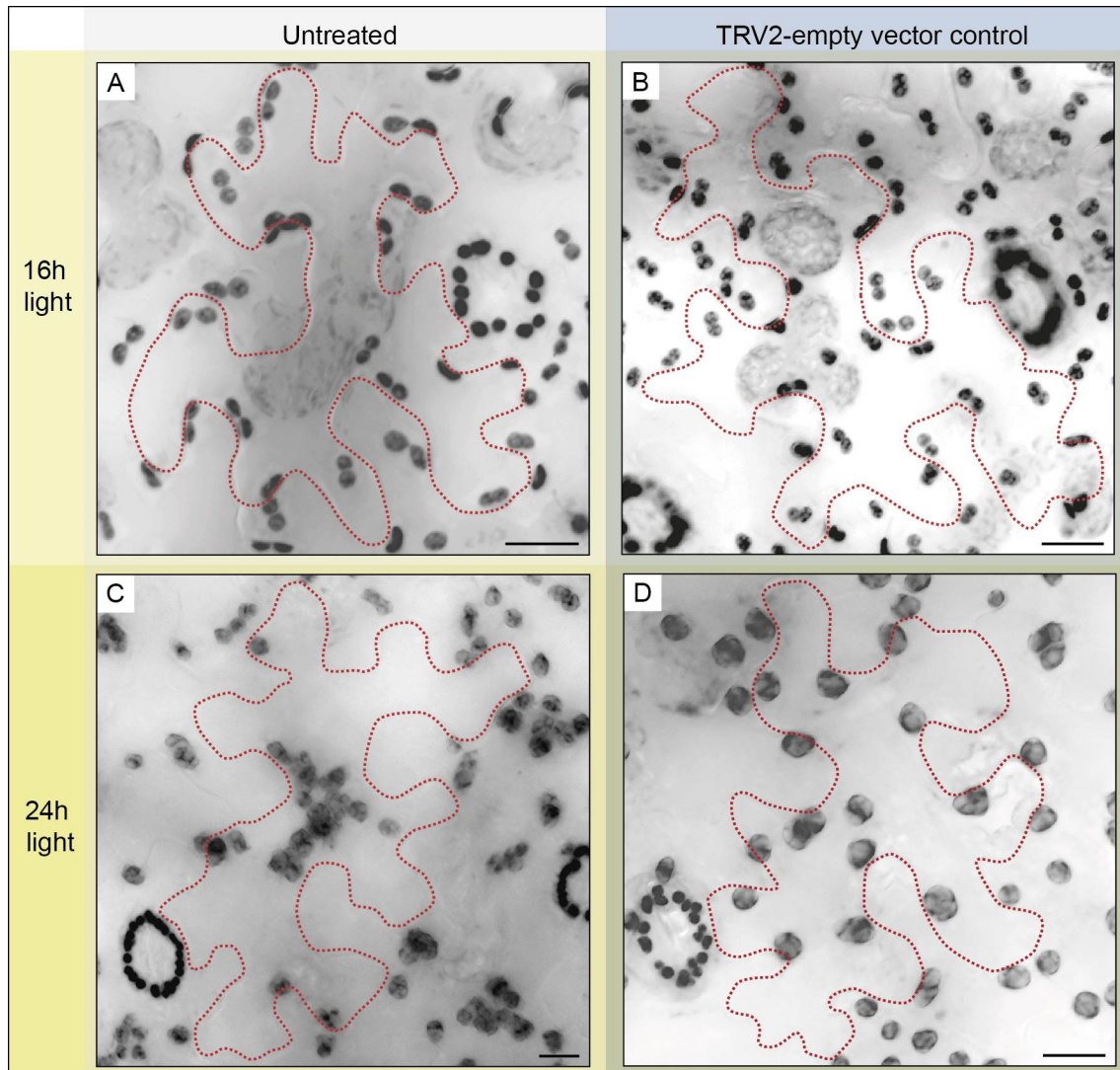


Figure 7.4.: Plastid morphology differs depending on light conditions. Plastid morphology in *N. bethamiana* (*FNRtp:eGFP* stable transgenics) lower leaf epidermis under 16 h (A and B) and 24 h (C and D) light conditions in both untreated tissue (A and C) as well as tissue infiltrated with VIGS silencing vectors *TRV1* and *TRV2* vector control (B and D). Plants in (B) and (D) were silenced with the *TRV1/TRV2* at the 4 leaf stage and images were taken from leaf 6, after 14 days of silencing. Plants grown under 24 h light show drastic starch accumulation, visible as GFP free spots within the plastid body. For ease of visualization plastids were converted to gray scale and inverted, so plastids are visible in dark gray-black. Dotted lines denote boundaries of single cells. Scale = 20 μ m.

with stromule frequencies that were not significantly different than the non-infiltrated control (Rank Sum: $U = 143$, $p = 0.31$) (Figure 7.5, panel B, and compare panels E and F). This confirmed the results of the original screen, suggesting the importance of *Sl17E6* to stromule formation via *A. tumefaciens* strain GV3101.

Growth phenotype of *Sl17E6* silenced plants

It should be noted, independent of the silencing construct used, that the presence of the TRV resulted in retarded growth and development compared to plants that were not infiltrated with the virus. Untreated plants flowered sooner and were usually slightly bigger. However, apart from being slightly smaller than 'No VIGS' plants, silencing using *Sl17E6* produced plants that appeared healthy (Figure 7.6 on page 111, panel B). *Sl17E6* plants were indistinguishable

from plants silenced with other randomly silenced clones tested during the VIGS silencing screen (data not shown), confirming the small difference in growth rate is very likely due to the presence of the virus and not *Sl17E6* silencing. In contrast, it was found that the *TRV2* silencing controls, although exhibiting no stromule phenotype, show a more drastic decrease in plant size relative to *Sl17E6* silenced plants (Figure 7.6 on page 111, panels C and D). Empty *TRV2* is a standard silencing control (Padmanabhan et al., 2013) and based on the lack of stromule phenotype we continued to use it for further experiments.

7.2.2. Over-expression of *Sl17E6* results in mild stromule induction

Since silencing of *Sl17E6* in *N. benthamiana* suppresses stromules, the next step was to test whether over-expression of this gene has the opposite effect. To evaluate whether stromules are triggered via *Sl17E6* over-expression, the *Sl17E6* cDNA was placed under the control of the *A. thaliana* *UBIQUITIN 10* (*UBQ*) promoter and tagged with mRFP⁷. Transient *A. tumefaciens*-mediated over-expression of a *UBQ::mRFP* empty vector control, *UBQ::mRFP:Sl17E6* and *UBQ::Sl17E6:mRFP* was performed in *N. benthamiana* (*FNRtp:eGFP*) lower epidermis and stromule frequency was evaluated in expressing cells. LBA4404 was chosen to mediate over-expression assays, since it induces few stromules (stromule frequencies of 10-20%, Erickson et al., 2014), making it easier to recognize increases in stromule number triggered during protein over-expression. GV3101 was chosen as a positive control for stromule induction. In line with data presented in Erickson et al. (2014) the LBA4404-derivative mediating mRFP expression induced around 20% stromules (Figure 7.7 on page 111). Over-expression of *Sl17E6* with N and C-terminal mRFP tags showed a slight increase in mean stromule frequency compare to mRFP alone, however this increase was not significant (mRFP/mRFP-*Sl17E6* Rank Sum: $U = 22$, $p = 0,066$; mRFP/*Sl17E6*-mRFP Rank Sum: $U = 21$, $p = 0.093$; Figure 7.7, panel D). Comparison to the positive control indicated that there was no significant difference between GV3101-infiltrated tissues and *Sl17E6* over-expression treatments (mRFP-*Sl17E6*/GV3101 Rank Sum: $U = 37$, $p = 0.0540$; *Sl17E6*-mRFP/GV3101 Rank Sum: $U = 28$, $p = 0.289$). Stromule induction via *Sl17E6* over-expression appears to lie between the negative and positive controls. When taken in combination with the results from the VIGS experiments, the moderate over-expression phenotype was sufficient evidence to suggest that GRAM domain containing proteins could prove important for stromule induction in *N. benthamiana* and were worth investigating further.

mRFP tagged *Sl17E6* is localized to the cytoplasm and is nuclear excluded

Given that nearly nothing is known about tomato or *N. benthamiana* GRAM protein function or localization patterns, over-expression constructs were used to examine sub-cellular localization of *Sl17E6*. Expression of the *mRFP* control results in clear nuclear and cytoplasmic localization (Figure 7.8 on page 112, panel A). Cytoplasmic localization was evident by the labeling of cytoplasmic strands with mRFP (Figure 7.8, panel A shows examples labeled as 'cs')

⁷pUB-Dest vector series, Grefen et al. (2010)

and cell outlines were clearly visible. mRFP-S117E6 and S117E6-mRFP were also cytoplasmic in epidermal and mesophyll cells (Figure 7.8, panels B-G), but were largely excluded from the nucleus of epidermal cells when compared to the mRFP control (Figure 7.8 on page 112, panels B and C). At this point it is not clear whether nuclear exclusion represents that true sub-cellular localization of this protein, or whether this is a result of the increased size created by the fusion to mRFP.

Based on its influence on stromule frequency, one might suspect localization of S117E6 to the plastid. However, S117E6 did not visibly overlap with plastid autofluorescence signals in either the epidermis (Figure 7.8 on page 112, panel B and C) or the mesophyll (Figure 7.8, panels D-G). There are clear holes in the S117E6 expression in mesophyll cells in the location of chloroplast autofluorescence signals. It appears that despite being important to stromule induction, S117E6 is not localized to plastids.

7.2.3. Identifying silencing targets of *Sl17E6* in *N. benthamiana*

At this point the silencing targets of the *TRV2::Sl17E6* in *N. benthamiana* were not yet known, so the stromule suppression phenotype observed during the VIGS screen and confirmation experiments could not be attributed to the knockdown of any specific transcript in *N. benthamiana*. Although the ability of *Sl17E6* over-expression to cause moderate stromule induction caused us to suspect that *N. benthamiana* GRAM proteins are also important to stromule formation, we had to confirm that the silencing targets of *Sl17E6* included genes belonging to the GRAM family. An *in silico* approach was chosen to determine what *N. benthamiana* GRAM family transcripts were likely to be knocked-down during *Sl17E6* silencing, as well as to identify any potential off-targets.

SGN VIGS tool

In order to identify silencing targets of *TRV2::Sl17E6* in *N. benthamiana* we analyzed the sequence using the 'SGN VIGS tool'⁸. The SGN VIGS tool is free online software developed by the Sol Genomics Network (Bombarely et al., 2012) to simulate VIGS *in silico* for the purpose of simplifying VIGS construct design, facilitating effective and specific silencing, and predicting silencing targets and off-targets of any construct sequence used as an input. In order to predict targets, the input is broken down into 21 nucleotide fragments (called 'n-mers'), simulating the cleavage of dsRNA by DICER (Fernandez-Pozo et al., 2015). Fragments are then mapped to the *N. benthamiana* model transcriptome, simulating the recognition of homologous host mRNAs by the RISC-siRNA complex (Fernandez-Pozo et al., 2015). Gene models with regions homologous to the n-mers generated by the algorithm are considered potential silencing targets (Fernandez-Pozo et al., 2015). The VIGS tool output displays the gene number of all potential targets, as well as the number of n-mers that match the target sequence, the position of n-mers, and a functional description of proteins (Fernandez-Pozo et al., 2015). The ability of the algorithm to identify potential VIGS targets in this way, made

⁸<http://vigs.solgenomics.net/>

it ideal for analysis of *SL17E6*. When the *SL17E6* cDNA was used as an input and analyzed via default parameter settings (mismatches = 0, n-mer size = 21) only four potential targets were identified (Table 7.2). Setting 'mismatches' to 0 means that alignments between n-mers and targets have 100% base pair identity. According to the VIGS tool output each of the four targets identified has only 1 n-mer produced that perfectly matched the target sequence (See 'Matches' category of Table 7.2). Interestingly, only one of the targets identified by the VIGS tool was a GRAM domain containing protein (Niben101Scf00821g14009.1, Table 7.2).

Gene	Matches	Functional Description
Niben101Scf15760g00013.1	1	Unknown protein
Niben101Scf08137g05005.1	1	Tubulin-folding cofactor B
Niben101Scf08137g05007.1	1	UPF0614 protein C14orf102, putative isoform2 (<i>Theobroma cacao</i>)
Niben101Scf00821g14009.1	1	GRAM domain-containing protein / ABA responsive protein-related

Table 7.2.: SGN VIGS tool identifies four possible targets of *TRV2::SL17E6* in *N. benthamiana* (mismatches = 0, n-mer size = 21). The gene number of target identified is listed in column 1, the number of n-mers generated that match the target is shown in column 2, and the functional description based on sequence similarity to previously characterized proteins is in column 3. A single GRAM domain containing protein (in bold) was identified.

Although it was initially thought that VIGS requires an exact match between siRNA and the target mRNA for silencing to occur, it is now known that, in practice, the VIGS system frequently allows for at least one mismatch (Senthil-Kumar and Mysore, 2014). Therefore, a second analysis of *SL17E6* was performed, changing the parameter of 'mismatches' to 1, producing an output containing 9 additional putative targets (Table 7.3 on the facing page). Of these, the two top hits were GRAM domain containing proteins, one being Niben101Scf00821g14009.1, the candidate from the previous search, and a second being Niben101Scf04406g06011.1, which I chose to call Nb17E6-1 and Nb17E6-2 respectively.

A SGN BLAST of *SL17E6* nucleotide sequence to the *N. benthamiana* genome⁹ revealed *Nb17E6-1* and *Nb17E6-2* as the only hits (Figure 11.2 on page 145, panel A), thus confirming their similarity to *SL17E6*. DNA alignments demonstrate the similarity between predicted cDNA sequences of the two *N. benthamiana* GRAM genes (sequences extracted from the SGN) and *SL17E6* (Figure 11.2, panels B and C). Since *Nb17E6-1* and *Nb17E6-2* appear to be the top candidates for silencing during VIGS, we chose to focus on their characterisation in the context of stromule regulation.

Corrections to the SGN predicted cDNA sequence of *Nb17E6-1*

For further analysis of *Nb17E6-1* and *Nb17E6-2* I wanted to ensure that the predicted cDNA sequences annotated by the SGN were accurate. For this purpose these genes were cloned into pDONR221 and sequenced. During primer design, RNA sequencing data was referenced via the SGN 'JBrowse' tool¹⁰ to determine the likely start and stop codons of *Nb17E6-1* and *Nb17E6-2*. Due to sequence similarity between the ends of the coding sequence of these

⁹ *N. benthamiana* Genome v1.0.1 predicted cDNA, <https://solgenomics.net/tools/blast/>

¹⁰ *N. benthamiana* draft genome v1.0.1, https://solgenomics.net/jbrowse_solgenomics/,

Gene	Matches	Functional Description
Niben101Scf00821g14009.1 (Nb17E6-1)	20	GRAM domain-containing / ABA-responsive protein-related
Niben101Scf04406g06011.1 (Nb17E6-2)	5	GRAM domain-containing / ABA-responsive protein-related
Niben101Scf15760g00013.1	4	Unknown protein
Niben101Scf08137g05007.1	3	UPF0614 protein C14orf102, putative isoform2 (Theobroma cacao)
Niben101Scf01143g01009.1	3	18S pre-rib gar2-related, putative isoform 2 (Theobroma cacao)
Niben101Scf08137g05005.1	3	Tubulin-folding cofactor B
Niben101Scf11235g04013.1	2	Insulin-degrading enzyme
Niben101Scf04185g04010.1	2	BnaA05g04350D (Brassica napus)
Niben101Scf06013g00008.1	2	peptidase M16 (Vibrio parahaemolyticus)
Niben101Scf01587g02009.1	2	Serine/threonine-protein kinase 3
Niben101Scf06966g00015.1	1	BnaA05g04350D (Brassica napus)
Niben101Scf02964g00008.1	1	Tic22-like family protein
Niben101Scf28230g00015.1	1	Tic22-like family protein

Table 7.3.: SGN VIGS tool identifies thirteen possible targets of *TRV2::Sl17E6* in *N. benthamiana* (mismatches = 1, n-mer size = 21). The gene number of target identified is listed in column 1, the number of n-mers generated that match the target (allowing for \leq one mismatched base) is shown in column 2, and the functional description based on sequence similarity to previously characterized proteins is in column 3. Two GRAM domain containing proteins (in bold) were identified.

genes one primer pair was used to simultaneously amplify both products from *N. benthamiana* cDNA. A single nucleotide difference between *Nb17E6-1* and *Nb17E6-2* makes these two genes distinguishable via a *BamHI* digest, where *Nb17E6-1* is cut at position 224, but not *Nb17E6-2*. Isolated clones were digested and sequenced to confirm their identity as *Nb17E6-1* or *Nb17E6-2*, and to determine the exact cDNA sequence. We found that *Nb17E6-2* perfectly matched the predicted cDNA sequence. In contrast, we found a mistake in the *Nb17E6-1* predicted sequence; an intron was mistakenly included in the coding sequence, making the predicted protein sequence far too long. Additionally, we found one silent single nucleotide polymorphism at base pair 267. An alignment between the predicted and the cloned *Nb17E6-1* can be found in Figure 11.3 on page 146.

With the corrected *Nb17E6-1* sequence in hand, an alignment to the *Nb17E6-2* cDNA and translated protein sequences revealed that two loci are remarkably similar (Figure 11.4 on page 147). The main difference between these proteins is a small region near the N-terminus which is missing in *Nb17E6-2* (amino acids 11-16 of *Nb17E6-1*), but otherwise these two predicted proteins are nearly identical.

7.2.4. Confirming silencing of *Nb17E6-1* and *Nb17E6-2* via real-time PCR

Although, based on sequence similarity, *Nb17E6-1* and *Nb17E6-2* were likely targets of *TRV2::Sl17E6*, this needed to be confirmed via quantitative Real-Time PCR (qRT-PCR). Due to the similarity of *Nb17E6-1* and *Nb17E6-2* sequences, real-time primers could not

be designed in a way that would distinguish between the the two transcripts. As a result, primers were designed to amplify both transcripts simultaneously. Reference genes and primer sequences were chosen based on work by Liu et al. (2012), where *APR*, *EF1a* and *PP2A* were identified as the most stably-expressed transcripts in VIGS experiments in *N. benthamiana*. Tissue was collected from one full VIGS experiment (3 plants for each treatment), and RNA from each treatment was pooled to allow for processing of a whole experiment in one 69-well plate with all four primer pairs (three reference genes plus *Nb17E6*). The first qRT-PCR experiment shows a 37% reduction in *Nb17E6* transcripts during *Sl17E6* silencing, relative to the *TRV2* control treatment (Figure 7.9 on page 113). The silencing of *Nb17E6* was even more effective in GV3101-infiltrated tissue, where there was a 66% reduction in transcript levels. Results shown here are preliminary, and this experiment should be repeated two more times in order to ensure that the impact on *Nb17E6* expression is reproducible. Although more biological repeats are needed, this data provides strong indications that *N. benthamiana 17E6* transcripts are targeted for silencing utilizing *TRV2::Sl17E6*.

7.2.5. Confirming stromule suppressing effect of *Nb17E6* silencing

Selecting appropriate cDNAs for silencing using the SGN VIGS tool

One disadvantage of VIGS is the potential for the silencing of off-targets. Although we identified two GRAM family transcripts that are likely silencing candidates for *Sl17E6*, we have identified 11 potential off-targets that could also be causing the stromule suppression phenotype (Table 7.3 on the previous page). To eliminate the silencing of off-targets, the SGN VIGS tool was used a second time to design a more specific silencing construct. When using the full length *Sl17E6* cDNA sequence as the query the algorithm identified base pairs 131-430 as the 'best target region' for specific silencing of *Nb17E6-1* (highlighted in yellow in Figure 11.5 on page 148). This region of *Sl17E6* features 10 n-mers matching only *Nb17E6-1*. According to this result, base pairs 131-430 were amplified from the original *Sl17E6* clone and incorporated into the *TRV2* vector to be used for silencing. The short version of the *Sl17E6* (henceforth referred to as *Sl17E6*¹³¹⁻⁴³⁰) results in highly specific silencing, but the reduction in the number of n-mers could result in reduced silencing efficiency.

As an alternative to *Sl17E6*¹³¹⁻⁴³⁰, we chose to generate one final silencing construct using the the full length of *Nb17E6-1*. Although this re-introduces potential off-target silencing, the VIGS tool predicts a massive number of n-mers specific to both *Nb17E6-1* (1062 n-mers) and *Nb17E6-2* (677 n-mers), compared to 4 or less n-mers produced for all off-targets (Figure 11.6 on page 149 and Table 7.4 on the facing page). Interestingly, we identified two additional GRAM domain containing sequences during the *Nb17E6-1* silencing simulation, one which is described as an ABA-responsive protein (Niben101Scf20961g00007.1) and FIP1 (Niben101Scf04950g06001.1). In contrast to *Sl17E6*¹³¹⁻⁴³⁰, the clone *Nb17E6-1* was designed to facilitate very thorough silencing of both *Nb17E6-1* and *Nb17E6-2*, while potentially sacrificing specificity. Via the generation of these two constructs, two different strategies were used to confirm that our phenotype is really the result of the knockdown of *Nb17E6-1*, and perhaps *Nb17E6-2* as well.

Gene	Matches	Functional Description
Niben101Scf00821g14009.1	1062	GRAM domain-containing / ABA-responsive protein-related
Niben101Scf04406g06011.1	677	GRAM domain-containing / ABA-responsive protein-related
Niben101Scf05559g01009.1	4	Chalcone-flavanone isomerase family protein
Niben101Scf20961g00007.1	3	ABA-responsive protein [Zea mays]
Niben101Scf04950g06001.1	3	FIP1 [Zea mays]
Niben101Scf00849g01018.1	2	Chalcone-flavanone isomerase family protein
Niben101Scf06819g05002.1	2	BnaC04g54350D [Brassica napus]
Niben101Scf02915g08013.1	2	Syntaxin-81
Niben101Scf03380g01009.1	1	Protein TIME FOR COFFEE
Niben101Scf02739g01002.1	1	Protein TIME FOR COFFEE
Niben101Scf07728g01019.1	1	Pentatricopeptide repeat-containing protein
Niben101Scf02803g01009.1	1	Exocyst complex component SEC8
Niben101Scf10505g00003.1	2	Syntaxin-81
Niben101Scf11688g01018.1	1	Exocyst complex component SEC8
Niben101Scf1171g08017.1	1	26S proteasome non-ATPase regulatory subunit 1 homolog B

Table 7.4.: SGN VIGS tool identifies possible targets of *TRV2::Nb17E6-1* in *N. benthamiana* (mismatches = 1, n-mer size = 21). The gene number of target identified is listed in column 1, the number of n-mers generated that match the target (allowing for \leq one mismatched base) is shown in column 2, and the functional description based on sequence similarity to previously characterized proteins is in column 3. GRAM domain family members emphasized in **bold** font.

Silencing utilizing *SI17E6*¹³¹⁻⁴³⁰ and *Nb17E6-1* reduced GV3101-induced stromules

Armed with *TRV2::17E6* constructs which were predicted to be either highly specific (*SI17E6*¹³¹⁻⁴³⁰), or highly effective (*Nb17E6-1*) for the silencing of *Nb17E6*, the VIGS experiment was repeated. The result was that both constructs showed the same ability to suppress GV3101-induced stromule formation as the original *SI17E6* clone (Figure 7.10 on page 114). Stromule levels were very low (5-10 %) in non-infiltrated tissue following silencing using both *SI17E6*¹³¹⁻⁴³⁰ (Figure 7.10, panel C) and *Nb17E6-1* (Figure 7.10, panel D), and largely resemble unsilenced or *TRV2* control silenced tissue (shown in Figure 7.5 on page 110, panel C). Stromule frequency values remained at this level or lower following infiltration with GV3101. Therefore, silencing with three independent constructs, two of which were specifically designed to target *Nb17E6-1*, has provided us with the same stromule suppressing phenotype, strongly suggesting that this GRAM domain containing protein plays a role in stromule formation.

7.2.6. Over-expression of *Nb17E6* proteins confirm their relevance to stromule formation

VIGS experiments suggest that silencing of *Nb17E6* reduces stromules frequency. To confirm the link between *Nb17E6* and stromules, *Nb17E6-1* and *Nb17E6-2* were transiently over-expressed in *N. benthamiana* (*FNRtp:eGFP*) to determine if stromules could be induced. As previously mentioned, *SI17E6* over-expression showed a 'tendency' toward stromule induction, however, it was not significantly different from control infiltrations. Suspecting that moderate stromule induction could be the result of the promoter used to drive over-expression of *SI17E6* (*A. thaliana UBQ10*), the stronger, *35S* Cauliflower Mosaic Virus (CaMV) promoter was chosen to direct over-expression of *Nb17E6-1* and *Nb17E6-2*. Therefore, both *Nb17E6* cDNAs were cloned into *pGWB554* and *pGWB555* vectors¹¹ to create C-terminal and N-terminal mRFP tagged fusions.

Excitingly, transient over-expression of *Nb17E6-1* and *Nb17E6-2* driven by the *35S* promoter resulted in significant and obvious stromule induction relative to the negative control, regardless of whether mRFP tags were on the C or N terminus of the protein (Figure 7.11 on page 115). Although the over-expression clearly resulted in stromule induction, individual spots or cells chosen for microscopy showed high variability in stromule number. For example the *Nb17E6-1:mRFP* over-expression yielded a maximum stromule frequency of 58% in one image, and as low as 18% in another image taken from the same leaf disc. Importantly, all cells chosen for stromule quantification showed fusion protein expression, as indicated by the presence of mRFP. Although this variability in stromule induction was puzzling, induction by GRAM domain containing proteins is exciting given that very few proteins have been identified that induce stromules when over-expressed.

Localization studies of *Nb17E6-1* and *Nb17E6-2* showed an expression pattern identical to that of *SI17E6*; cytosolic and nuclear excluded (Figure 7.12 on page 116). As was the case with *SI17E6*, the significance of the nuclear exclusion of these proteins is unclear at this

¹¹Provided by Tsuyoshi Nakagawa, of Shimane University, Matsue, Japan.

point, since adding the mRFP increases the size of the protein significantly (from 31.8kDa to 58.6kDa). Weak mRFP signals were often observed in the nucleus (Figure 7.12, panel B-E).

7.2.7. Over-expression of GRAM only and no GRAM constructs

In combination, the results from the VIGS and the over-expression experiments indicate the Nb17E6-1 and Nb17E6-2 are important for stromule formation, but raise new questions regarding the mechanism by which this occurs. Since the GRAM domain is the only known protein domain that could be identified (Table 7.5), the next step was to determine what role this domain plays in stromule induction.

Input	Pfam motif identified	Amino Acid Position (Independent E-value)	Pfam Annotation, Description
Nb17E6-1	GRAM	152-269 ($4.9e^{-24}$)	PF02893, GRAM domain
Nb17E6-2	GRAM	146-263 ($4.4e^{-24}$)	PF02893, GRAM domain

Table 7.5.: The GRAM domain is the only conserved protein domain identified in Nb17E6-1 and Nb17E6-2. 'Motif Search' (<http://www.genome.jp/tools/motif/>) output following analysis of the translated ORF of the *Nb17E6-1* and *Nb17E6-2* sequenced clones. Pfam database was used, E-value cut-off = 1.

To test whether the GRAM domain is important for stromule induction two truncated fusion proteins were designed, the first featured a deletion of the GRAM domain (referred to as 'noGRAM' construct), and the second contained only the GRAM domain (referred to as 'GRAM') (Figure 7.13 on page 117, panel A). Nb17e6-1 and Nb17e6-2 are nearly identical in amino acid sequence and stromule inducing capacity, so it was decided that truncating both proteins would be unnecessary. Therefore, only Nb17E6-1 was used for creating truncated fusions. Additionally, since both C and N-terminal mRFP fusions seemed to result in stromule induction during the transient over-expression assays utilizing the full length protein fusions (refer to Figure 7.11 on page 115), only C-terminal mRFPs were used to label truncated proteins. The results of LBA4404-mediated transient expression of the GRAM domain alone did not result in an increase in stromule levels. While, the noGRAM construct showed significantly higher stromule frequencies than the mRFP control and, surprisingly, also induced more stromules than the full length Nb17E6-1 (Figure 7.13 on page 117, panel B). Although the full length Nb17E6-1 construct showed a significant increase in stromule frequency relative to the mRFP control in initial experiments, this was not always the case during these infiltrations (Figure 7.13, panel B). As mentioned previously, stromule induction via Nb17E6-1 was sporadically very high, or did not appear any different from the mRFP control. However, there was a tendency for stromule induction in all experiments. In contrast, noGRAM over-expression resulted in consistently higher stromule frequencies than control infiltrations in all experiments (p values of <0.001). Indicating that not only is the GRAM domain not required for induction, but that its elimination from the Nb17E6-1 protein seems to enhance induction.

In contrast to the full length Nb17E6-1-mRFP, the truncated versions both exhibited nuclear-localization (Figure 7.13 on page 117, panel C and D). While the noGRAM was very highly expressed, the GRAM suffered very low expression levels. The detection of the GRAM signal via epifluorescence microscopy required a combination of high lamp intensities (between 73-90%) and high exposure times (1000-1800 ms), and/or further manipulation of display settings to see weak mRFP fluorescence. This is in comparison to a lamp setting of 50% and between 250-500 ms exposure times for mRFP, Nb17E6-1 full length and noGRAM constructs. A more quantitative comparison of protein stability and confirmation of protein size will need to be performed in the future via Western Blot using an mRFP antibody.

7.2.8. Identification of *N. benthamiana* GRAM domain family members

One way to gain insight into protein function is to determine the amino acid similarity of the protein of interest to that of previously characterised proteins, and to other gene family members. The *A. thaliana* GRAM family is fully annotated and some of the proteins have been characterised, making it ideal for comparison with the Nb17E6 GRAM proteins. There are 15 GRAM domain-containing proteins in *A. thaliana*, and these were used in a series of SGN BLAST searches against the '*N. benthamiana* Genome v1.0.1 predicted proteins' database to identify all homologous GRAM proteins in *N. benthamiana*. This resulted in the identification of 25 putative GRAM domain-containing proteins (See Table 7.6 on page 106). Sequences of predicted proteins were extracted from SGN, and GRAM domains were annotated according to predictions by 'Motif Search'. Analysis of all GRAM domain containing sequences from *N. benthamiana* and *A. thaliana* revealed that there is a huge variation in the size of these proteins, the largest being 1051 amino acids long and the smallest only 133 amino acids. The lengths of the predicted GRAM domains themselves also varied in size from 49-149 amino acids long. Although the GRAM domain is often the only domain identified (16/25 *N. benthamiana* proteins), it was also found in combination with the C2 (lipid-binding domain), with DUFs (domain of unknown function) and, less frequently, in combination with other domains.

Chapter 7. VIGS identifies a GRAM protein that regulates stromules

Gene number	Protein length (aa)	Length of GRAM (aa)	Location of the GRAM	Other protein domains
Niben101Scf05188g01002	133	88	40-127	-
Niben101Scf00917g03010	138	49	61-109	-
Niben101Scf05177g01002	165	120	40-159	-
Niben101Scf01267g11013	173	121	52-172	-
Niben101Scf05177g01023	194	115	69-183	-
Niben101Scf05188g01021	201	115	83-197	-
Niben101Scf05177g01019	206	120	81-200	Sterol_MT_C
GRE7At5g23360	210	117	90-206	-
GRE8 At5g23370	219	117	98-215	-
GRE4 At5g08350	222	119	96-214	DUF1492
PRSL1/GRE3 At4g40100	225	89	129-217	RPEL, DUF2285
Niben101Scf05177g01031	227	116	106-221	-
Niben101Scf05177g01029	232	120	107-226	-
Niben101Scf05188g01019	232	120	107-226	-
GRE2 At4g01600	233	120	107-226	-
Niben101Scf06424g00001	234	119	114-232	-
Niben101Scf07440g00009	257	119	137-255	-
Niben101Scf02622g11005	257	59	54-112	-
FIP1/GRE1 At1g28200	259	121	138-258	-
Niben101Scf04950g06001	265	94	171-264	-
GER5/GRE5 At5g13200	272	115	144-258	-
Niben101Scf05697g03012	273	59	54-112	Myotub-related
GRE6 At5g23350	280	118	160-277	-
Nb17E6-2 Niben101Scf04406g06011	285	118	146-263	-
Nb17E6-1 Niben101Scf00821g14009	291	118	152-269	-
Niben101Scf20961g00007	292	120	171-290	-
GEM At2g22475	299	117	176-292	-
Niben101Scf05173g02013	343	83	72-154	DUF 4782
Niben101Scf03457g00003	564	54	212-265	C2, DUF4782
Niben101Scf01077g02010	586	73	225-297	C2, DUF4782
At3g59660	594	73	232-304	C2, DUF4782
Niben101Scf02400g02015	597	149	288-436	DUF 4782
VAD1 At1g02120	598	101	71-171	DUF 4782
MTM2 AT5G04540	833	68	42-109*	Myotub-related, DUF4055, DUF3150, EzrA, HIP1_clath_bdg

Gene number	Protein length (aa)	Length of GRAM (aa)	Location of the GRAM	Other protein domains
MTM1 AT3G10550	840	68	45-112*	Myotub-related, DUF4055
Niben101Scf06423g03027	1012	108	656-763	C2 (2x), DUF4782 (2x)
At1g03370	1020	109	689-797	C2 (2x), DUF4922, DUF4782 (2x)
Niben101Scf04148g00002	1020	71	691-762	C2 (2x), DUF4782 (2x)
At5g50170	1027	81	693-774	C2 (2x), DUF4782 (2x)
Niben101Scf17612g01007	1051	108	695-802	C2 (2x), DUF4782 (2x)

Table 7.6.: GRAM domain containing proteins from *A. thaliana* and *N. benthamiana* show variability in length and combinations with other protein domains. List of all GRAM proteins identified in *A. thaliana* and *N. benthamiana* listed according to ascending size (column 2; aa = amino acids). 'Motif Search' annotations of GRAM domain size and position are listed in columns 3 and 4, and additional protein domains are listed in column 5. Domain annotations are as follows: DUF (domain of unknown function), C2 (phospholipid binding domain), Sterol_MT_C (sterol methyltransferase C-terminal), Myotub-related (myotubularin-like phosphatase domain), RPEL (actin binding motif), EzrA (septation ring formation regulator), HIP1_clath_bdg (clathrin-binding domain). *GRAM annotated by TAIR using InterProScan.pl program and the SMART database. All other GRAM domains annotated via 'Motif Search'.

7.2.9. Nb17E6 in the context of the GRAM family

The amino acid sequences of the GRAM domains of all GRAM-containing proteins were compared to determine the amino acid homology relationship among them (Figure 7.14 on page 118). Sl17E6 was included in the analysis, as well as CaABR1 (ABA RESPONSIVE 1), a previously characterized GRAM domain protein from pepper (Choi and Hwang, 2011). The yeast ScYSP2 GRAM domain was used as an out-group for comparison.

The result of the phylogenetic analysis in Figure 7.14 once again demonstrates the prevalence of proteins harbouring only the GRAM domain. The tree also makes it clear that ABA responsive proteins are scattered throughout the GRAM family (indicated with asterisks), seemingly independent of the other conserved domains present, and independent of protein size (Table 7.6 on the facing page). Indicating, either that ABA-inducibility is conserved among GRAM proteins, or evolved independently in at least 6 instances.

7.2.10. Nb17E6 homologs required for plant resistance to pathogens

The phylogeny clearly displays that 17E6 proteins are part of a small clade containing the previously characterised proteins ABA RESPONSIVE1 (CaABR1, CA01g05510) from pepper (Choi and Hwang, 2011) and GEM-RELATED5 (AtGER5/AtGRE5, At5g13200) (Choi and Hwang, 2011; Baron et al., 2014) (Figure 7.14 on page 118). An alignment of AtGER5, CaABR1, Sl17E6 and Nb17E6-1 confirms high amino acid sequence similarity, both in the GRAM domains, and throughout length of the proteins (Figure 11.7 on page 150). SGN BLASTs using AtGER5 and CaABR1 as queries confirmed Nb17E6-1 as the top hit, with 58% identity (167/284 amino acids) and 74% identity (205/277 amino acids), respectively. Given the clear results of the GRAM domain homology tree and the full-length alignment of these proteins, it was concluded that the previously characterised CaABR1 and AtGER5 are likely homologs of Nb17E6 proteins.

Basal expression of CaABR1 and AtGER5 in leaf tissue is low, however both genes are up-regulated following exogenous ABA application (Choi and Hwang, 2011), as is the barley homolog, 'aba45' (Liu et al., 1999). AtGER5 is also induced under a wide variety of ABA-related abiotic stress stimuli, including mannitol, salt stress, and dehydration (Liu et al., 2013; Jiang et al., 2008; Baron et al., 2014), however the exact role of this protein in abiotic stress response is unclear up to now. In contrast, CaABR1 and AtGER5 have a clearer role during biotic stress and participate in plant defense reactions. CaABR1 is up-regulated in pepper during exposure to an avirulent *Xcv* strain (Bv5-4a) and is required for HR-based plant resistance (Choi and Hwang, 2011).

A quick reminder about HR:

Phytopathogenic viruses, bacteria, fungi and oomycetes all deliver effector proteins into the host cytoplasm where they specifically target a variety of plant cellular processes related to plant immune response and promote pathogen proliferation (Toruño et al., 2016). The recognition of effector proteins by plant R genes or proteins trigger defense responses, initiating effector-triggered immunity (ETI) (Khan et al., 2016). ETI often ends in hypersensitive response (HR), a rapid local cell death that inhibits phytopathogen spread within plant tissue (Klement and Goodman, 1967).

CaABR1 over-expression also enhanced cell death in *A. thaliana* exposed to avirulent *Pseudomonas syringae* pv. *tomato* (*Pst*), a reaction that was accompanied by a strong spike in ROS, a known contributor to programmed cell death (Choi and Hwang, 2011). AtGER5 was also shown to be important for resistance to *Pst* and the biotrophic oomycete pathogen *Hyaloperonospora arabidopsis* (*Hpa*). Silencing or knockouts in these genes in pepper and *A. thaliana* results in increased susceptibility to pathogens (Choi and Hwang, 2011). These proteins were shown to manipulate ABA-SA antagonism during defense reactions by participating in a negative feedback loop with ABA, reducing its concentration and thus increasing the level of SA (Choi and Hwang, 2011). The examination Nb17E6 in the context of the GRAM family provides strong indications that this gene is ABA inducible, and may play a role in hormone level regulation and induction of ROS during immune reactions in *N. benthamiana*.

7.2.11. Nb17E6 silencing inhibits HR in *N. benthamiana*

To get an idea of whether Nb17E6 proteins are involved in plant defense like homologs in pepper and *A. thaliana*, a preliminary test was performed to evaluate the importance of this protein during HR response in *N. benthamiana*. Plants were silenced using the *TRV2* control or the *TRV2::Nb17E6-1* construct and transient over-expression of the *Bs3* resistance gene from pepper was used to induce HR in silenced tissue.¹² Typically *Bs3*-dependent HR occurs in response to the *Xcv* effector *AvrBs3* (Van den Ackerveken et al., 1996), however, transient over-expression of the resistance gene alone is also sufficient to initiate HR in *N. benthamiana* (Römer et al., 2007). Electrolyte leakage was used as a measure of cell death (Mackey et al., 2002) in silenced plants at 24, 48 and 72 hours post-inoculation (hpi). Little difference was seen between the control and *Nb17E6*-silenced tissue at the first time points, however at 72 hpi *Nb17E6* showed less cell-death (Rank sum test: $p = 0.057$, $U = 0$) than the *TRV2* control (Figure 7.15 on page 119). This preliminary experiment provides the first indication that Nb17E6 may be important for HR in *N. benthamiana*, and suggests that this protein may function in a similar manner to the CaABR1 homolog in pepper, however it will have to be repeated. The *TRV2* silencing showed highly variable cell death, suggesting that, although suitable for plastid morphology experiments, it may not be a suitable control for electrolyte leakage assays. This may be due to the silencing of off-targets by the empty vector (Figure 11.8 on page 151 and Table 12.4 on page 157). *TRV2::GFP* would be a better choice going forward.

¹²*35S::Bs3*, kindly provided by Thomas Lahaye, University of Tübingen.

7.2.12. Nb17E6-1 interacting proteins

Although there are indications that Nb17E6 is involved in pathogen response and ABA signaling, little is known about the mechanism of its action. In order to learn more about how Nb17E6 is acting in the cell, and therefore how it could be acting to increase stromule number, a pull-down was done with Nb17E6-1 to identify putative protein interacting partners. This experiment was performed at the Sainsbury Laboratory in Cambridge with the help of Edouard Evangelisti (AG Schornack). N and C-terminal mRFP or sGFP-tagged Nb17E6-1 were transiently over-expressed (LBA4404-mediated) in wild-type *N. benthamiana* for two days, proteins were extracted and co-immunoprecipitation (Co-IP) was performed using RFP-Trap or GFP-Trap beads from Chromotek¹³. Samples were run on 10% SDS gels, Coomassie stained and selected gel pieces were cut out and sent to the Cambridge Centre for Proteomics (Cambridge, UK) for LC-MS/MS (liquid chromatography-mass spectrometry and liquid chromatography - tandem mass spectrometry) analysis (gel pictures in Figure 7.16 on page 119). sGFP-Nb17E6, and Nb17E6-mRFP were sent alongside two unrelated samples (E7 and E14) from E. Evangelisti. GFP and RFP control samples were pooled for the analysis.

Pathogen defense-related genes identified as putative Nb17e6-1 interaction partners

A total of 174 putative interacting proteins were pulled down by Nb17E6-1 fusions during the Co-IP. From the 174 a final short list of 15 proteins were chosen as potential candidates for future work (Table 7.7 on page 124, criteria for selection is outlined in the materials and methods section). 14/15 of proteins identified interacted with Nb17E6-1-mRFP, while only 3/15 interacted with the sGFP-Nb17E6-1 fusion, only 2/15 protein interacted with both Nb17e6-1 fusion proteins. This was not so surprising given that C-terminal protein fusions (sGFP and mRFP) showed more prominent bands on the Coomassie gel (Figure 7.16 on page 119), indicating that an N-terminal tag may interfere with protein interactions *in planta*.

Of the interacting proteins 7/15 have been linked to plant defense reactions, with roles in pathogen-triggered immunity (OMT I-b), resistance to the tobacco mosaic virus (TMV) (OMTI-b, 14-3-3 d-1, 14-3-3 i-2), hormone-driven pathogen response (GSNOR, NbPDR1b), scavenging of reactive nitrogen species (GSNOR) and scavenging of reactive oxygen species (APX, cytosolic ascorbate peroxidase) (Table 7.7 on page 124). Based on the known function of Nb17E6 homologs in pepper and *A. thaliana*, it was already suspected that Nb17E6 is important for HR via the manipulation of hormones levels and ROS, and the identification of interacting proteins related to these processes supports this idea. Further analysis of Nb17E6-1 interacting proteins will provide insight into the mechanism of Nb17e6-1 action, which is not understood up to now. It will also bring us closer to understanding the pathways, proteins and signaling molecules important for stromule formation.

¹³Planegg-Martinsried, Germany

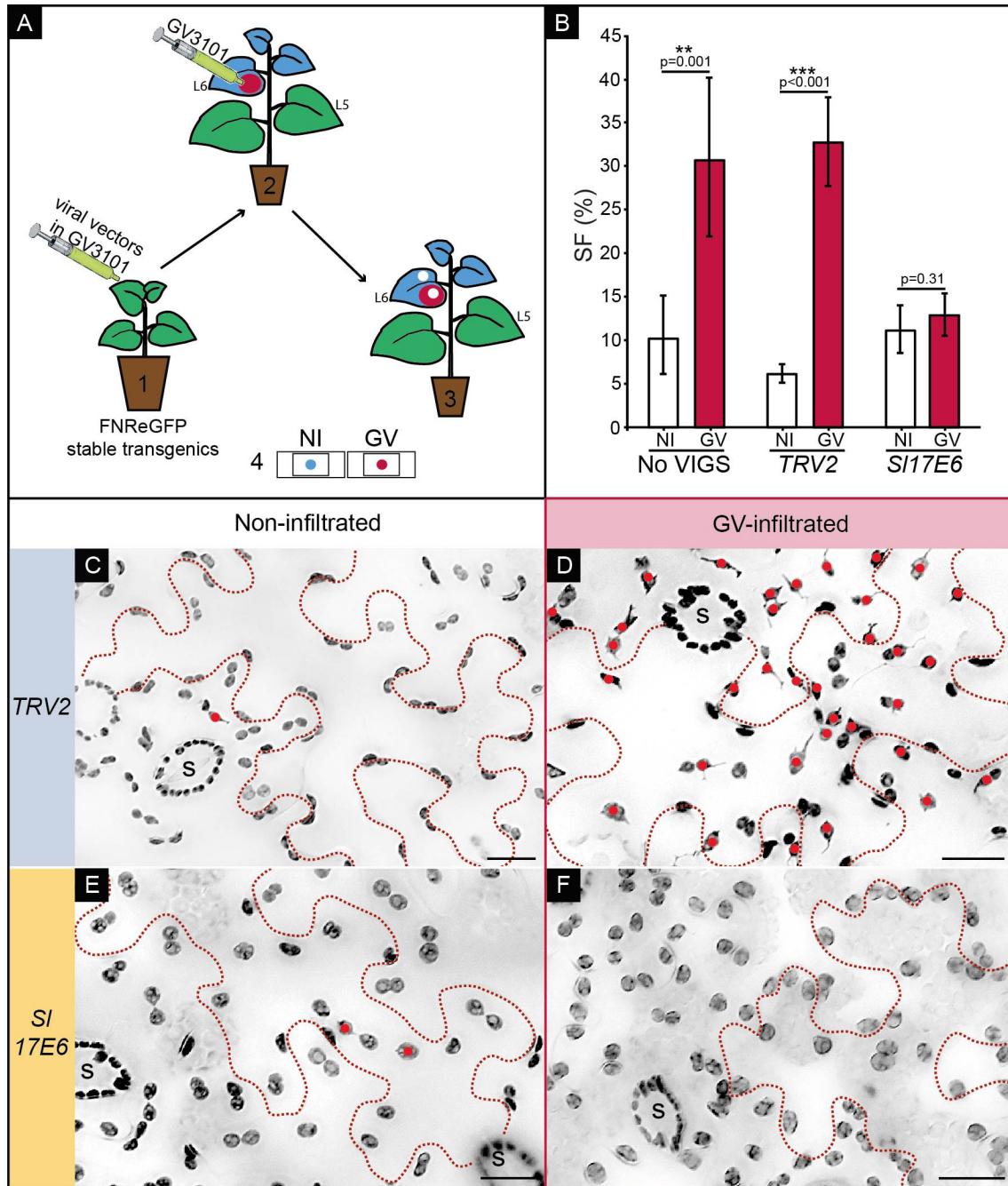


Figure 7.5.: Silencing of *Sl17E6* suppresses the induction of stromules by *A. tumefaciens* strain GV3101 in *N. benthamiana* lower epidermis. (A) The experimental setup used for VIGS silencing of *Sl17E6* and the *TRV2* control plants. The procedure is as follows: **1**) Young plants were infiltrated with GV3101 containing plasmids harboring the recombinant virus: *TRV1* combined with the empty *TRV2* negative control, or *TRV2::Sl17E6*. **2**) Silencing occurred in all new leaves after approximately 15 days (silenced leaves marked in blue), and at this point a silenced leaf was infiltrated with GV3101 to induce stromules (infiltration spot outlined in red). **3**) At 3 dpi with GV3101, leaf punches were isolated from the silenced, non-infiltrated tissue and tissue infiltrated with GV3101. **4**) Leaf punches were evaluated via epifluorescence microscopy, and stromules were quantified. (B) A bar graph of mean back-transformed stromule frequencies (SF) in *N. benthamiana* following silencing (*TRV2* control and *Sl17E6*), in non-infiltrated (white bars/NI) or infiltrated with GV3101 (red bars/GV). Graph shows that *Sl17E6* silencing represses the ability of plants to form GV3101-induced stromules in the epidermis. In addition, data from tissue without VIGS has been included from Erickson et al. (2014) on page 45, panel F as a reference for what the system looks like without VIGS present (first and second bars). $n = 3$ plants for No VIGS treatments, and $n = 4$ plants for VIGS treatments (labeled *TRV2* and *Sl17E6*), and 3 or more images were quantified for each plant. Rank sum test results performed on arcsine transformed data are indicated above the appropriate bars. Error bars represent back-transformed 95% confidence intervals. (C-F) Example images from treatments quantified in (B). Stromule induction following infiltration with GV3101 in *TRV2*-silenced tissues (compare C to D), and a lack of stromule induction in *Sl17E6*-silenced tissues (compare E to F). For ease of visualization images were converted to gray scale and inverted, so plastids are visible in dark gray-black. Dotted lines denote boundaries of single cells. Plastids with stromules indicated with red circles. Scale = 20 μ m.

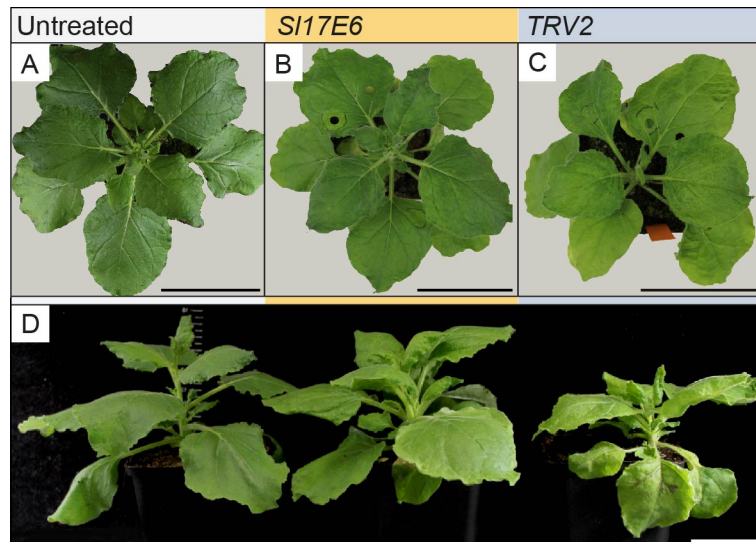


Figure 7.6.: Silencing utilizing *SI17E6* causes no outward signs of decreased plant fitness. Top down view of untreated *N. benthamiana* (A), a *SI17E6*-silenced plant (B), and a *TRV2*-silenced plant (C) 15 days post-viral inoculation. Scale = 10 cm. (D) Side view of an untreated *N. benthamiana*, *SI17E6*-silenced, and *TRV2* control plants (consecutively) at 15 days post-viral inoculation. Scale = 5 cm.

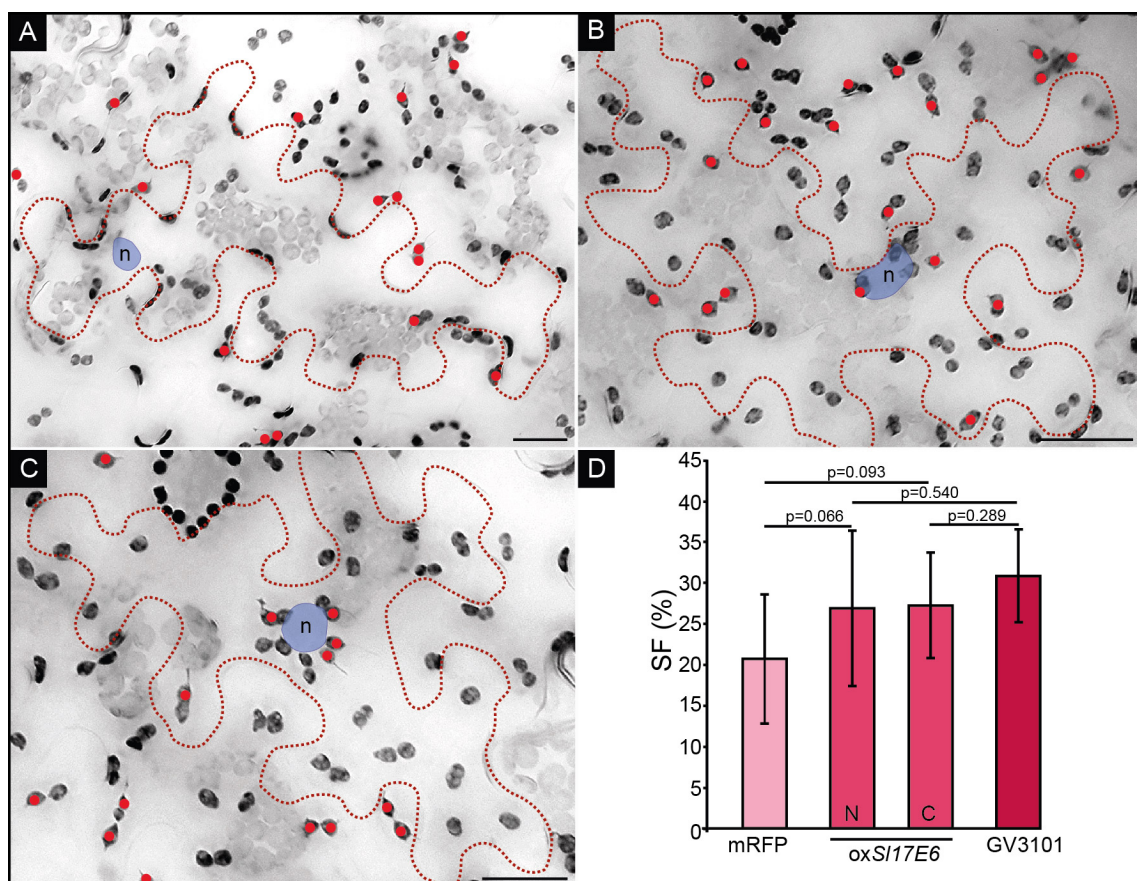


Figure 7.7.: *SI17E6* transient over-expression in *N. benthamiana* lower epidermis via LBA4404 results in slight stomule induction. LBA4404-mediated transient overexpression of (A) *mRFP*, (B) *mRFP:SI17E6* and (C) *SI17E6:mRFP* in *N. benthamiana* lower epidermis (*FNRtp:eGFP*). For ease of visualization images were converted to gray scale and inverted, plastids are visible in dark gray-black. Dotted lines denote boundaries of single cells and the position of the nucleus is highlighted in blue (labeled with 'n'). Plastids with stomules indicated with red dots. Images are combined z-stacks. Scale = 20 μ m. (D) Quantification of the stomule phenotypes shown in (A-C) GV3101 was included as a positive control for stomule induction. Bars represent back-transformed mean stomule frequencies, and error bars represent back-transformed 95% confidence intervals. Rank sum test results performed on arcsine transformed data are indicated above the appropriate bars (n = 3 plants for all treatments with 3 images quantified per plant).

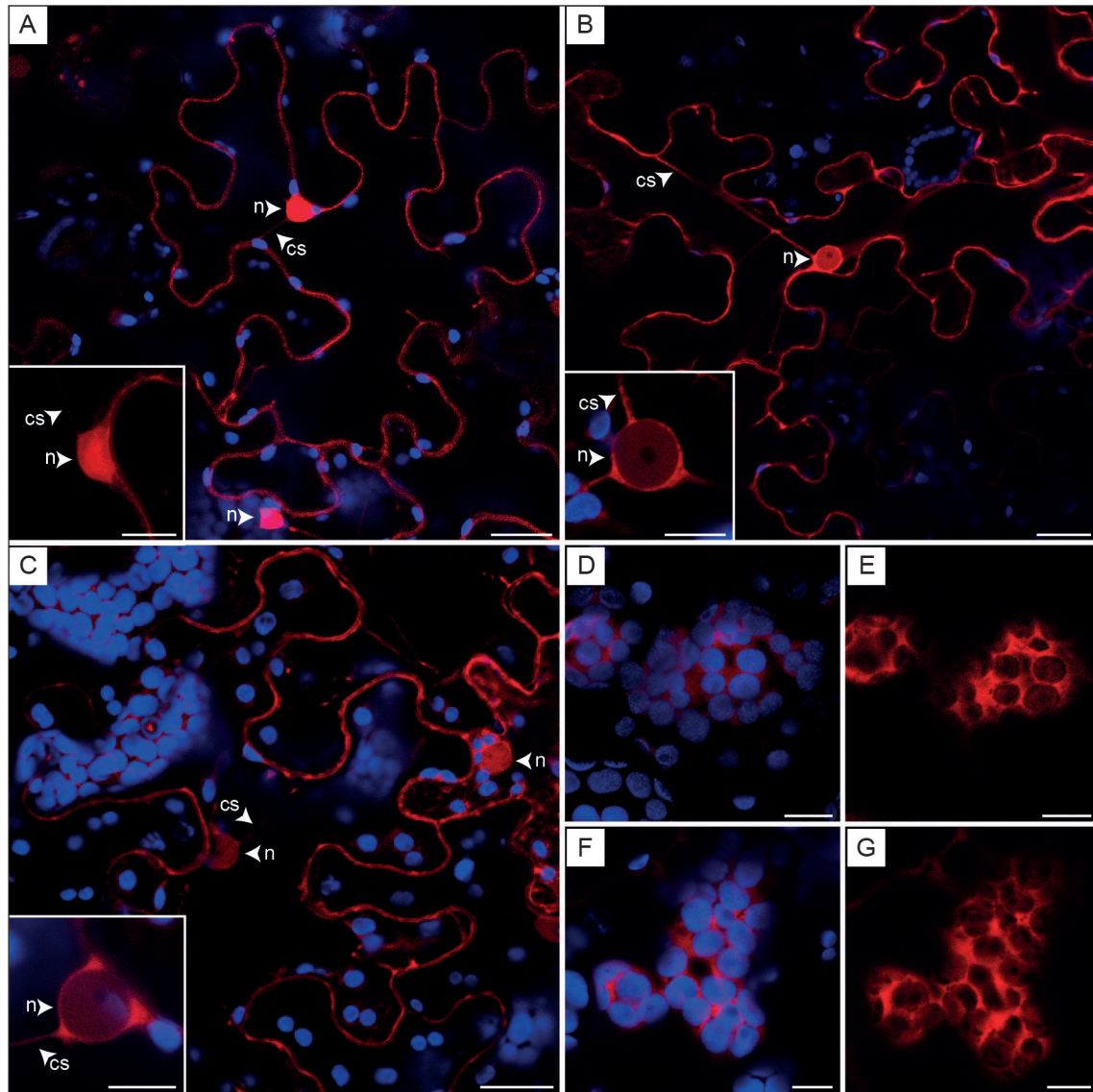


Figure 7.8: Sub-cellular localization of S117E6 in transient assays is cytoplasmic and nuclear excluded. Confocal images taken of wild-type *N. benthamiana* (A-C) lower leaf epidermis and (D-G) mesophyll, inoculated with LBA4404 derivatives mediating the overexpression of mRFP constructs. mRFP channel is visible in red, while plastid autofluorescence is visible in blue. Nuclei are labeled 'n' and cytoplasmic strands are labeled 'cs'. Scale bars in (A-C) are 20 μm (10 μm for all insets) and 10 μm for panels (D-G). (A) *mRFP* negative control shows expression in the nucleus and cytoplasm. Inset shows expression of mRFP in a nucleus at higher magnification. (B) mRFP-S117E6 is cytoplasmic and nuclear excluded. Inset shows a nucleus at higher magnification, a red ring of mRFP-S117E6 is visible around the nucleus with lower levels of mRFP visible inside, an expression pattern that is clearly distinct when compared to the mRFP only control (A). (C) S117E6-mRFP expression appears the same as that of the N-terminally tagged construct, cytoplasmic and mostly excluded from the nucleus. Inset shows a nucleus at higher magnification. Sub-cellular localization of mRFP-S117E6 (D-E) and S117E6-mRFP (F-G) in mesophyll is also cytoplasmic.

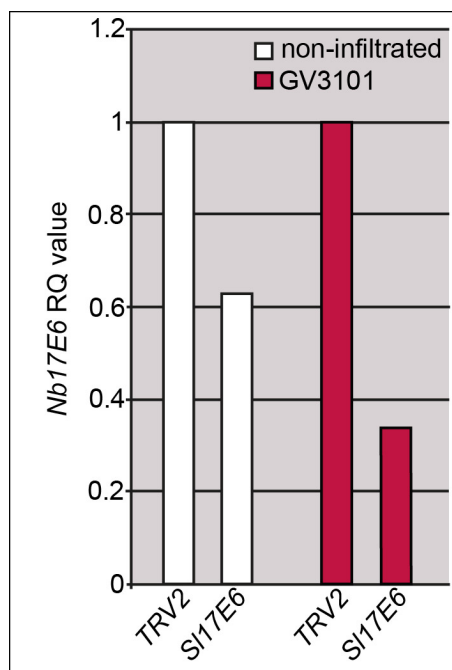


Figure 7.9.: Silencing utilizing *SI17E6* reduces *Nb17E6* transcript levels. Relative quantity of *Nb17E6* transcripts in plants silenced with the *TRV2* control and *SI17E6*, non-infiltrated (white) and infiltrated with GV3101 (red). Bars represent relative quantity of transcripts compared to the *TRV2* control measured from RNA pooled from three plants, and the average of four technical replicates. Error bars are not included, since this data represents only one biological replicate and needs to be repeated.

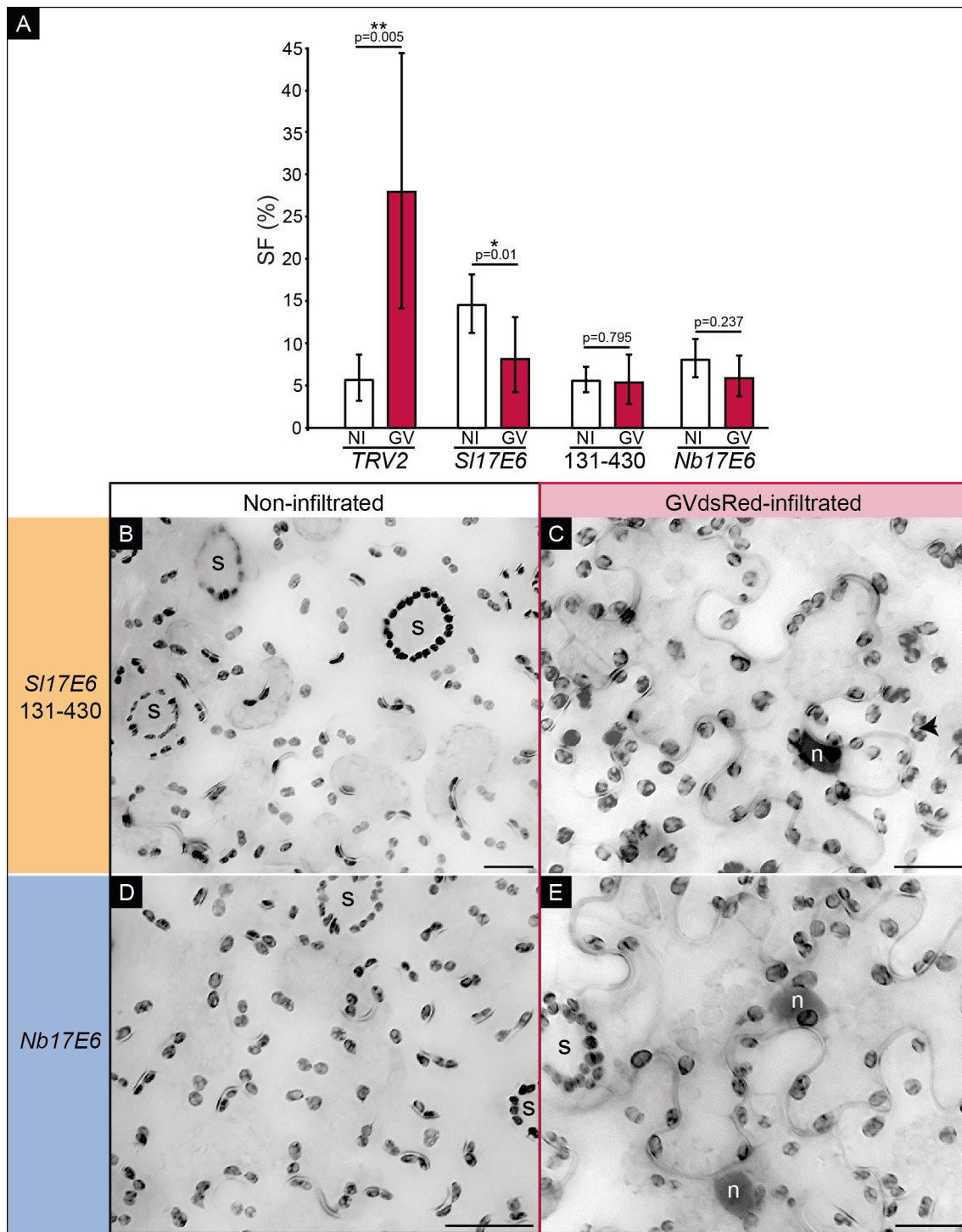


Figure 7.10.: VIGS utilizing the highly specific *SI17E6*¹³¹⁻⁴³⁰ and *Nb17E6-1* full length results in the suppression of GV3101-induced stromules. (A) Quantification of stromule frequencies (SF) in *N. benthamiana* lower epidermis following silencing using the *TRV2* empty vector control, *SI17E6*, *SI17E6*¹³¹⁻⁴³⁰ (labeled 131-430), and *Nb17E6-1* (labeled *Nb17E6*). Silenced tissue was either non-infiltrated (white bars/NI) or infiltrated with GV3101 (red bars/GV). Graph shows that silencing using all three *17E6* constructs significantly represses the ability of plants to form stromules in the epidermis following infiltration with GV3101. Raw data was arcsine transformed and bars represent back-transformed means. Error bars represent back-transformed 95% confidence intervals. Rank-Sum test results are shown above the appropriate bars. $n = 4$ plants with 3 or more images quantified per plant. (B - E) VIGS example images illustrating the lack of stromule induction following infiltration with GV3101 when *17E6* constructs are utilized. (B) and (D) represent tissue silenced with *17E6* constructs but not infiltrated with GV3101, and show phenotypes comparable to control silencing with *TRV2* (compare to Figure 7.5 on page 110, panel C). Tissue in (C) and (E) is silenced with *17E6* and then infiltrated with GV3101, and show a phenotype similar to tissue silenced with the full length *SI17E6*, with very few stromules (compare to Figure 7.5, panel F). Treatment with GV3101 results in an accumulation of starch, which is visible as 'holes' in the eGFP expression (in C an example is labeled with a black arrow). 's' denotes the position of stomata, which were not considered in the analysis, and 'n' denotes the position of nuclei labeled with dsRed. In this case GV3101 expressing dsRed was used for induction because it allows us to monitor the presence of this stromule-inducing bacteria. For ease of visualization images were converted to gray scale and inverted, plastids are visible in dark gray-black. Images are combined z-stacks. Scale bars = 20 μ m.

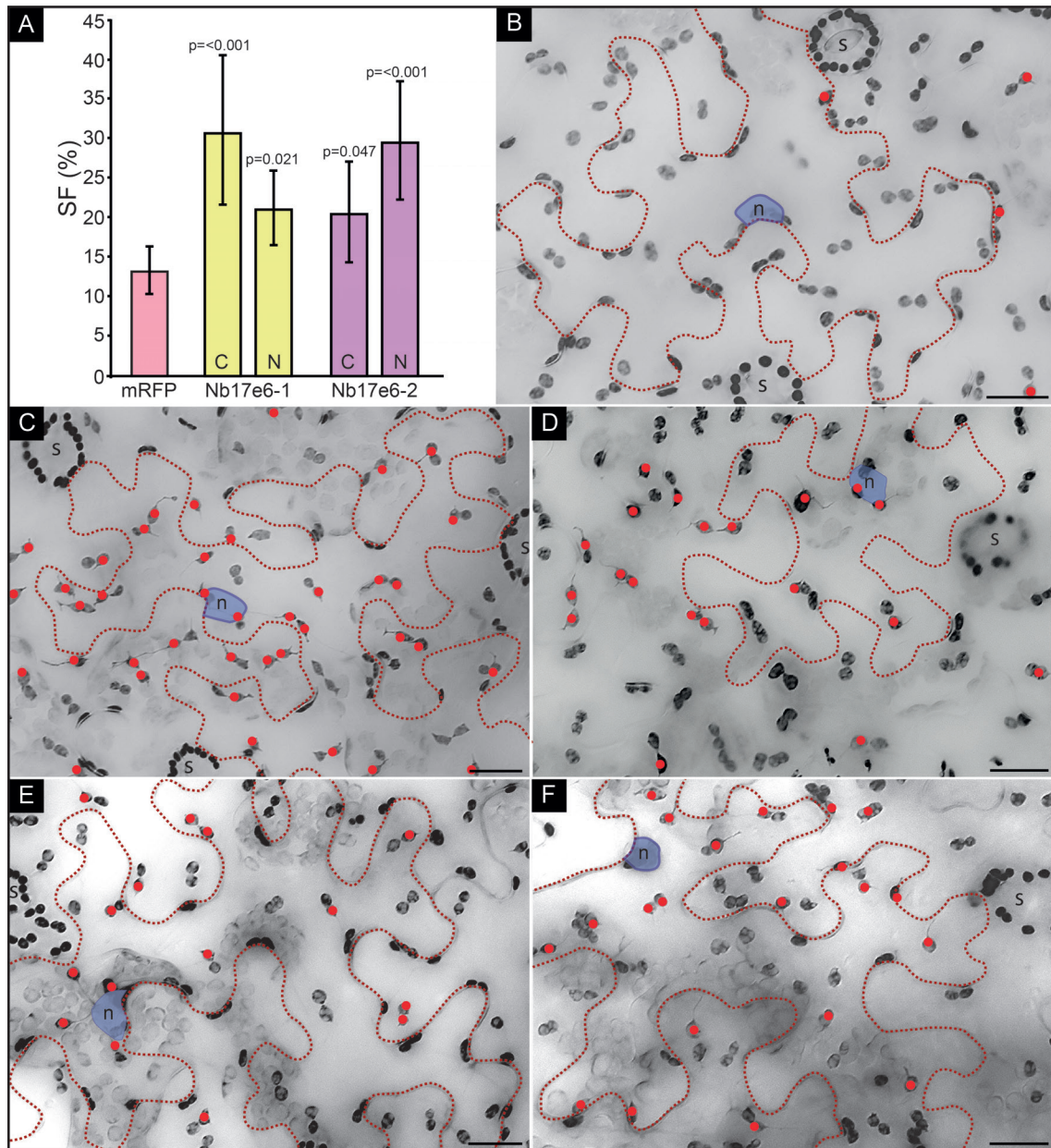


Figure 7.11.: Transient over-expression of *Nb17E6-1* and *Nb17E6-2* leads to significant stomule induction. (A) Mean stomule frequencies during transient over-expression (mediated by *A. tumefaciens* strain LBA4404) of *Nb17E6* fusion proteins. The letters 'C' and 'N' within bars denote fusions with C-terminal and N-terminal mRFP. Raw data was arcsine transformed and bars represent back-transformed means. Error bars represent back-transformed 95% confidence intervals. Rank-Sum test results comparing mRFP alone and *Nb17E6* shown above the corresponding bars. $n = 3-4$ plants for *Nb17E6* and $n = 10$ plants for the mRFP control, with 3 images quantified per plant. (B-F) Example epifluorescence microscopy images (combined z-stacks) of *N. benthamiana* (*FNRtp:eGFP*) lower epidermis expressing (B) mRFP, (C) *Nb17E6-1*-mRFP (D) mRFP-*Nb17E6-1*, (E) *Nb17E6-2*-mRFP and (F) mRFP-*Nb17E6-2*. For ease of visualization images were converted to gray scale and inverted, plastids are visible in dark gray-black. Dotted lines denote boundaries of single cells, the position of nuclei is highlighted in blue (labeled with 'n') and the position of stomata are labeled with 's'. Plastids with stomules indicated with red circles. Scale bars = 20 μ m.

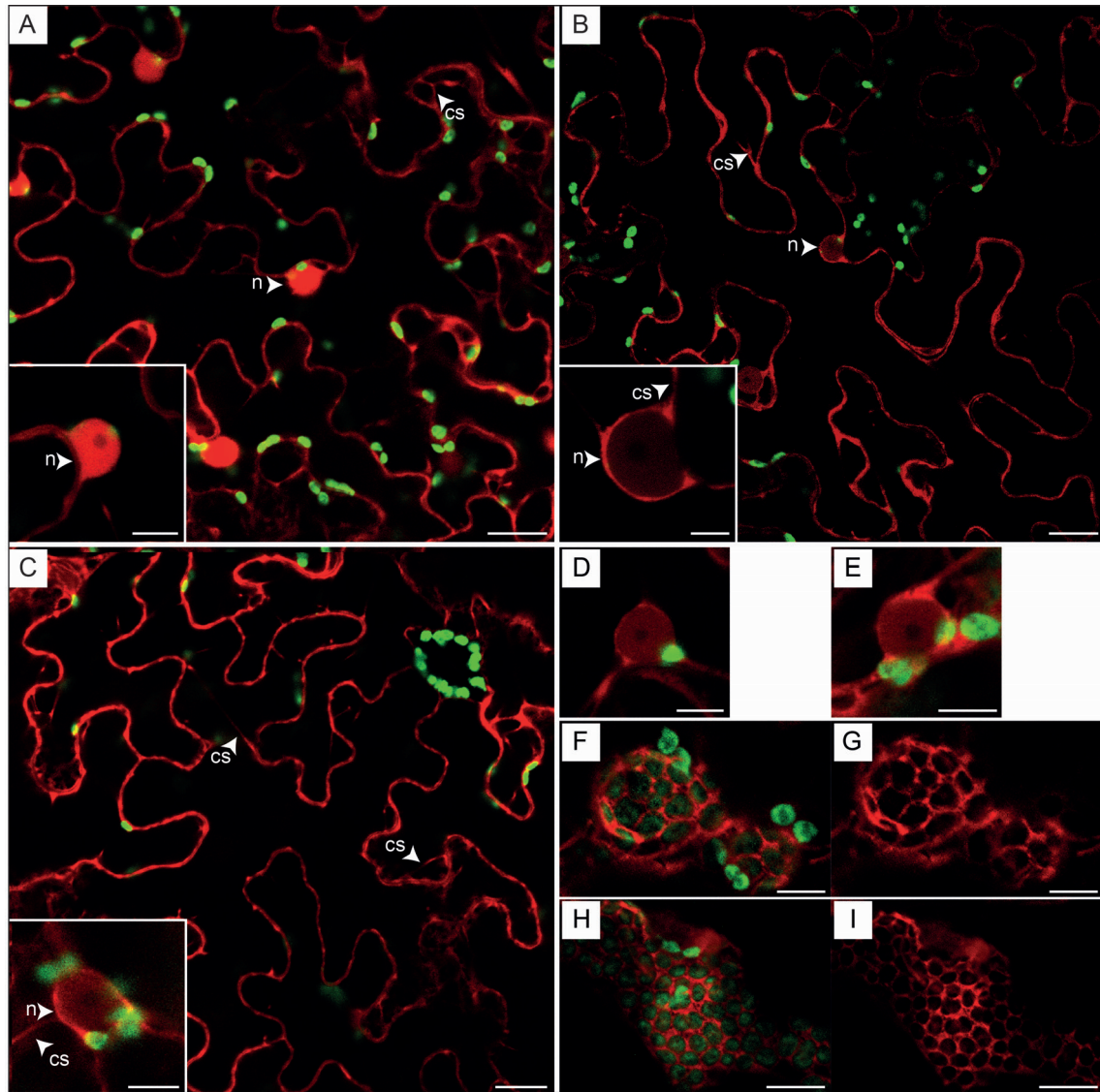


Figure 7.12.: mRFP tagged Nb17E6-1 and Nb17E6-2 are localized to the cytosol and are excluded from the nucleus. Confocal images taken of *N. benthamiana* (*FNRtp:eGFP*) (A-C) lower leaf epidermis and (D-I) mesophyll, inoculated with LBA4404 derivatives mediating the overexpression of mRFP constructs. mRFP channel is visible in red, while plastid fluorescence is visible in green. Nuclei are labeled 'n' and cytoplasmic strands are labeled as 'cs'. Scale bars in (A-C) are 20 µm (10 µm for all insets) and 10 µm for panels (D-I). (A) mRFP negative control shows expression in the nucleus and cytoplasm. Inset shows mRFP in a nucleus at higher magnification. (B) mRFP-Nb17E6-1 and (C) Nb17E6-1-mRFP are cytoplasmic and nuclear excluded. Insets show nuclei at higher magnification. A red ring of Nb17E6-1 is visible around the nucleus with lower levels of mRFP visible inside, an expression pattern that is clearly distinct when compared to the mRFP only control. Nb17E6-2 constructs showed the same localization pattern as Nb17E6-1. Nuclei of mRFPNb17E6-2 and Nb17E6-2mRFP shown in (D) and (E) respectively. Examples images of a Nb17E6-1-mRFP expressing mesophyll cell (F-G), and a mRFPNb17E6-2 expressing mesophyll cell (H-I), show clear cytoplasmic localization. Nb17E6-1 and Nb17E6-2 showed no co-localization with the plastid marker.

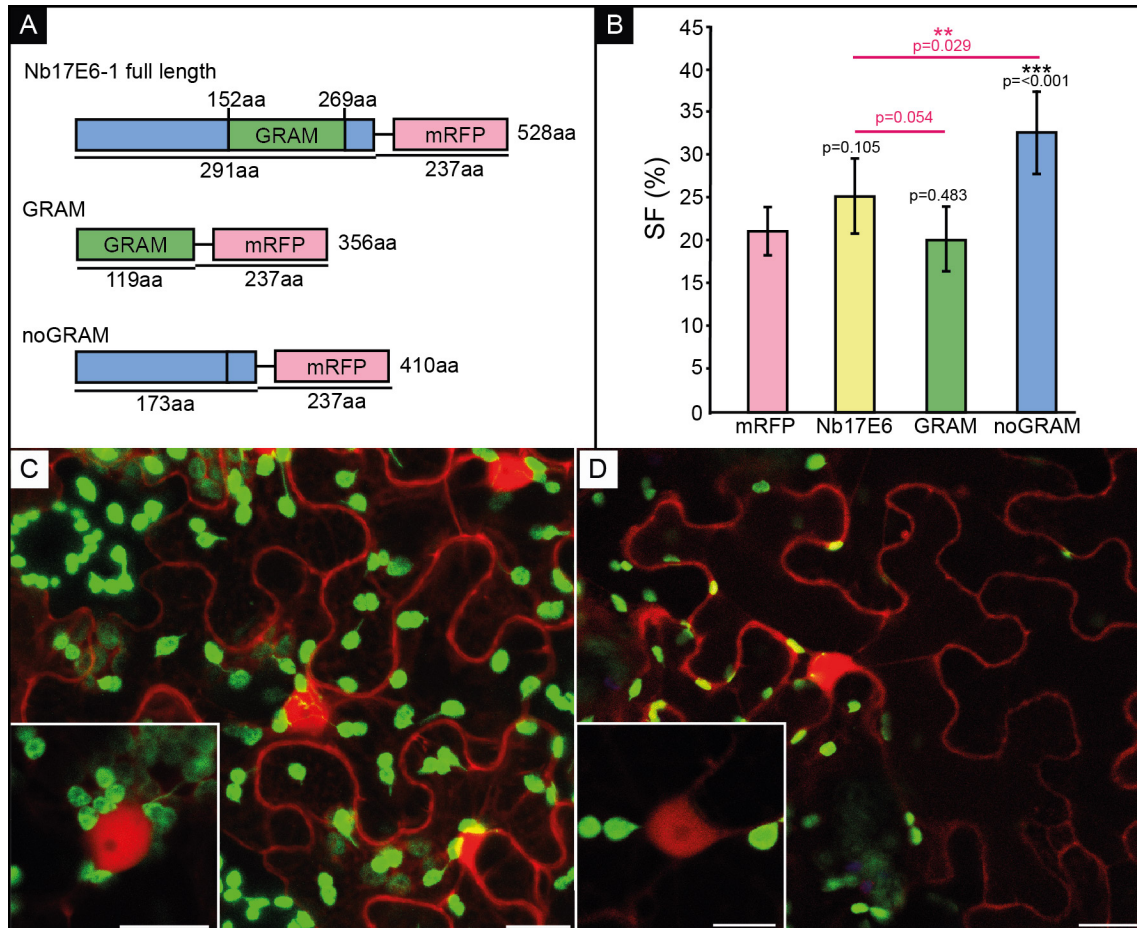


Figure 7.13. Deletion of the GRAM domain increases stomule induction by Nb17E6-1 over-expression. (A) Schematic of Nb17E6-1 and truncated mRFP fusion proteins (GRAM and noGRAM) transiently expressed (mediated by LBA4404) in *N. benthamiana* (*FNRtp:eGFP*). (B) Mean stomule frequencies following overexpression of mRFP, Nb17E6-1-mRFP (Nb17E6), GRAM-mRFP (GRAM), and noGRAM-mRFP (noGRAM) fusion proteins in lower leaf epidermis. Raw data was arcsine transformed and bars represent back-transformed means. Error bars represent back-transformed 95% confidence intervals. Rank-Sum test results comparing mRFP control and Nb17E6/mRFP fusions are shown above the corresponding treatment, while other comparisons are denoted with a line and highlighted in red. $n = 10$ plants for mRFP and Nb17E6-1 infiltrations, $n = 7$ plants for the GRAM and $n = 8$ plants for the noGRAM, with 3 images quantified per plant. (C-D) Confocal images of lower leaf epidermis expressing (C) noGRAM-mRFP and (D) GRAM-mRFP (combined z-stacks). Both protein fusions are cytosolic and nuclear. The mRFP channel is visible in red, while plastid fluorescence is visible in green. Scale bars in (C-D) are 20 μm (10 μm for insets).

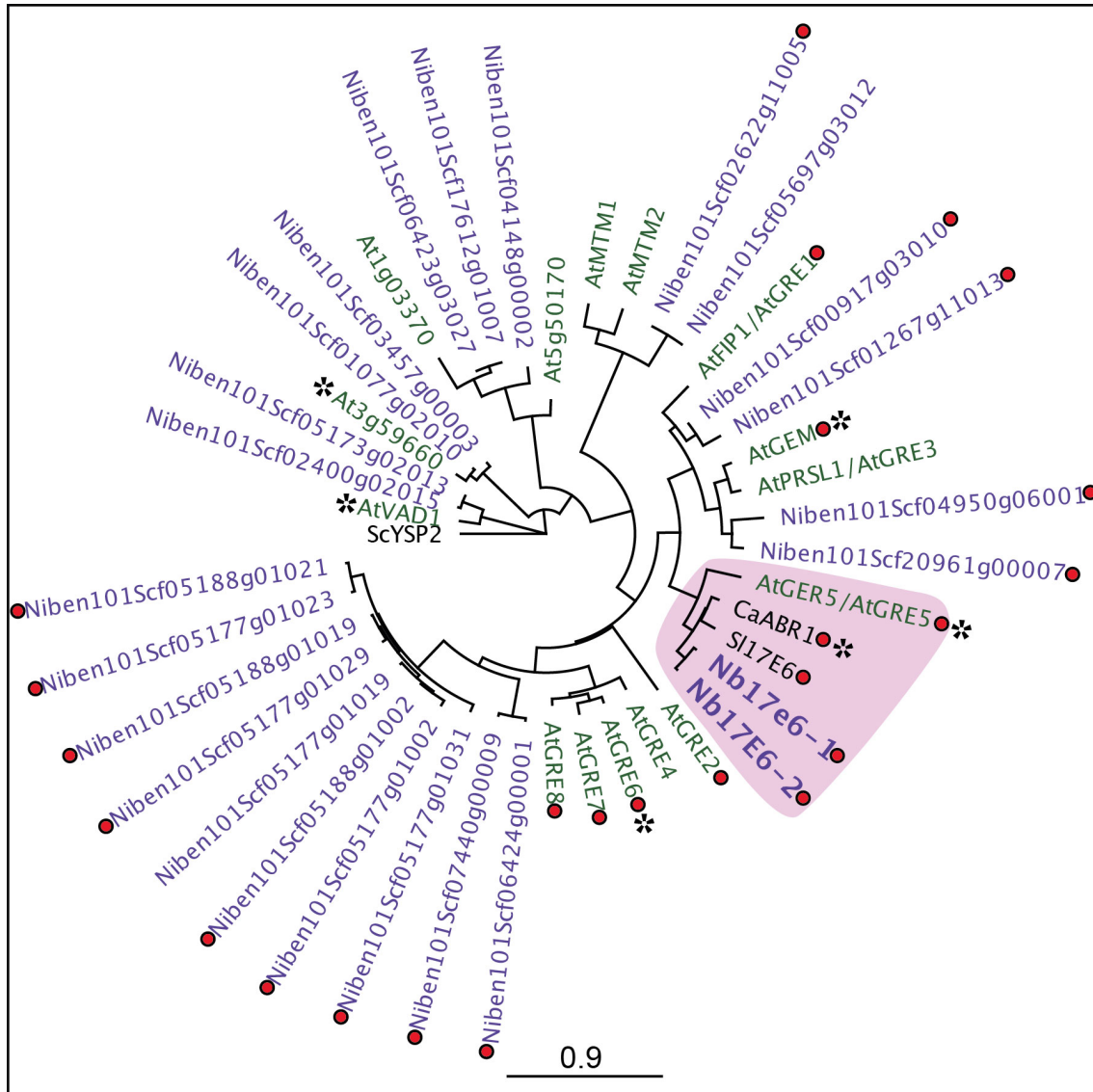


Figure 7.14.: Amino acid homology relationship between GRAM domains from *A. thaliana* (shown in green) and *N. benthamiana* (shown in purple). *Nb17E6-1* and *Nb17E6-2* are part of a small clade including the previously characterized *AtGER5* and *CaABR1* (highlighted in pink). Most GRAM domain containing proteins have the GRAM as their only known conserved protein domain (marked with a red dot). Genes found throughout the tree have been experimentally shown to be ABA responsive (marked with asterisks), including *AT3g59660*, *AtVAD1* (Jiang et al., 2008), *GRE6* (Jiang et al., 2008), *AtGER5/AtGRE5* (Choi and Hwang, 2011), *ABR1* (Choi and Hwang, 2011) and *AtGEM* (Mauri et al., 2016). Scale bar represents evolutionary distance in substitutions per nucleotide. The yeast YSP2 GRAM protein was included as an outgroup.

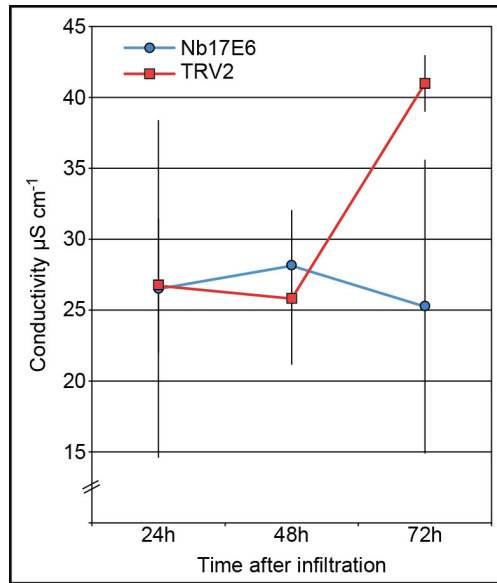


Figure 7.15.: Silencing with *TRV2::Nb17E6-1* inhibits HR during triggered by transient *Bs3* over-expression. Empty vector (*TRV2*) and *TRV2::Nb17E6* silencing in *N. benthamiana* (*FNRtp:eGFP*) was followed by GV3101-mediated over-expression of the *Bs3* gene to induced hypersensitive response (HR). Electrolyte leakage was measured at 24, 48, and 72 hpi. Three plants were silenced with *TRV2*, and four with *Nb17E6-1*. Error bars represent standard deviation.

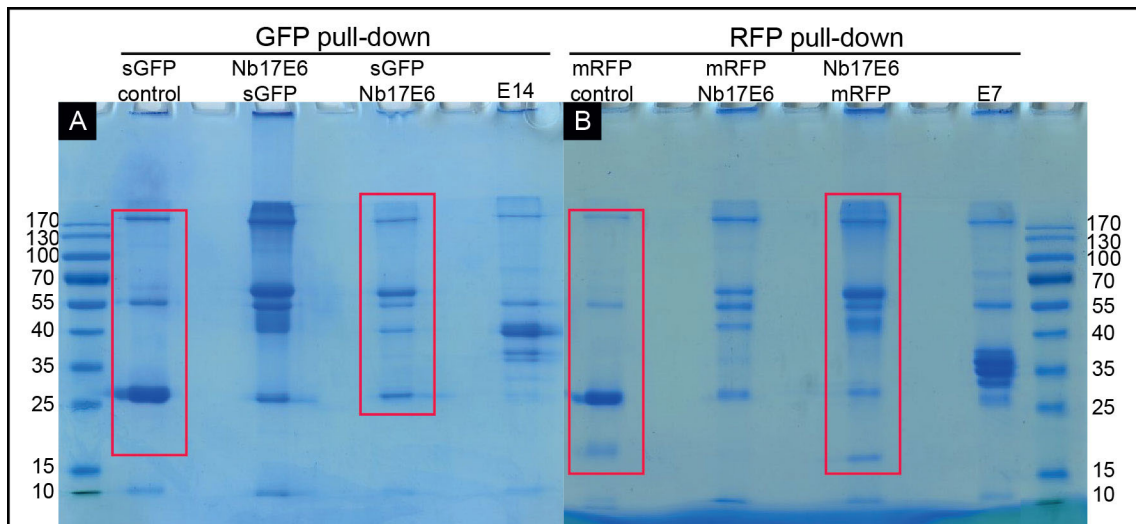


Figure 7.16.: Coomassie stained 10% SDS gels of Nb17E6-1 Co-IP. (A) GFP-Trap Co-IP from tissue over-expressing sGFP alone, C or N-terminal sGFP-tagged Nb17E6-1 (Nb17E6-sGFP and sGFP-Nb17E6, respectively) and an unrelated, GFP-tagged sample (E14). (B) RFP-Trap Co-IP from tissue over-expressing mRFP alone, N or C-terminal mRFP-tagged Nb17E6-1 (mRFP-Nb17E6 and Nb17E6-mRFP, respectively) and an unrelated, RFP-tagged sample (E7). Red boxes outline the gel pieces cut out and analysed by LC-MS/MS. Protein ladder and annotation can be found at each end (kDa).

Accession number	Name	Function	Probable localization	Control	GFP-Nb17E6	Nb17E6-mRFP	E14	E7
Plant defense related								
Q04065 _TOBAC	OMT I-b Catechol O-methyltransferase	phenylpropanoid gene strongly upregulated during PTI (<i>P. syringae</i> Δ <i>hrcC</i>) (Szatmári et al., 2014) NtOMT I accumulates in leaf epidermis in tobacco infected with TMV (Jaeck et al., 1996)	?	0	0	3(3) 12%(42/364)	0	0
Q5KTN4 _TOBAC	14-3-3 d-1 protein	protein domain specific binding (InterPro) Nt14-3-3 d-1 interacts with the N-resistance protein (confers resistance to TMV) (Konagaya et al., 2004) 14-3-3 proteins typically act as adaptors and relocate proteins to their sites of action. 14-3-3s usually recognize phosphorylated protein motifs (Comparot et al., 2003)	?	0	0	2(2) 21%(53/249)	0	0

Accession number	Name	Function	Probable localization	Control	GFP-Nb17E6	Nb17E6-mRFP	E14	E7
Q75ZD3 _TOBAC	14-3-3 i-2 protein	protein domain specific binding (InterPro) Nt14-3-3 i-2 identified as an protein interacting with the N-resistance protein (confers resistance to TMV) (Konagaya et al., 2004)	?	0	2(2) 19%(49/260)	0	0	0
A0A0H5B1M _NICBE	NbPDR1b PDR-type ABC transporter	NpPDR1 transports antifungal compound, is involved in general and JA-dependent defense response (Stukkens et al., 2005)	plasma membrane (UniProtKB)	0	0	4(4) 3%(44/1435)	0	0
Uncharacterised 14-3-3 proteins								
Q762F2 _TOBAC	Nt14-3-3 proteinkappa2	protein domain specific binding (InterPro)	?	0	0	2(2) 17%(42/252)	0	0
Q948K3 _TOBAC	14-3-3 protein 9-like	protein domain specific binding (InterPro)	?	0	0	2(2) 16%(41/261)	0	0

Accession number	Name	Function	Probable localization	Control	GFP-Nb17E6	Nb17E6-mRFP	E14	E7
Reactive nitrogen and oxygen scavengers								
E9NX75_NICAT	GSNOR S-(hydroxymethyl) glutathione dehydrogenase	removal of reactive nitrogen species NaGSNOR is important for JA/JA-Ile and ethylene biosynthesis during herbivory (Wünsche et al., 2011) AtGSNOR1 (75% identity) positively regulates plant immunity to phytopathogens. Regulates SA signaling and abundance (Feechan et al., 2005)	AtGSNOR1 cytosol and peroxisome (GO Database)	0	0	2(3) 7%(23/322)	2(3) 7%(23/322)	2(3) 7%(23/322)
F8WQS3_NICBE	APX (ascorbate peroxidase)	response to oxidative stress (InterPro) AtAPX1 (66% identity) is a ROS scavenger important for desiccation and immune response (Yang et al., 2015)	AtAPX1 is cytosolic	0	0	2(2) 27%(51/192)	2(2) 27%(51/192)	0
Q40589_TOBAC	Cytosolic ascorbate peroxidase	response to oxidative stress (InterPro) AtAPX1 (83% identity) is a ROS scavenger important for desiccation and immune response (Yang et al., 2015)	cytosol (UniProtKB)	0	6(12) 28%(71/250)	8(16) 40%(99/250)	8(13) 39%(97/250)	9(15) 40%(100/250)

Accession number	Name	Function	Probable localization	Control	GFP-Nb17E6	Nb17E6-mRFP	E14	E7
26S proteasome components								
Q076B1_NICBE	RPN9	19S subunit of the proteasome Silencing of <i>NbRPN9</i> induces PCD (Kim et al., 2003) Required for systemic viral transport (Jin et al., 2006)	cytosol	0	2(2) 5%(19/359)	2(3) 9%(32/359)	0	2(2) 5%(19/359)
Q076B0_NICBE	RPN8	19S lid complex of the 26S proteasome (InterPro)	cytosol	0	0	4(4) 14%(32/229)	0	0
Other proteins								
D2CFI9_TOBAC	LRR1 (leucine-rich repeat protein 1)	DNA-damage-repair/tolerance protein DRT100-like (UniProt)	?	0	0	2(2) 7%(24/365)	0	2(2) 7%(24/365)
C9DFB6_NICBE	Uncharacterized protein	oxidoreductase activity (InterPro)	?	0	0	5(6) 23%(38/167)	3(4) 16%(26/167)	2(2) 12%(20/167)
Q40556_TOBAC	protein phosphatase 2A	AtPP2AA2 (90% identity) homolog is part protein phosphatase 2A (PP2A) holoenzyme holoenzyme has roles in plant metabolism, development, stress response and signaling (Kataya et al., 2015)	cytosol, peroxisomes (AtPP2AA2) (Kataya et al., 2015)	0	0	2(2) 3%(19/586)	0	0

Accession number	Name	Function	Probable localization	Control	GFP-Nb17E6	Nb17E6-mRFP	E14	E7
O24112_NICPL	small GTP-binding protein	AtRabD2C (89% identity) - pollen tube growth (Peng et al., 2011)	cytosol, organelle membranes (AtRab1C; GO database)	0	0	2(2) 9%(19/203)	0	0

Table 7.7.: Short list of putative Nb17E6-1 interacting proteins identified during LC-MS/MS analysis of proteins isolated from Co-IP. The first column shows the accession number of putative interacting proteins identified via a 'Mascot' search of peptides against the UniProt Nicotiana database. The second column shows the protein name assigned by UniProt (uniprot.org). The third column shows predicted and experimentally tested protein functions based on publications specific to the gene of interest, or homologs in other species (amino acid sequence identity to *A. thaliana* homologs in brackets; Geneious global alignment with free-end gaps). Column 4 shows predicted sub-cellular protein localization based on scans of UniProt databases (database used in brackets), or on the localization of homologs from other species. Question marks indicate that localization is uncharacterised. The last four columns show which proteins were pulled-down by the sGFP+mRFP control (column 5), the two Nb17E6-1 fusions (column 6 and 7), E14 (column 8) and E7 (column 9). The first number is the number of unique peptides identified during LC-MS/MS analysis, in brackets it shows the total number of peptides. Below peptide number is the percent coverage by peptides of the full length protein, in brackets is the number amino acids covered by peptides/total number of amino acids in the full length protein. Abbreviations are as follows: 'PTI' = pattern-triggered immunity' 'Nb' = *Nicotiana benthamiana*, 'Na' = *Nicotiana attenuata*, 'Nt' = *Nicotiana tabacum* 'Np' = *Nicotiana glauca*, 'At' = *Arabidopsis thaliana*, 'TMV' = tobacco mosaic virus.

7.3. Discussion and outlook

While most of this thesis has discussed the molecular machinery necessary for stromule formation, the idea of the VIGS screen was to identify novel genetic or signaling pathways regulating stromule formation. Silencing and over-expression of *Nb17E6-1* and *Nb17E6-2*, both of which contain a single conserved GRAM domain, identified them as a novel genes important for GV3101-induced stromule formation. *Nb17E6-1* and *Nb17E6-2* showed high sequence similarity to the previously characterised *AtGER5* and *CaABR1*; proteins that are ABA-responsive with a known role in plant immune response and HR (Choi and Hwang, 2011). *CaABR1* enhances HR in pepper via the manipulation of ABA-SA balance and enhancing accumulation of H_2O_2 ; a ROS molecule and key cell death-inducing signal during HR (Choi and Hwang, 2011). However, the exact mechanism by which *CaABR1* acts to alter hormone balance or H_2O_2 is not known. In a preliminary experiment it was also found that *Nb17E6* may be important for Bs3-triggered HR, suggesting that this protein may serve a similar function to *CaABR1* in pepper. A Co-IP experiment with *Nb17E6-1* also identified of a large proportion of protein interacting partners with roles related to plant defense.

7.3.1. *Nb17E6-1* may have a role in regulating ROS and RNS pools

Given the sequence similarity to *CaABR1* (Figure 11.7 on page 150), and the potential importance of *Nb17E6* to HR in *N. benthamiana*, one would expect that *Nb17E6-1* and/or *Nb17E6-2* may have a role in the manipulation of H_2O_2 abundance. Therefore it was very exciting to see that several of the putative interacting proteins have been shown to directly or indirectly influence H_2O_2 levels during immune response.

Two ascorbate peroxidases were pulled-down in the Co-IP, and although little is known about these proteins in *N. benthamiana*, they both showed quite high sequence identity (66 and 83%) to APX1 from *A. thaliana* (*AtAPX1*). *AtAPX1* is a cytosolic scavenger of H_2O_2 , using ascorbate as a substrate to convert H_2O_2 into water (Yang et al., 2015). One could hypothesize that through an interaction with *Nb17E6*, *NbAPX1* scavenging activity is inhibited, thus promoting H_2O_2 accumulation (Figure 7.17 on page 127).

During plant immune response H_2O_2 abundance is influenced by cross-talk with pathways regulating reactive nitrogen species (RNS). An increase in the abundance of the RNS molecule, NO, triggers increased S-nitrosylation of APX1, a modification which increases its activity (Yang et al., 2015). Therefore, high NO indirectly decreases H_2O_2 accumulation (Yang et al., 2015). Due to the high reactivity of NO it has a short half-life in planta, NO is maintained via a reaction with sulfhydryl-containing molecules to produce S-nitrosothiols (SNOs) which are more stable, and therefore more mobile (Leterrier et al., 2011). One putative *Nb17E6-1* interacting protein was the S-(hydroxymethyl) glutathione dehydrogenase, *GSNOR*. *AtGSNOR* reduces S-nitroso-glutathione (GSNO; a SNO molecule), to produce GSSG and NH_3 (Leterrier et al., 2011), thus diminishing the NO pool and APX1 activity (Yang et al., 2015). Like *CaABR1*, *GSNOR* positively regulates HR response through indirect enhancing of H_2O_2 accumulation in *A. thaliana* (Feechan et al., 2005). A physical interaction with *Nb17E6-1* may

positively regulate GSNOR (Figure 7.17 on the facing page).

Putative interactions between Nb17E6-1 and ascorbate peroxidases as well as GSNOR suggest that Nb17E6-1 may contribute to HR through the manipulation of the NO-H₂O₂ balance in the cell, possibly to encouraged H₂O₂ accumulation. As mentioned previously, SA is also considered a pro-HR signal, and although there were no interacting proteins which provided a direct link to SA biosynthesis, it is known that H₂O₂ and SA participate in a positive feedback loop during immune reactions (Vlot et al., 2009). CaABR1 induces SA accumulation, and it could be that Nb17E6 induces SA accumulation in a similar fashion, possibly mediated by H₂O₂.

7.3.2. The disturbance of Nb17E6 interactions could influence stromule induction

Caplan et al. (2015) and Gray et al., (2012) showed that treatments with exogenous H₂O₂ induce stromules in multiple plant species and tissues. Caplan et al. (2015) also reported that stromules are induced via SA treatment of *N. benthamiana* leaves. Data described above indicates that Nb17E6-1 may increase the concentration of both H₂O₂ and SA, providing one explanation for stromule induction following Nb17E6-1 over-expression, and indicating the potential importance H₂O₂ and SA signaling to stromule formation. Initially it was puzzling that the noGRAM construct induced even more stromules than the full length construct. However, GRAM domains have been proposed to act in protein-protein interaction (Doerks et al., 2000), and it could be that the removal of the GRAM domain influences interactions important for controlling the H₂O₂ pool or SA biosynthesis (such as those with ascorbate peroxidases and GSNOR). To test this one should measure H₂O₂ and SA accumulation following over-expression of both the full-length and noGRAM Nb17E6-1. The generation of stable transgenic plants with an inducible promoter system would be preferable, to avoid the influence of *A. tumefaciens* on H₂O₂ levels during transient infiltrations.

7.3.3. Regulation of Nb17E6-1 via 14-3-3 proteins?

Interestingly, a total of six 14-3-3 proteins were also identified as interacting with *Nb17E6-1*, several of which are known to interact with the N-resistance protein responsible for conferring resistance to TMV, and some uncharacterised. However, 2/6 showed unspecific interactions with fluorescence protein controls and so were not included in the short list. 14-3-3s are small regulatory proteins that recognize phosphorylated protein motifs on a wide range of 'client' proteins, and subsequently regulate their activity and/or localization (Comparot et al., 2003). In addition to a variety of housekeeping processes, these proteins have clearly been linked to both abiotic and biotic stress response, including roles in ABA signal transduction, R-gene mediated plant resistance, and reactive oxygen species production during defense response (reviewed in Denison et al., 2011).

Phosphoproteome analyses have identified phosphorylation sites in AtGER5 (the *A. thaliana* homolog of Nb17E6) at serines in positions 4, 30, 31, 32 and 33 (Reiland et al., 2009; Roitinger

et al., 2015; Zhang et al., 2016). Therefore, one could look into the potential phosphorylation sites of Nb17E6 proteins to determine if they are 14-3-3 recognition sites. It could be that they are differentially phosphorylated under different conditions and that this phosphorylation influences 14-3-3 binding and stromule induction. Assuming the interaction between Nb17E6-1 and 14-3-3 can be confirmed, one could also design Nb17E6 constructs with amino acid exchanges at phosphorylation sites and test interactions with 14-3-3 proteins to see which sites are essential to the interaction. Interestingly, none of the phosphorylation sites identified in AtGER5 were within the GRAM domain but are clustered at the N-terminus. Assuming the phosphorylation pattern is similar in *N. benthamiana* it may be that the GRAM domain is not essential for interaction with 14-3-3 proteins.

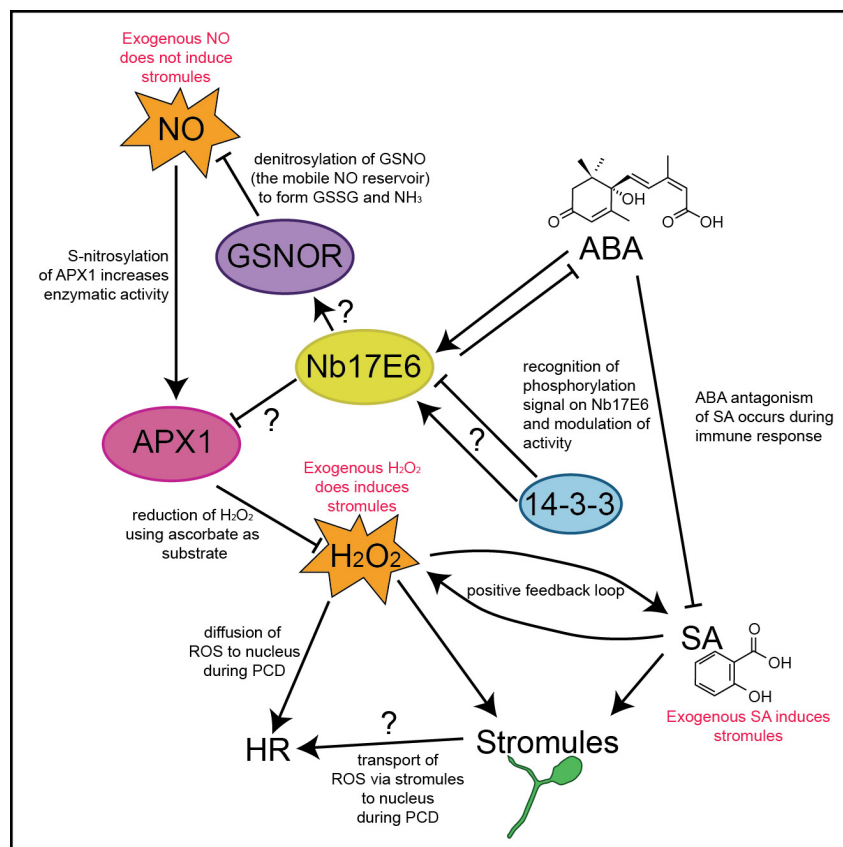


Figure 7.17: Model for potential Nb17E6 interactions based on the identification of putative interacting proteins GSNOR, APX1 and 14-3-3 proteins via Co-IP and exogenous application of hormones and signaling molecules. Based on the activity of its homolog, CaABR1 from pepper (Choi and Hwang, 2011), Nb17E6-1 may act to increase endogenous H₂O₂ levels during immune reactions and stromule formation. Nb17E6-1 may also participate in the negative feedback loop with ABA, manipulating the SA-ABA balance. Further, putative interactions with GSNOR and APX1 suggest Nb17E6-1 manipulates endogenous H₂O₂, a potent stromule inducing stimuli (Gray et al., 2012, Caplan et al., 2015). GSNOR acts to reduce the pool of reactive nitrogen species through the reduction of GSNO (mobile pool of NO) (Leterrier et al., 2011). When NO is limiting the enzymatic activity of APX1 is lower (which occurs via S-nitrosylation), resulting in less H₂O₂ scavenging and, ultimately, H₂O₂ accumulation (Yang et al., 2015). Co-IP results also indicate that Nb17E6-1 interacts with APX1. Overall Nb17E6-1 appears likely to interact with multiple phytohormones and proteins to increase endogenous H₂O₂. Further, stromules induced by over-expression of Nb17E6-1 may be a result of multiple inputs affecting H₂O₂ level, or the direct result of SA (which was also shown to induce stromules in some experiments; Caplan et al., 2015). Stromules occur with ETI and have been hypothesized to transmit pro-defense signals like SA and H₂O₂ to the nucleus (Caplan et al., 2015; Kumar et al., 2018).

7.3.4. Is Nb17E6 important for ETI-induced stromules?

Over the past 3 years ETI and HR induction via multiple effector/receptor combinations has been shown to result in stromule induction (Table 12.5 on page 157), implicating stromules immunity (Caplan et al., 2008, 2015). So far we know that Nb17E6 is important for GV3101-induced stromules and that it could be important for HR, however we have not addressed the question of whether Nb17E6 is important for ETI-induced stromules. *Nb17E6* silencing and subsequent induction of ETI using transient XopQ expression (as in Erickson et al., 2017a), or one of the other receptor/effector pairs listed in Table 12.5, would determine whether Nb17E6 is needed for ETI-induced stromules or only for those induced by GV3101.

7.4. Summary

Stromules are known to be induced following treatment with a wide range of stress-associated stimuli, but no genes involved in signaling stromule induction have been identified up to now. Here we have identified a GRAM domain-containing protein, Nb17E6, as the first stromule-regulating protein in the pathway between GV3101 inoculation and stromule induction. The characterisation of Nb17E6-1 in more detail allows us to more precisely manipulate parts of this pathway to determine which parts are key to stromule formation. More generally, a better understanding of the physiological changes occurring in response to multiple stromule-inducing stimuli and identifying commonalities between them will help us identify key molecules for stromule induction. Immediate future experiments should evaluate the importance of Nb17E6 to ETI-induced stromules, and the confirmation of protein interactions through yeast two-hybrid, a second Co-IP or split-YFP experiments.

7.5. Materials and methods

7.5.1. Plant material and growth conditions

Wild-type *N. benthamiana* stably expressing ferredoxin NADP(H) oxidoreductase transit peptide fused to eGFP (*FNRtp:eGFP*) were used, as in Schattat et al. (2012). Unless otherwise stated, plant growth conditions are as described in Erickson et al. (2017a).

7.5.2. Bacterial strains and constructs

A. tumefaciens strain GV3101 (Koncz and Schell, 1986) was used for mediating the expression of VIGS vectors, while LBA4404 (Hoekema et al., 1983) was used for transient over-expression experiments. Bacterial transformation, and growth procedure is described in Erickson et al. (2017a).

Constructs generated for over-expression and silencing experiments were cloned using the

Gateway cloning system¹⁴ (list of primers and constructs listed in Table 12.7 on page 158). Deletion of the GRAM domain for the noGRAM construct was completed using PCR-mediated deletion (Hansson et al., 2008) using the *pDONR221::Nb17E6-1* as a template.

7.5.3. Virus induced gene silencing

Two *A. tumefaciens* derivatives (GV3101), one harbouring *TRV1* (*pYL192*)¹⁵ and one with the *TRV2* (*pYL276a*)¹⁶ plasmid containing the gene-specific silencing fragment, were cultured and diluted with AIM¹⁷ to an OD₆₀₀ of 0.1 and 0.4 respectively, then mixed 1:1. At the four leaf stage *N. benthamiana* (*FNRtp:eGFP*) were inoculated with mixed *A. tumefaciens* strains, and silencing was allowed to occur over 14-17 days. *NbPDS* silencing was used as a control in each experiment to gauge when effective silencing occurred. Growth chambers were set to long-day conditions (16 h light/8 h dark), 22°C, with a light intensity of 120 $\mu\text{E m}^{-2}$ (unless otherwise stated).

7.5.4. Epifluorescence microscopy

Epifluorescence images were collected as z-stacks (.czi files) as described in Erickson et al. (2017a). The 38HE filter was used for imaging of eGFP labeled plastids and the 43HE filter was used to image mRFP labeled 17E6 fusion proteins.

7.5.5. Image analysis

Images were exported as single .tif files and flatten for images analysis using ImageJ/Fiji as described in Erickson et al. (2017a).

7.5.6. Confocal microscopy

Confocal microscopy was performed as described in Erickson et al. (2017a), with a few modifications. A Zeiss LSM 780, inverted AxioObserver, with a x63 water lens (C-Apochromat963/1.20 W Korr M27) and a x100 oil immersion lens (Plan-Apoc-hromat 9100/1,46 Oil DIC) was used. eGFP fluorescence was induced via a 488 nm laser line of a multiline argon laser (25 mW) and mRFP fluorescence was induced via a 561 nm laser. Fluorescence was recorded in single-track mode. Individual channels for eGFP (493-523 nm), for mRFP (576-629 nm) and for chlorophyll (684–721 nm) were defined. ZenBlack software was used for image capture and controlling the microscope. All equipment and software from Zeiss GmbH (Jena, Germany).

¹⁴Gateway technology was developed by Hartley et al. (2000), cloning kit by Thermo Fisher Scientific, Braunschweig, Germany.

¹⁵ABRC, www.arabidopsis.org, stock number CD3-1039

¹⁶AG Bonas/S. Schornack, currently in The Sainsbury Laboratory, Cambridge, UK

¹⁷acetosyringone containing infiltration medium: 10mM MgCl₂, 5mM MES pH 5.3 (both from Roth, Karlsruhe, Germany), 150 μM acetosyringone (Sigma-Aldrich, Deisenhofen, Germany).

7.5.7. Real-time PCR to test VIGS silencing efficiency

Isolation of total RNA was performed from 100mg of tissue using a NucleoSpin RNA Plant kit from Macherey-Nagel (MN)¹⁸. The RNA of three plants from each treatment was pooled (each plant contributed 1 µg of RNA to the pool), 1 µg of pooled RNA was then used for the cDNA synthesis.

Generation of cDNAs utilized the RevertAid H Minus First Strand cDNA Synthesis Kit¹⁹, according to kit instructions utilizing the Oligo dT₁₈ primer. cDNAs were diluted to 1:4, 1:10, 1:16 and 1:64 for qRT-PCR.

Real time primers for reference genes were published in Lui et al. (2012). *Nb17E6* primers were designed to amplify a region of 133 base pairs, with the forward primer annealing within the first exon and the second primer annealing on the boarder between the first and second exons. Primer sequences can be found in Table 12.6 on page 157.

qRT-PCR was performed in 15 µL reactions using SsoAdvanced Universal SYBR Green Supermix²⁰, 4.5 pmol of gene specific primer and 2 µL of diluted cDNA (in control reactions 1 µg of total RNA was added to ensure that no unspecific products were amplified). PCR was performed using a CFX connect Real-time PCR Detection System from Bio-Rad²¹. The $2^{-\Delta\Delta CT}$ method Livak and Schmittgen (2001) was used to calculate the relative quantity (RQ value) of *Nb17E6* compared to *NbEF1*, *NbPP2A*, and *NbAPR*. The RQ value reported represents the average of normalization against all three reference genes.

7.5.8. Generation of the homology tree

As mentioned amino acid sequences of GRAM domain-containing proteins from *A. thaliana* were used in a series of SGN BLAST searches²² to identify all homologous GRAM proteins. This resulted in the identification of 25 putative GRAM domain-containing proteins in *N. benthamiana*. These proteins were run through 'Motif Search'²³ to identify conserved protein domains from the Pfam database²⁴. GRAM domain sequences were isolated and the homology tree was generated using Geneious Tree Builder²⁵. GRAM domain containing proteins are highly variable in sequence outside the GRAM domain, which is why the GRAM domain was chosen for tree generation.

7.5.9. Ion leakage assay

The ion leakage assay was performed as described in (Szczesny et al., 2010), with a few modifications. Leaf discs (5) were harvested from each plant (silenced with *TRV2::Nb17E6-1*

¹⁸Düren, Germany, mn-net.com

¹⁹Thermo Fisher Scientific, Braunschweig, Germany

²⁰Bio-Rad, München, Germany

²¹München, Germany

²²*N. benthamiana* Genome v1.0.1 predicted proteins, <https://solgenomics.net/tools/blast/>

²³<https://www.genome.jp/tools/motif/>

²⁴Protein families database Finn et al., 2013

²⁵Settings for tree building: global alignment, cost matrix = Blosum65, genetic distance model = Jukes-Cantor, tree building method = Neighbor-Joining.

or empty *TRV2*) using a size 4 cork borer at 24, 48 and 72 hpi with a GV3101 derivative mediating the expression of the *Bs3* gene from pepper (induces HR in *N. benthamiana*). Leaf discs were placed in 15 mL falcon tubes, plastic fly screen was placed into the tube and discs were immersed in millipore water. Samples were vacuum-infiltrated for 1 min, and rotated in an overhead shaker for 1 h at room temperature. Conductivity was measured with a Knick conductometer²⁶. Maximum conductivity of the samples was measured by boiling samples for 10 min, allowing them to cool to room temperature, and measuring conductivity a second time. Leakage is calculated by dividing the 1st measurement by the 2nd measurement x 100.

7.5.10. Co-Immunoprecipitation

Preparation of beads - GFP-Trap and RFP-Trap beads (30 μ L per sample) were pipetted into 1.5 mL tubes, centrifuged (1min, 800 xg) and washed in 1 mL IP buffer²⁷. Washing was repeated 2 times and beads were resuspended in a final volume of 30 μ L.

Protein extraction - Whole leaves (with major veins removed) from wild-type *N. benthamiana* transiently expressing N and C-terminal mRFP or sGFP-tagged Nb17E6-1 were collected at 2 days post inoculation. 2-3 leaves were ground in liquid nitrogen using a mortar and pestle, powder was transferred to a 15 mL tube, and 4mL of IP buffer was added. After a 5min centrifugation (>3000 g at 4°C) the supernatant was transferred to a 2 mL tube on ice.

Co-IP - pre-prepared beads were added, and incubated for 3 h at 4°C with gently rotation. Samples were centrifuged for 2 min (800 xg at room temperature), and supernatant was discarded. Beads were washed 5 times with 1 mL IP buffer.

Elution - 30 μ L Laemmli buffer was added to beads followed by incubation at 95°C for 5 min. After centrifugation for 1-2 min at maximum speed, the supernatant was transferred to a new tube and used for SDS-page.

Samples were run on 10% gels and Coomassie stained, and selected gel pieces were cut out for LC-MS/MS analysis at the Cambridge Centre for Proteomics²⁸.

7.5.11. LC-MS/MS

Gel pieces provided to the company were cut into 1 mm² pieces, destained, reduced via DTT, alkylated via iodoacetamide, and digested with chymotrypsin overnight at 37°C. Samples were loaded onto an auto-sampler for LC-MS/MS analysis.²⁹

A Dionex Ultimate 3000 RSLC nanUPLC and a Q Exactive Orbitrap mass spectrometer³⁰ was used to analyse samples. Reverse-phase chromatography (flow rate of 300 nL min⁻¹) and a Thermo Scientific reverse-phase nano Easy-spray column (Thermo Scientific PepMap C18,

²⁶Knick, Berlin, Germany

²⁷10% glycerol, 25 mM Tris-HCl pH 7.5, 1 mM EDTA pH 8.0, 150 mM NaCl, 0.1% Tween-20

²⁸Cambridge, UK

²⁹LC-MS/MS experiments were performed at by the Cambridge Centre for Proteomics (Cambridge, UK) and information pertaining to LC-MS/MS methods was provided by Mike Deery.

³⁰Both from Thermo Fisher Scientific Inc, Waltham, MA, USA

2 μm particle size, 100A pore size, 75 μm i.d. x 50 cm length) was used to separate peptides. Peptides were loaded onto a pre-column (Thermo Scientific PepMap 100 C18, 5 μm particle size, 100A pore size, 300 μm i.d. x 5 mm length) from the Ultimate 3000 auto-sampler with 0.1% formic acid for 3 min at a flow rate of 10 $\mu\text{L min}^{-1}$. After this period, the column valve was switched to allow elution of peptides from the pre-column onto the analytical column. Solvent A was water + 0.1% formic acid and solvent B was 80% acetonitrile, 20% water + 0.1% formic acid. The linear gradient employed was 2-40% B in 30 min.

The LC eluant was sprayed into the mass spectrometer by means of an Easy-Spray source³¹. All m/z values of eluting ions were measured in an Orbitrap mass analyzer, set at a resolution of 70000 and was scanned between m/z 380-1500. Data dependent scans (Top 20) were employed to automatically isolate and generate fragment ions by higher energy collisional dissociation (HCD, NCE:25%) in the HCD collision cell and measurement of the resulting fragment ions was performed in the Orbitrap analyser, set at a resolution of 17500. Singly charged ions and ions with unassigned charge states were excluded from being selected for MS/MS and a dynamic exclusion window of 20 sec was employed.

7.5.12. Database searching

Post-run, all MS/MS data were converted to .mgf files and the files were then submitted to the Mascot search algorithm (Matrix Science, London UK) and searched against the UniProt Nicotiana database and a common contaminant sequences database. Variable modifications of oxidation (M), deamidation (NQ) and carbamidomethyl were applied. The peptide and fragment mass tolerances were set to 5 ppm and 0.1 Da, respectively. A significance threshold value of $p < 0.05$ and a peptide cut-off score of 20 were also applied. All data was then imported into the Scaffold program³².

³¹Thermo Fisher Scientific Inc.

³²Version_4.5.4, Proteome Software Inc, Portland, OR

Part III.

General Discussion

8. Elucidating cytoskeletal involvement in stromule formation

As previously mentioned, 15 years ago Kwok and Hanson (2003) suggested that actin and microtubules both play a unique role in the formation of stromules, although the exact mechanisms were not elucidated. As we begin to understand how stromules are made it seems that these statements made years ago still hold true. Through the quantification of plastid-nucleus relationships, the targeted knockout of myosins in *A. thaliana*, as well as a blind screening approach (effector screen) in *N. benthamiana*, work presented in this thesis confirms the involvement of both actin and microtubules in stromule formation and contributes to the elucidation of the distinct mechanisms by which they each promote stromule elongation.

8.1. Actin

8.1.1. Actin and myosins influence stromule extension via nucleus movement

Through the screening of all 13 myosin T-DNA insertion lines for stromule phenotypes in the *A. thaliana* upper epidermis, we found that the role of myosins and actin in stromule formation is important, but may not occur as initially expected. Based on the literature available at the time, we started screening myosin mutants with the expectation that we might find the myosin(s) that pulls on the plastid envelope to extend stromules along actin. Although we found no data suggesting the myosins act to pull stromules along actin, we did find that actin and myosin XI-I play an indirect role in stromule formation via the movement of the nucleus in this tissue. *Myosin xi-i* showed reduced stromule frequencies, and the analysis of another mutant with impaired nucleus movement, *wit12* (an adaptor between myosin XI-I and the nuclear envelope) further confirmed the importance of nucleus movement to basal stromule levels in this tissue. Indeed, movie data clearly shows stromules anchored at points near the nucleus were elongated when the nucleus (and associated stromule tip) moved away (Figure 8.1A) (Erickson et al., 2017b). As a result, the majority of stromules in this tissue were formed in close proximity to the nucleus, and pointed towards it (Erickson et al., 2017b). Further, plastids sitting on the nucleus without a stromule, gain a stromule as the nucleus moves away (Erickson et al., 2017b), suggesting that the membrane of plastids both with and without stromules are anchored near the nucleus.

8.1.2. What anchors stromules to the nucleus?

Although the identity of the nuclear-associated anchor point was not confirmed in Erickson et al. (2017b), we suggested that stromules are likely affiliated with the actin cage surrounding the nucleus, and when the nucleus moves, the actin cage and stromule tip moves with it. In a paper the following year, Kumar et al. (2018) showed that stromules form stable associations (>18 min) with actin filaments surrounding the nucleus, and showed the plastid bodies sitting at the nucleus also formed associations with actin. Despite the fact that these observations were made in *N. benthamiana* where ETI was triggered¹, it provides support for the hypothesis we made in Erickson et al. (2017b). Based on our work and the work of Kumar et al. (2018) it seems likely that plastids close to the nucleus are normally anchored to actin, and triggering of nucleus movement provides the force necessary to form a stromule.

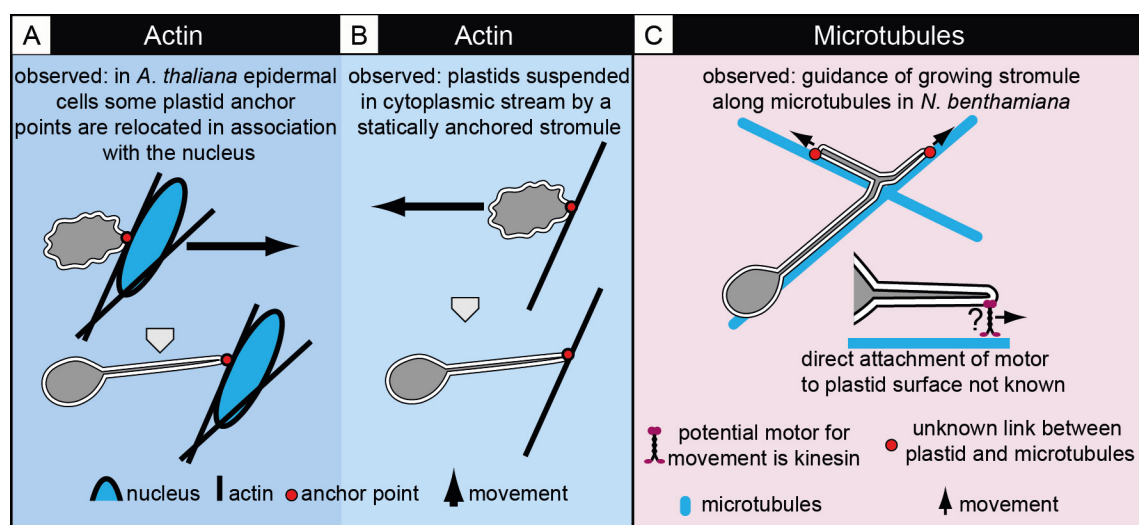


Figure 8.1.: Likely models for stromule formation. (A) Movement of actin anchor point: the plastid membrane is anchored to actin, and the anchor point is moved away from the plastid body resulting in stromule elongation (Erickson et al., 2017b; Kwok and Hanson, 2003). During live-cell imaging in *A. thaliana* it was observed that stromules anchored near the nucleus (likely to the actin cage) were elongated when the nucleus plus the associated stromule anchor moved away from the main plastid body (Erickson et al., 2017b). (B) Static anchor point: movement of the plastid body away from a stromule anchor point (potentially on actin) results in stromule extension (Gunning, 2005; Kwok and Hanson, 2003). (C) Pulling motors (microtubules): microtubules guide growing stromules and determine branching patterns in *N. benthamiana* (Erickson et al., 2017a; Kumar et al., 2018). Kinesins are likely involved in stromule extension, but the mode of kinesin interaction with the plastid membrane is unknown.

8.1.3. Anchoring of the plastid body

The model proposed above assumes that the plastid body is resistant to movement and is anchored in place. It is known that plastid position within the cell is tightly controlled in order to maximize photosynthetic efficiency and prevent photo-damage (Oikawa et al., 2008). In addition to the role of actin in nucleus movement and stromule anchoring, actin is also clearly linked to the positioning/anchoring of plastid bodies in place. Chloroplasts have been shown to associate with actin bundles as well as fine filaments, which create a 'basket' around the plastid (Kandasamy and Meagher, 1999). Additionally, treatments with actin depolymerizing chemicals completely disrupt chloroplast positioning in mesophyll cells of *A. thaliana*

¹p50 effector and Lifeact-TagRFP (actin label) were transiently expressed via *A. tumefaciens* in N-containing NRIP1-Cerulean plants.

(Kandasamy and Meagher, 1999). Mediation of actin-dependent chloroplast positioning relies on CHUP1 (CHLOROPLAST UNUSUAL POSITIONING 1), a protein which localizes to the outer plastid envelope and is essential for both actin organization during light avoidance movement, as well as anchoring of the plastid to the plasma membrane. Mutants in *chup1* showed accumulation of chloroplasts at the bottom of mesophyll cells and no photo-relocation (Oikawa, 2003). In epidermal cells of *A. thaliana*, plastids in *chup1* cluster around nucleus (Figure 11.9 on page 152). If plastid membranes anchor at the nucleus, as our model suggests, then plastid bodies that are no longer held in position (as in *chup1*) would be expected to accumulate at the nucleus in exactly this way. This provides support for our model, but future work should examine how removing the plastid body anchor impacts stromule abundance, number of stromule elongation events, stromule length and orientation near the nucleus.

8.1.4. Why should the plastid membrane anchor near the nucleus?

As summarized in Erickson et al. (2017b) the transport of so-called 'retrograde signals' from the plastid to the nucleus is needed to regulate the expression of pertinent chloroplast genes that were transferred to the nucleus during evolution. Retrograde signal transfer allows the plastid to communicate its protein requirements to the nucleus base on developmental status, or when challenged with biotic or abiotic stress (reviewed in Erickson et al., 2017b). A close association of the nucleus and plastid may be necessary for retrograde signaling. Indeed, we showed that almost all cells have between 2 or more plastids close to the nucleus at all times, suggesting that this might be an important constellation (Erickson et al., 2017b). I would suggest that anchoring of the plastid membrane near the nucleus may provide a means for the plastid to maintain close proximity to the nucleus. The stretching of the plastid membrane to form a stromule may represent a means of keeping track of a mobile nucleus in *A. thaliana* upper epidermis (Erickson et al., 2017b). In the future, focus should be placed on identifying the anchor point at the nucleus and knocking out its function in order to evaluate the importance of stromule-nucleus associations.

8.2. Microtubules

8.2.1. Microtubule scaffold contributes to stromules formation

During a blind screen utilizing T3Es from *Xcv*, we found that microtubules contribute to stromule formation in *N. benthamiana* via a completely different mechanism what we have described for actin in *A. thaliana*. As summarized in Erickson et al. (2017a), stromules use microtubules as a scaffold for extension, branching and kinking. Alternatively, depolymerization of microtubules was shown prevent elongation, and to alter stromules shape. A few weeks after our publication of these findings a second group confirmed this relationship between microtubules and stromules with remarkably similar movies (Kumar et al., 2018). Stromule tips and kinks were also seen in close association with microtubules using transmission electron microscopy. Additionally, it was reported that treatment with a microtubule stabilizer increase stromule frequencies (Kumar et al., 2018). Movies of tissue fluorescently labeled with actin, microtubule and plastid stroma marker suggest that in *N. benthamiana* microtubules serve as a scaffold for extension, while actin provides static anchor points along the way.

8.2.2. Microtubules as an interface for interaction

The significance of microtubule-dependent stromules is unknown so far, although there has been speculation that they are extended for the purpose of transporting signals to the nucleus (Kumar et al., 2018). One could also speculate that microtubules act as a cellular 'compartment', bringing together specific organelles by creating an interface for their interaction. Multiple organelles that move utilizing actin pause at microtubules, including mitochondria as well as ER tubules, which appear to be more stable at junctions with microtubules (Hamada et al., 2012)². Authors speculated that microtubules may act to increase the incidence of organelle interactions at fixed points in the cortex (Hamada et al., 2012). Careful observations of ER and stromules revealed that stromules extend into ER channels, and appeared to form associations at defined points (Schattat et al., 2011b). Interestingly, recent work by Kumar et al. (2018) actually found that microtubules direct stromules into ER channels (described by Schattat et al., 2011a) and that microtubules are the site of ER-stromule interfaces. Indeed, microtubules provide a chance for interaction between organelles, the biological relevance of these interactions remains to be explored.

Other mechanisms for stromule formation?

Results presented here do not rule out pulling by myosins on the plastid membrane during stromules formation, or investigate the contributions of cytoplasmic streaming to stromule formation. As shown in Figure 8.1 on page 135B, plastid bodies have also been observed suspended in the cytoplasmic stream by a stromule attached to actin (Gunning, 2005; Kwok and Hanson, 2003) suggesting yet another mode of formation.

²*A. thaliana* shoot epidermis of seedlings.

8.3. Significance

I would argue that the most important contribution of my thesis to the stromule field was the finding that stromules form via at least two different cytoskeleton-dependent mechanisms. Although it is possible that both of these mechanisms make stromules for the same purpose, it is also possible that stromules formed via different mechanisms have different functions. Perhaps nucleus-dependent stromule extension is important for retrograde signaling, whereas microtubule-dependent stromule extension is important for interactions with other organelles. Now that this work has made us aware of the existence of more than one stromule type, we can distinguish between the mechanism of stromule elongation and evaluate the importance of each mechanism under different stress conditions and in different tissues or species.

9. Genetic elements contributing to stromule formation

In addition to addressing the mechanistic aspects of stromule elongation, a second goal of this thesis was to identify genetic elements important for the regulation of stromule formation. As mentioned previously, few mutants have been identified that influence stromules, and most of these mutants give more insight into the mechanism than the regulatory pathways required for making stromules. Defects in the plastid division apparatus caused by the deletion of *ACCUMULATION AND REPLICATION OF CHLOROPLAST (ARC)* genes *ARC3*, *ARC5*, *ARC6*, and *PARC6 (PARALOG OF ARC6)* resulted in the formation of much fewer, larger, mesophyll plastids than in wild type (Pyke, 1999; Holzinger et al., 2008; Itoh et al., 2018) with a large increase in stromule number and length (Holzinger et al., 2008). However, with whole host of abnormal plastid and stromule morphologies, and very long folded stromules (Holzinger et al., 2008), phenotypes seem to be a side effect of excessive plastid membrane. In contrast ion channel mutants *mssl2-1/mssl3-1* which are impaired in osmotic regulation, produce perfectly round plastids that do not make any stromules (Haswell and Meyerowitz, 2006), further emphasizing the importance of membrane availability to stromules.

Another mutant, the aforementioned *chup1*, was described as having constitutive stromule induction in *A. thaliana* by Caplan et al. (2015). Although we found that stromule frequency was slightly elevated in this mutant (Figure 11.10 on page 152), we found that the difference in stromule frequencies between *chup1* and wild-type was not as striking as described. In absence of functional CHUP1, plants also showed enhanced HR, and although authors say this is due to an increase in stromules and stromule-nucleus contacts (Caplan et al., 2015), this is not necessarily the case. As mentioned previously, *chup1* also has more plastids clustered around the nucleus (Figure 11.9 on page 152), which could also contribute to enhanced HR, independent of stromule induction.

So far there are only four mutants identified that provide information about stromule function or regulation. The previously discussed *atg5-1* (Subsection 1.5.2 on page 6) shows elevated stromule frequencies and implicates stromules in autophagy (Ishida et al., 2008). Mutants in MORE AXILLARY BRANCHES genes, *max3-9*¹ and *max2-1*², convincingly correlated increases in stromule frequency with strigolactone biosynthesis during phosphate starvation (Vismans et al., 2016), however the cascade by which strigolactones trigger stromules is unexplored so far (Vismans et al., 2016). Interestingly, ABA induction of stromules (also observed

¹Strigolactone biosynthesis impaired resulting impaired stromule induction under phosphate stress.

²Strigolactone signaling mutant, which exhibits higher strigolactone biosynthesis and enhances stromule induction under phosphate stress.

by Gray et al., 2012) was inhibited in *max3-9* mutant, suggesting that downstream accumulation of strigolactone is required for ABA-induced stromules in some cases (Vismans et al., 2016). Lastly, VIGS of NADPH-dependent thioredoxin reductase C (NbNTRC) induced stromules in *N. benthamiana* (Brunkard et al., 2015). NbNTRC is a chloroplast stromal protein responsible for the detoxification of H₂O₂ in the chloroplast (Pérez-Ruiz et al., 2006) and the activation of ADP-glucose pyrophosphorylase (AGPase), an enzyme important for starch synthesis (Michalska et al., 2009). In *A. thaliana*, *nrtc* had higher H₂O₂, malformed mesophyll cells, altered thylakoid organization and impaired photosynthesis (Pérez-Ruiz et al., 2006), suggesting broad defects that likely cause significant stress. Such extensive impairment to plastid structure and function make it difficult to decipher which pathways are important for the stromule inducing phenotype.

Although mutants characterized so far re-enforce the idea that hormones, altered sugar metabolism and reactive oxygen species induce stromules, no proteins involved in downstream signaling pathways that lead to stromule formation had been identified. Starting from the observation that GV3101-derived cytokinin induces stromules (Erickson et al., 2014), we used VIGS screen to identify Nb17E6 as the first protein downstream of hormone/bacterial exposure that is important for regulating stromules. Nb17E6 silencing does not result in severe plant growth defects, or severe chloroplast abnormalities, other than the fact that it suppresses stromules, making it different than many of the mutants discussed above.

While silencing of Nb17E6 knocks-down stromules, over-expression of Nb17E6 induces stromules. Insight into the mode of Nb17E6-triggered stromule induction comes from examining the homolog, CaABR1 (from pepper), which was previously shown to induce an increase in H₂O₂ (Choi and Hwang, 2011), a molecule that both induces stromules (Gray et al., 2012; Caplan et al., 2015) and is key to resistance reactions (Caplan et al., 2015). Until now, the mechanism by which H₂O₂ could be regulated by GRAM proteins was completely unknown. Putative Nb17E6 interacting proteins provide an idea of how this protein might act in the signaling pathway between hormone perception and the accumulation of H₂O₂. A Co-IP experiment with full length Nb17E6-1 revealed putative interactions with two ascorbate peroxidases and one S-(hydroxymethyl) glutathione dehydrogenase, suggesting that Nb17E6 interactions influence H₂O₂ scavenging, rather than triggering production of this molecule (Figure 7.17). In addition to being important for signal transduction in response to GV3101, sequence homology to characterized GRAM domain proteins suggest that *Nb17E6* is also likely to be ABA-inducible. As a result, one could speculate that this protein may be capable of integrating several stimuli leading to a specific H₂O₂ output. Providing more evidence for Nb17E6 interactions, exploring the dependence of stromule-inducing stimuli on Nb17E6 and interacting proteins, exploring Nb17E6 response to different hormone and stress signals, and showing that Nb17E6 can influence H₂O₂ are all exciting prospects for future work.

9.1. H₂O₂, a key regulator of stromules?

One challenge of elucidating stromule function is that stromules are not induced by specific stimuli, but are a general characteristic of cells under stress. The question then becomes:

is there a common factor among stromule inducing stress conditions that is key to their regulation? Nb17E6 data suggests that we need to look into the links between stromules and H₂O₂, which may be a good candidate for a key stromule regulator based on its importance in responding to most abiotic and biotic stress conditions (Livanos et al., 2014; Saxena et al., 2016). Exogenous application of H₂O₂ to multiple tissues and species reliably induces stromules (Caplan et al., 2015; Brunkard et al., 2015). H₂O₂ is less reactive than other ROS species, and at non-toxic levels works as a signaling molecule during development, growth and stomatal closure (Saxena et al., 2016). At toxic concentrations it contributes to programmed cell death (Saxena et al., 2016). Given its potential toxicity, H₂O₂ levels are tightly controlled through the regulation of enzymes involved in producing and scavenging H₂O₂, and through controlling the abundance of compounds such as ascorbate and glutathione (GSH), which are used up during H₂O₂ reduction (reviewed in Saxena et al., 2016). H₂O₂ production is tightly intertwined with JA, OPDA, GA, ABA, ethylene, SA, calcium, and NO signaling, and ultimately H₂O₂ levels reflect the integration of multiple signals in times of stress (Saxena et al., 2016). H₂O₂ could act as part of a signaling cascade to trigger stromule induction, however there is also evidence to suggest that H₂O₂ alters microtubule dynamics *in vitro* (Islam et al., 2016)³ and *in planta* (Yao et al., 2011), which we now know to be important for stromule extension (Erickson et al., 2017a).

Stromules as mediators of H₂O₂ transport?

During resistance reactions, the chloroplast is a primary source of the reactive oxygen species (ROS) H₂O₂ and O₂⁻ which promote the onset of HR (Maruta et al., 2012). H₂O₂ produced in the chloroplast during ETI ultimately relocates to the nucleus (Caplan et al., 2015). Stromules are also induced during ETI, and H₂O₂ was seen to diffuse into stromules in contact with the nucleus during ETI reactions, leading authors to speculate that stromules are required for the retrograde movement of the H₂O₂ signal (Caplan et al., 2015). However H₂O₂ can freely diffuse through membranes, so it is not clear what mechanism prevents it from escaping the stromule on its way to the nucleus.

9.2. Significance

Nb17E6 is the first protein to be identified as part of a hormone signaling pathway leading to stromule induction. Exploring Nb17E6 function, and identifying putative interacting proteins, has provided specific gene targets downstream of the GV3101/cytokinin stimulus that we can use to explore how stromules are regulated. Nb17E6 interactions with H₂O₂ scavenging enzymes has brought H₂O₂ back to our attention as potent stromule inducer, and provides us with specific targets that can be utilized to explore the importance of H₂O₂ under different stromule-inducing stimuli.

³Addition of H₂O₂ to microtubules *in vitro* led to decreases in microtubule growth rate and shrinkage rate, inducing more instances of catastrophe, and much fewer instances of microtubule rescue.

10. Conclusion

Elucidating stromule function and significance to cell/plant survival is not a simple task. The central obstacle to this field is that no mutant has been identified that lacks stromules completely, making it difficult to pin down the exact processes where stromules are important. At the onset of this thesis my goal was to identify cellular machinery and genetic components necessary for stromule formation in order to identify a more precise means of knocking-out stromules. Although this work did not yield a 100% stromule knock-out, it has provided crucial insights that will change the way we approach the problem of stromule function. This thesis describes at least two distinct modes of stromule elongation (microtubule-dependent and nucleus-dependent). The existence of two stromule types offers one explanation for why a single mutant lacking all stromules has not yet been identified. Now the challenge for the field will be to address whether stromules formed via different mechanisms have different functions. My findings should be used to direct the search for targets specific to the the different stromule types, in order to evaluate the importance of each stromule type under different conditions or in different tissues. For example, a knock-out of the kinesin(s) involved in microtubule-dependent elongation, or of the anchor point of stromules at the nucleus, would provide ways to distinguish between the two stromules types in the future.

Another challenge in the stromule field is the wide range of stresses and hormones that induce stromule formation and make it difficult to identify signaling pathways or common regulatory molecules leading to stromules. Nb17E6 is the first instance of a protein identified as part of a signaling cascade leading to stromules, making it particularly valuable. By knocking-out *Nb17E6* it is now possible to evaluate the reliance of different stromule-inducing stimuli on this signaling pathway. Further, putative Nb17E6 interacting proteins manipulate cellular H₂O₂ levels, suggest a role for this molecule as a potential stromule regulator. These interacting proteins can now be used as targets for evaluating the importance of H₂O₂ during stromule induction via different stimuli.

Overall, work presented in this thesis contributes to a better understanding of the mechanistic and regulatory components involved in '**Shaping plastid stromules**', and in doing so, provides exciting prospective targets for the investigation of stromule function going forward.

Part IV.

Supplemental Data

11. Figures

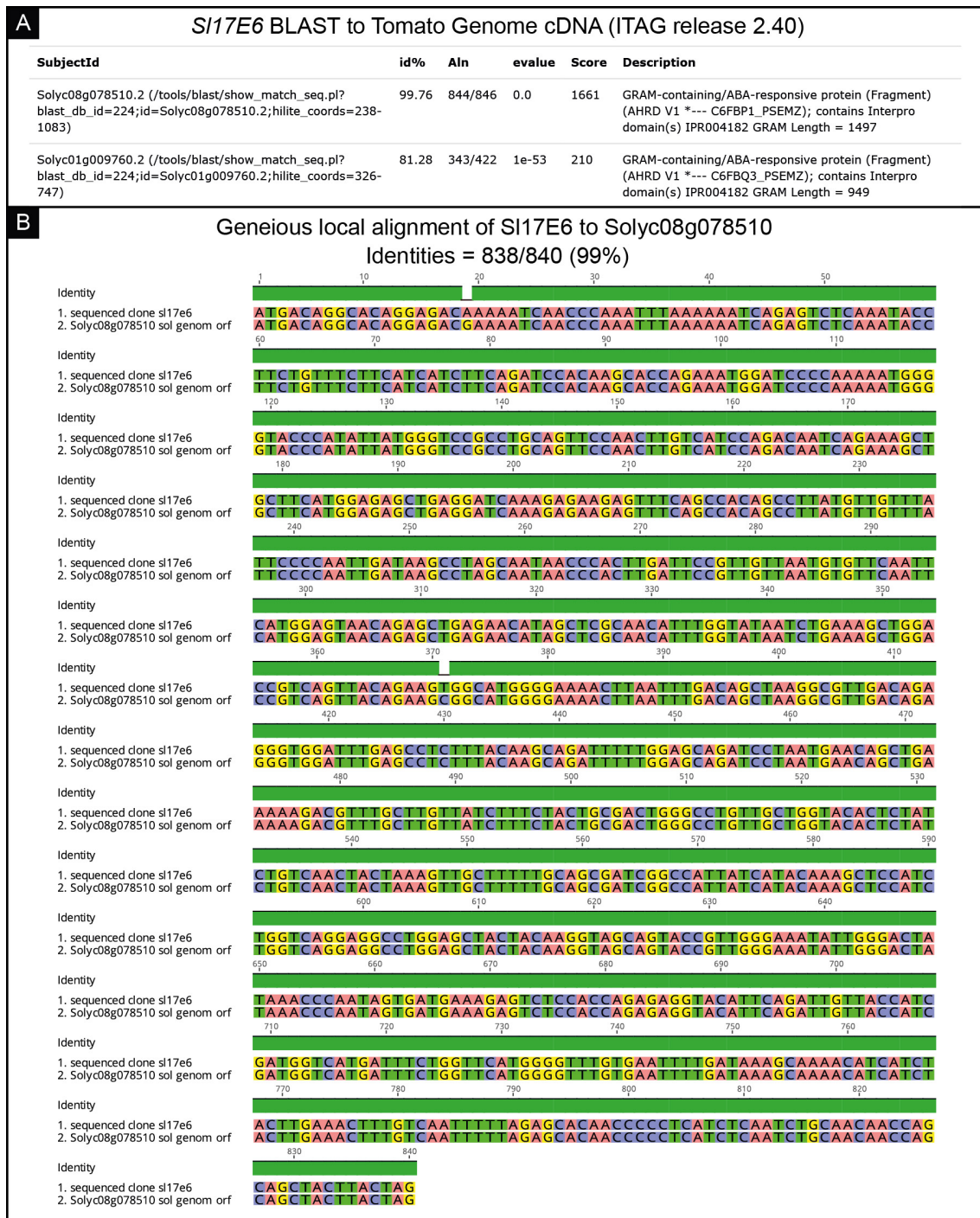


Figure 11.1.: Identity of *SI17E6* sequenced clone. (A) is the BLAST result from SGN and (B) is the Geneious local alignment (Smith-Waterman) of the cloned *SI17E6* sequence with tomato cDNA sequence extracted from the SGN. Nucleotides are labeled in different colors (pink = A, green = T, yellow = G, purple = C). Green graph above the sequence indicates regions where the sequences match.

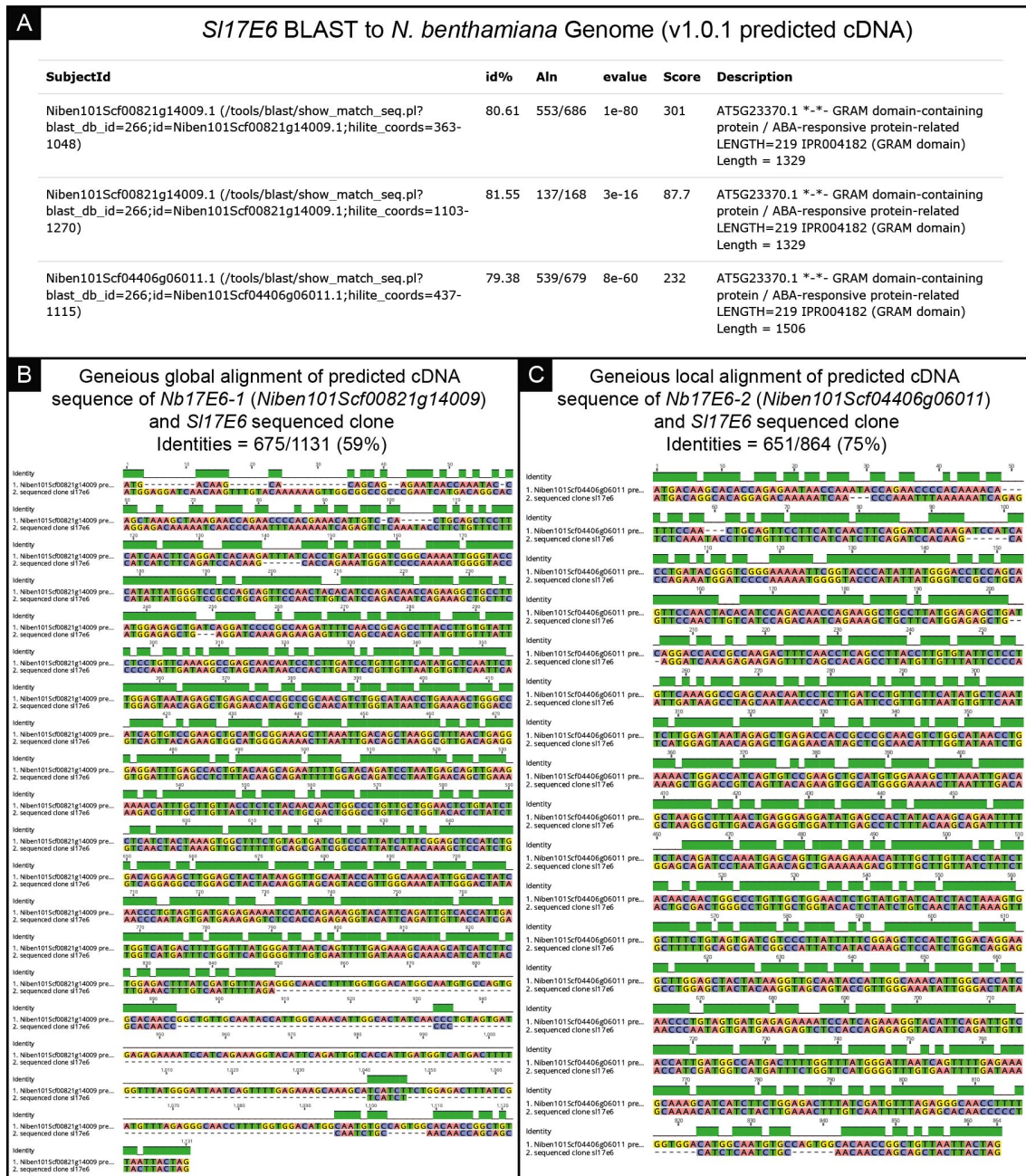


Figure 11.2.: SGN BLAST of *Sl17E6* against the *N. benthamiana* genome. (A) BLAST of *Sl17E6* against the *N. benthamiana* draft genome identifies two predicted cDNAs in *N. benthamiana* with similar sequences, deemed *Nb17E6-1* and *Nb17E6-2*. (B and C) Geneious alignments between *Sl17E6* and (B) *Nb17E6-1* or (C) *Nb17E6-2*. A global alignment (Needleman-Wunsch) was chosen for the comparison of *Sl17E6* and *Nb17E6-1*, to illustrate the large gap in sequence similarity at the 3' end of these genes, while a local alignment (Smith-Waterman) was chosen for *Sl17E6* and *Nb17E6-2*, since there was sequence similarity throughout the sequences and did little to change identity scores. Nucleotides are labeled in different colors (pink = A, green = T, yellow = G, purple = C). Green graph above the sequence indicates regions where the sequences match.



Figure 11.3: A Geneious global alignment (Needleman-Wunsch) between the predicted *Nb17E6-1* and the cloned sequence, reveals the incorrect retention of an intron in the predicted sequence. (A) DNA alignment. Nucleotides are labeled in different colors (pink = A, green = T, yellow = G, purple = C) and the green graph above the sequence indicate regions where the sequences match. Alignment reveals that base pairs 643-864 of the predicted *Nb17E6-1* are not found in the cloned sequence. (B) Protein alignment. Green graph above the top of the sequence represents 100% match between amino acid sequences, yellow shows similar amino acids and white indicates no similarity. The alignment reveals a 100% match, except at amino acids 215-288 of the predicted *Nb17E6-1* sequence, where this region is missing in the translate clone sequence. The purple line spans the predicted GRAM domain.



Figure 11.4.: Geneious global alignment (Needleman-Wunsch) of the *Nb17E6-1* and *Nb17E6-2* cloned sequences, reveals striking similarity between these two loci. **(A)** DNA alignment. Nucleotides are labeled in different colors (pink = A, green = T, yellow = G, purple = C) and green graph above the sequence indicate regions where the sequences match. **(B)** Protein alignment. Green graph across the top of the sequence represents 100% match between amino acid sequences, yellow shows similar amino acids and white indicates no similarity. The purple line spans the predicted GRAM domain.

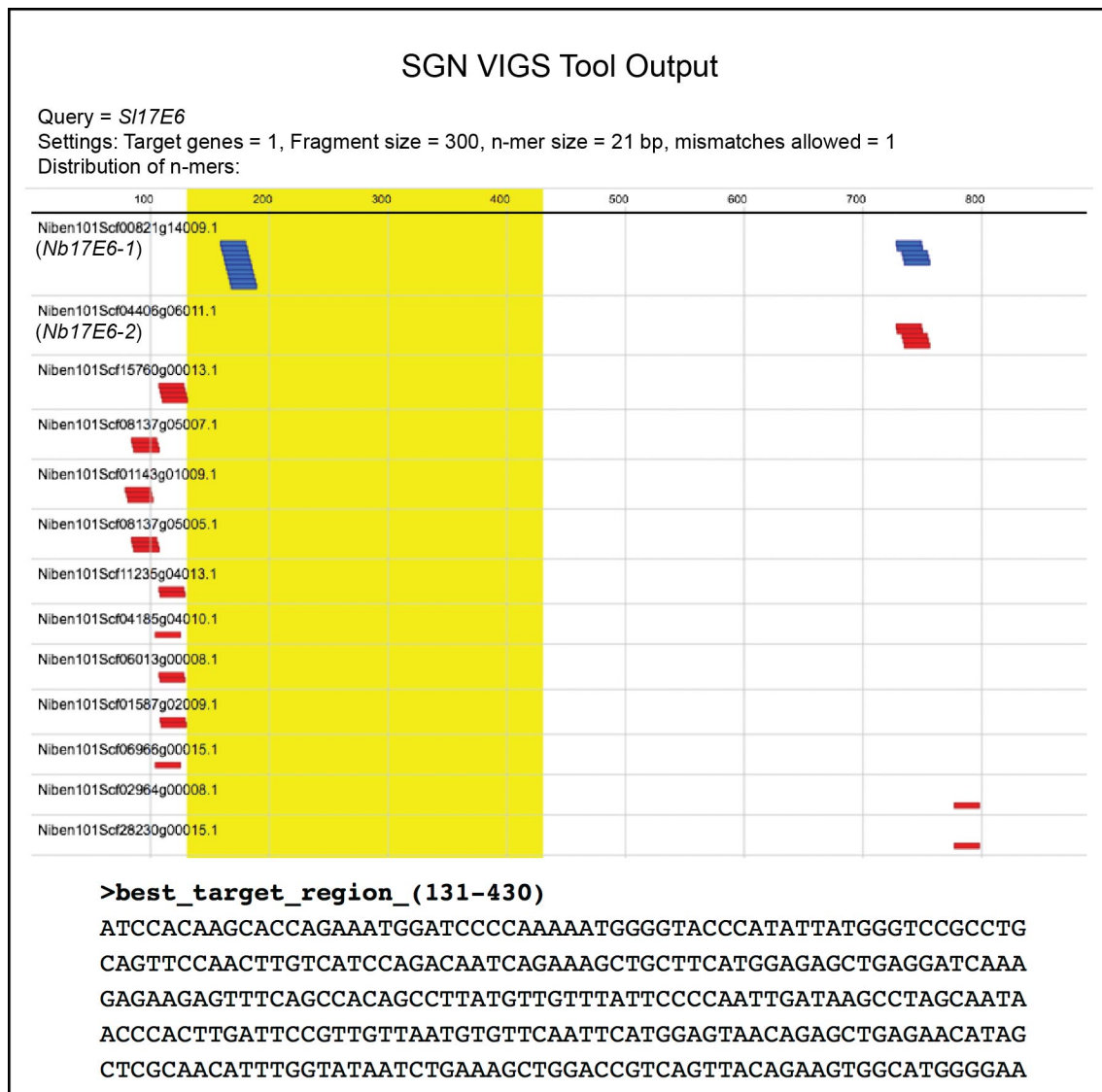


Figure 11.5: Simulation of *Sl17E6* silencing using the SGN VIGS tool reveals a region specific for silencing of *Nb17E6-1*. Using the full length *Sl17E6* cDNA sequence as a query, the SGN VIGS tool identified a region of the cDNA (base pairs 131-430, highlighted in yellow) that will specifically silence *Nb17E6-1* (alignment of n-mers highlighted in blue). The sequence of the highlighted region is found under the heading 'best_target_region'. Alignment of *Sl17E6* n-mers to non-target sequences are shown in red. Map of n-mer distribution as well as 'best_target_region' sequence was extracted from SGN (<http://vigs.solgenomics.net/>)

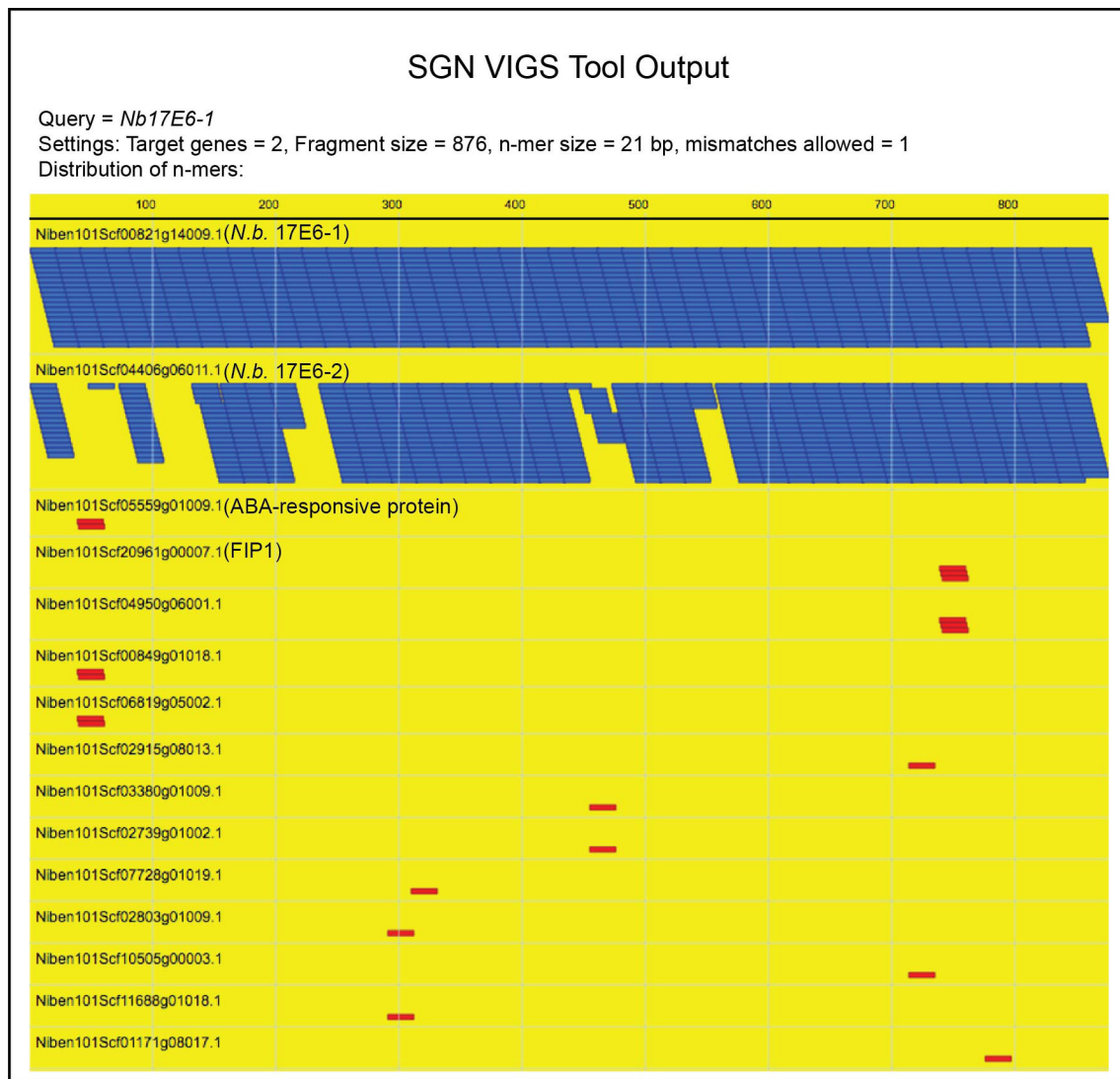


Figure 11.6.: Simulation of *Nb17E6-1* silencing using the SGN VIGS tool reveals high abundance of n-mers specific to GRAM domain containing proteins. Using the full length *Nb17E6-1* cDNA sequence as a query the SGN VIGS tool was used to predict silencing targets. *Nb17E6-1* and *Nb17E6-2* silencing should be thorough due to the large number of specific n-mers produced (alignment of target n-mers highlighted in blue, and off-targets shown in red). It should be noted that if mismatches = 0 only these two genes are targeted, with no off-targets. Additional GRAM domain-containing off-targets included an 'ABA-responsive protein' and 'FIP1'. Yellow region highlights region of the cDNA utilized for silencing (in this case, the whole cDNA). Map of n-mer distribution was extracted from SGN (<http://vigs.solgenomics.net/>).

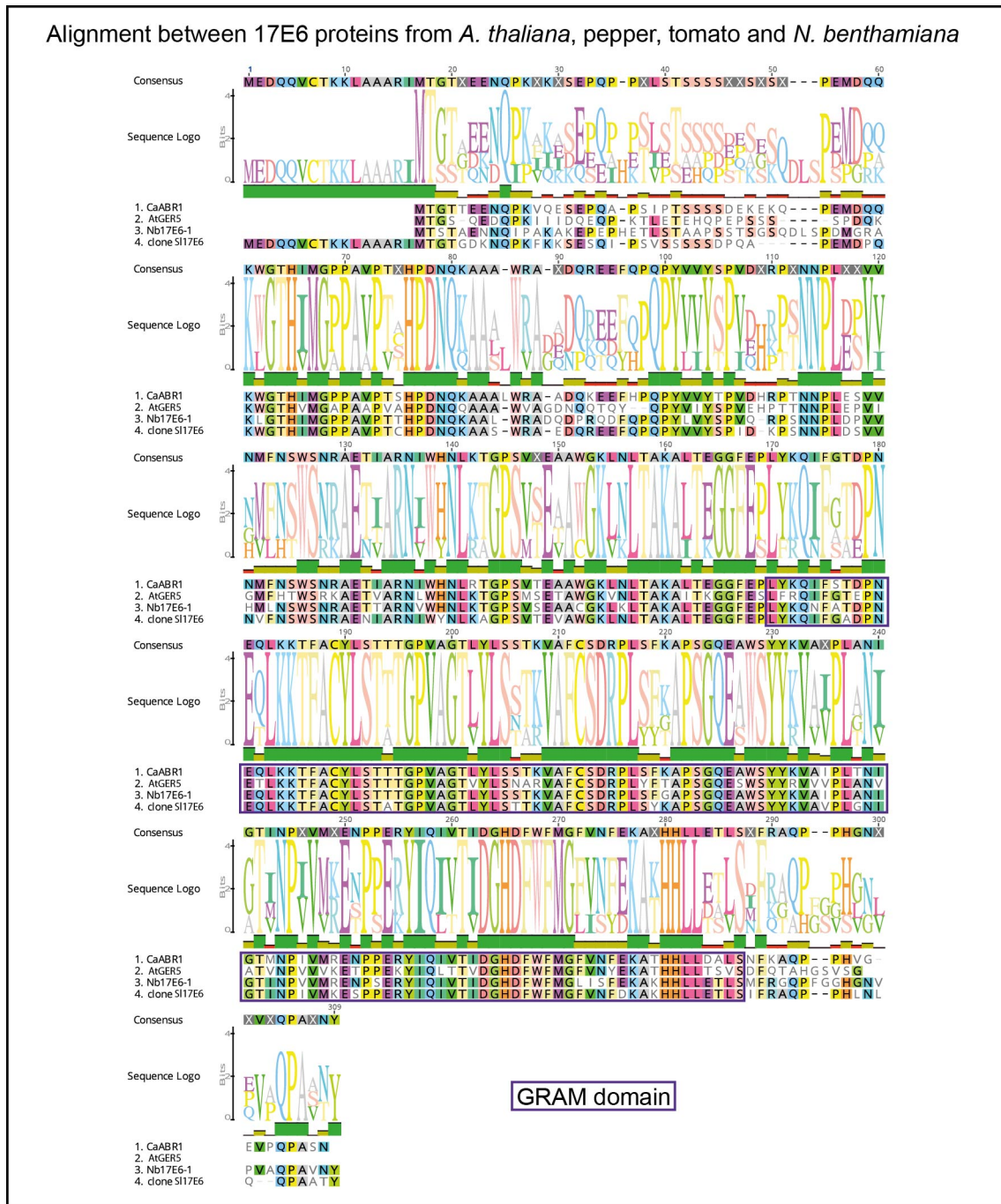


Figure 11.7.: Geneious full length protein alignment (Global alignment with free end gaps) of Nb17E6 and homolog sequences from pepper (CaABR1), *A. thaliana* (AtGER5) and tomato (S117E6). Amino acids are color coded according to identity. Sequence logo indicates the prevalence of the various amino acids at each position, while the graph indicates amino acid identity. The GRAM domain is outlined in purple.

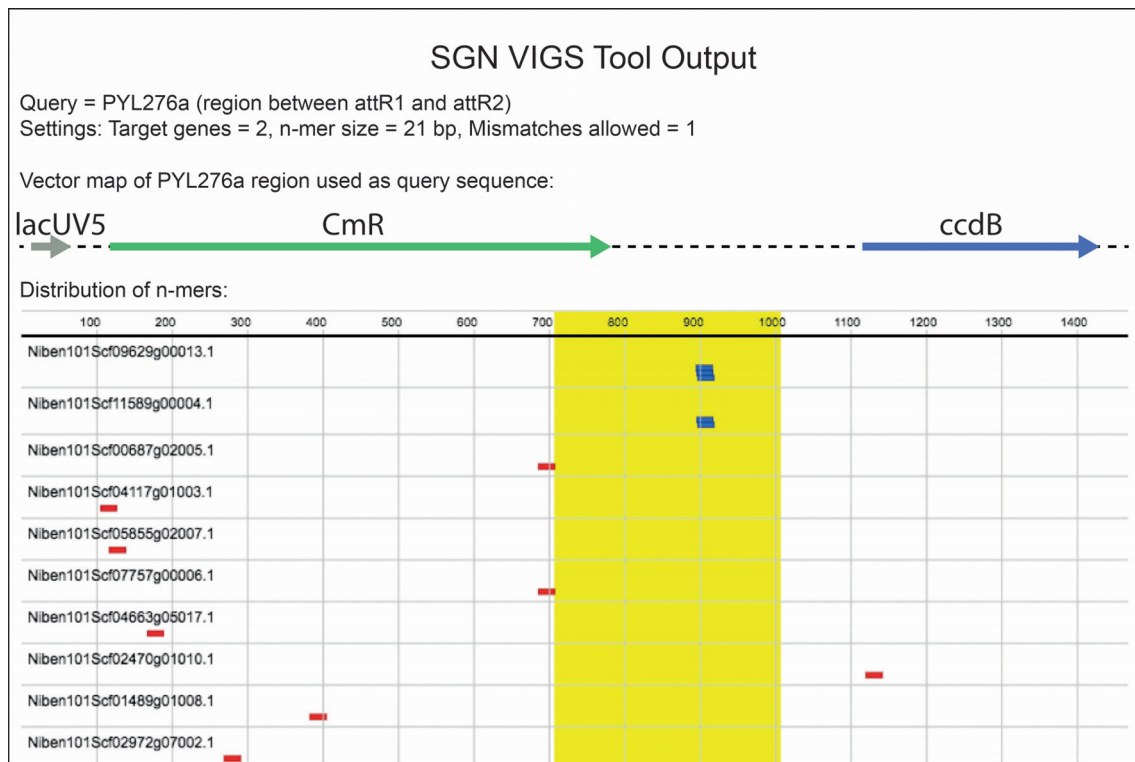


Figure 11.8.: SGN VIGS tool n-mer alignments reveal potential off-targets of the *TRV2* silencing control. The 'Query' was the portion of PYL276a (*TRV2*) between the two Gateway recombination sites (represents the region utilized to facilitate silencing). Default VIGS tool settings were used, excluding 'mismatches allowed' which was set to 1. When mismatches = 0 no targets were identified. Yellow region highlights region recommended for most effective silencing of target genes (alignments illustrated in blue), however this is not relevant when using the SGN VIGS tool for the identification of potential off targets (typically the SGN VIGS tool is used for construct design). Included above the distribution of n-mer alignments is a scale map of the portion of the vector used as a query sequence, illustrating the *lacUV5* promoter (*lacUV5*; grey), the *chloramphenicol resistance* gene (*CmR*; green) and the *control of cell death* gene (*ccdB*; blue). Map of n-mer distribution was extracted from SGN (<http://vigs.solgenomics.net/>).

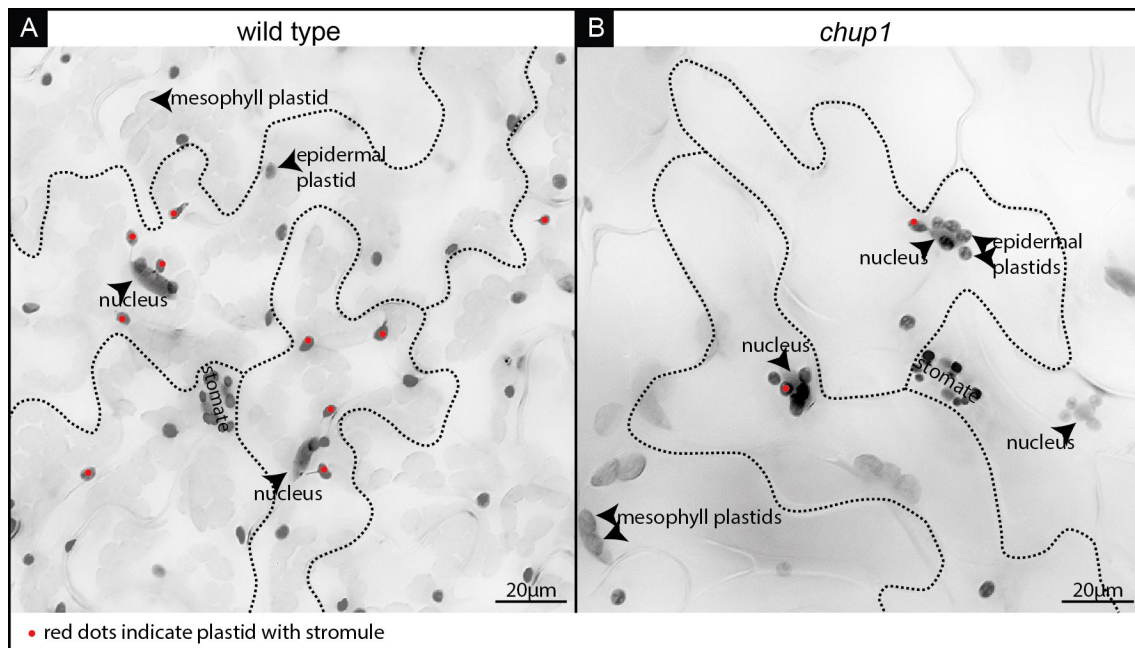


Figure 11.9.: Comparison of plastid position in upper leaf epidermis between wild-type *A. thaliana* and *chup1* mutant. *FNR:eGFP* labeled plastids and stromules and nuclei are labeled with DAPI. Dotted black lines represents cell boundaries and red dots indicate the plastids with stromules. Images are flattened z-stacks which were converted to gray-scale and inverted.

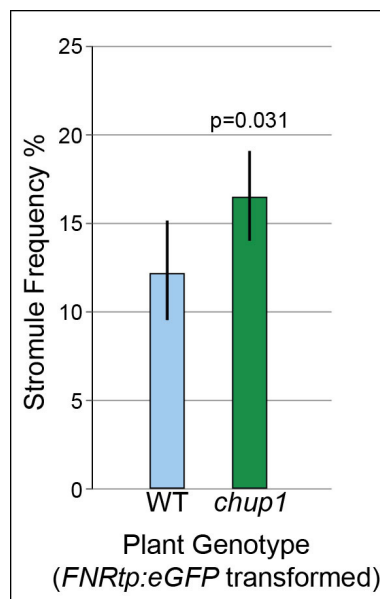


Figure 11.10.: Stromules frequencies in wild type and *chup1* rosette leaf of the upper epidermis in *A. thaliana* (ecotype Col-0) *FNRtp:eGFP* stable transgenics. Stromule frequencies in wildtype (WT-blue) tissue are slightly, but significantly lower than the *chup1* mutant (green).

12. Tables

Genotype	Locus	Insertion line	Plant lines	Total lines	Total plants	Images analysed
WT	-	-	3, 6, 8	3	48	144
<i>xi-a</i>	At1g04600	GABI_622E02 ¹	4, 7, 9	3	9	27
<i>xi-b</i>	At1g04160	SALK_113062 ¹	8, 14, 15	3	9	27
<i>xi-c</i>	At1g08730	GABI_262B03 ¹	1, 2, 3	3	9	27
<i>xi-d</i>	At2g33240	SALK_082078 ¹	4, 5, 6	3	9	27
<i>xi-e</i>	At1g54560	SALK_072023 ¹	5, 9, 11	3	9	27
<i>xi-f</i>	At2g31900	GABI_070F03 ²	1, 2, 4	3	9	27
<i>xi-g</i>	At2g20290	SALK_018032 ¹	3, 5, 9	3	9	27
<i>xi-h</i>	At4g28710	SAIL_365_D03 ¹	7, 4, 2	3	9	27
<i>xi-i</i>	At4g33200	SALK_082443 ¹	2, 3, 5, 9	4	17	51
<i>xi-j</i>	At3g58160	SALK_063159 ¹	2, 3, 4	3	9	27
<i>xi-k</i>	At5g20490	SALK_067972 ¹	1, 2, 7	3	9	27
<i>xi-1</i>	At1g17580	SALK_019031 ¹	1, 5, 9	3	9	27
<i>xi-2</i>	At5g43900	SALK_055785 ¹	2, 3, 4	3	9	27
3KO ³	At1g17580	SALK_055785	2, 3, 7	3	18	54
<i>xi-1, xi-2, xi-k</i>	At5g43900	SALK_019031				
	At5g20490	SALK_067972				
4KO ³	At1g17580	SALK_055785	1, 2, 3	3	9	27
<i>xi-1, xi-2, xi-k,</i>	At5g43900	SALK_019031				
<i>xi-i</i>	At5g20490	SALK_067972				
	At4g33200	SALK_082443				

Table 12.1.: Myosin mutant lines analysed for stromule quantification in Figure 4.1. A. thaliana (ecotype Columbia-0) wild type (WT) and T-DNA insertion mutants in all 13 myosins as well as triple and quadruple mutants were stably transformed with *FNHtp::eGFP* to visualize plastids and stromules. Stromule frequency counts were collected from multiple plants originating from at least three different primary transformants (plant lines chosen are listed in column 4). Plant samples sizes used for data displayed in Figure 4.1, as well as total images analysed are seen in columns 6 and 7, respectively. Seeds were provided by: The Arabidopsis Information Resource (TAIR), www.arabidopsis.org¹, The Nottingham Arabidopsis Stock Centre (NASC), <http://arabidopsis.info/>² and Valerian Dolja, Oregon State University, Corvallis, Oregon, USA, published in Peremyšlov et al. (2010)³.

Genotype	Locus	Insertion line	Plant lines	Total lines	Total plants	Total images analysed
WT	-	-	2, 3, 10	3	6	19
<i>wit12</i> ¹	At5g11390 AT1G68910	CS445078 SALK_127765	8, 12, 13	3	12	34
WT	-	-	10, 3, 2	3	6	20
<i>xt-i</i>	At4g33200	SALK_082443 ²	17, 12, 6	3	11	32
WT	-	-	18, 3, 2	3	3	9
4KO ²	At1g17580 At5g43900 At5g20490 At4g33200	SALK_055785 SALK_019031 SALK_067972 SALK_082443	1, 2, 3	3	10	31
WT	-	-	18, 3	2	3	9
3KO ²	At1g17580 At5g43900 At5g20490	SALK_055785 SALK_019031 SALK_067972	2, 3, 4	3	9	27

Table 12.2.: Mutant lines analysed for stromule quantification in Figure 4.3. *A. thaliana* (ecotype Columbia-0) wild type (WT) and T-DNA insertion mutants *wit12*, *myosin xt-i*, and triple (3KO) and quadruple myosin (4KO) mutants were stably transformed with a single plasmid containing *FNR:eGFP* to visualize plastids and stromules, and *H2B:mCherry* to visualize nuclei. Stromule frequency counts were collected from multiple plants originating from at least three different primary transformants (plant lines chosen are listed in column 4). Plant sample sizes used for data displayed in Figure 4.3, as well as total images analysed are seen in columns 6 and 7, respectively. Seeds were provided by: Iris Meier, Ohio State University, Columbus, Ohio, USA (Zhou and Meier, 2014)¹, seed information for myosin mutants in Table 12.1 on the facing page² and The Arabidopsis Information Resource (TAIR) - www.arabidopsis.org³.

	AIM-LBR	AIM-GVC7	AIM-GVR	AIM-Ltz4	LBR-GVR	LBR-Ltz4	GVC7-GVR	GVC7-Ltz4
ABA	18, 0.161	2, <0.001	0, <0.001	0, <0.001	14, 0.065	11, 0.028	9, 0.015	9, 0.015
ACC	1, <0.001	4, 0.002	0, <0.001	0, <0.001	19, 0.535	4.5, 0.004	4, 0.004	0, <0.001
IAA	13, 0.094	26.5, 0.574	11.5, 0.054	12.5, 0.038	18, 0.456	28, 1	6, 0.009	15, 0.083
SA	6, 0.009	5, 0.003	4, 0.004	0, <0.001	24, 1	25, 0.779	15, 0.152	14, 0.065
OPDA	23, 0.613	25, 0.505	2, 0.001	0, <0.001	4, 0.007	3, 0.002	4, 0.004	1, <0.001
JA	14, 0.121	31, 0.959	22.5, 0.536	27, 0.645	21.5, 0.710	24, 0.694	26, 0.867	29.5, 0.798
JA-IIe	12, 0.072	16, 0.105	20, 0.397	24, 0.442	18, 0.456	26, 0.867	23, 0.613	30, 0.878

Table 12.3.: Rank sum test results corresponding to pair-wise comparisons of treatments shown in Figure 5.1. The first value of the pair represents the U-statistic, while the second number is the p-value. Red represents significant differences in hormone levels between infiltration medium (AIM) and the different bacterial strains, while green highlights instances where *A. tumefaciens* strains with (GVR and Ltz4) and without (LBR and GVC7) the *tsz* gene are compared.

Gene	Matches	Functional description
Niben101Scf09629g00013.1	3	Pentatricopeptide repeat-containing protein
Niben101Scf11589g00004.1	2	Pentatricopeptide repeat-containing protein
Niben101Scf00687g02005.1	1	Protein phosphatase 2C family protein
Niben101Scf04117g01003.1	1	1-aminocyclopropane-1-carboxylate oxidase homolog 1
Niben101Scf05855g02007.1	1	ubiquitin-protein ligase [<i>Setaria italica</i>]
Niben101Scf07757g00006.1	1	Protein phosphatase 2C family protein
Niben101Scf04663g05017.1	1	Unknown protein
Niben101Scf02470g01010.1	1	Unknown protein
Niben101Scf01489g01008.1	1	Decapping nuclease rail
Niben101Scf02972g07002.1	1	Protein yippee-like

Table 12.4.: VIGS tool results using region of *pYL276a* (*TRV2*) between the *attR1* and *attR2* Gateway recombination sites as the query. This includes the *lacUV5* promoter, chloramphenicol resistance gene and the control of *cell death gene* (*ccdB*). Settings for analysis were: mismatches = 1, n-mer size = 21.

Donor organism	Effector	Plant receptor
TMV	p50 (GV3101)	<i>Nb</i> stably expressing N receptor plus transient NRIP1 Caplan et al. (2008, 2015)
<i>Xcv</i>	AvrBs2 (GV3101)	<i>Nb</i> transiently expressing pepper Bs2 Tai et al. (1999)
<i>Xcv</i> (85-10)	XopQ (GV3101)	<i>Nb</i> ; recognition by endogenous Roq1 Schultink et al. (2017)
<i>Pst</i> (DC3000)	AvrRpt2 (<i>Pst</i>)	<i>At</i> (Col-0); recognition by endogenous RPS2 Kunkel et al. (1993)
<i>Pst</i> (DC3000)	AvrRpm1 (<i>Pst</i>)	<i>At</i> (Col-0); recognition by endogenous RPM1 Grant et al. (1995)
<i>Pst</i> (DC3000)	AvrRps4 (<i>Pst</i>)	<i>At</i> (Col-0); recognition by endogenous RPS4 Gassmann et al. (1999)

Table 12.5.: Description of the origin of effector/receptor combinations used to induce ETI and stromules in *N. benthamiana* and *A. thaliana*. 'Donor organism' describes the pathogen from which the effector was isolated (strain is in brackets); 'Effector' provides the effector name and the name of the bacteria used to mediate expression/translocation of the effector *in planta*; 'Plant receptor' lists the receptor necessary for triggering ETI and the reference describing the effector/receptor interaction, as well as the mode of receptor expression utilized. Experiments describing stromule induction during ETI were reported by Caplan et al., (2015), with the exception of XopQ, which was reported by Erickson et al. (2017a). Abbreviations are as follows: TMV = tobacco mosaic virus, *Xcv* = *Xanthomonas campestris* pv. *vesicatoria*, *Pst* = *Pseudomonas syringe* pv. *tomato*, *Nb* = *N. benthamiana*, *At* = *A. thaliana*.

Gene	Reference	Forward primer (5' - 3')	Reverse primer (5' - 3')
<i>NbEF1a</i>	Liu et al., 2012	agctttacctcccaagtcac	agaacgcctgtcaatcttgg
<i>NbPP2A</i>	Liu et al., 2012	gaccctgatgttgatgttcgct	gagggatttgaagagagatttc
<i>NbAPR</i>	Liu et al., 2012	catcagtgtcgttcaggtatt	gcaacttctgggttctcat
<i>Nb17E6-1/2</i>	This thesis	cagcttaccttgtgtattct	cagttttcaggttatgccag

Table 12.6.: Primers utilized for qRT-PCR. Primer sequences for *NbEF1*, *NbPP2A* and *NbAPR* were extracted from (Liu et al., 2012).

Vector	Method	Construct	Forward primer (5' - 3')	Reverse primer (5' - 3')
<i>pUB-Dest</i> (N-mRFP)	Gateway	<i>mRFP::Sl17E6</i>	17E6_TFL_B1: ggggacaagttt gta- <i>caaaaagcaggctctc</i> atgaggaggatcaacaagttt gtaca	17E6_TFLs_B2: ggggaccacttt gtacaa- <i>gaaagctgggtc</i> ctagtaagtagtagctgctgctgctg
<i>pUB-Dest</i> (C-mRFP)	Gateway	<i>Sl17E6::mRFP</i>	17E6_TFL_B1: ggggacaagttt gta- <i>caaaaagcaggctctc</i> atgaggaggatcaacaagttt gtaca	17E6_TFLns_B2: ggggaccacttt gtacaa gaaagctgggtc <i>glaagtagctgctgctgctgctg</i>
<i>TRV2</i> (<i>pYL276a</i>)	Gateway	<i>Sl17E6¹³¹⁻⁴³⁰</i>	17E6_131-430_B1: ggggacaagttt gtacaaaaaagcaggct <i>atccacaagcaccagaatg</i>	17E6_131-430_B2: ggggaccacttt gtacaa gaaagctgggt <i>tcccacatgcccactctg</i>
<i>TRV2</i> (<i>pYL276a</i>)	Gateway	<i>Nb17E6-1</i>	14009_B1: ggggacaagttt gta- <i>caaaaagcaggctctc</i> atgacaagcacaagcaggagaataa	14009_B2: ggggaccacttt gtacaa gaaagctgggtc <i>ctagtaataacagccggttgtgc</i>
<i>pGWB 555</i> (N-mRFP)	Gateway	<i>mRFP::Nb17E6-1</i>	14009_B1: ggggacaagttt gta- <i>caaaaagcaggctctc</i> atgacaagcacaagcaggagaataa	14009_B2: ggggaccacttt gtacaa gaaagctgggtc <i>ctagtaataacagccggttgtgc</i>
<i>pGWB 554</i> (C-mRFP)	Gateway	<i>Nb17E6-1::mRFP</i>	14009_B1: ggggacaagttt gta- <i>caaaaagcaggctctc</i> atgacaagcacaagcaggagaataa	0601Ins_B2: ggggaccacttt gtacaa gaaagctgggtc <i>gtaattaacagccggttgtgc</i>
<i>pGWB 555</i> (N-mRFP)	Gateway	<i>mRFP::Nb17E6-2</i>	06011_B1: ggggacaagttt gta- <i>caaaaagcaggctctc</i> atgacaagcacaagcaggagaataa	14009_B2: ggggaccacttt gtacaa gaaagctgggtc <i>ctagtaataacagccggttgtgc</i>
<i>pGWB 554</i> (C-mRFP)	Gateway	<i>Nb17E6-2::mRFP</i>	06011_B1: ggggacaagttt gta- <i>caaaaagcaggctctc</i> atgacaagcacaagcaggagaataa	0601Ins_B2: ggggaccacttt gtacaa gaaagctgggtc <i>gtaattaacagccggttgtgc</i>
<i>pDONR221</i>	PCR based deletion	<i>no GRAM</i>	GRAMDeINb17_1_F: <i>gaggaggattgagccaatgcttagagggcaacctt</i>	GRAMDeINb17_1_R: <i>aggttgcctctaaccatggctcaatcctccctcag</i>
<i>pGWB 554</i> (C-mRFP)	Gateway	<i>no GRAM::mRFP</i>	14009_B1: ggggacaagttt gta- <i>caaaaagcaggctctc</i> atgacaagcacaagcaggagaataa	0601Ins_B2: ggggaccacttt gtacaa gaaagctgggtc <i>gtaattaacagccggttgtgc</i>
<i>pGWB 554</i> (C-mRFP)	Gateway	<i>GRAM::mRFP</i>	GRAMonlyF: ggggacaagttt gta- <i>caaaaagcaggctctc</i> atgctgtacaagcaggaaattt gtctacag	GRAMonly_R: ggggaccacttt gtacaa- <i>gaaagctgggtc</i> cgataaagctc ccagaagatgatg

Table 12.7.: List of plasmids generated and primer sequences. Column 1 lists the plasmids utilized and abbreviations C and N stand for C-terminal and N-terminal tags, respectively. The cloning method utilized can be found in column 2. Final construct names and primer sequences can be found in columns 3-5. Gene specific part of the primer underlined, att sites in red (green are base pairs added maintain frame when fused to an N terminal fluorescence protein). *pUB-Dest* vectors published and provided by (Greten et al., 2010), *pYL276a* provided by AG Bonas (*pYL276a*; is *YL276* (Lin et al., 2002) modified by S. Schomack to include an ampicillin resistance cassette), *pGWB* vectors published and provided by (Nakagawa et al., 2007) and *pDONR221* was purchased from Thermo Fisher Scientific, Braunschweig, Germany.

13. DNA and protein sequences

Sl17E6 clone/*Soly08g078510* DNA sequence (888 bp)

```
1 ATGACAAGCA CAGCAGAGAA TAACCAAATA CCAGCTAAAG CTAAAGAACC AGAACCCAC
61 GAAACATTGT CCACTGCAGC TCCTTCATCA ACTTCAGGAT CACAAGATTT ATCACCTGAT
121 ATGGGTCTGG CAAAATTGGG TACCCATATT ATGGGTCTCT CAGCAGTTCC AACTACACAT
181 CCAGACAACC AGAAGGCTGC CTTATGGAGA GCTGATCAGG ATCCCCGCCA AGATTTTCAA
241 CCGCAGCCTT ACCTTGTGTA TTCTCCTGTT CAAAGGCCGA GCAACAATCC TCTTGATCCT
301 GTTGTTTATA TGCTCAATTC TTGGAGTAAT AGAGCTGAGA CCACCGCCCG CAACGTCTGG
361 CATAACCTGA AAAGTGGGCC ATCAGTGTCC GAAGCTGCAT GCGGAAAGCT TAAATTGACA
421 GCTAAGGCTT TAACTGAGGG AGGATTTGAG CCACTGTACA AGCAGAATTT TGCTACAGAT
481 CCTAATGAGC AGTTGAAGAA AACATTTGCT TGTTACCTCT CTACAACAAC TGGCCCTGTT
541 GCTGGAATCT TGTATCTCTC ATCTACTAAA GTGGCTTTCT GTAGTGATCG TCCCTTATCT
601 TTCGGAGCTC CATCTGGACA GGAAGCTTGG AGCTACTATA AGGTTGCAAT ACCATTGGCA
661 AACATTGGCA CTATCAACCC TGTAGTGATG AGAGAAAATC CATCAGAAAG GTACATTCAG
721 ATTGTCACCA TTGATGGTCA TGACTTTTGG TTTATGGGAT TAATCAGTTT TGAGAAAGCA
781 AAGCATCATC TTCTGGAGAC TTTATCGATG TTTAGAGGGC AACCTTTTGG TGGACATGGC
841 AATGTGCCAG TGGCACAACC GGCTGTTAAT TACTAG
```

Sl17E6 ORF translation (295 aa, 32.8 kDa)

```
1 MEDQQVCTKK LAAARIMTGT GDKNQPKFKK SESQIPSVSS SSSDPQAPEM DPQKWGTHIM
61 GPPAVPTCHP DNQKAASWRA EDQREEFQPQ PYVVYSPIDK PSNNPLDSV NVFNSWSNRA
121 ENIARNIWYN LKAGPSVTEV AWGKLNLTAK ALTEGGFEPL YKQIFGADPN EQLKKTFCY
181 LSTATGPVAG TLYLSTTKVA FCSRPLSYK APSGQEAWSY YKVAVPLGNI GTINPIVMKE
241 SPPERVIQIV TIDGHDFWFM GFVNFDAKAKH HLETLISIFR AQPPHLNLQQ PAATY*
```

Nb17E6-1/Niben101Scf00821g14009 DNA sequence- corrected version (876 bp)

```
1 ATGACAAGCA CAGCAGAGAA TAACCAAATA CCAGCTAAAG CTAAAGAACC AGAACCCAC
61 GAAACATTGT CCACTGCAGC TCCTTCATCA ACTTCAGGAT CACAAGATT ATCACCTGAT
121 ATGGGTCGGG CAAAATTGGG TACCCATATT ATGGGTCCTC CAGCAGTTCC AACTACACAT
181 CCAGACAACC AGAAGGCTGC CTTATGGAGA GCTGATCAGG ATCCCCGCCA AGATTTTCAA
241 CCGCAGCCTT ACCTTGTGTA TTCTCCTGTT CAAAGGCCGA GCAACAATCC TCTTGATCCT
301 GTTGTTTATA TGCTCAATTC TTGGAGTAAT AGAGCTGAGA CCACCGCCCG CAACGTCTGG
361 CATAACCTGA AAAGTGGGCC ATCAGTGTCC GAAGCTGCAT GCGGAAAGCT TAAATTGACA
421 GCTAAGGCTT TAACTGAGGG AGGATTTGAG CCACTGTACA AGCAGAATTT TGCTACAGAT
481 CCTAATGAGC AGTTGAAGAA AACATTTGCT TGTTACCTCT CTACAACAAC TGGCCCTGTT
541 GCTGGAAGCT TGTATCTCTC ATCTACTAAA GTGGCTTTCT GTAGTGATCG TCCCTTATCT
601 TTCGGAGCTC CATCTGGACA GGAAGCTTGG AGCTACTATA AGGTTGCAAT ACCATTGGCA
661 AACATTGGCA CTATCAACCC TGTAGTGATG AGAGAAAATC CATCAGAAAG GTACATTCAG
721 ATTGTCACCA TTGATGGTCA TGAATTTTGG TTTATGGGAT TAATCAGTTT TGAGAAAGCA
781 AAGCATCATC TTCTGGAGAC TTTATCGATG TTTAGAGGGC AACCTTTTGG TGGACATGGC
841 AATGTGCCAG TGGCACAACC GGCTGTTAAT TACTAG
```

Nb17E6-1 protein sequence (291 aa, 31.8 kDa)

```
1 MTSTAENNQI PAKAKEPEPH ETLSTAAPSS TSGSQDLSPD MGRAKLGTHI MGPPAVPTTH
61 PDNQAALWR ADQDPRQDFQ PQPVLVYSPV QRPSNNPLDP VVHMLNSWSN RAETTARNVW
121 HNLKTGPSVS EAACGKLLT AKALTEGGFE PLYKQNFATD PNEQLKKTFA CYLSTTTGPV
181 AGTLYLSSTK VAFCSRPLS FGAPSGQEAW SYKVAIPLA NIGTINPVVM RENPSERYIQ
241 IVTIDGHDFW FMGLISFEKA KHHLLETLSM FRGQPFGGHG NVPVAQPAVN Y*
```


Nb17E6-2/Niben101Scf04406g06011 DNA sequence (858 bp)

```

1 ATGACAAGCA CACCAGAGAA TAACCAAATA CCAGAACCCC AAAAAACATT TCCAACCTGCA
61 GTTCCTTCAT CAACTTCAGG ATTACAAGAT CCATCACCTG ATACGGGTCTG GGAAAAATTC
121 GGTACCCATA TTATGGGACC TCCAGCAGTT CCAACTACAC ATCCAGACAA CCAGAAGGCT
181 GCCTTATGGA GAGCTGATCA GGACCACCGC CAAGACTTTC AACCTCAGCC TTACCTTGTG
241 TATTCTCCTG TTCAAAGGCC GAGCAACAAT CCTCTTGATC CTGTTCTTCA TATGCTCAAT
301 TCTTGGAGTA ATAGAGCTGA GACCACCGCC CGCAACGTCT GGCATAACCT GAAAACTGGA
361 CCATCAGTGT CCGAAGCTGC ATGTGGAAAG CTTAAATTGA CAGCTAAGGC TTTAACTGAG
421 GGAGGATATG AGCCACTATA CAAGCAGAAT TTTTCTACAG ATCCAAATGA GCAGTTGAAG
481 AAAACATTTG CTTGTTACCT ATCTACAACA ACTGGCCCTG TTGCTGGAAC TCTGTATGTA
541 TCATCTACTA AAGTGGCTTT CTGTAGTGAT CGTCCCTTAT TTTTCGGAGC TCCATCTGGA
601 CAGGAAGCTT GGAGCTACTA TAAGGTTGCA ATACCATTGG CAAACATTGG CACCATCAAC
661 CCTGTAGTGA TGAGAGAAAA TCCATCAGAA AGGTACATTC AGATTGTCAC CATTGATGGC
721 CATGACTTTT GGTTTATGGG ATTAATCAGT TTTGAGAAAAG CAAAGCATCA TCTTCTGGAG
781 ACTTTATCGA TGTTTAGAGG GCAACCTTTT GGTGGACATG GCAATGTGCC AGTGGCACAA
841 CCGGCTGTTA ATTACTAG

```

Nb17E6-2 protein sequence (285 aa, 31.5 kDa)

```

1 MTSTPENNQI PEPHKTFPTA VPSSTSLQD PSPDTGREKF GTHIMGPPAV PTHHPDNQKA
61 ALWRADQDHR QDFQPQPYLV YSPVQRPSNN PLDPVLHMLN SWSNRAETTA RNVVHNLKTG
121 PSVSEAACGK LKLTAKALTE GGYEPLYKQN FSTDPNEQLK KTFACYLSTT TGPVAGTLYV
181 SSTKVAFCSD RPLFFGAPSG QEAWSYYKVA IPLANIGTIN PVVMRENPS ERYIQIVTIDG
241 HDFWFMGLIS FEKAKHLLLE TLSMFRGQPF GGHGNVPVAQ PAVNY*

```

CaABR1/Ca01g05510 DNA sequence (855bp)

```
1 ATGACAGGCA CAACAGAAGA AAATCAACCC AAAGTTCAAG AATCAGAGCC TCAAGCACCC
61 TCTATTCCTA CATCTTCTTC TTCTGATGAG AAAGAGAAAC AACCAGAAAT GGATCAACAA
121 AAATGGGGCA CACACATAAT GGGTCCACCA GCAGTTCCAA CAAGTCATCC AGATAATCAG
181 AAAGCTGCTG CGTTATGGAG AGCTGCAGAC CAAAAAGAAG AGTTTCACCC ACAGCCTTAC
241 GTTGTTTATA CTCCAGTTGA TCATAGGCCT ACTAATAATC CACTTGAATC TGTTGTTAAT
301 ATGTTTAATT CTTGGAGTAA TCGAGCTGAG ACCATCGCCC GCAACATCTG GCATAATCTG
361 AGAACTGGAC CATCAGTGAC AGAAGCAGCG TGGGGAAAAGC TTAATTTGAC AGCCAAGGCC
421 TTAACAGAAG GCGGATTCGA GCCGCTTTAC AAGCAGATTT TCTCTACGGA CCCTAATGAG
481 CAGCTGAAGA AGACATTTGC TTGTTATCTT TCAACAATA CTGGTCCTGT TGCTGGAACA
541 CTCTATTTGT CATCTACTAA GGTGCTTTT TGCAGTGATC GACCTTTATC CTTCAAAGCT
601 CCATCAGGTC AGGAGGCTTG GAGCTACTAC AAGGTAGCAA TACCATTGAC AAACATTGGG
661 ACTATGAACC CAATAGTGAT GAGAGAGAAT CCACCAGAGA GGTACATTCA GATTGTTACA
721 ATCGATGGTC ATGACTTCTG GTTCATGGGG TTTGTCAATT TTGAGAAAAGC AACACATCAT
781 CTCCTTGACG CCTTGTCTAA TTTTAAGGCC CAACCTCCTC ATGTTGGGGA AGTGCCACAA
841 CCAGCTAGTA ACTAG
```

CaABR1/Ca01g05510 protein sequence (284 aa, 31.7 kDa)

```
1 MTGTTEENQP KVQESEPPAP SIPTSSSSDE KEKQPEMDQQ KWGTHIMGPP AVPTSHPDNQ
61 KAAALWRAAD QKEEFHPQPY VVYTPVDHRP TNNPLESVFN MFNSWSNRAE TIARNIWHNL
121 RTGPSVTEAA WGKLNLTAKA LTEGGFEPLY KQIFSTDPNE QLKKTFACYL STTTGVPVAGT
181 LYLSSTKVAF CSDRPLSFKA PSGQEAWSYY KVAIPLTNIG TMNPIVMREN PPERYIQIVT
241 IDGHDFWFMG FVNFEEKATHH LLDALSNFKA QPPHVGEVPQ PASN*
```

Ger5/Gre5/AtABR1/AT5G13200 DNA sequence (819bp)

```

1 ATGACAGGAT CACAAGAAGA CCAACCTAAG ATCATCATTG ATCAAGAGCA ACCCAAAACT
61 CTAGAAACAG AGCACCAACC AGAACCTTCT TCATCGTCTC CGGATCAGAA GAAATGGGGT
121 ACTCACGTGA TGGGAGCTCC GGCAGCTCCA GTTGCTCATC CCGATAACCA ACAGGCGGCG
181 GCGTGGGTCG CTGGAGATAA CCAGCAGACG CAGTACCAAC CGTACGTCAT CTA CTCTCTCT
241 GTCGAACATC CAACA ACTAA CAACCCTCTC GAGCCAGTCA TCGGAATGTT CCATACCTGG
301 AGTCGCAAGG CAGAAACCGT CGCACGTAAC CTCTGGCACA ATCTGAAGAC AGGACCGTCT
361 ATGTCGGAAA CGGCGTGGGG GAAGGTTAAT TTGACGGCCA AAGCGATAAC AAAAGGAGGA
421 TTCGAGTCGC TTTTCAGACA GATTTTCGGA ACAGAGCCAA ACGAGACGCT GAAGAAA ACT
481 TTCGCTTGTT ATCTCTCGAC GACGACAGGT CCTGTTGCTG GAACTGTCTA TCTTTCGAAT
541 GTCGCTGTCG CTTTTTGTAG CGATCGTCCT CTGTACTTCA CAGCACCTTC TGGTCAAGAA
601 TCTTGAGACT ACTACAGGGT GGTGTACCT TTGGCGAATG TAGCGACGGT GAATCCGGTG
661 GTGGTGAAAG AACTCCACC TGAGAAGTAT ATTCAGTTGA CGACGGTGGG TGGTCATGAC
721 TTCTGTTTCA TGGGTTTTGT GAATTATGAG AAGGCTACGC ATCATCTGCT GACCAGTGTCT
781 TCCGATTTTC AAACCGCACA CGGCTCTGTG TCTGGTTAA

```

Ger5/Gre5/AtABR1/AT5G13200 protein sequence (272 aa, 30.1 kDa)

```

1 MTGSQEDQPK IIIDQEQPKT LETEHQPEPS SSSPDQKKWG THVMGAPAAP VAHPDNQQAA
61 AWWAGDNQQT QYQPYVIYSP VEHPPTNPL EPVIGMFHTW SRKAETVARN LWHNLKTGPS
121 MSETAWGKVN LTAKAITKGG FESLFRQIFG TEPNETLKKT FACYLSTTTG PVAGTVYLSN
181 ARVAFCSDRP LYFTAPSGQE SWSYRVRVVP LANVATVNPV VVKETPPEKY IQLTTVDGHD
241 FWFMGFVNYE KATHLLTSV SDFQTAHGSV SG*

```

protein sequence of attB2 linker (highlighted in yellow) plus C-terminal mRFP (highlighted in red) resulting from Gateway reaction of Nb17e6 and truncations into pGWB554 (26.8 kDa)

```

1 DPAFLYKVVD NSMASEDVI KEFMRFKVRM EGSVNGHEFE IECEGEGRPY EGTQTAKLKV
61 TKGGPLPFAW DILSPQFQYG SKAYVKHPAD IPDYLLKLSFF EGFKWERVMN FEDGGVVTVT
121 QDSSLQDGEF IYKVKLRGTN FPSDGPVMQK KTMGWEASTE RMYPEDGALK GEIKMRLKLK
181 DGGHYDAEVK TTYMAKKPVQ LPGAYKTDIK LDITSHNEDY TIVEQYERAE GRHSTGA

```

Part V.

Appendix

14. List of abbreviations

3KO - triple knockout myosin mutant (<i>xi-1</i> , <i>xi-2</i> , <i>xi-k</i>)	ER - endoplasmic reticulum
4KO - quadruple knockout myosin mutant (<i>xi-1</i> , <i>xi-2</i> , <i>xi-k</i> , <i>xi-i</i>)	ETI - effector triggered immunity
ABA - abscisic acid	FIP1 - FH INTERACTING PROTEIN 1
ABD2 - actin binding domain 2 from FIMBRIN 1	FNRtp - FERREDOXIN-NADP(H) OXIDOREDUCTASE transit peptide
CaABR1 - ABA RESPONSIVE 1	GEM - GL2-EXPRESSION MODULATOR
ACC - 1 aminocyclopropane-1-carboxylic acid	GER - GEM-RELATED (also abbreviated GRE)
AgNO ₃ - silver nitrate	GRAM - Glucosyltransferases, Rab-like GTPase activators and Myotubularins
AGPase - ADP-glucose pyrophosphorylase	GSH - glutathione
AIM - acetosyringone infiltration medium	GSNO - S-nitroso-glutathione (an SNO molecule)
APM - aminoprophosphomethyl	GSNOR - S-(HYDROXYMETHYL) GLUTATHIONE DEHYDROGENASE
APR- APS REDUCTASE	GV - GV3101
APX 1 - ASCORBATE PEROXIDASE 1	GVC - GV3101 transformed with <i>pCP60::35S:DsRed2</i> cured of the Ti-plasmid
ARC - ACCUMULATION AND REPLICATION OF CHLOROPLAST	GVR - GV3101 transformed with <i>pCP60::35S:DsRed2</i>
ATG - AUTOPHAGY GENE	H2B - HISTONE 2B
ATP - adenosine triphosphate	H ₂ O ₂ - hydrogen peroxide (ROS molecule)
<i>A. thaliana</i> - <i>Arabidopsis thaliana</i>	hpi- hours post-infiltration
<i>A. tumefaciens</i> - <i>Agrobacterium tumefaciens</i>	HR - hypersensitive response
AvrBs3 - avirulence protein bacterial spot 3	h - hours
BAP - 6-Benzylaminopurine	IAA - indole-3-acetic acid
Bs3 - bacterial spot resistance 3	JA - jasmonic acid
<i>C. annuum</i> - <i>Capsicum annuum</i> (pepper)	JA-Ile - jasmonoyl-isoleucine
CaMV - Cauliflower Mosaic Virus	Lat B - latriculin B
CD - cytochalasin D	LBA - LBA 4404
CHUP1 - CHLOROPLAST UNUSUAL POSITIONING 1	LBR - LBA4404 transformed with <i>pCP60::35S:DsRed2</i>
Co-IP - co-immunoprecipitation	LC-MS/MS - liquid chromatography-mass spectrometry and liquid chromatography - tandem mass spectrometry
dpi - days post-infiltration	LRR - leucine-rich repeat
DsRed - drFP583 (ref) fluorescent protein	Ltz - LBA4404 transformed with <i>pLSU::ptzs:tzs</i>
dsRNA - double-stranded RNA	MCS - membrane contact sites
EF1 - ELONGATION FACTOR 1	
eGFP - enhanced green fluorescent protein	

Chapter 14. List of abbreviations

MeJA - methyl-jasmonate	PTGS - post-transcriptional gene silencing
min - minutes	qRT-PCR - quantitative real-time polymerase chain reaction
mOrange2 - monomeric orange fluorescent protein 2	R-gene - resistance gene
mRFP - monomeric red fluorescent protein	RPN - 19S REGULATORY PARTICLE NON-ATPASE
MAP4 - MICROTUBULE ASSOCIATED PROTEIN 4 (from mouse)	SA - salicylic acid
MAX - MORE AXILLARY BRANCHES	SDS - sodium dodecyl sulfate
MSL2 - MSCS-LIKE 2	sec - seconds
MSL3 - MSCS-LIKE 3	SGN - Sol Genomics Network
NADPH - nicotinamide adenine dinucleotide phosphate hydrogen	siRNA - small interfering RNA
NO - nitric oxide (RNS molecule)	Sl17E6 - tomato clone number 17E6 from VIGS library
noGRAM - mutant Nb17E6-1 without the GRAM domain	<i>S. lycopersicum</i> - <i>Solanum lycopersicum</i> (tomato)
<i>N. tabacum</i> - <i>Nicotiana tabacum</i> (tobacco)	SNO - S-nitrosothiol
Nb17E6 - <i>N. benthamiana</i> clone number 17E6 from VIGS library	ROS - reactive oxygen species
<i>N. benthamiana</i> - <i>Nicotiana benthamiana</i>	RNS - reactive nitrogen species
NTRC - NADPH-DEPENDENT THIOREDOXIN REDUCTASE C	T3E - type III effector
OMT I-b - Catechol O-methyltransferase I-b	TMV - tobacco mosaic virus
OPDA - 12-oxo-phytodienoic acid	TRV - tobacco rattle virus
ORF - open reading frame	TUA - TUBULIN ALPHA
pARC - PARALOG OF ARC6	<i>tZ</i> - <i>trans</i> -Zeatin
PCR - polymerase chain reaction	<i>tzs</i> - <i>trans</i> -zeatin synthase
PDR1 - PDR-type ABC transporter 1	UBQ 10 - UBIQUITIN 10
PDS - PHYTOENE DESATURASE	VIGS - virus induced gene silencing
Pfam - Protein families database	WIT - WPP DOMAIN-INTERACTING TAIL-ANCHORED PROTEIN
pn marker- plastid (<i>FNRtp:eGFP</i>) - nucleus marker (<i>H2B:mCherry</i>)	WT - wild type
PP2A - PROTEIN PHOSPHATASE 2A	<i>Xcv</i> - <i>Xanthomonas campestris</i> pv. <i>vesicatoria</i>
<i>P. syringe</i> - <i>Pseudomonas syringe</i>	Xop - Xanthomonas outer protein
	XopLmut - E3-ligase dead mutant variant of XopL (XopL _{H584A_L585A_G586E})

15. List of figures

1.1	Defining a stromule.	4
1.2	Summary of stromule-nuclear interactions reported in the literature.	6
1.3	Budding and segmentation of stromules.	7
1.4	Osmotic status of the plastid dictates stromule formation.	8
1.5	Membrane availability limits stromule formation.	9
1.6	A model for direct pulling of class XI myosins on the plastid membrane.	11
4.1	Mutants lacking myosin XI-I show decreased stromule frequency.	35
4.2	Nucleus movement-driven stromule elongation.	36
4.3	Mutants with impaired nucleus movement have less stromules.	37
5.1	<i>A. tumefaciens</i> derivatives expressing the <i>tzs</i> gene alter plant hormone levels.	64
5.2	Application of stress-associated compounds leads to stromule formation.	67
6.1	XopL triggers depolymerization of microtubules.	86
7.1	Mechanism of Virus Induced Gene Silencing.	90
7.2	Schematic of blind VIGS screen for stromule-relevant genes.	91
7.3	VIGS silencing of <i>PDS</i> is most efficient under 24 h light.	94
7.4	Plastid morphology differs depending on light conditions.	95
7.5	Silencing of <i>Sl17E6</i> suppresses the induction of stromules.	110
7.6	Plant phenotype following silencing utilizing <i>Sl17E6</i>	111
7.7	<i>Sl17E6</i> transient over-expression results in slight stromule induction.	111
7.8	Sub-cellular localization of transient Sl17E6.	112
7.9	Silencing utilizing <i>Sl17E6</i> reduces <i>Nb17E6</i> transcript levels.	113
7.10	VIGS with shortened <i>Sl17E6</i> ¹³¹⁻⁴³⁰ and full <i>Nb17E6-1</i>	114
7.11	Transient over-expression of <i>Nb17E6</i> induces stromules.	115
7.12	mRFP tagged Nb17E6 proteins are cytosolic and nuclear excluded.	116

7.13	Deletion of the GRAM domain increases stromule induction.	117
7.14	Amino acid homology between GRAM domains.	118
7.15	Silencing with <i>TRV2::Nb17E6-1</i> inhibits HR.	119
7.16	Comassie stained 10% SDS gels of Nb17E6-1 Co-IP.	119
7.17	Model for potential Nb17E6 interactions.	127
8.1	Likely models for stromule formation.	135
11.1	Identity of <i>Sl17E6</i> sequenced clone.	144
11.2	SGN BLAST of <i>Sl17E6</i> against the <i>N. benthamiana</i> genome.	145
11.3	Alignment between the predicted and cloned <i>Nb17E6-1</i>	146
11.4	Alignment of the <i>Nb17E6-1</i> and <i>Nb17E6-2</i> cloned sequences.	147
11.5	SGN VIGS tool reveals a region of <i>Sl17E6</i> specific for silencing of <i>Nb17E6-1</i>	148
11.6	Simulation of <i>Nb17E6-1</i> silencing using the SGN VIGS tool.	149
11.7	Alignment of Nb17E6, CaABR1, AtGER5 and Sl17E6 proteins.	150
11.8	SGN VIGS tool with empty <i>TRV2</i> as query.	151
11.9	Comparison of plastid position in wild-type and <i>chup1</i> mutant.	152
11.10	Stromules frequencies in wild type and <i>chup1</i>	152

16. List of tables

7.1	The GRAM domain of Sl17E6.	91
7.2	SGN VIGS tool identifies four possible targets of <i>TRV2::Sl17E6</i>	98
7.3	SGN VIGS tool identifies thirteen possible targets of <i>TRV2::Sl17E6</i>	99
7.4	SGN VIGS tool identifies possible targets of <i>TRV2::Nb17E6-1</i>	101
7.5	The GRAM domains of Nb17E6-1 and Nb17E6-2.	103
7.6	GRAM domain containing proteins from <i>A. thaliana</i> and <i>N. benthamiana</i>	106
7.7	Short list of putative Nb17E6-1 interacting proteins.	124
12.1	Myosin mutant lines analysed for stromule quantification.	154
12.2	<i>wit</i> mutant lines analysed for stromule quantification.	155
12.3	Rank sum test results of treatments shown in 5.1.	156
12.4	VIGS tool results using <i>TRV2</i> sequence as query.	157
12.5	Effector/receptor combinations used to induce ETI and stromules.	157
12.6	Primers utilized for qRT-PCR.	157
12.7	List of plasmids generated and primer sequences.	158

17. References

A

Argueso, C. T., Ferreira, F. J., Epple, P., To, J. P. C., Hutchison, C. E., Schaller, G. E., Dangl, J. L., and Kieber, J. J. (2012). Two-component elements mediate interactions between cytokinin and salicylic acid in plant immunity. *PLoS Genetics*, 8(1):e1002448.

Avisar, D., Abu-Abied, M., Belausov, E., Sadot, E., Hawes, C., and Sparkes, I. A. (2009). A comparative study of the involvement of 17 Arabidopsis myosin family members on the motility of Golgi and other organelles. *Plant Physiology*, 150(2):700–709.

B

Baron, K. N., Schroeder, D. F., and Stasolla, C. (2014). GEM-Related 5 (GER5), an ABA and stress-responsive GRAM domain protein regulating seed development and inflorescence architecture. *Plant Science : an international journal of experimental plant biology*, 223:153–166.

Bartel, D. P. (2004). MicroRNAs: genomics, biogenesis, mechanism, and function. *Cell*, 116(2):281–297.

Barton, K., Wozny, M., Mathur, N., Jaipargas, E.-A., and Mathur, J. (2017). Chloroplast behaviour and interactions with other organelles in *Arabidopsis thaliana* pavement cells. *Journal of Cell Science*, 131(2):1–11.

Bobik, K. and Burch-Smith, T. (2015). Chloroplast signaling within, between and beyond cells. *Frontiers in Plant Science*, 6(1872):307.

Bombarely, A., Rosli, H. G., Vrebalov, J., Moffett, P., Mueller, L. A., and Martin, G. B. (2012). A draft genome sequence of *Nicotiana benthamiana* to enhance molecular plant-microbe biology research. *Molecular Plant-Microbe Interactions*, 25(12):1523–1530.

Boroske, E., Elwenspoek, M., and Helfrich, W. (1981). Osmotic shrinkage of giant egg-lecithin vesicles. *Biophysical Journal*, 34(1):95–109.

Borucki, W., Bederska, M., and Sujkowska-Rybkowska, M. (2015). Visualisation of plastid outgrowths in potato (*Solanum tuberosum* L.) tubers by carboxyfluorescein diacetate staining. *Plant Cell Reports*, 34(5):853–860.

Bowsher, C. G. and Tobin, A. K. (2001). Compartmentation of metabolism within mitochondria and plastids. *Journal of Experimental Botany*, 52(356):513–527.

Brunkard, J. O., Runkel, A. M., and Zambryski, P. C. (2015). Chloroplasts extend stromules independently and in response to internal redox signals. *Proceedings of the National Academy of Sciences of the United States of America*, 112(32):10044–10049.

Burch-Smith, T. M., Anderson, J. C., Martin, G. B., and Dinesh-Kumar, S. P. (2004). Applications and advantages of virus-induced gene silencing for gene function studies in plants. *The Plant Journal*, 39(5):734–746.

Büttner, D. and He, S. Y. (2009). Type III protein secretion in plant pathogenic bacteria. *Plant Physiology*, 150:1656–1664.

C

- Caplan, J. L., Kumar, A. S., Park, E., Padmanabhan, M. S., Hoban, K., Modla, S., Czymmek, K., and Dinesh-Kumar, S. P. (2015). Chloroplast stromules function during innate immunity. *Developmental Cell*, 34(1):45–57.
- Caplan, J. L., Mamillapalli, P., Burch-Smith, T. M., Czymmek, K., and Dinesh-Kumar, S. P. (2008). Chloroplastic protein NRIP1 mediates innate immune receptor recognition of a viral effector. *Cell*, 132(3):449–462.
- Chae, H. S., Faure, F., and Kieber, J. J. (2003). The *eto1*, *eto2*, and *eto3* mutations and cytokinin treatment increase ethylene biosynthesis in *Arabidopsis* by increasing the stability of ACS protein. *The Plant Cell*, 15(2):545–559.
- Chiba, A., Ishida, H., Nishizawa, N. K., Makino, A., and Mae, T. (2003). Exclusion of ribulose-1,5-bisphosphate carboxylase/oxygenase from chloroplasts by specific bodies in naturally senescing leaves of wheat. *Plant & Cell Physiology*, 44(9):914–921.
- Choi, D. S. and Hwang, B. K. (2011). Proteomics and functional analyses of pepper abscisic acid-responsive 1 (ABR1), which is involved in cell death and defense signaling. *The Plant Cell*, 23(2):823–842.
- Comparot, S., Lingiah, G., and Martin, T. (2003). Function and specificity of 14-3-3 proteins in the regulation of carbohydrate and nitrogen metabolism. *Journal of Experimental Botany*, 54(382):595–604.

D

- Denison, F. C., Paul, A.-L., Zupanska, A. K., and Ferl, R. J. (2011). 14-3-3 proteins in plant physiology. *Seminars in Cell & Developmental Biology*, 22(7):720–727.
- Doerks, T., Strauss, M., Brendel, M., and Bork, P. (2000). GRAM, a novel domain in glucosyltransferases, myotubularins and other putative membrane-associated proteins. *Trends in Biochemical Sciences*, 25(10):483–485.
- Dyall, S. D., Brown, M. T., and Johnson, P. J. (2004). Ancient invasions: from endosymbionts to organelles. *Science*, 304(5668):253–257.

E

- El-Yazal, S. A. S., El-Yazal, M. A. S., Dwidar, E. F., and Rady, M. M. (2015). Phytohormone crosstalk research: cytokinin and its crosstalk with other phytohormones. *Current Protein & Peptide Science*, 16(5):395–405.
- Erickson, J. L., Adlung, N., Lampe, C., Bonas, U., and Schattat, M. H. (2017a). The *Xanthomonas* effector XopL uncovers the role of microtubules in stromule extension and dynamics in *Nicotiana benthamiana*. *The Plant Journal*, 93(5):856–870.
- Erickson, J. L., Kantek, M., and Schattat, M. H. (2017b). Plastid-nucleus distance alters the behavior of stromules. *Frontiers in Plant Science*, 8:1135.
- Erickson, J. L. and Schattat, M. H. (2018). Shaping plastid stromules-principles of in vitro membrane tubulation applied in planta. *Current Opinion in Plant Biology*, 46:48–54.
- Erickson, J. L., Ziegler, J., Guevara, D., Abel, S., Klösgen, R. B., Mathur, J., Rothstein, S. J., and Schattat, M. H. (2014). Agrobacterium-derived cytokinin influences plastid morphology and starch accumulation in *Nicotiana benthamiana* during transient assays. *BMC Plant Biology*, 14:127.

F

- Feechan, A., Kwon, E., Yun, B.-W., Wang, Y., Pallas, J. A., and Loake, G. J. (2005). A central role for S-nitrosothiols in plant disease resistance. *Proceedings of the National Academy of Sciences*, 102(22):8054–8059.

Chapter 17. References

- Fernandez-Pozo, N., Rosli, H. G., Martin, G. B., and Mueller, L. A. (2015). The SGN VIGS tool: user-friendly software to design virus-induced gene silencing (VIGS) constructs for functional genomics. *Molecular Plant*, 8(3):486–488.
- Fester, T. and Hause, G. (2005). Accumulation of reactive oxygen species in arbuscular mycorrhizal roots. *Mycorrhiza*, 15(5):373–379.
- Fester, T., Strack, D., and Hause, B. (2001). Reorganization of tobacco root plastids during arbuscule development. *Planta*, 213(6):864–868.
- Finn, R. D., Bateman, A., Clements, J., Coggill, P., Eberhardt, R. Y., Eddy, S. R., Heger, A., Hetherington, K., Holm, L., Mistry, J., Sonnhammer, E. L. L., Tate, J., and Punta, M. (2013). Pfam: the protein families database. *Nucleic Acids Research*, 42:D222–D230.

G

- Gabaldón, T. and Pittis, A. A. (2015). Origin and evolution of metabolic sub-cellular compartmentalization in eukaryotes. *Biochimie*, 119:262–268.
- Gassmann, W., Hinsch, M. E., and Staskawicz, B. J. (1999). The Arabidopsis *RPS4* bacterial-resistance gene is a member of the TIR-NBS-LRR family of disease-resistance genes. *The Plant Journal*, 20(3):265–277.
- Gillespie, T., Boevink, P., Haupt, S., Roberts, A. G., Toth, R., Valentine, T., Chapman, S., and Oparka, K. J. (2002). Functional analysis of a dna-shuffled movement protein reveals that microtubules are dispensable for the cell-to-cell movement of *Tobacco mosaic virus*. *The Plant Cell*, 14(6):1207–1222.
- Golomb, L., Abu-Abied, M., Belausov, E., and Sadot, E. (2008). Different subcellular localizations and functions of Arabidopsis myosin VIII. *BMC Plant Biology*, 8(1):3.
- Grant, M. R., Godiard, L., Straube, E., Ashfield, T., Lewald, J., Sattler, A., Innes, R. W., and Dangl, J. L. (1995). Structure of the Arabidopsis *RPM1* gene enabling dual specificity disease resistance. *Science*, 269(5225):843–846.
- Gray, J. C., Hansen, M. R., Shaw, D. J., Graham, K., Dale, R., Smallman, P., Natesan, S. K. A., and Newell, C. A. (2012). Plastid stromules are induced by stress treatments acting through abscisic acid. *The Plant Journal*, 69(3):387–398.
- Gray, J. C., Sullivan, J. A., Hibberd, J. M., and Hansen, M. R. (2001). Stromules: mobile protrusions and interconnections between plastids. *Plant Biology*, 3:223–233.
- Grefen, C., Donald, N., Hashimoto, K., Kudla, J., Schumacher, K., and Blatt, M. R. (2010). A *ubiquitin-10* promoter-based vector set for fluorescent protein tagging facilitates temporal stability and native protein distribution in transient and stable expression studies. *The Plant Journal*, 64(2):355–365.
- Großkinsky, D. K., van der Graaff, E., and Roitsch, T. (2014). Abscisic acid–cytokinin antagonism modulates resistance against *Pseudomonas syringae* in tobacco. *Phytopathology*, 104(12):1283–1288.
- Gunning, B. E. S. (2005). Plastid stromules: video microscopy of their outgrowth, retraction, tensioning, anchoring, branching, bridging, and tip-shedding. *Protoplasma*, 225(1-2):33–42.

H

- Hamada, T., Tominaga, M., Fukaya, T., Nakamura, M., Nakano, A., Watanabe, Y., Hashimoto, T., and Baskin, T. I. (2012). RNA processing bodies, peroxisomes, Golgi bodies, mitochondria, and endoplasmic reticulum tubule junctions frequently pause at cortical microtubules. *Plant & Cell Physiology*, 53(4):699–708.
- Hamilton, A. J. and Baulcombe, D. C. (1999). A species of small antisense RNA in posttranscriptional gene silencing in plants. *Science*, 286(5441):950–952.

- Hanson, M. R. and Hines, K. M. (2018). Stromules: probing formation and function. *Plant Physiology*, 176(1):128–137.
- Hanson, M. R. and Sattarzadeh, A. (2008). Dynamic morphology of plastids and stromules in angiosperm plants. *Plant, Cell & Environment*, 31(5):646–657.
- Hanson, M. R. and Sattarzadeh, A. (2011). Stromules: recent insights into a long neglected feature of plastid morphology and function. *Plant Physiology*, 155(4):1486–1492.
- Hansson, M. D., Rzeznicka, K., Rosenbäck, M., Hansson, M., and Sirijovski, N. (2008). PCR-mediated deletion of plasmid DNA. *Analytical Biochemistry*, 375(2):373–375.
- Hartley, J. L., Temple, G. F., and Brasch, M. A. (2000). DNA cloning using *in vitro* site-specific recombination. *Genome Research*, 10(11):1788–1795.
- Haswell, E. S. and Meyerowitz, E. M. (2006). MscS-like proteins control plastid size and shape in *Arabidopsis thaliana*. *Current Biology*, 16(1):1–11.
- Hoekema, A., Hirsch, P. R., Hooykaas, P. J. J., and Schilperoort, R. A. (1983). A binary plant vector strategy based on separation of *vir*-region and T-region of the *Agrobacterium tumefaciens* Ti-plasmid. *Nature*, 303:79–180.
- Holthuis, J. C. M. and Levine, T. P. (2005). Lipid traffic: floppy drives and a superhighway. *Nature Reviews Molecular Cell Biology*, 6(3):209–220.
- Holzinger, A., Buchner, O., Lütz, C., and Hanson, M. R. (2007a). Temperature-sensitive formation of chloroplast protrusions and stromules in mesophyll cells of *Arabidopsis thaliana*. *Protoplasma*, 230(1-2):23–30.
- Holzinger, A., Kwok, E. Y., and Hanson, M. R. (2008). Effects of *arc3*, *arc5* and *arc6* mutations on plastid morphology and stromule formation in green and nongreen tissues of *vArabidopsis thaliana*. *Photochemistry and Photobiology*, 84(6):1324–1335.
- Holzinger, A., Wasteneys, G. O., and Lütz, C. (2007b). Investigating cytoskeletal function in chloroplast protrusion formation in the arctic-alpine plant *Oxyria digyna*. *Plant Biology*, 9(3):400–410.

I

- Ishida, H., Yoshimoto, K., Izumi, M., Reisen, D., Yano, Y., Makino, A., Ohsumi, Y., Hanson, M. R., and Mae, T. (2008). Mobilization of rubisco and stroma-localized fluorescent proteins of chloroplasts to the vacuole by an *ATG* gene-dependent autophagic process. *Plant Physiology*, 148(1):142–155.
- Islam, M. S., Kabir, A. M. R., Inoue, D., Sada, K., and Kakugo, A. (2016). Enhanced dynamic instability of microtubules in a ROS free inert environment. *Biophysical Chemistry*, 211:1–8.
- Itoh, R. D., Ishikawa, H., Nakajima, K. P., Moriyama, S., and Fujiwara, M. T. (2018). Isolation and analysis of a stromule-overproducing *arabidopsis* mutant suggest the role of PARC6 in plastid morphology maintenance in the leaf epidermis. *Physiologia Plantarum*, 162(4):479–494.

J

- Jaack, E., Martz, F., Stiefel, V., Fritig, B., and Legrand, M. (1996). Expression of class I O-methyltransferase in healthy and TMV-infected tobacco. *Molecular Plant-Microbe Interactions*, 9(8):681–688.
- Jiang, S.-Y., Ramamoorthy, R., and Ramachandran, S. (2008). Comparative transcriptional profiling and evolutionary analysis of the GRAM domain family in eukaryotes. *Developmental Biology*, 314(2):418–432.
- Jin, H., Li, S., and Villegas, A. (2006). Down-regulation of the 26S proteasome subunit RPN9 inhibits viral systemic transport and alters plant vascular development. *Plant Physiology*, 142(2):651–661.
- Jones, B., Gunnerås, S. A., Petersson, S. V., Tarkowski, P., Graham, N., May, S., Doležal, K., Sandberg, G., and Ljung, K. (2010). Cytokinin regulation of auxin synthesis in *Arabidopsis* involves a homeostatic feedback loop regulated via auxin and cytokinin signal transduction. *The Plant Cell*, 22(9):2956–2969.

Jones, B. and Ljung, K. (2011). Auxin and cytokinin regulate each other's levels via a metabolic feedback loop. *Plant Signaling & Behavior*, 6(6):901–904.

K

Kandasamy, M. K. and Meagher, R. B. (1999). Actin-organelle interaction: Association with chloroplast in Arabidopsis leaf mesophyll cells. *Cytoskeleton*, 44(2):110–118.

Kataya, A. R. A., Heidari, B., Hagen, L., Kommedal, R., Slupphaug, G., and Lillo, C. (2015). Protein phosphatase 2A holoenzyme is targeted to peroxisomes by piggybacking and positively affects peroxisomal β -oxidation. *Plant Physiology*, 167(2):493–506.

Keilwagen, J., Wenk, M., Erickson, J. L., Schattat, M. H., Grau, J., and Hartung, F. (2016). Using intron position conservation for homology-based gene prediction. *Nucleic Acids Research*, 44(9):e89.

Khan, M., Subramaniam, R., and Desveaux, D. (2016). Of guards, decoys, baits and traps: pathogen perception in plants by type III effector sensors. *Current Opinion in Microbiology*, 29:49–55.

Kim, M., Ahn, J.-W., Jin, U.-H., Choi, D., Paek, K.-H., and Pai, H.-S. (2003). Activation of the programmed cell death pathway by inhibition of proteasome function in plants. *The Journal of Biological Chemistry*, 278(21):19406–19415.

Klement, Z. and Goodman, R. N. (1967). The hypersensitive reaction to infection by bacterial plant pathogens. *Annual Review of Phytopathology*, 5:17–44.

Köhler, R. H., Cao, J., Zipfel, W. R., Webb, W. W., and Hanson, M. R. (1997). Exchange of protein molecules through connections between higher plant plastids. *Science*, 276(5321):2039–2042.

Köhler, R. H. and Hanson, M. R. (2000). Plastid tubules of higher plants are tissue-specific and developmentally regulated. *Journal of Cell Science*, 113(1):81–89.

Konagaya, K.-i., Matsushita, Y., Kasahara, M., and Nyunoya, H. (2004). Members of 14-3-3 protein isoforms interacting with the resistance gene product N and the elicitor of *Tobacco mosaic virus*. *Journal of General Plant Pathology*, 70(4):221–231.

Koncz, C. and Schell, J. (1986). The promoter of TL-DNA gene 5 controls the tissue-specific expression of chimaeric genes carried by a novel type of Agrobacterium binary vector. *Molecular and General Genetics*, 204(3):383–396.

Krenz, B., Jeske, H., and Kleinow, T. (2012). The induction of stromule formation by a plant DNA-virus in epidermal leaf tissues suggests a novel intra- and intercellular macromolecular trafficking route. *Frontiers in Plant Science*, 3:1–12.

Krenz, B., Windeisen, V., Wege, C., Jeske, H., and Kleinow, T. (2010). A plastid-targeted heat shock cognate 70kDa protein interacts with the *Abutilon* mosaic virus movement protein. *Virology*, 401(1):6–17.

Kumagai, M. H., Donson, J., della Cioppa, G., Harvey, D., Hanley, K., and Grill, L. K. (1995). Cytoplasmic inhibition of carotenoid biosynthesis with virus-derived RNA. *Proceedings of the National Academy of Sciences of the United States of America*, 92(5):1679–1683.

Kumar, A. S., Park, E., Nedo, A., Alqarni, A., Ren, L., Hoban, K., Modla, S., McDonald, J. H., Kambhamettu, C., Dinesh-Kumar, S. P., and Caplan, J. L. (2018). Stromule extension along microtubules coordinated with actin-mediated anchoring guides perinuclear chloroplast movement during innate immunity. *Elife*, 7:e23625.

Kunkel, B. N., Bent, A. F., Dahlbeck, D., Innes, R. W., and Staskawicz, B. J. (1993). *RPS2*, an Arabidopsis disease resistance locus specifying recognition of *Pseudomonas syringae* strains expressing the avirulence gene *avrRpt2*. *The Plant Cell*, 5(8):865–875.

Kwok, E. Y. and Hanson, M. R. (2003). Microfilaments and microtubules control the morphology and movement of non-green plastids and stromules in *Nicotiana tabacum*. *The Plant Journal*, 35(1):16–26.

- Kwok, E. Y. and Hanson, M. R. (2004a). *In vivo* analysis of interactions between GFP-labeled microfilaments and plastid stromules. *BMC Plant Biology*, 4(1):2.
- Kwok, E. Y. and Hanson, M. R. (2004b). Plastids and stromules interact with the nucleus and cell membrane in vascular plants. *Plant Cell Reports*, 23(4):188–195.
- Kwok, E. Y. and Hanson, M. R. (2004c). Stromules and the dynamic nature of plastid morphology. *Journal of Microscopy*, 214(2):124–137.

L

- Lee, C.-W., Efetova, M., Engelmann, J. C., Kramell, R., Wasternack, C., Ludwig-Müller, J., Hedrich, R., and Deeken, R. (2009). *Agrobacterium tumefaciens* promotes tumor induction by modulating pathogen defense in *Arabidopsis thaliana*. *The Plant Cell*, 21(9):2948–2962.
- Leister, D. (2012). Retrograde signaling in plants: from simple to complex scenarios. *Frontiers in Plant Science*, 3:135.
- Letierrier, M., Chaki, M., Airaki, M., Valderrama, R., Palma, J. M., Barroso, J. B., and Corpas, F. J. (2011). Function of S-nitrosoglutathione reductase (GSNOR) in plant development and under biotic/abiotic stress. *Plant Signaling & Behavior*, 6(6):789–793.
- Liu, D., Shi, L., Han, C., Yu, J., Li, D., and Zhang, Y. (2012). Validation of reference genes for gene expression studies in virus-infected *Nicotiana benthamiana* using quantitative real-time PCR. *PLoS ONE*, 7(9):e46451.
- Liu, E. and Page, J. E. (2008). Optimized cDNA libraries for virus-induced gene silencing (VIGS) using tobacco rattle virus. *Plant Methods*, 4(1):5.
- Liu, J.-H., Luo, M., Cheng, K.-J., Mohapatra, S. S., and Hill, R. D. (1999). Identification and characterization of a novel barley gene that is ABA-inducible and expressed specifically in embryo and aleurone. *Journal of Experimental Botany*, 50(334):727–728.
- Liu, L., Li, N., Yao, C., Meng, S., and Song, C. (2013). Functional analysis of the ABA-responsive protein family in ABA and stress signal transduction in *Arabidopsis*. *Chinese Science Bulletin*, 58(31):3721–3730.
- Liu, Y., Schiff, M., and Dinesh-Kumar, S. P. (2002). Virus-induced gene silencing in tomato. *The Plant Journal*, 31(6):777–786.
- Livak, K. J. and Schmittgen, T. D. (2001). Analysis of relative gene expression data using real-time quantitative PCR and the 2⁻delta delta CT method. *Methods*, 25(4):402.
- Livanos, P., Galatis, B., and Apostolakos, P. (2014). The interplay between ROS and tubulin cytoskeleton in plants. *Plant Signaling & Behavior*, 9(1):e28069.

M

- Mackey, D., Holt, B. F., Wiig, A., and Dangl, J. L. (2002). RIN4 interacts with *Pseudomonas syringae* type III effector molecules and is required for RPM1-mediated resistance in *Arabidopsis*. *Cell*, 108(6):743–754.
- Madison, S. L. and Nebenführ, A. (2013). Understanding myosin functions in plants: are we there yet? *Current Opinion in Plant Biology*, 16(6):710–717.
- Maruta, T., Noshi, M., Tanouchi, A., Tamoi, M., Yabuta, Y., Yoshimura, K., Ishikawa, T., and Shigeoka, S. (2012). H₂O₂-triggered retrograde signaling from chloroplasts to nucleus plays specific role in response to stress. *The Journal of Biological Chemistry*, 287(15):11717–11729.
- Mathur, J., Mammone, A., and Barton, K. (2012). Organelle extensions in plant cells. *Journal of Integrative Plant Biology*, 54(11):851–867.
- Mauri, N., Fernández-Marcos, M., Costas, C., Desvoyes, B., Pichel, A., Caro, E., and Gutierrez, C. (2016). GEM, a member of the GRAM domain family of proteins, is part of the ABA signaling pathway. *Nature Publishing Group*, 6(1):22660–11.

Michalska, J., Zauber, H., Buchanan, B. B., Cejudo, F. J., and Geigenberger, P. (2009). NTRC links built-in thioredoxin to light and sucrose in regulating starch synthesis in chloroplasts and amyloplasts. *Proceedings of the National Academy of Sciences of the United States of America*, 106(24):9908–9913.

N

Nakagawa, T., Kurose, T., Hino, T., Tanaka, K., Kawamukai, M., Niwa, Y., Toyooka, K., Matsuoka, K., Jinbo, T., and Kimura, T. (2007). Development of series of gateway binary vectors, pGWBs, for realizing efficient construction of fusion genes for plant transformation. *Journal of Bioscience and Bioengineering*, 104(1):34–41.

Naseem, M., Kunz, M., and Dandekar, T. (2014). Probing the unknowns in cytokinin-mediated immune defense in Arabidopsis with systems biology approaches. *Bioinformatics and Biology Insights*, 8:35–44.

Natesan, S. K. A., Sullivan, J. A., and Gray, J. C. (2005). Stromules: a characteristic cell-specific feature of plastid morphology. *Journal of Experimental Botany*, 56(413):787–797.

Natesan, S. K. A., Sullivan, J. A., and Gray, J. C. (2009). Myosin XI is required for actin-associated movement of plastid stromules. *Molecular Plant*, 2(6):1262–1272.

Nishiyama, R., Watanabe, Y., Fujita, Y., Le, D. T., Kojima, M., Werner, T., Vankova, R., Yamaguchi-Shinozaki, K., Shinozaki, K., Kakimoto, T., Sakakibara, H., Schmölling, T., and Tran, L.-S. P. (2011). Analysis of cytokinin mutants and regulation of cytokinin metabolic genes reveals important regulatory roles of cytokinins in drought, salt and abscisic acid responses, and abscisic acid biosynthesis. *The Plant Cell*, 23(6):2169–2183.

Nonaka, S., Yuhashi, K.-I., Takada, K., Sugawara, M., Minamisawa, K., and Ezura, H. (2008). Ethylene production in plants during transformation suppresses *vir* gene expression in *Agrobacterium tumefaciens*. *New Phytologist*, 178(3):647–656.

Nott, A., Jung, H.-S., Koussevitzky, S., and Chory, J. (2006). Plastid-to-nucleus retrograde signaling. *Annual Review of Plant Biology*, 57:739–759.

O

Oikawa, K. (2003). CHLOROPLAST UNUSUAL POSITIONING1 is essential for proper chloroplast positioning. *The Plant Cell*, 15(12):2805–2815.

Oikawa, K., Yamasato, A., Kong, S.-G., Kasahara, M., Nakai, M., Takahashi, F., Ogura, Y., Kagawa, T., and Wada, M. (2008). Chloroplast outer envelope protein CHUP1 is essential for chloroplast anchorage to the plasma membrane and chloroplast movement. *Plant Physiology*, 148(2):829–842.

P

Padmanabhan, M. S., Ma, S., Burch-Smith, T. M., Czymmek, K., Huijser, P., and Dinesh-Kumar, S. P. (2013). Novel positive regulatory role for the SPL6 transcription factor in the N TIR-NB-LRR receptor-mediated plant innate immunity. *PLoS Pathogens*, 9(3):e1003235.

Peng, J., Ilarslan, H., Wurtele, E. S., and Bassham, D. C. (2011). AtRabD2b and AtRabD2c have overlapping functions in pollen development and pollen tube growth. *BMC Plant Biology*, 11(1):25.

Peremyslov, V. V., Klocko, A. L., Fowler, J. E., and Dolja, V. V. (2012). Arabidopsis myosin XI-K localizes to the motile endomembrane vesicles associated with F-actin. *Frontiers in Plant Science*, 3(184):1–10.

Peremyslov, V. V., Prokhnevsky, A. I., and Dolja, V. V. (2010). Class xi myosins are required for development, cell expansion, and F-actin organization in Arabidopsis. *The Plant Cell*, 22(6):1883–1897.

Pérez-Ruiz, J. M., Spínola, M. C., Kirchsteiger, K., Moreno, J., Sahrawy, M., and Cejudo, F. J. (2006). Rice NTRC is a high-efficiency redox system for chloroplast protection against oxidative damage. *The Plant Cell*, 18(9):2356–2368.

- Prokhnevsky, A. I., Peremyslov, V. V., and Dolja, V. V. (2008). Overlapping functions of the four class XI myosins in Arabidopsis growth, root hair elongation, and organelle motility. *Proceedings of the National Academy of Sciences of the United States of America*, 105(5):19744–19749.
- Pyke, K. A. (1999). Plastid division and development. *The Plant Cell*, 11:549–556.
- Pyke, K. A. (2002). Plastid and stromule morphogenesis in tomato. *Annals of Botany*, 90(5):559–566.

R

- Reichelt, S., Knight, A. E., Hodge, T. P., Baluska, F., Samaj, J., Volkmann, D., and Kendrick-Jones, J. (1999). Characterization of the unconventional myosin VIII in plant cells and its localization at the post-cytokinetic cell wall. *Plant Journal*, 19(5):555–567.
- Reiland, S., Messerli, G., Baerenfaller, K., Gerrits, B., Endler, A., Grossmann, J., Gruissem, W., and Baginsky, S. (2009). Large-scale Arabidopsis phosphoproteome profiling reveals novel chloroplast kinase substrates and phosphorylation networks. *Plant Physiology*, 150(2):889–903.
- Reisen, D. and Hanson, M. R. (2007). Association of six YFP-myosin XI-tail fusions with mobile plant cell organelles. *BMC Plant Biology*, 7(1):6.
- Rico, A., Bennett, M. H., Forcat, S., Huang, W. E., and Preston, G. M. (2010). Agroinfiltration reduces ABA levels and suppresses *Pseudomonas syringae*-elicited salicylic acid production in *Nicotiana tabacum*. *PLoS ONE*, 5(1):e8977.
- Robert-Seilaniantz, A., Grant, M., and Jones, J. D. G. (2011). Hormone crosstalk in plant disease and defense: more than just jasmonate-salicylate antagonism. *Annual Review of Phytopathology*, 49(1):317–343.
- Roitinger, E., Hofer, M., Köcher, T., Pichler, P., Novatchkova, M., Yang, J., Schlögelhofer, P., and Mechtler, K. (2015). Quantitative phosphoproteomics of the Ataxia Telangiectasia-Mutated (ATM) and Ataxia Telangiectasia-Mutated and Rad3-related (ATR) dependent DNA damage response in *Arabidopsis thaliana*. *Molecular & Cellular Proteomics*, 14(3):556–571.
- Römer, P., Hahn, S., Jordan, T., Strauss, T., Bonas, U., and Lahaye, T. (2007). Plant pathogen recognition mediated by promoter activation of the pepper *Bs3* resistance gene. *Science*, 318(5850):645–648.
- Roux, A. (2013). The physics of membrane tubes: soft templates for studying cellular membranes. *Soft Matter*, 9(29):6726–6736.

S

- Sah, S. K., Reddy, K. R., and Li, J. (2016). Abscisic acid and abiotic stress tolerance in crop plants. *Frontiers in Plant Science*, 7(15013):63.
- Sattarzadeh, A., Krahmer, J., Germain, A. D., and Hanson, M. R. (2009). A myosin XI tail domain homologous to the yeast myosin vacuole-binding domain interacts with plastids and stromules in *Nicotiana benthamiana*. *Molecular Plant*, 2(6):1351–1358.
- Saxena, I., Srikanth, S., and Chen, Z. (2016). Cross talk between H₂O₂ and interacting signal molecules under plant stress response. *Frontiers in Plant Science*, 7:570.
- Scalschi, L., Sanmartín, M., Camañes, G., Troncho, P., Sánchez-Serrano, J. J., García-Agustín, P., and Vicedo, B. (2015). Silencing of *OPR3* in tomato reveals the role of OPDA in callose deposition during the activation of defense responses against *Botrytis cinerea*. *The Plant Journal*, 81(2):304–315.
- Schattat, M., Barton, K., Baudisch, B., Klösgen, R. B., and Mathur, J. (2011a). Plastid stromule branching coincides with contiguous endoplasmic reticulum dynamics. *Plant Physiology*, 155(4):1667–1677.
- Schattat, M., Barton, K., and Mathur, J. (2011b). Correlated behavior implicates stromules in increasing the interactive surface between plastids and ER tubules. *Plant Signaling & Behavior*, 6(5):715–718.

Chapter 17. References

- Schattat, M. H., Griffiths, S., Mathur, N., Barton, K., Wozny, M. R., Dunn, N., Greenwood, J. S., and Mathur, J. (2012). Differential coloring reveals that plastids do not form networks for exchanging macromolecules. *The Plant Cell*, 24(4):1465–1477.
- Schattat, M. H. and Klösgen, R. B. (2011). Induction of stomule formation by extracellular sucrose and glucose in epidermal leaf tissue of *Arabidopsis thaliana*. *BMC Plant Biology*, 11:115.
- Schultink, A., Qi, T., Lee, A., Steinbrenner, A. D., and Staskawicz, B. (2017). Roq1 mediates recognition of the *Xanthomonas* and *Pseudomonas* effector proteins XopQ and HopQ1. *The Plant Journal*, 92(5):787–795.
- Sellers, J. R. (2000). Myosins: a diverse superfamily. *Biochimica et Biophysica Acta*, 1496(1):3–22.
- Senn, G. (1908). Die Gestalts- und Lageveränderung der Pflanzen-Chromatophoren. *Nature Publishing Group, Leipzig, Germany*, pages 1–397.
- Senthil-Kumar, M. and Mysore, K. S. (2014). Tobacco rattle virus-based virus-induced gene silencing in *Nicotiana benthamiana*. *Nature Protocols*, 9(7):1549–1562.
- Shalla, T. A. (1964). Assembly and aggregation of *Tobacco mosaic virus* in tomato leaflets. *Journal of Cell Biology*, 21:253–264.
- Sparkes, I. (2011). Recent advances in understanding plant myosin function: life in the fast lane. *Molecular Plant*, 4(5):805–812.
- Sparkes, I. A., Teanby, N. A., and Hawes, C. (2008). Truncated myosin XI tail fusions inhibit peroxisome, Golgi, and mitochondrial movement in tobacco leaf epidermal cells: a genetic tool for the next generation. *Journal of Experimental Botany*, 59(9):2499–2512.
- Stukkens, Y., Bultreys, A., Grec, S., Trombik, T., Vanham, D., and Boutry, M. (2005). NpPDR1, a pleiotropic drug resistance-type ATP-binding cassette transporter from *Nicotiana plumbaginifolia*, plays a major role in plant pathogen defense. *Plant Physiology*, 139(1):341–352.
- Subramoni, S., Nathoo, N., Klimov, E., and Yuan, Z.-C. (2014). *Agrobacterium tumefaciens* responses to plant-derived signaling molecules. *Frontiers in Plant Science*, 5:322.
- Suttle, J. C. (1986). Cytokinin-induced ethylene biosynthesis in nonsenescent cotton leaves. *Plant Physiology*, 82(4):930–935.
- Swartzberg, D., Kirshner, B., Rav-David, D., Elad, Y., and Granot, D. (2007). *Botrytis cinerea* induces senescence and is inhibited by autoregulated expression of the *IPT* gene. *European Journal of Plant Pathology*, 120(3):289–297.
- Szatmári, Á., Zvara, Á., Móricz, Á. M., Besenyi, E., Szabó, E., Ott, P. G., Puskás, L. G., and Bozsó, Z. (2014). Pattern triggered immunity (PTI) in tobacco: Isolation of activated genes suggests role of the phenylpropanoid pathway in inhibition of bacterial pathogens. *PLoS ONE*, 9(8):e102869.
- Szczesny, R., Büttner, D., Escolar, L., Schulze, S., Seiferth, A., and Bonas, U. (2010). Suppression of the AvrBs1-specific hypersensitive response by the YopJ effector homolog AvrBsT from *Xanthomonas* depends on a SNF1-related kinase. *The New Phytologist*, 187(4):1058–1074.

T

- Tai, T. H., Dahlbeck, D., Clark, E. T., Gajiwala, P., Pasion, R., Whalen, M. C., Stall, R. E., and Staskawicz, B. J. (1999). Expression of the *bs2* pepper gene confers resistance to bacterial spot disease in tomato. *Proceedings of the National Academy of Sciences of the United States of America*, 96(24):14153–14158.
- Tamura, K., Iwabuchi, K., Fukao, Y., Kondo, M., Okamoto, K., Ueda, H., Nishimura, M., and Hara-Nishimura, I. (2013). Myosin XI-I links the nuclear membrane to the cytoskeleton to control nuclear movement and shape in *Arabidopsis*. *Current Biology*, 23(18):1776–1781.
- Thompson, A. R., Doelling, J. H., Suttangkakul, A., and Vierstra, R. D. (2005). Autophagic nutrient recycling in *Arabidopsis* directed by the ATG8 and ATG12 conjugation pathways. *Plant Physiology*, 138(4):2097–2110.

- Tirlapur, U. K., Dahse, I., Reiss, B., Meurer, J., and Oelmüller, R. (1999). Characterization of the activity of a plastid-targeted green fluorescent protein in Arabidopsis. *European Journal of Cell Biology*, 78(4):233–240.
- Toruño, T. Y., Stergiopoulos, I., and Coaker, G. (2016). Plant-pathogen effectors: Cellular probes interfering with plant defenses in spatial and temporal manners. *Annual Review of Phytopathology*, 54(1):419–441.

V

- Van den Ackerveken, G., Marois, E., and Bonas, U. (1996). Recognition of the bacterial avirulence protein AvrBs3 occurs inside the host plant cell. *Cell*, 87(7):1307–1316.
- Velásquez, A. C., Chakravarthy, S., and Martin, G. B. (2009). Virus-induced gene silencing (VIGS) in *Nicotiana benthamiana* and tomato. *Journal of Visualized Experiments*, 28.
- Veley, K. M., Marshburn, S., Clure, C. E., and Haswell, E. S. (2012). Mechanosensitive channels protect plastids from hypoosmotic stress during normal plant growth. *Current Biology*, 22(5):408–413.
- Viallat, A., Dalous, J., and Abkarian, M. (2004). Giant lipid vesicles filled with a gel: shape instability induced by osmotic shrinkage. *Biophysical Journal*, 86(4):2179–2187.
- Vismans, G., van der Meer, T., Langevoort, O., Schreuder, M., Bouwmeester, H., Peisker, H., Dörman, P., Ketelaar, T., and van der Krol, A. (2016). Low-phosphate induction of plastidal stromules is dependent on strigolactones but not on the canonical strigolactone signaling component MAX2. *Plant Physiology*, 172(4):2235–2244.
- Vlot, A. C., Dempsey, D. A., and Klessig, D. F. (2009). Salicylic acid, a multifaceted hormone to combat disease. *Annual Review of Phytopathology*, 47(1):177–206.

W

- Wang, Z. and Benning, C. (2012). Chloroplast lipid synthesis and lipid trafficking through ER-plastid membrane contact sites. *Biochemical Society Transactions*, 40(2):457–463.
- Wildman, S. G., Hongladarom, T., and Honda, S. I. (1962). Chloroplasts and mitochondria in living plant cells: cinephotomicrographic studies. *Science*, 138(3538):434–436.
- Wünsche, H., Baldwin, I. T., and Wu, J. (2011). S-Nitrosoglutathione reductase (GSNOR) mediates the biosynthesis of jasmonic acid and ethylene induced by feeding of the insect herbivore *Manduca sexta* and is important for jasmonate-elicited responses in *Nicotiana attenuata*. *Journal of Experimental Botany*, 62(13):4605–4616.

Y

- Yang, H., Mu, J., Chen, L., Feng, J., Hu, J., Li, L., Zhou, J.-M., and Zuo, J. (2015). S-nitrosylation positively regulates ascorbate peroxidase activity during plant stress responses. *Plant Physiology*, 167(4):1604–1615.
- Yao, L.-L., Zhou, Q., Pei, B.-L., and Li, Y.-Z. (2011). Hydrogen peroxide modulates the dynamic microtubule cytoskeleton during the defence responses to *Verticillium dahliae* toxins in Arabidopsis. *Plant, Cell & Environment*, 34(9):1586–1598.

Z

- Zhang, T., Chen, S., and Harmon, A. C. (2016). Protein-protein interactions in plant mitogen-activated protein kinase cascades. *Journal of Experimental Botany*, 67(3):607–618.
- Ziegler, J., Qwegwer, J., Schubert, M., Erickson, J. L., Schattat, M., Bürstenbinder, K., Grubb, C. D., and Abel, S. (2014). Simultaneous analysis of apolar phytohormones and 1-aminocyclopropan-1-carboxylic acid by high performance liquid chromatography/electrospray negative ion tandem mass spectrometry via 9-fluorenylmethoxycarbonyl chloride derivatization. *Journal of Chromatography. A*, 1362:102–109.

18. Publication list

Publications included in this thesis:

1. **Erickson, J.L.** and Schattat, M. (2018) Shaping plastid stromules - principles of *in vitro* membrane tubulation applied *in planta*. (Invited review) *Current Opinion in Plant Biology*, 46: 48-54.
2. **Erickson, J.L.**, Adlung, N., Lampe, C., Bonas, U. and Schattat, M. (2017) The *Xanthomonas* effector XopL uncovers the role of microtubules in stromules extension and dynamics in *N. benthamiana*. *The Plant Journal*, 93(5): 856-870.
3. **Erickson, J.L.**, Kantek, M. and Schattat, M. (2017) Plastid-nucleus distance alters the behavior of stromules. *Frontiers in Plant Science*, 8: 1135.
4. **Erickson, J.L.**, Ziegler, J., Guevara, D., Abel, S., Klösgen, R.B., Mathur, J., Rothstein S.J. and Schattat, M.H. (2014) Agrobacterium-derived cytokinin influences plastid morphology and starch accumulation in *Nicotiana benthamiana* during transient assays. *BMC Plant Biology*, 14: 127.
5. Ziegler, J., Qwegwer, J., Schubert, M., **Erickson, J.L.**, Schattat M.H., Bürstenbinder, K., Grubb, D.C. and Abel, S. (2014). Simultaneous analysis of apolar phytohormones and 1-aminocyclopropan-1-carboxylic acid by high performance liquid chromatography/electrospray negative ion tandem mass spectrometry via 9-fluorenylmethoxycarbonyl chloride derivatization. *Journal of Chromatography A.*, 1362:102-109.

Additional publications related to PhD work:

6. Keilwagen, J., Wend, M., **Erickson, J.L.** and Schattat, M.H. (2016) Using intron position conservation for homology-based gene prediction. *Nucleic Acids Research*, 44(9): e89.
7. Franke, L., **Erickson, J.L.**, Rödel, D., Schröter, D., Storbeck, B., Möller, B. and Schattat, M.H. (2015). The “MTB Cell Counter” a versatile tool for the semi-automated quantification of sub-cellular phenotypes in fluorescence microscopy images. A case study on plastids, nuclei, and peroxisomes. *Endocytobiosis Cell Research*, 26: 031-042.

Additional unrelated publications:

8. Pahari, S., Cormark, R.D., Blackshaw, M.T., Lieu, C., **Erickson, J.L.** and Schultz, E.A. (2014) Arabidopsis *UNHINGED* encodes a VPS51 homolog and reveals a role for the GARP complex in leaf shape and vein patterning. *Development*, 141(9): 1894-1905.
9. **Erickson, J.L.** (2011). Formation and maintenance of morphogen gradients; and essential role for the endomembrane system in *Drosophila melanogaster* wing development. *Fly*, 5(3): 266-271.
10. Hou, H., **Erickson, J.**, Meservy, J. and Schultz, E.A. (2010). *FORKED1* encodes a PH domain protein that is required for PIN1 localization in developing leaf veins. *The Plant Journal*, 63(6): 960-973.

19. *Curriculum vitae* / Lebenslauf

Personal Information:

Name	Jessica Lee Erickson
Address	Kleine Schlossgasse 5, 06108, Halle (Saale)
Birthday	05.05.1986
Sex	Female
Birthplace	Pincher Creek, AB, Canada
Nationality	Canadian

Education:

2004	High School Diploma - Livingstone School, Lundbreck, AB, Canada
2009	Bachelor's Degree (with Honours thesis) - University of Lethbridge; Alberta, Canada Topic - General Biology
2011	Master's Degree - Dr. Elizabeth Schultz's lab (Plant Genetics and Development), Department of Biology, University of Lethbridge, Alberta, Canada Master's topic - A yeast two-hybrid screen in <i>Arabidopsis thaliana</i> suggests FORKED1 forms homodimers and the ARFA1 family has a role in cotyledon vein patterning.
2013-2018 1 year maternity leave (2014-2015)	Doctoral Candidate - Dr. Martin Schattat's lab (Plant organelle shape and dynamics), Department of Plant Physiology, Martin-Luther-University Halle-Wittenberg Topic - Shaping plastid stromules.

20. Declaration / Erklärung

I hereby declare that I have completed this thesis independently, without external help. I also declare that sources and auxiliary materials used in this thesis are identified as such; otherwise outside works have not been used literally or in terms of content. This is the first time I have applied for a doctoral degree with this work.

21. Acknowledgements

Martin - We have been a fantastic team over the last years. I can't tell you how much I have enjoyed the brainstorming, the excitement, and the challenges of doing science with you. I would be sad if I thought we would stop working together, but I know we will be dreaming and scheming together for the rest of our careers.

Leif - My munchkin, you keep me grounded.

Ulla Bonas - Thank you for supporting me while writing this thesis, both financially and as a mentor. I am so grateful for the opportunity to work with you and your amazing group. I have already learned so much and look forward to working together in the future.

Christina Lampe - You are amazing! You make my life so much easier. You are reasonable, logical, steady, and smart. You being calm has kept me calm over these last stressful months.

Oliver Nagel - Thanks for reading my first draft of this thesis, even though you have absolutely no time! You are awesome, and I am excited to work with you in the years to come.

Friends and Family - Caro, Elli, Ekki, Arvid, Smilla, you make Halle feel like home. Marco, thank you for being a great trainer, and fitness role model. It is always inspiring to see people who follow their passion and love what they do. Mom, Dad, Katie, Mitchel, Kelsey, Lisa and Benji thanks for the encouragement, love and patience. Without you I would not be here. Lily and Rosa, Auntie is free to play now!

Rabe Klösigen - Thanks for including us in lab meetings, providing insight into projects, and contributing to our co-authored publication. Thank you for hosting our group and, of course, for reading my thesis.

Lab members of AG Schattat and Klösigen, past and present - Thanks for providing a stimulating, supportive and welcoming environment during my PhD time. Jolina Marx and Rachel Gormanns you made my last months in AG Schattat especially fun.

Co-authors - "Alone we can do so little; together we can do so much." - Hellen Keller

I am so grateful to my co-authors for reading and contributing ideas and data to the manuscripts. A special thanks to Norman Adlung, who shared first authorship with me on the XopL paper and who suffered through endless questions and interruptions with incredible patience.

Committee members - Thank you in advance for the time you spent reading this thesis. I am sorry it is so long!